THE UNIVERSITY
of EDINBURGH

Preclinical investigation of the novel SRC inhibitor eCF506 in cancer

Carolin Temps

THE UNIVERSITY *of* EDINBURGH

Doctor of Philosophy

The University of Edinburgh

2019

Declaration

I declare that this thesis has been composed by myself and describes my own research, except where explicitly stated otherwise in the text. No part of this thesis has been submitted for any other degree or professional qualification.

Carolin Temps

March 2020

Abstract

The non-receptor tyrosine kinase SRC plays an important and context-dependent role in a variety of cell signalling pathways that regulate cell motility, survival, division and growth factor signalling. SRC activity has been closely linked to several hallmarks of cancer (cell proliferation, metastasis, angiogenesis) and treatment resistance. Multiple studies found SRC to be aberrantly activated and/or overexpressed in solid tumours, such as breast, colorectal and ovarian cancer, which often correlated with malignancy and poor prognosis.

Dual SRC/ABL kinase inhibitors (e.g. dasatinib, bosutinib) are already in clinical use for the treatment of chronic myeloid leukaemia. However, attempts to repurpose them for their SRC inhibition alone have so far failed in clinical trials. Several studies suggest that ABL kinase can act as a tumour suppressor in solid cancers and its inhibition has been linked to cardiotoxic events in patients. This complicates the use of SRC/ABL inhibitors in combination with other anti-cancer agents with cardiac side effects, such as chemotherapeutics, certain monoclonal antibodies and other kinase inhibitors; yet resistance to several of these drugs was found to involve the activation of SRC signalling pathways. Consequently, there is a clear need for more selective SRC inhibitors which have the potential to exhibit greater efficacy and fewer side effects than the ones currently available.

The novel small molecule SRC inhibitor eCF506 has recently been discovered by the Innovative Therapeutics Lab at the University of Edinburgh [1]. It exhibits nanomolar potency, thousand-fold selectivity for SRC over ABL kinase and superior drug-like properties compared to the current gold-standard SRC inhibitor dasatinib. This thesis continues the preclinical development of eCF506 by (i) investigating its potency against different cancers in *in vitro* and *in vivo* models, (ii) assessing its safety and pharmacokinetic properties and (iii) identifying a unique binding mode to SRC kinase.

Lay summary

Kinases are proteins that add phosphate groups to other molecules in the cell. This often activates the target molecule and can cause it to phosphorylate others, leading to the activation of complex signalling pathways in the cell. SRC is a type of kinase that phosphorylates the amino acid tyrosine on its target proteins. SRC and its family members are found in many cell types of the human body and their activity plays an important role in the growth, division and movement of cells. However, abnormal SRC activity has been linked to the growth and spread of cancer and to treatment resistance. Higher levels of active SRC have been found in many different cancers (e.g. breast, ovarian and colorectal) and this has been associated with worse outcomes for patients.

There are currently no drugs available that inhibit only SRC kinase, but there are several that inhibit both SRC and another kinase called ABL (e.g. dasatinib, bosutinib). These dual SRC/ABL inhibitors are used in the clinic to treat patients with a type of blood cancer called chronic myeloid leukaemia (CML), which is caused by a mutation in ABL kinase. Several clinical trials have tested these drugs in other cancers for their SRC inhibition but so far they have not shown enough benefit for the patients to gain regulatory approval. A possible reason for this is that ABL may not be a good target in certain cancers, as some studies found ABL inhibition can contribute to cancer growth. Additionally, ABL inhibitors can cause heart problems that may limit the maximum dose patients can take and prohibit the combination with other anti-cancer drugs with similar side effects. This is a major drawback, as resistance to some of these drugs is thought to involve SRC activation. Based on these findings, there is a clear need for a selective SRC kinase inhibitor which has the potential to be more potent and safer than the current dual SRC/ABL inhibitors available.

The first potent and selective SRC kinase inhibitor eCF506 has recently been discovered by the Innovative Therapeutics Lab at the University of Edinburgh [1]. It can inhibit SRC kinase at very low concentrations, has high selectivity over ABL kinase and has better properties to be made into a drug than the current gold-standard SRC/ABL inhibitor dasatinib. This PhD thesis continues the preclinical development of eCF506 by (i) testing its effects in different models of cancer in isolated cancer cells and in animals, (ii) investigating its safety and fate in the body and (iii) finding out more about how it binds and inhibits its target SRC kinase.

Acknowledgements

First and foremost, I would like to thank my amazing supervisors Asier and Neil, who always had an open door, fresh ideas and motivation at hand when needed. The last three years would not have been as much fun without them. I am very grateful they believed in me back when I was a bachelor student and gave me this great opportunity.

I would also like to thank Val and Bin-Zhi for their critical input during thesis committee meetings and beyond, as well as their vital support in performing the *in vivo* experiments. These would not have been possible without the hard work of Xue-Feng, John and Morwenna, who performed all of the animal work and did not complain when we kept changing our minds about the experimental design. A special thank you to our collaborators Dr Daniel Lietha, Dr Alaide Morcavallo, Dr Michael Porcu and Dr Mathew Garnet, who tested eCF506 in their models and kindly let me show their results in this thesis. Thank you also to Prof Charlie Gourley and his group for providing the ovarian cancer cell lines and to Prof Margaret Frame for supporting the project.

I would like to thank Neil's group and in particular John, who always had a minute to spare to help me throughout my PhD. Thank you also to Kenny, who did the RPPA and cytokine assay, Rich, who included eCF506 in the oesophageal screen, as well as Alison, who never said no when I wanted to test yet another one of their cell lines. A big thanks to the level 3 support group, who never made me feel like the second-floor intruder that I was. I would like to thank Henry especially for helping me with the spheroids and subcellular fractionations, giving me his cell lines and listening to my endless updates about every small success and failure in my project.

I would like to thank my whole group, who have always been there for me during all my ups and downs in the last few years. Even though I mostly just ran in and out of the chemistry lab all day and couldn't stomach 2pm lunch times, I very much enjoyed my time with you and our epic Christmas parties! Thank you to Rafa, who spent many days in the lab making more compound. I also had the pleasure of supervising Anna during her bachelor dissertation and I am grateful for all her hard work and great attitude during her time with us.

Zuletzt möchte ich gerne meinen Eltern und meinem Bruder danken für ihre bedingungslose Unterstützung während meiner Schulzeit, meines Studiums und darüber hinaus. Ohne euch hätte ich es nicht geschafft! Danke auch an David, der immer für mich da war.

Contents

List of Figures

List of Tables

Abbreviations

Table I. List of abbreviations.

Abbreviation	Definition
A	Ascites
AC	Adenocarcinoma
ADME	Absorption, distribution, metabolism and excretion
ADP	Adenosine diphosphate
AJ	Adherens junction
ALL	Acute lymphoblastic leukaemia
ANOVA	Analysis of variance
AR	Androgen receptor
ATP	Adenosine triphosphate
AUC	Area under curve
BCA	Bicinchoninic acid
BCRP	Breast cancer resistance protein
BLI	Bioluminescence intensity
BSA	Bovine serum albumin
BLQ	Below limit of quantification
C	Completed
CAR-T	Chimeric antigen receptor T-cells
CBR	Clinical benefit rate
CCC	Clear cell carcinoma
cDNA	Complementary deoxyribonucleic acid
CL	Clearance
CL_{int}	Intrinsic clearance
C_{max}	Maximum plasma concentration
CML	Chronic myeloid leukaemia
CR	Complete response
CST	Cell Signalling Technology
CT	Cycle threshold
DAB	3,3-Diaminobenzidine
DAPI	4,6-Diamidino-2-phenylindole
DC	Ductal carcinoma
DCM	Dichloromethane
DMEM	Dulbecco's Modified Eagle's Medium
DMSO	Dimethyl sulfoxide
DNA	Deoxyribonucleic acid
EC	Endometrioid adenocarcinoma
EC_{50}	Half maximal effective concentration
ECL	Enhanced chemiluminescence
EDTA	Ethylenediaminetetraacetic acid
EGTA	Ethylene glycol-bis(β-aminoethyl ether)-N,N,N′,N′-tetraacetic acid
EMT	Epithelial-to-mesenchymal transition
ER	Oestrogen receptor
F	Bioavailability
FAT	Focal adhesion targeting
FBS	Foetal bovine serum
FDA	Food and Drug Administration
FERM	Protein 4.1, ezrin, radixin and moesin

FRET	Fluorescence resonance energy transfer
GABA	Gamma-aminobutyric acid
GDP	Guanosine diphosphate
GDSC	Genomics of Drug Sensitivity in Cancer
GI_{50}	Half maximal growth inhibition
GIST	Gastrointestinal stromal tumours
GPCR	G-protein coupled receptors
GTP	Guanosine triphosphate
H&E	Haematoxylin and eosin
HEPES	4-(2-Hydroxyethyl)-1-piperazineethanesulfonic acid
HGSOC	High-grade serous ovarian cancer
hRMVEC	Human retinal microvascular endothelial cells
HRP	Horseradish peroxidase
hTERT	Human telomerase reverse transcriptase
HUVEC	Human umbilical vein endothelial cells
IA	Intraarterial
IC_{50}	Half maximal inhibitory concentration
ICH	International Council for Harmonisation of Technical Requirements for Registration of Pharmaceuticals for Human Use
IPF	Idiopathic pulmonary fibrosis
IPT	Intraportal
ITAM	Immunoreceptor tyrosine-based activation motif
ITIM	Immunoreceptor tyrosine-based inhibitory motif
IV	Intravenous
K_d	Binding constant
K_i	Inhibitory constant
LC	Lobular carcinoma
LC-MS/MS	Liquid chromatography with tandem mass spectrometry
LPS	Lipopolysaccharide
M	Medullary carcinoma
MC	Metaplastic carcinoma
MF	Myelofibrosis
MFE	Mammosphere forming efficiency
MHC	Major histocompatibility complex
MTC	Medullary thyroid cancer
MTD	Maximum tolerated dose
NES	Nuclear export sequence
NLS	Nuclear localisation sequence
NMDAR	N-methyl-D-aspartate receptor
NR	Not recruiting
NS	Not significant
NSCLC	Non-small-cell lung cancer
ORR	Objective response rate
OS	Overall survival
PBr	Primary breast
PBS	Phosphate buffered saline
PBST	Phosphate buffered saline tween
PCR	Polymerase chain reaction
PCV	Polycythemia vera
PDB	Protein database
PE	Pleural effusion

PFS	Progression-free survival
Pgp	P-glycoprotein
Ph+	Philadelphia chromosome positive
pHEMA	Poly(2-hydroxyethyl methacrylate)
PI	Protease and phosphatase inhibitors
PK	Pharmacokinetic
PMSF	Phenylmethylsulfonyl fluoride
PO	*Per os* (orally)
PR	Partial response
PrR	Progesterone receptor
R	Recruiting
R^2	Coefficient of determination
RFI	Relative fluorescence intensity
RIPA	Radioimmunoprecipitation assay
RNA	Ribonucleic acid
RPPA	Reverse phase protein array
RSV	Rous sarcoma virus
RTK	Receptor tyrosine kinase
S	Suspended
SCB	Santa Cruz Biotechnology
SCLC	Small-cell lung cancer
SD	Stable disease
SDS	Sodium dodecyl sulfate
SDS-PAGE	Sodium dodecyl sulfate polyacrylamide gel electrophoresis
SFK	SRC family kinase
SH	SRC homology domain
siRNA	Small interfering RNA
STR	Short tandem repeat
T	Terminated
$t_{1/2}$	Half-life
TBS	Tris-buffered saline
TBST	Tris-buffered saline tween
TCEP	Tris(2-carboxyethyl)phosphine
TCR	T-cell receptor
TFA	Trifluoroacetic acid
TGI	Total growth inhibition
TGS	Tris glycine saline
THF	Tetrahydrofuran
TLR	Toll-like receptor
T_{max}	Time to reach maximum concentration
TNBC	Triple negative breast cancer
Tris	Tris(hydroxymethyl)aminomethane
UPLC-MS/MS	Ultra performance liquid chromatography with tandem mass spectrometry
UV	Ultraviolet
Vd_{ss}	Volume of distribution (steady state)
W	Withdrawn

Chapter 1. Introduction

1.1. Cancer and kinases

Cancer

Cancer is a group of diseases characterised by aberrant cell proliferation and invasion of other tissues that can lead to the disruption of normal body functions. More than 18 million patients were diagnosed with cancer in 2018 and it is the second-leading cause of mortality in the world after heart disease [2]. Cancer is caused by the accumulation of genetic mutations in the cell that lead to the activation of oncogenes or inactivation of tumour suppressor or DNA repair genes [3]. Despite their genetic complexity, most cancers share common traits defined as the hallmarks of cancer by Hanahan and Weinberg (see Table 1.1) [3,4].

Table 1.1. Hallmarks of cancer [3,4].

1	Self-sufficiency in growth signals
2	Insensitivity to anti-growth signals
3	Evading apoptosis
4	Limitless replicative potential
5	Sustained angiogenesis
6	Tissue invasion and metastases
7	Abnormal metabolic pathways
8	Evading the immune system

Risk factors for cancer include genetic predisposition, certain infections and/or lifestyle factors, including obesity, lack of exercise, malnutrition, smoking and alcohol use [5]. Extensive research into cancer has led to the development of many different classes of anti-cancer agents, including chemo-, hormone, targeted and immune therapies [6]. The success of these differs between the type of cancer, stage of the disease and individual patients, and personalised medicine aims to match the unique tumour biology of each patient to tailored treatment regimens [7]. This process has accelerated the development of targeted therapies, which inhibit specific molecular targets that are involved in the development or spread of the cancer. These targets include modulators of cell signalling, gene expression, apoptosis or angiogenesis [3]. One important group of proteins involved in cell signalling are kinases, which connect extracellular signals with intracellular signalling pathways [8].

Role of kinases in cancer

Kinases are proteins which phosphorylate other biomolecules in the cell by catalysing the following reaction: $MgATP^{1-}$ + *substrate*-$OH \rightarrow MgADP$ + *substrate*-OPO_3^{2-} + H^+. This transfer of the γ-phosphate of ATP onto the hydroxyl group of a substrate is one of the most common post-translational modifications and plays a critical part in many cellular and extracellular processes [9]. Eukaryotic protein kinases phosphorylate specific amino acid residues, either tyrosine, serine/threonine or both tyrosine and threonine residues of a wide range of proteins, and separate groups of kinases can phosphorylate other molecules such as sugars and lipids. There are 538 protein kinases encoded in the human genome and their actions are countered by protein phosphatases, which catalyse the dephosphorylation of their substrates [8]. Most proteins are activated by phosphorylation, with some exceptions, which makes kinases the key activators of signalling pathways in the cell.

Aberrant phosphorylation has been linked to many pathologies, including cancer, immunodeficiencies, endocrine and cardiovascular diseases [8–10]. It can be caused by increased kinase activity, decreased phosphatase activity or a combination of both. Several malignancies have been directly linked to chromosomal rearrangements or activating mutations in kinases; examples are the BCR-ABL fusion protein in chronic myeloid and lymphoblastic leukaemia, ALK rearrangements in a subset of non-small-cell lung cancers, the BRAF V600E mutation in melanoma, and mutations in FLT3, EGFR and KIT in acute leukaemia, lung and gastrointestinal tumours [8,10]. Furthermore, amplification of kinase genes or their overexpression can lead to tumour development, as can hyperactivation of these kinases through phosphorylation (e.g. EGFR or MET in non-small-cell lung cancer; HER2 in breast, ovarian, oesophageal and gastric cancer; AKT2 in pancreatic, ovarian and breast cancers; ERK in breast cancer). Kinase mutations, expression levels and activation status are already being used as biomarkers in diagnosis and prognosis and to stratify treatment options [11]. More than 240 kinase inhibitors have been evaluated in the clinic and many have received regulatory approval for use in cancer and other diseases, comprising both small molecule drugs (currently 55 compounds FDA approved) and biologicals such as antibodies [12]. Intensive research into the development of novel kinase inhibitors continues, as the current collection targets less than half of the human kinome and many small molecule inhibitors are highly promiscuous or liable to the development of resistance mechanisms in patients.

1.2. SRC kinase

1.2.1. Discovery of SRC kinase

SRC kinase has been closely linked to cancer since its discovery more than a century ago [13,14]. In 1911, Peyton Rous showed that injecting a healthy chicken with the cell-free filtrate of a chicken sarcoma led to the development of the same tumour [15]. His hypothesis, that these sarcomas are caused by a tumour-secreted “ultramicroscopic organism”, went largely unacknowledged due to the prevalent assumption that cancers are non-infectious and of endogenous origin. It was not until 1955 that the Rous sarcoma virus (RSV) was identified in pock assays as the cancer-causing agent and studies in the following years confirmed it could trigger cancer in mammals [16–18]. Rous received the Nobel prize for his original discovery in 1966 [19]. Three years later Huebner and Todaro first proposed the existence of a transforming “oncogene” in RSV, which led to the identification of the *v-Src* gene [20]. Hybridisation studies with a DNA probe complementary to *v-Src* revealed that it was also present in the cellular genome and had probably been captured and repurposed by viruses [21]. Since the cellular homologue, called *c-Src*, did not have the same transforming ability as *v-Src*, it was classified as a “proto-oncogene” and a second Nobel Prize linked to SRC was awarded for this discovery in 1989 [22,23].

Further studies of SRC largely focussed on the protein, which was first isolated in 1977 [24]. Two independent groups revealed the kinase activity of SRC a year later, with much higher activity observed for v-Src than c-Src [25,26]. The serendipitous use of an aged buffer in 1980 then revealed that SRC can phosphorylate tyrosine residues on other proteins as well as on itself; the phosphorylated residue of v-Src was identified to be tyrosine 416 [27]. c-Src was phosphorylated at the same residue *in vitro* but a different one *in vivo*, later identified as tyrosine 527 in the C-terminus, which is missing in v-Src [28,29]. An important study showed that c-Src can be activated by dephosphorylation of tyrosine 527, which led to the understanding that phosphorylation of tyrosine 416 or 527 results in SRC activation or inhibition, respectively [30]. It emerged that SRC is predominantly inactive in non-transformed cells due to phosphorylation of its C-terminus but can be activated by phosphatases as part of normal cellular processes or aberrantly in cancer.

1.2.2. Structure and regulation of SRC kinase

SRC is a non-receptor tyrosine kinase and the prototype of an eleven-member family of kinases named SRC family kinases (SFKs) [31]. SFKs are further divided into subfamilies based on their sequence similarity, forming the SRC-like subfamily (SRC, YES, FYN, FGR), the LYN-like subfamily (LYN, HCK, LCK, BLK) and a third more distantly related subfamily containing FRK, BRK and SRM.

Not all SFKs are expressed ubiquitously in all cell types and their specific roles are summarised in Table 1.2. While SRC is expressed in all tissues, its levels are especially high in osteoclasts, platelets and neurons [32].

Table 1.2. Main tissues of expression of SRC family kinases [31].

SFK	Subfamily	Tissue
SRC	SRC-related	Ubiquitous
YES		Ubiquitous
FYN		Ubiquitous
FGR		Haematopoietic (Myeloid cells, B-cells)
LYN	LYN-related	Haematopoietic (Myeloid cells, B-cells)
HCK		Haematopoietic (Myeloid cells)
LCK		Haematopoietic (T-cells)
BLK		Haematopoietic (B-cells)
FRK	SFK-related	Bladder, brain, breast, colon, lymphoid
BRK		Colon, prostate, small intestine, (breast)
SRM		Keratinocytes

SRC-like and LYN-like SFKs share a conserved structure which consists of (from N- to C-terminus): a myristoylated membrane-targeting region in the N-terminus, a unique domain, a SH3 domain, a SH2 domain, a linker domain, the SH1 protein-tyrosine kinase domain, and a short regulatory C-terminus (see Figure 1.1a) [33]. The SH2 and SH3 domains are important for protein-protein interactions, while the SH1 domain contains the active site of the kinase. The SFK-like kinases of the third subfamily differ from the other two as they lack the myristoyl group and C-terminus but they still contain all three SH domains. The human SRC, chicken c-Src and viral v-Src proteins have different lengths of 536, 533 and 527 amino acids, respectively,

and this thesis will use the established chicken c-Src numbering throughout for consistency [31]. Figure 1.1a shows the species-dependent numbering of important residues. While chicken Src and human SRC are nearly identical, v-Src lacks seven residues in its C-terminus, including the important autoinhibition residue tyrosine 527.

SRC kinase activity is regulated by phosphorylation of two important residues: the autoinhibition site at tyrosine 527 in the C-terminus and the autophosphorylation site at tyrosine 416 in the activation loop of the kinase domain [33]. The carboxyterminal tyrosine can be phosphorylated by C-terminal SRC kinase (CSK) or CHK (CSK homologous kinase). This inactivates SRC by promoting its assembly into a closed, autoinhibited conformation in which the phosphorylated C-terminus binds the SH2 domain (see Figure 1.1b). Further interactions between the SH3 domain, linker region and kinase domain help maintain this state. SRC can be activated by dephosphorylation of tyrosine 527 by phosphatases such as SHP-1, PTP-α and PTP1B or by interactions with high-affinity proteins that bind the SH2 or SH3 domain, such as growth factor receptors [34]. While phosphorylation of tyrosine 416 by another SRC molecule has been thought to activate SRC as well, is has recently been shown that SRC can exist in a double phosphorylated state, suggesting that tyrosine 416 phosphorylation on its own is not enough to induce an open conformation [35]. The lack of the regulatory C-terminus is the reason for v-Src's oncogenic activity [34].
In its open and active state, intramolecular phosphorylation of tyrosine 416 is required for full kinase activity, as it stabilises the activation loop in a conformation that facilitates substrate binding [31]. In its activated state, SRC can phosphorylate tyrosine residues on many different substrates and it is involved in signalling via growth factor receptors, integrins, G-protein coupled receptors, T-cell and B-cell receptors, steroid hormone receptors, cytokine receptors and NMDA receptors [36]. Some of these interactions, such as SRC's role in cell migration due to its activation of focal adhesion kinase (FAK), have been characterised extensively and are explained in more detail in chapter 1.2.3.

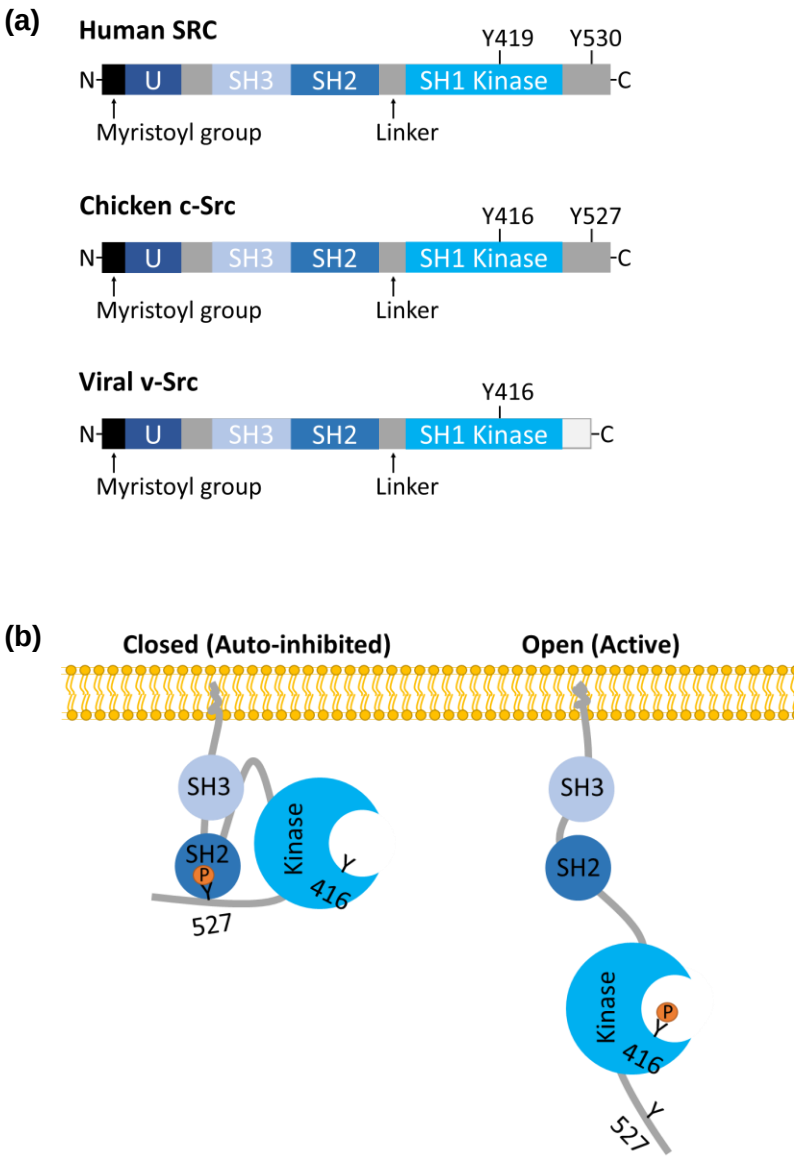

Figure 1.1. Structure and activation of SRC kinase. a) Structure of human, chicken and viral SRC showing the conserved SRC homology domains (SH1, SH2, SH3), the linker domain, the unique domain (U), the myristoyl group and key tyrosine phosphorylation sites. b) Conformation of inhibited and active SRC kinase: SRC is inactivated by phosphorylation of tyrosine 527, which results in binding of the C-terminus to the SH2 domain. Dephosphorylation of the C-terminus and autophosphorylation of tyrosine 416 activates SRC.

1.2.3. Functions of SRC kinase

SRC family kinases interact with and phosphorylate many different substrates in the cell [37]. Their role is often context-dependent and can differ between cell types and extracellular stimuli. The most prominent roles of SRC are its involvement in the transduction of growth factor signalling via receptor tyrosine kinases as well as cell migration and invasion. However, may other functions of SRC have been discovered and the following will give an overview of the key areas.

1.2.3.1. Cell adhesion, migration and invasion

SRC plays an important role in the adhesion of cells to the extracellular matrix (ECM) as well as other cells, thus controlling cell polarity, tissue integrity and cell migration.

Cell-ECM contacts through focal adhesions

Cells adhere to the extracellular matrix through dynamic macromolecular assemblies called focal adhesions. The central component of focal adhesions are heterodimeric transmembrane proteins called integrins, which connect the actin cytoskeleton to the substratum, thereby allowing the transmission of mechanical force and biochemical signals [37]. Integrins do not possess intrinsic catalytic activity but aggregate upon ligand binding, which allows intracellular proteins to bind. Focal adhesion kinase (FAK) plays a key role in integrin-mediated signal transduction and localises to integrin clusters via interactions between its C-terminal domain and the β1 integrin cytoplasmic domain [38]. This triggers its autophosphorylation on tyrosine 397, which enables transient binding of SRC kinase via its SH2 domain or interaction with other proteins such as phosphatidylinositol 3-kinase (PI3K) or phospholipase Cγ [39]. SRC, in turn, phosphorylates FAK on several tyrosine residues (576, 577, 861, 925) which form binding sites for other focal adhesion proteins, such as GRB2, leading to the formation of a multiprotein complex tethered to the actin cytoskeleton (see Figure 1.2 and Figure 1.3) [40].

The exact dynamics of focal adhesions as still not fully understood due to their complexity and the involvement of over 50 proteins [37]. The dynamic formation and turnover of focal adhesions is essential for cell migration, as new protrusions form at the leading edge while the trailing edge detaches from the substratum [41]. Phosphorylation of p130Cas by the active SRC-FAK complex can stimulate Rac1 activity, leading to actin polymerisation at the cell periphery and the formation of

membrane protrusions [42]. SRC also appears to be essential for the disassembly of focal adhesions, for example through its phosphorylation of integrin cytoplasmic domains, enhancement of the proteolytic cleavage of FAK by calpains and activation of the RhoA antagonist p190 RhoGAP, which disrupts the actin cytoskeleton [39,41–43]. Cell migration beyond matrix barriers (e.g. the basement membrane) leads to invasion of other tissues, which is often seen in cancer, and SRC contributes to this phenotype by promoting the expression of matrix degrading proteins, such as matrix metalloproteinases [44,45]. Taken together, SRC kinase plays a central role in the dynamic regulation of focal adhesions, actin remodelling and ECM degradation, which is necessary for cell migration and invasion.

Cell-cell contacts through adherens junctions

SRC kinase is also involved in the assembly and disassembly of cell-cell interactions called adherens junctions (AJs). These contacts are important in the integration of individual cells into tissues, epithelial cell polarity and the suppression of tumour invasion [39].

AJs are organised similar to focal adhesions and connect the actin cytoskeleton of neighbouring cells. The transmembrane proteins of AJs are calcium-dependent cadherin receptors; E-cadherin is the prototype cadherin that is ubiquitously expressed in epithelial cells, while VE-cadherin is commonly found in endothelial tissues. Cadherins form homodimers which bind other cadherin molecules on neighbouring cells via their extracellular domains, while their intracellular tails connect to actin filaments through adaptor proteins such as α-, β-, and p120-catenin, plakoglobin, actinin and vinculin [37]. SRC kinase can associate with this complex and phosphorylate p120-catenin, β-catenin or its homologue plakoglobin, and to a lesser degree E-cadherin; this has been linked to AJ turnover and E-cadherin internalisation via endocytosis and hyperactive SRC was found to decrease cell-cell adhesion [39,46,47]. In contrast, lower levels of SRC activity have been shown to support cadherin function and SRC deletion or inactivation is associated with the lack of AJ formation and turnover [39,48]. SRC therefore appears to be important in both the assembly and disassembly of AJs, with differing roles depending on its level of activation.

Due to the role of SRC in the turnover of both cell-cell and cell-ECM adhesions, as well as matrix degradation, its activity has been linked to a biological process called epithelial-to-mesenchymal transition (EMT) [49–51]. EMT is associated with normal

development and wound healing but also cancer invasion; it causes epithelial cells to lose their polarity and adhesion to neighbouring cells, as they acquire an invasive mesenchymal phenotype that is resistant to senescence or apoptosis.

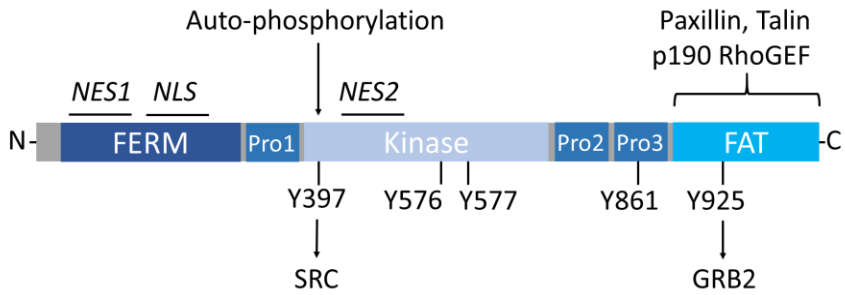

Figure 1.2. FAK structure and phosphorylation sites. Focal adhesion kinase protein contains a FERM (protein 4.1, ezrin, radixin and moesin homology), kinase and FAT (focal adhesion targeting) domain. There are three proline-rich domains (Pro1-3) which can bind SH3 sites. The FERM and kinase domains contain two NES (nuclear export sequence) and one NLS (nuclear localisation sequence). Integrin clusters trigger autophosphorylation of tyrosine 397 which forms a binding site for SH2 domain containing proteins, such as SRC, p85 subunit of PI3K, PLCγ and others. SRC phosphorylates other tyrosine residues on FAK (576, 577, 861, 925) which enables FAK to bind GRB2 and interact with other focal adhesion proteins.

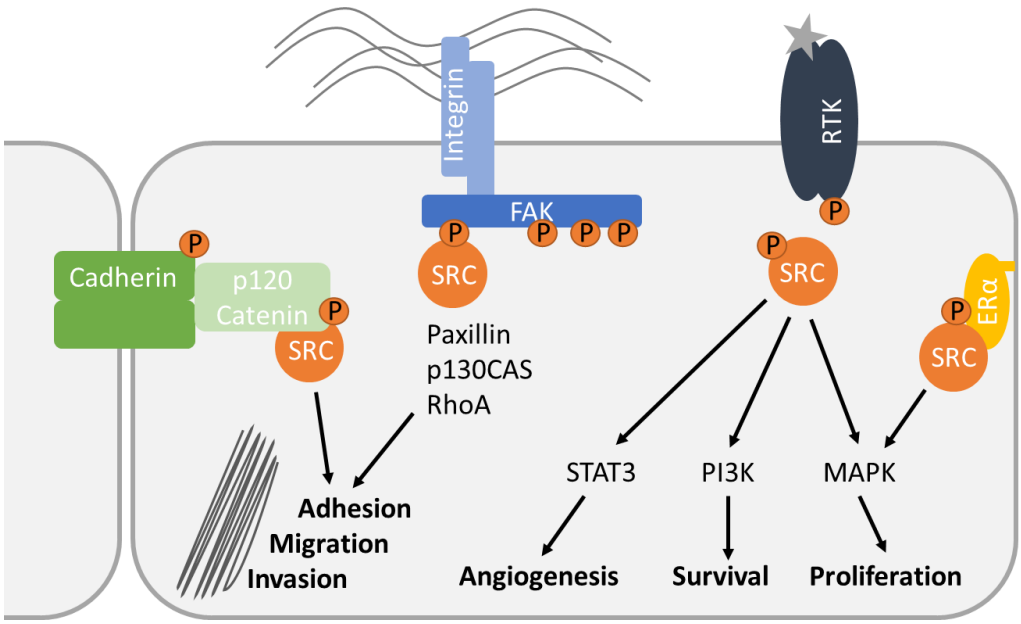

Figure 1.3. SRC signalling pathways. SRC kinase is located downstream of adherens junctions, focal adhesions, receptor tyrosine kinases, steroid receptors and other signalling pathways. Context-dependent SRC activation leads to substrate phosphorylation and promotes cell motility, invasion, angiogenesis, cell survival and proliferation.

1.2.3.2. Cell proliferation and survival

SRC kinase plays a key role in the transduction of pro-survival and proliferation signals across the cell membrane through its interactions with receptor tyrosine kinases, G-protein coupled receptors, and steroid hormone receptors [36]. Some of these interactions lead to the activation of downstream signalling pathways that facilitate cell cycle progression from G1 to S phase [52].

Receptor tyrosine kinases

SRC kinase is involved in the mitogenic signalling of several receptor tyrosine kinases (RTKs); these include the platelet-derived growth factor receptor (PDGFR), epidermal growth factor receptor (EGFR), human epidermal growth factor receptor 2 (HER2), fibroblast growth factor receptor (FGFR), insulin-like growth factor receptor (IGFR), hepatocyte growth factor receptor (HGFR/c-Met), colony-stimulating factor receptor (CSFR) and several others [53,54].

RTKs contain an extracellular N-terminal ligand-binding domain, a hydrophobic transmembrane domain and a highly conserved intracellular C-terminal domain with catalytic kinase activity. Binding of a ligand (e.g. growth factors, cytokines or hormones) usually triggers receptor dimerization, which leads to trans-phosphorylation of residues within their carboxyterminal domain by the other receptor and results in receptor activation [55]. This creates binding sites for other substrates, such as SRC, which binds RTKs via its SH2 domain and subsequently becomes activated by phosphorylation [53]. SRC can then signal via different pathways, depending on the RTK, resulting in specific gene expression changes. For example, activation of the MAPK pathway (SHC-GRB2-RAS-RAF-MEK1/2-ERK1/2) increases cell proliferation, while signalling via the PI3K-AKT-IKK-NFkB pathway promotes cell survival (see Figure 1.3) [56]. Other molecules involved in SRC downstream signalling are STAT3 and protein kinase C (PKC) [45,53,57]. SRC is also involved in the RTK-induced remodelling of the actin cytoskeleton, for example in the EGF-stimulated phosphorylation of p190 RhoGAP. In addition to relaying RTK signalling, studies have found that SRC activity can also modulate RTK turnover by affecting endocytosis and ubiquitination of these receptors [53].

G-protein coupled receptors

G-protein coupled receptors (GPCRs) are transmembrane proteins which, upon ligand-binding, exchange GDP for GTP in their associated G proteins; this triggers the dissociation of G proteins into GTP-Gα and Gβγ subunits, which then regulate enzymes or ion channels that generate second messengers [58]. These enzymes and second messengers can be involved in cell proliferation and differentiation but do not traditionally signal through tyrosine kinases. However, studies found that SRC family kinases can bind some GPCRs, either directly (e.g. β2 and β3-adrenergic receptor) or via β-arrestins [59]. Further, GPCRs can activate SFKs directly via the Gα subunit or via crosstalk with RTKs or focal adhesions, and SFKs in turn were shown to regulate Gα activity by phosphorylation [58,59]. SFKs can also mediate the internalisation of some GPCRs (e.g. M1 muscarinic receptors) [58]. In general, GPCR signalling has been shown to include the activation of SFKs, either directly or indirectly, expanding the role of SFKs as transductors of extracellular signalling beyond RTKs.

Steroid hormone receptors

Nuclear steroid hormone receptors are typically characterised as ligand-activated transcription factors that directly bind the DNA. While they are not traditionally associated with kinases, studies found that these receptors can also trigger rapid signalling outside the nucleus, some of it mediated via tyrosine kinases, and that SRC can affect receptor function [60–62].

One study showed that SRC can phosphorylate oestrogen receptor alpha (ERα) on tyrosine 537, which increased binding affinity for the ligand estradiol and triggers cytoplasmic localisation that promotes cell cycle progression; another one discovered that SRC promotes oestrogen-induced ERα proteolysis [63,64]. Estradiol treatment also induced rapid phosphorylation events in MCF-7 cells that could be blocked by a SRC inhibitor [61]. SRC was further found to mediate ligand-independent transcriptional activation of the androgen receptor (AR) and potentiate its activation [65–67].

ERα can be palmitoylated and localised to the plasma membrane where it can signal through multiple proteins including SRC (see Figure 1.3) [68]. Similarly, the AR and progesterone receptor (PrR) were also found at the cell membrane where their signalling via SRC kinase regulates cell proliferation [60]. It is thought that nuclear steroid receptors located at the membrane interact with caveolin-1, which facilitates the activation of signalling pathways [60].

Cell Cycle Progression

One of the effects of oncogenic SRC is anchorage- and growth factor-independent cell proliferation, which is mediated through its effects on the cyclin-dependent kinase (CDK) inhibitor p27 in the cell cycle [69,70].

The cell cycle consists of four distinct stages that lead to cell division (gap 1, synthesis, gap 2, mitosis) and a fifth resting phase (gap 0). During gap 1 (G1), the cell increases in size and activates control mechanisms (G1 checkpoint) that ensure it is ready for DNA synthesis. This is followed by the synthesis (S) phase, during which the cell duplicates its genome. The gap 2 (G2) phase allows further growth and contains the G2 checkpoint that determines whether the cell is ready for division. During the final mitosis (M) phase, the cell divides into two under control of the metaphase checkpoint, after which the daughter cells may either re-enter the cell cycle to divide again or enter the gap 0 (G0) resting phase.

Transition of cells from G1 to S phase involves the binding of cyclin D to CDK4 or CDK6, which leads to hyperphosphorylation of the Rb protein and causes it to dissociate from the transcription factor E2F (Figure 1.4) [52]. Unbound E2F can then activate gene expression, including that of cyclin E and cyclin A, and ensuing binding of CDK2 to cyclin E triggers S phase entry. SRC can directly phosphorylate p27, an inhibitor of cyclin E-CDK2, at tyrosine 74 and 88 [71]. SRC overexpression reduced p27's binding and inhibition of cyclin E-CDK2 and lead to its proteolysis, which facilitates G1 to S transition. The use of pharmacological SRC inhibitors was able to stabilise p27, inhibit cyclin E-CDK2, downregulate cyclin D1 and induce G1 cell cycle arrest [52,71]. Both SRC siRNA and ERK1/2 or AKT inhibition reduced the expression of cyclin D and cyclin E and increased p27, which shows that SRC downstream signalling also promotes cell cycle progression. Overexpression of EGFR or HER2 amplification in breast cancer is known to induce p27 proteolysis, which highlights the central role of SRC in driving oncogenic transformation through RTK signalling [71].

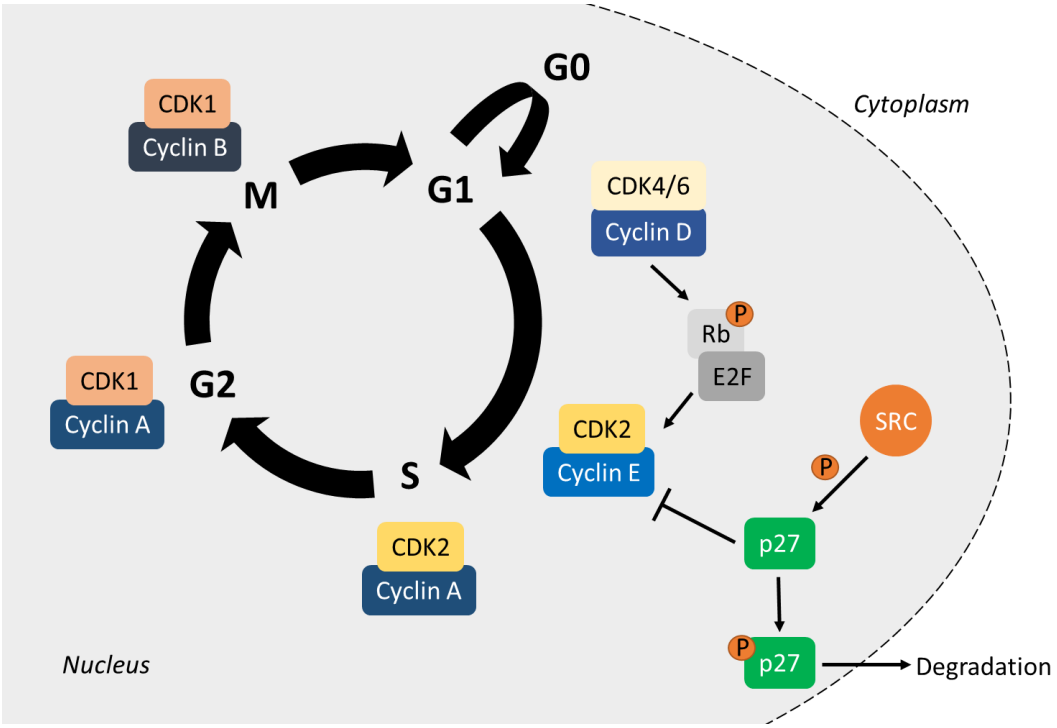

Figure 1.4. Role of SRC kinase in the cell cycle. p27 inhibits transition from G1 to S phase by interacting with CDK2 and Cyclin E in the nucleus. Phosphorylation of p27 by SRC triggers its cytoplasmic translocation and degradation, allowing the cell to enter S phase.

1.2.3.3. Cell metabolism

A less well-known role of SFKs in the cell is their involvement in the mitochondrial energy production by oxidative phosphorylation and the Warburg effect in cancer. Several mitochondrial proteins are phosphorylated by SRC which results in positive modulation of the oxidative phosphorylation machinery (e.g. mitochondrial cytochrome C oxidase, adenine nucleotide translocase 1) and evasion of hypoxia-induced apoptosis via Hif1α-SRC-NFkB signalling [72–74]. SRC-mediated phosphorylation also appears to play a role in the switch of malignant cells from oxidative phosphorylation to anaerobic glycolysis, as it attenuates pyruvate dehydrogenase activity while activating the rate-limiting glycolysis enzymes HK1 and HK2 [75,76]. SRC-stimulated ATP production also facilitates activation of mTORC1 and PRC2 in a model of HER2 positive breast cancer [77].

1.2.3.4. Angiogenesis

Angiogenesis, the formation of new blood vessels from existing ones, is an important physiological process in development and wound healing but also involved in cancer [3]. Multiple steps are involved in angiogenesis, including the local breakdown of the basement membrane followed by the migration and proliferation of endothelial cells [78]. Several molecules are known to stimulate angiogenesis, in particular growth factors (e.g. FGF, VEGF), their receptors (e.g. VEGFR) and proteases (e.g. matrix metalloproteinases) [3,78]. Particular attention has been paid to the role of VEGF, and several inhibitors of this growth factor or its receptors (VEGFR1-3) have been approved for use in cancer and degenerative eye diseases (antibodies: bevacizumab, aflibercept, ramucirumab; small molecule inhibitors: axitinib, cabozantinib, lenvatinib, pazopanib, regorafenib, sunitinib, sorafenib, vandetanib) [79,80]. SFKs are involved in the downstream signalling of growth factor receptors such as VEGFR and required for VEGF-induced endothelial cell proliferation, migration, tube formation and vascular permeability [81,82]. Reduced migration of SRC-inhibited endothelial and vascular smooth muscle cells has been linked to its role in the organisation of the actin cytoskeleton [83]. Moreover, SRC activation can increase VEGF expression through activation of STAT3 signalling [57,84]. Other studies have shown that targeting FAK can also inhibit angiogenesis by disrupting the SRC-FAK-Rho GTPase signalling pathway [85–88]. Taken together, SFKs play an important role in angiogenesis by mediating growth factor signalling in endothelial cells and enabling cell migration.

1.2.3.5. Bone resorption

The remodelling and integrity of bones is governed by a carefully controlled balance between bone formation by osteoblasts and resorption by osteoclasts. The major phenotype of SRC knockout mice is osteopetrosis, an accumulation of excess bone due to impaired osteoclast function [32]. Indeed, SRC is highly expressed in osteoclasts and essential for their ability to resorb bone; specifically, it is involved in their ability to form ruffled borders and maintain high levels of ATP through phosphorylation of mitochondrial cytochrome C oxidase [72,89,90]. SRC activity has also been linked to the formation of bone metastases, which is a primary metastatic site for breast and prostate cancer but also a frequent site for thyroid, lung and bladder cancer [91–94]. Inhibitors of SRC kinase are therefore being investigated both for their ability to reduce the occurrence of metastatic bone disease and associated pain [95–98].

1.2.3.6. Immune system and platelets

SFKs are involved in the functioning of the immune system through their roles in T-cells, B-cells, platelets and cytokine signalling [36].

T-cells

LCK is expressed and active in T-cells where it is involved in the signal transduction of T cell receptors (TCRs) that is necessary for effector T-cell activation [99]. TCRs respond to pathogen or tumour-derived antigenic peptides presented by antigen presenting cells (e.g. macrophages, dendritic cells, B-cells) via the major histocompatibility complex (MHC). Upon binding of TCR to MHC, CD4 or CD8 are recruited and trigger TCR phosphorylation by LCK [99]. LCK then recruits and phosphorylates ZAP70 via its SH2 domain and binds the ZAP70 substrate LAP via its SH3 domain, allowing LAP activation and signalling via multiple downstream pathways (e.g. GRB2, PI3K, PLC) [100,101]. Some activated LCK also translocates inside lipid rafts where it activates FYN and further downstream signalling leading to changes in gene transcription [102]. Taken together, LCK and FYN activity is necessary for the formation of both helper and cytotoxic T-cells by inducing cell differentiation, proliferation and cytokine secretion [103].

The SFK target FAK was found to negatively regulate TCR-mediated signalling in CD4 T-cells, as FAK knockdown resulted in lower levels of LCK inhibition [104]. The paper suggests that FAK expression is necessary to recruit CSK to the membrane, which phosphorylates the autoinhibition site on LCK and thus hinders its activation. However, a second study that utilised the FAK inhibitor PF562271 found that pharmacological inhibition impairs CD4 T-cell activation; while these results may be due to off-target effects, it shows the challenges of defining FAK's role in T-cells [105].

B-cells

SFKs can have both activating and inhibitory effects on B-cells which are involved in antibody-mediated immune responses [106]. Multiple SFKs (LYN, BLK, FYN, FGR, YES) are expressed in B-cells and LYN in particular is involved in signalling via the B-cell receptor and downstream activation of SYK. LYN-deficient mice exhibited fewer mature B-cells but also a lower threshold for B-cell activation and autoreactive antibodies [107], while continuously active LYN similarly reduced the number of peripheral B-cells and induced autoimmunity [108]. This suggests that LYN is important in balancing B-cell activity rather than switching it on or off [109].

Macrophages

SFKs in macrophages appear to act as rheostats that modulate the activity of signalling pathways, rather than having a specific function [110]. They can affect signal transduction by phosphorylating two motifs that are found in several receptors or their associated signalling molecules: the immunoreceptor tyrosine-based activation motif (ITAM) and the immunoreceptor tyrosine-based inhibitory motif (ITIM). ITAMs can be found for example in DAP12 and FcRγ, which associate with integrins, and their phosphorylation by SFKs leads to the recruitment of SYK kinase and downstream phosphorylation events [111]. ITIMs are often contained in the receptors themselves, such as in the IL-4 alpha chain, and their phosphorylation leads to the recruitment of phosphatases that inhibit downstream signalling [110].

Another role of SFKs in macrophages may be in Toll-like receptor (TLR) signalling, as HCK and LYN were found to be activated by the TLR4 ligand lipopolysaccharide (LPS); TLR4 was in turn phosphorylated in an SFK-dependent manner, which attenuates the inflammatory response to LPS [112,113]. However, SFK knockout macrophages showed no significant defects in the LPS response and the importance of SFKs in TLR signalling in macrophages currently remains unclear [110].

Neutrophils

Several studies found that SFKs play a role in the ability of neutrophils to generate an inflammatory environment. The inhibition of SFKs or SYK was found to hinder inflammatory cytokine production by neutrophils by reducing the phosphorylation of proteins involved in the control of translation [114]. Further, $Hck^{-/-}$, $Fgr^{-/-}$, $Lyn^{-/-}$ knockout mice were protected from inflammatory responses, not because of changes in neutrophil migratory ability, but due to their failure to release pro-inflammatory mediators in response to immune complexes [115]. Neutrophils have several receptors containing ITAMs and ITIMs, like macrophages, and SFKs were found to phosphorylate the ITAM-containing FcRγ chain of the activating Fc receptor, with $FcR\gamma^{-/-}$ mice showing a similar immune phenotype as the $Hck^{-/-}$, $Fgr^{-/-}$, $Lyn^{-/-}$ mice [115].

Dendritic cells

Dendritic cells process antigens and subsequently present them on their cell surface to the immune system. Two studies found that SRC may play a role in TIM-3 mediated dendritic cell suppression and that its inhibition can improve the anti-tumour effects of DNA vaccines [116,117].

Cytokine receptors

Cytokine receptors have no intrinsic enzymatic activity and rely on kinases for the signal transduction of extracellular cytokine signals. Type I and II receptors (e.g. interleukin, growth hormone, prolactin and interferon receptors) signal via the JAK-STAT pathway to change gene expression [118]. However, some studies have found that the growth hormone receptor can also signal via LYN kinase, independent of JAK, and that SRC can regulate JAK signalling in the prolactin receptor in a kinase-independent manner [119,120]. SFKs are activated by pro-inflammatory cytokines in both inflammation and cancer and have been proposed as a mechanistic link between both diseases [121]. Furthermore, SFKs can activate STAT signalling independent of JAK, for example through growth factor receptors, although this only includes a subset of the STAT molecules that can be activated by cytokines [122].

Platelets

SFKs are highly expressed in platelets and play a pivotal role in platelet activation in response to injury [123]. They are involved in the signal transduction of various tyrosine kinase-linked receptors (e.g. α2β1 integrin, collagen receptor, von Willebrand factor receptor) and GPCRs (e.g. PAR-4 thrombin receptor) which enable platelet adhesion and thrombus formation. SFK inhibitors have been shown to induce bleeding and thrombocytopenia in patients and reduce platelet count and reactivity *in vivo*, suggesting an important role for SRC in platelet-producing megakaryocytes [124–127].

1.2.3.7. Central nervous system

Several SFKs (SRC, FYN, YES, LCK, LYN) are highly expressed in neurons, which was a surprising finding as these are differentiated cells that no longer proliferate [128]. It was discovered that the role of SFKs in the CNS is to upregulate the activity of ion channels, including ionotropic glutamate receptors (e.g. *N*-methyl-D-aspartate receptor, NMDAR), voltage-gated ion channels (e.g. potassium, calcium) and ionotropic neurotransmitter receptors (e.g. $GABA_A$, nicotinic acetylcholine receptor). Studies of the NMDAR revealed that SRC phosphorylates the carboxyterminal of NR2 subunits which potentiates NMDAR currents by increasing channel gating and might reduce internalisation of the receptor [129]. Its actions are opposed by STEP phosphatase [128]. SFKs signalling has been implicated in neurodegenerative diseases such as Alzheimer's, which is discussed in more detail in chapter 1.2.4.4.

1.2.3.8. Kinase-independent scaffolding roles

Most actions of SFKs are mediated via their kinase activity, which allows them to phosphorylate other proteins and activate cell signalling pathways. However, their SH2 and SH3 domains also enable them to bind other proteins and act as an adapter protein [33]. Several studies have tried to distinguish between SRC's kinase and scaffolding activity by using kinase-defective SRC K295M, which is mutated in the ATP binding site [130]. They found that the osteopetrosis phenotype observed in SRC knockout mice (see chapter 1.2.3.5) was partially rescued by re-expression of kinase-defective SRC by improving cytoskeletal organisation in osteoclasts [131]. Further evidence for its scaffolding role in the cytoskeleton comes from the observation that reduced cell spreading of SRC -/- fibroblasts on fibronectin could be rescued by SRC K295M, which exhibited similar distribution to focal adhesions during attachment as wild-type SRC [132]. Kinase-defective SRC was found to mediate FAK-dependent phosphorylation of p130Cas and downstream ERK activation in fibroblasts by binding FAK and p130Cas via its SH2 and SH3 domains, respectively [133]. Activation of p130Cas through SRC's adapter function alone also occurs in cardiomyocytes during pressure overload [134]. The phosphorylation of several SRC-linked tyrosine residues on FAK in colorectal cancer cells was also found to be independent of SRC kinase activity but dependent on its SH2 domain, although other papers reported opposite findings [135,136]. In the same cells, kinase-defective SRC was able to induce the formation of cell-matrix adhesions but not the disruption of adherens junctions [47].
Moreover, the SH2 and SH3 domains are necessary to mediate signalling of the prolactin receptor via JAK2-STAT5 in kinase-defective SRC, and kinase-defective LYN was able to reverse the increase of B-cell receptor-dependent PLC activation observed with LYN knockout back to wild-type levels [119,137]. LCK-mediated TCR activity was reduced by mutations in either the kinase and SH2 domain, but only fully ablated when both were mutated, although another study found that Y394 phosphorylation is essential for TCR function [138,139]. These examples highlight potential roles for SFKs beyond their kinase activity through their SH2 and SH3 domains.

1.2.4. The role of SRC kinase in cancer and disease

1.2.4.1. SRC and the hallmarks of cancer

SRC is a critical component of various signalling pathways, cellular processes and physiological functions and was the first proto-oncogene to be discovered. It is closely linked to several of the eight hallmarks of cancer (see Table 1.1), as its activity can stimulate cell proliferation and survival (chapter 1.2.3.2), angiogenesis (chapter 1.2.3.4), cell migration, invasion and metastasis (chapter 1.2.3.1 and 1.2.3.5), and mitochondrial ATP production and glycolysis (chapter 1.2.3.3).

Due to its role as a central signalling node for many receptors and cell types, SRC activation can have multiple interconnected outcomes that promote cancer progression. For example, signalling through growth factor receptors traditionally involved in mitogenic signalling can also induce EMT and promote an invasive phenotype [49–51]. Furthermore, SRC activity in endothelial cells plays a dual-role in tumour progression; it stimulates angiogenesis in the absence of nutrients and oxygen, allowing tumours to grow beyond 1-2 mm^2 in size, and increases vascular permeability that enables the dissemination of cancer cells across the body [81,140,141]. SRC activity is also at the centre of a vicious cycle in the development of latent bone metastasis. Cancer cells release osteolytic factors and disrupt the RANK-RANKL loop between osteoclasts and osteoblasts, while the metastatic bone microenvironment releases factors (e.g. CXCL12, TRAIL) that lead to SRC-mediated activation of survival pathways and evasion of apoptosis [92,142,143].

1.2.4.2. SRC expression and activity in cancer

Increased SRC expression or activity has been found in several different solid tumours. Early studies showed SRC activity and/or expression was upregulated in a subset of sarcomas, breast and colorectal cancers compared to normal tissues [144–148]. Aberrant SRC activity or overexpression was later also identified in several other tumours, including prostate, lung, pancreatic, head and neck and ovarian cancer [149–153]. It was also increased in hepatocellular carcinoma, which correlated with reduced expression of the SRC inactivator CSK [154,155]. HER2 amplification in breast cancer was found to increase SRC levels by enhancing both its translation and stability [156].

Increased SRC activation or expression in cancer is generally associated with later stages of the disease, metastatic potential and poor clinical prognosis [157–161].

A recent study found that aberrant SRC signalling is a key hallmark of Group 4 medulloblastoma, which is the most common malignant brain tumour in children [162]. It showed that genomic, epigenetic and transcriptomic data does not necessarily correlate with protein abundance and post-translational pathway activation and can miss the activation of kinase signalling pathways. An integrated multi-omics approach was able to identify the distinct activation of ErbB4 and SRC signalling in a defined subgroup of medulloblastoma, which could lead to future applications for SRC and RTK inhibitors in this disease.

1.2.4.3. SRC in treatment resistance

SRC activity is frequently upregulated in cancers after treatment with chemo-, hormone or targeted therapies and can contribute to resistance by activating alternative signalling or survival pathways [54]. It has been proposed to combine these drugs with SRC kinase inhibitors to delay or overcome resistance and many studies reported positive results in *in vitro* and *in vivo* resistance and combination studies.
Examples of resistance to chemotherapy include the SRC-mediated activation of EGFR signalling by cisplatin and 5-fluorouracil in breast and pancreatic cancer cell lines, respectively [163,164]. Cisplatin resistance was also linked to SRC-mediated downregulation of cell-cell communication via gap junctions [165]. SRC is known to be overexpressed and activated with HER2 amplification and this contributes to breast cancer resistance to paclitaxel [156,166]. Inhibition of SRC kinase, either by siRNA or small molecule inhibitors, was further found to re-sensitise paclitaxel-resistant breast and ovarian cancer cells and gemcitabine-resistant pancreatic cancer models [167–171]. Moreover, the SRC inhibitor dasatinib combined with doxorubicin or oxaliplatin produced synergistic effects in breast and colon carcinoma cells, respectively [172,173].
SRC activation has also been linked to hormone therapy resistance in breast and prostate cancers, which is associated with the role of SRC in hormone receptor signalling (see chapter 1.2.3.2) [54]. Resistance of breast cancer cells to the selective oestrogen modulator tamoxifen is modulated by SRC-induced signalling through EGFR-STAT5b and SRC inhibition can prevent tamoxifen-resistance *in vitro* [71,174,175]. Moreover, only hormone-refractory prostate cancer cells stopped proliferation in

response to SRC inhibition and downregulation of the SRC inhibitor CSK was found to promote resistance to anti-androgen therapy [176,177].

Aberrant activation of EGFR involving SRC has been identified in multiple resistance pathways; conversely, SRC also becomes activated in response to EGFR inhibitors (e.g. cetuximab, afatinib, gefinitib, erlotinib, osimertinib) or ALK inhibition (e.g. alectinib) and contributes to treatment resistance in NSCLC models [178–180]. It is also involved in acquired sorafenib resistance in KRAS mutant NSCLC xenografts [181]. SRC activation by HER2 in some breast cancers was also found to contribute to *de novo* and acquired resistance to the HER2 inhibitors trastuzumab and lapatinib and their combination with the SRC inhibitor saracatinib re-sensitised resistant tumours *in vitro* and *in vivo* [182,183].

There are many examples in which SRC has been involved in resistance in preclinical studies, which re-emphasises its role as a central signalling node in the cell. However, clinical trials of drug combinations with SRC inhibitors have so far failed to demonstrate sufficient additional benefit to warrant their regulatory approval in solid tumours (see chapter 1.3.2). Further studies are needed to determine whether this is due to insufficient patient stratification, lack of efficacy of current SRC inhibitors or inadequacy of SRC kinase as a drug target.

1.2.4.4. SRC family kinases in other diseases

SRC kinase activity has been linked to cancer since its discovery (see chapter 1.2.1). However, the central role of SRC in cellular signalling pathways means it has also been implicated in other diseases associated with diabetes, fibrosis, neuronal excitation and viral infections.

Diabetes-associated morbidities

SRC kinase signalling has been implicated in multiple pathways of diabetes associated morbidities. It plays an important role in the glucose-induced secretion of insulin by pancreatic β-cells and is involved in the diabetes-induced disruption of the endothelial barrier and vascular hyperpermeability[184,185]. The SRC inhibitor dasatinib was able to reduce VEGF-induced retinal vascular leakage in a mouse model and SRC might be a promising target in diabetic retinopathies [186,187]. Moreover, SRC is involved in diabetic nephropathy as it activates EGFR signalling in the presence of

high glucose leading to collagen IV accumulation; this pathway was disrupted when streptozotocin-induced diabetic mice were treated with a SRC inhibitor [188].

Fibrosis-associated diseases

SFKs have been implicated in multiple fibrosis-associated diseases, such as idiopathic pulmonary fibrosis (IPF), chronic kidney disease, pancreatic fibrosis and liver fibrosis [189]. Myofibroblasts play an important role in wound healing and fibrosis and TGFβ1 stimulation leads to SFK-mediated differentiation of lung fibroblasts into myofibroblasts which was blocked by the SFK inhibitor saracatinib [190]. Indeed, this inhibitor has recently been granted orphan drug status by the FDA after a phase I clinical trial in IPF [191]. Multiple roles for SFKs have also been identified in chronic kidney diseases, including renal fibrosis, glomerulonephritis and nephropathies [189]. The SFK LYN plays an important role in the migration, proliferation and collagen production of chronic pancreatitis myofibroblasts and its inhibition prevented pancreatic fibrosis in a mouse model [192]. LYN is also involved in hepatic fibrosis by modulating hepatic stellate cell activation [193]. The JAK1/2 and SRC inhibitor ruxolitinib has already been approved for use in myelofibrosis and its efficacy may in part be due to its potent SFK inhibition (see Table 1.3 in chapter 1.3.1) [194].

Alzheimer's disease and other neuronal disorders

SFKs kinase upregulate the activity of the excitatory ionotropic glutamate receptor NMDAR by phosphorylation (see chapter 1.2.3.7). Excessive NMDAR activity can cause excitotoxicity which has been linked to neurodegeneration and Alzheimer's disease (AD) [195–197]. FYN is known to bind Tau, a protein closely linked to AD, and this interaction is necessary to target FYN to NMDARs and enable their phosphorylation [198]. The binding of cellular prion protein to amyloid beta oligomers is also associated with AD phenotypes; this interaction leads to the activation of FYN which then phosphorylates the NR2 subunit of NMDARs [199]. Further studies also suggest a role for SFKs in AD through their involvement in amyloid beta plaque-induced microglial activation in microgliosis [200,201]. Indeed, inhibition of FYN by saracatinib was able to reverse spatial memory deficits and synapse density loss in AD mice and reduced microglial activation [202]. However, a phase IIa clinical trial of the SFK inhibitor saracatinib in patients with mild Alzheimer's dementia has recently reported no significant changes in its primary outcome (cerebral metabolic rate for glucose) or secondary measures of cognitive assessment [203].

Dysregulated NDMAR signalling also plays a critical role in the genetic neurodegenerative disorder Huntington's disease; SFK inhibition or mutation of its target tyrosine residues on NR2B subunit was found to significantly attenuate mutant huntingtin-induced neuronal death [204]. Upregulated NMDAR signalling by SFKs has also been linked to pain hypersensitivity in neuropathic or inflammatory pain, while an NRG1-ErbB4-mediated inhibition of SRC may play a role in schizophrenia [205].

Viral infections

SFK activity can facilitate the infection, replication, assembly and release of different viruses. FYN is necessary for the assembly of dengue virus particles in the endoplasmic reticulum and FYN inhibition by dasatinib or saracatinib lead to reduced dengue virus replication, assembly and secretion [206,207]. However, prolonged treatment of dengue virus-infected cells led to viral mutations that rendered it resistant to SFK-mediated replication inhibition, although the other processes remained unaffected [207]. Similarly, SFK activity is involved in the replication of Herpes simplex virus 1, while an SFK inhibitor prevented secretion of the West Nile Virus from infected cells [208,209]. Inhibition of HCK also prevented reactivation of the cytomegalovirus *in vitro* [210]. SRC has further been implicated in the transfer of HIV-1 from dendritic cells to CD4+ T-cells and SRC inhibitors reduced infection *in vitro*; however, another study suggests SRC protects CD4+ T-cells from infection [211–213].

SFKs may be involved in virus-associated morbidities, for example in Epstein-Barr induced EMT of human corneal epithelial cells [214]. On top of that, HCK/LCK/FGR were found to downregulate the antiviral response of zebrafish and mice in a negative feedback loop [215]. This highlights the opportunity to repurpose selective SFK inhibitors in viral diseases, some of which (e.g. dengue virus) only have limited treatment options at the moment.

1.3. SRC kinase inhibitors

The role of SRC family kinases as central nodes for cell signalling pathways and their involvement in several diseases make them attractive targets for pharmaceutical manipulation. Several dual SRC/ABL kinase inhibitors are already in use clinically for the treatment of chronic myeloid leukaemia (CML). However attempts to repurpose these drugs for their SRC inhibition alone have so far failed (see chapter 1.3.2) [54]. Several studies found that ABL kinase may act as a tumour suppressor in a subset of solid tumours, and its inhibition has been linked to cardiotoxic events in CML patients (see chapter 1.3.3). Recently, the first selective small molecule SRC kinase inhibitor eCF506 has been discovered [1]. It has equally high potency as the current best-in-class SRC inhibitors and approximately 1000-fold selectivity over ABL. This thesis will investigate eCF506 further in different preclinical models of cancer.

1.3.1. Current competitive landscape

The linkage between SRC activation, disease progression and treatment resistance, as well as promising results in pre-clinical studies, all support the premise that SRC represents an important therapeutic target in cancer. Consequently, efforts have been made to develop potent and selective SRC inhibitors since the approval of the first targeted therapies in the 1990s [54,216,217]. The ABL kinase inhibitor imatinib (Gleevec®) was the first targeted tyrosine kinase inhibitor that gained FDA approval in 2001 [217]. It is used in Philadelphia chromosome-positive cancers (e.g. chronic myeloid leukaemia), which are caused by a chromosomal translocation that gives rise to the constitutively active oncogenic BCR-ABL fusion protein. The emergence of imatinib resistance in patients led to the development of second-generation ABL inhibitors with higher potency and delayed resistance; these include dasatinib and bosutinib, promiscuous inhibitors which also potently inhibit SFKs at nanomolar concentrations [218,219]. Further ABL and other kinase inhibitors were developed and gained regulatory approval over the years, with several of them also inhibiting SRC and other SFKs (see Table 1.3).

Most small molecule kinase inhibitors target the highly conserved ATP-binding pocket of kinases; this is the reason why many of them exhibit high promiscuity across the kinome and should therefore be regarded as multi-kinase inhibitors (e.g. staurosporine, ponatinib) [12,220,221]. Most discovered SFK inhibitors exhibit similar

potency against SRC and ABL kinase, which is in part due to their targeted development in CML but also due to the high sequence similarity between these two kinases [222]. This lack in selectivity is important, as ABL kinase may not be a desirable target in some solid tumours (see chapter 1.3.3).

Table 1.3 compares the reported potency of all SFK inhibitors for SRC and ABL. Only three compounds exhibit both high potency (IC_{50} <5 nM in cell-free assays) against SRC kinase and selectivity over ABL: ruxolitinib, eCF506 and saracatinib. Ruxolitinib gained FDA-approval for its potent JAK1/2 inhibition (3.3 and 2.8 nM, respectively) and is therefore not SFK-selective [223]. While it does not inhibit proliferation of a BCR-ABL-expressing cell line, no confirmation is provided from cell-free ABL kinase assays. Saracatinib has similar potency for SRC as ruxolitinib and exhibits approximately 10-fold selectivity over ABL kinase [224]. However, the recently discovered eCF506 (see chapter 1.3.4) is over 5-times more potent than saracatinib for SRC (<0.5 nM and 2.7 nM, respectively), and exhibits approximately 1000-fold selectivity over ABL kinase [1]. The only other inhibitors with similar potency against SRC are dasatinib (<0.5 nM), bosutinib (1.2 nM) and AP23464 (0.45 nM), all of which are equipotent against ABL kinase. This comparison highlights the superior potency and selectivity profile of eCF506 in comparison to currently available SRC inhibitors, which warrants further investigation into its anti-cancer properties.

Table 1.3. Approved and experimental SFK inhibitors. Listed in order of IC_{50} for SRC kinase. IC_{50} describes the concentration (in nM) needed for 50% inhibition of maximal kinase activity in a cell-free assay, except: $^{+}$ binding constant (K_d); * in cells (EC_{50}); ° inhibitory constant (K_i). Indications: Ph+ CML = Philadelphia chromosome positive chronic myeloid leukaemia; Ph+ ALL = Philadelphia chromosome positive acute lymphoblastic leukaemia; MF = myelofibrosis; PCV = polycythemia vera; IPF = idiopathic pulmonary fibrosis; NSCLC = non-small-cell lung cancer; MTC = medullary thyroid cancer.

Inhibitor	CAS No.	IC_{50} SRC	IC_{50} ABL	Other main targets	Indication / Cl. trials	Brand name (Manufacturer)	Ref
FDA-approved							
Dasatinib (BMS-354825)	302962-49-8	<0.5	<0.5	EphB2, CSF1R, c-KIT, PDGFR, RET	Ph+ CML, Ph+ ALL	Sprycel (Bristol-Myers Squibb	1,218
Bosutinib (SKI-606)	380843-75-4	1.2	1	MAP4K, MINK, ERBB4, SIK2, EGFR	Ph+ CML	Bosulif (Wyeth/Pfizer)	219
Ruxolitinib (INCB018424)	941678-49-5	2.93	Unknown	JAK1/2, Tyk2	MF, PCV	Jakafi, Jakavi (Incyte Corp)	223,225
Ponatinib (AP24534)	943319-70-8	5.4	0.37	PDGFRα, VEGFR2, FGFR1, c-KIT	Ph+ CML, Ph+ ALL	Iclusig (ARIAD Pharmaceuticals)	226
Nintedanib (BIBF 1120)	656247-17-5	156 (LCK 16)	Unknown	VEGFR, PDGFR, FGFR, FLT3	IPF, NSCLC	Ofev, Vargatef (Boehringer Ingelheim)	227
Vandetanib (ZD6474)	443913-73-3	Yes (same as ABL)	Yes (same as SRC)	VEGFR, EGFR, KDR	MTC	Caprelsa (Genzyme)	221
Clinical development or experimental							
AP23464	845895-51-4	0.45	0.67	EGFR, HER2, PDGFR, FGFR			228
eCF506 (06, 52, 11a)	1914078-41-3	<0.5	479	ARAF, BMX, BTK, ERBB4			1
PP20		<1	<1	VEGFR2, EGFR, PDGFR			229
Saracatinib (AZD0530)	379231-04-6	2.7	30	EGFR, c-KIT, EphA2	Y (III)	(AstraZeneca)	224
UM-164	903564-48-7	2.7^{+}	2.9^{+}	p38β			230,231
XL-228	898280-07-4	5	5	IGF1R	Y (I)	(Exelixis)	232
Repotrectinib (TPX-0005)	1802220-02-5	5.3	Unknown	ALK	Y (I/II)	(Turning Point Therapeutics Inc.)	233

Table continued on next page

Table continued from previous page

Inhibitor	CAS No.	IC50 SRC	IC50 ABL	Other main targets	Indication / Cl. trials	Brand name (Manufacturer)	Ref
Staurosporine	62996-74-1	5.3	75	PKC, S6 kinase, Cdc2			234
WH-4-023	837422-57-8	6 (LCK 2)	Unknown	SIK			235
KX01 (KX2-391)	897016-82-9	9-60*	100-200*	Tubulin polymerisation	Y (II)	(Kinex)	236
PP121	1092788-83-4	14 (HCK 8)	18	PDGFR, VEGFR, mTOR			229
PP1	172889-26-8	17 (LCK 5, FYN 6)	147	KIT, EGFR			1,237
CCT196969	1163719-56-9	30 (LCK 20)	Unknown	c-RAF, V600E BRAF			238
SAB298		31 (YES <10)	87 (ABL2)	HER2			239
PP2	172889-27-9	33° (LCK 4, FYN 5)	Yes	PDGFRβ, BRK			237,240
Rebastinib (DCC2036)	1020172-07-9	34	0.8	FLT3, KDR, TIE2, PDGFRα	Y (II)	(Deciphera Pharm.)	241
SKI-1	179248-59-0	44	Unknown	VEGFR2			242
Compound 4		44°, 86^{+}	>125,000°	BRAF, c-RAF			240
LCK Inhibitor	213743-31-8	70 (LCK <1)	Unknown				221,243
SU6656	330161-87-0	280 (YES 20)	1,740				244
Bafetinib (INNO-406)	859212-16-1	1,700 (LYN 19)	5.8		Y (II)	(CytRx)	245
XL-999	705946-27-6	Yes	Unknown	VEGFR2, PDGFR, KIT	Y (II)	(Exelixis)	

1.3.2. SRC inhibitors in clinical trials

Several potent, albeit not very selective, SRC inhibitors are already approved for use in the clinic (e.g. dasatinib, bosutinib). Attempts have been made to repurpose these or approve novel SFK inhibitors (e.g. saracatinib) for use in different types of cancer. Multiple clinical trials have been conducted based on the promising preclinical activity of these compounds in breast, prostate, ovarian, NSCLC and pancreatic cancer patients, among many others [246]. While phase I studies of SRC inhibitors generally confirmed the safety of these compounds in humans, phase II trials mostly did not show sufficient additional benefit to proceed to phase III [54,217,247]. For example in breast cancer patients, dasatinib, bosutinib or saracatinib monotherapy only resulted in an objective response rate (ORR, combines complete and partial response) of 4-5%, 5% and 0%, respectively; the clinical benefit rate (CBR), which combines ORR and stable disease, was only marginally better at 10-13%, 27% and 0%, respectively (see Table 1.4) [248,249]. Similar results of CBR <25% were obtained with dasatinib in prostate cancer and melanoma; no clinical benefit was observed for dasatinib in NSCLC and colorectal cancer or for saracatinib in head and neck squamous cell carcinoma or prostate, pancreatic, gastric and breast cancer [54].

In most cancers, aberrant SRC kinase activity is not thought to be a primary driver of carcinogenesis, unlike BCR-ABL in CML, which is likely a reason for the poor results of SRC inhibitor monotherapy. However, SRC was found to play important roles in preventing and overcoming treatment resistance and showed synergistic effects with other anti-cancer agents in preclinical models, which provides a case for rational drug combinations (see chapter 1.2.4.3). In the case of breast cancer, several clinical trials investigated the combination of dasatinib, bosutinib or saracatinib with chemo-, hormone or targeted therapies (see Table 1.5). While two phase II trials reported improved progression-free survival (PFS) or CBR with dasatinib compared to hormone treatment alone, and two cases of complete response have been reported in others, the results of these trials have not yet led to phase III trials with dasatinib or other SFK inhibitors in breast cancer [250–253]. Two trials with bosutinib were terminated early due to too poor risk-to-benefit ratios [254,255].

Two phase III clinical trials with dasatinib combination therapy have been conducted in metastatic hormone resistant prostate cancer (NCT00744497) and gastrointestinal stromal tumours (GIST, NCT00688766); overall survival of prostate cancer patients was not improved by adding dasatinib to docetaxel and the GIST study was

terminated early [246,256]. A phase II trial of saracatinib with paclitaxel in platinum-resistant ovarian cancer (NCT01196741) showed no significant effects but a tendency towards worse outcomes with saracatinib; AstraZeneca has reportedly stopped its development in cancer, although it continues testing in other indications [257].

Overall, these results show that only a subset of patients respond moderately to current SRC inhibitors. It remains to be seen whether this can be improved with better biomarker-based patient stratification methods or more selective, potent inhibitors that can be used at higher doses.

Table 1.4. Phase II clinical trials of dasatinib, bosutinib or saracatinib as single agents in breast cancer. Status: C = completed, T = terminated, NR = not recruiting, S = suspended, W = withdrawn. Outcome: CR = complete response, PR = partial response, SD = stable disease, PFS = median progression-free survival, OS = overall survival.

Trial ID	Phase	Type	Status	Outcome	Ref
Dasatinib					
NCT00371254	II	TNBC	C	PR 5%, SD>16 wks 5%, PFS 8.3 wks	248
NCT00371345	II	HER2+, ER+, PrR+	C	PR 4%, SD>16 wks 9%	249
NCT00817531	II	untreated TNBC	T	Futility	246
NCT00780676	II	advanced	T	Futility	258
NCT00546104	II	advanced	C	Early closure due to low PFS	259
NCT00410813	II	bone mets	C	PFS 12.6 weeks	260
NCT01471106	II	no mets, ER-	NR	-	246
NCT02720185	II	TNBC	S	-	246
NCT01410708	II	untreated	W	-	246
Bosutinib					
NCT00319254	II	advanced, chemoresistance	C	PR 6%, SD>24 wks 21%, PFS 15 wks, OS>2 yrs 26.4%	261
Saracatinib					
NCT00559507	II	advanced, ER-, PR-	C	CR 0%, PR 0%, SD>6 mts 0%	262
NCT00558272	II	bone mets	C	-	246

Table 1.5. Phase I/II clinical trials of dasatinib, bosutinib or saracatinib in combination therapies in breast cancer. Status: C = completed, T = terminated, NR = not recruiting, R = recruiting. Outcome: CR = complete response, PR = partial response, SD = stable disease, PFS = median progression-free survival, OS = overall survival, CBR = clinical benefit rate (CR + PR + SD).

Combination	Trial ID	Phase	Type	Status	Outcome	Ref
Dasatinib						
Exemestane	NCT00767520	II	advanced, ER+	C	CBR higher with dasatinib (PR 6% vs 0%; SD>6 mts 43% vs 29%), PFS no difference (18.1 wks D+E vs 16.1 wks E)	246,250
Letrozole	NCT00696072	II	advanced, ER+, PrR+, HER2-	C	Higher PFS with dasatinib (20.1 mts vs 9.9 mts), CBR no difference (71% D+L vs 66% L)	251
Fulvestrant	NCT00754325	II	advanced, ER+, PrR+	C	PFS, CBR, OS not improved with dasatinib	263
Fulvestrant	NCT00903006	I/II	mets, ER+, PrR+, HER2-	T	Low accrual	246
Trastuzumab, Paclitaxel	NCT01306942	I/II	mets, HER2+	NR	PR 79%, SD 4%, PFS 24 mts	264
Capecitabine	NCT00452673	I	advanced	C	PR 24%, SD 32%, PFS 14.4 wks	265
Paclitaxel	NCT00820170	I/II	advanced, HER2-	C	Phase I: PR 31%, SD 29% Phase 2: CR 2.8%, PR 20%, SD>6 mts 20%, OS 20.6 mts, PFS 5.2 mts	266 252
Ixabepilone	NCT00924352	I	advanced, HER2-	C	PR 5%, SD 63%	267
Zoledronic Acid	NCT00566618	I/II	HER2-, bone mets	NR	PR 23%, SD 13%, PFS 2.7 mts	268
Bosutinib						
Exemestane	NCT00793546	II	advanced, ER+, PrR+, HER2-	T	PR 2.4%, SD>24 wks 7.1%, PFS 12.3 wks; risk:benefit ratio too high	254
Letrozole	NCT00880009	II	advanced, ER+, PrR+, HER2-	T	PR 6.7%, SD>24 wks 6.7%; risk:benefit ratio too high	255
Capecitabine	NCT00959946	I	advanced	T	PR 6%, SD>24 wks 13%	269
Fulvestrant, Palbociclib	NCT03854903	I	ER+, PrR+, HER2-	R		246
Saracatinib						
Anastrozole	NCT01216176	I/II	advanced, ER+, PrR+	C	CBR no difference (PR 70% S+A, 90% A)	246

1.3.3. The unclear role of ABL in solid tumours

Many attempts have been made to repurpose or approve dual SRC/ABL inhibitors for their SRC inhibition, but all showed insufficient efficacy to date to warrant regulatory approval (see previous chapter 1.3.2). One contributing factor may be the promiscuity and associated off-target effects of current inhibitors. ABL kinase appears to have a complex role in solid tumours, as different studies link its activity either to cancer invasiveness and treatment resistance or to p53-mediated tumour suppression [270,271].

ABL kinase was found to be highly activated in aggressive breast cancer cells, where it promotes invasion, proliferation and anchorage-independent growth *in vitro* that was reduced by the ABL inhibitor imatinib [272,273]. Aromatase-resistant patients were found to have higher levels of PDGFR and ABL kinase expression and ABL inhibition was able to re-sensitise lapatinib- or tamoxifen-resistant cells to treatment [274–276]. Moreover, ABL activity is necessary for the oncogenic transformation of fibroblasts and human breast cancer cells by SRC kinase, highlighting an interaction between both kinases [277].

Contradicting roles were found in an *in vivo* breast cancer model, in which knockdown of the ABL2 protein ARG increased tumour size and proliferation but simultaneously reduced tumour invasiveness [278]. Indeed, nuclear ABL kinase activity has long been linked to inhibition of cell growth, which was found to be mediated by its interaction with the tumour suppressor p53 and activation of p53-mediated transcription [279,280]. ABL activation was found to induce senescence in TNBC by upregulating p21 expression in a p53-dependent manner and wild-type p53 and ABL expression were identified as a prognostic factor for patient survival [281]. Recently, it was shown that the dual role of ABL in TNBCs can be linked to p53 status and subcellular localisation of the p53:ABL complex; mutant p53 triggers cytoplasmic accumulation of p53:ABL that inhibits ABL-mediated anti-tumour activity [282].

Another pathway distinct from ABL's nuclear function links signalling via the EphB4 receptor, ABL kinase and the CRK adapter protein to cytoskeletal changes that inhibit cell migration and tumour invasion [283–285]. Moreover, α3β1 integrin-mediated signalling through ABL was found to activate the Hippo pathway and suppress metastases in a prostate cancer model [286].

In addition to the role of ABL as a potential tumour suppressor, it also plays a key role in cardiac development by regulating cardiomyocyte proliferation [287]. Indeed, ABL

mutant mice exhibit cardiac hyperplasia and the same phenotype was found by Fraser *et al*. after treatment of Zebrafish embryos with the dual SRC/ABL inhibitor dasatinib but not with the SRC-selective inhibitor eCF506, even at a 50-fold higher concentration [1,287]. The ABL inhibitor imatinib was found to cause severe cardiotoxicity in some CML patients, although it should be noted that cardiac side effects of ABL inhibitors only occur in a small subset of patients [288,289].

The risk of ABL inhibition combined with the role of ABL in p53-mediated tumour suppression cautions against the long-term use of dual SRC/ABL inhibitors in indications of solid carcinomas and non-malignant diseases. Consequently, there is a clear case for the development and preclinical assessment of SRC selective, non-ABL inhibitors, which have the potential to exhibit greater potency and fewer side effects in the clinic.

1.3.4. The discovery of eCF506

The Innovative Therapeutics Lab at the University of Edinburgh has recently developed the first potent and highly selective small molecule SRC inhibitor eCF506 (see Figure 1.5) [1]. Its IC_{50} in isolated kinase screens of SRC was found to be <0.5 nM, which is on par with the current best-in-class inhibitor dasatinib. Notably, it is the only known SRC inhibitor to exhibit approx. one thousand-fold selectivity over ABL kinase (IC_{50} 479 nM) and does not inhibit c-KIT, PDGFR or RET, which are known targets of dasatinib (see Table 1.3).

Further testing by Fraser *et al*. confirmed that eCF506 can potently inhibit SRC activation in cells and in an *in vivo* xenograft model, as well as reduce the proliferation and migration of two breast cancer cell lines and neuromasts in Zebrafish [1]. Preliminary safety and pharmacokinetic studies show that it does not inhibit the hERG channel or cytochrome P450 enzymes and shows favourable plasma protein binding and metabolic stability. eCF506 is highly water soluble, unlike dasatinib, and its oral bioavailability and half-life in mice were also found to be superior. The high potency and selectivity of eCF506 combined with its excellent pharmacodynamic and pharmacokinetic properties warrant its continued preclinical development in cancer.

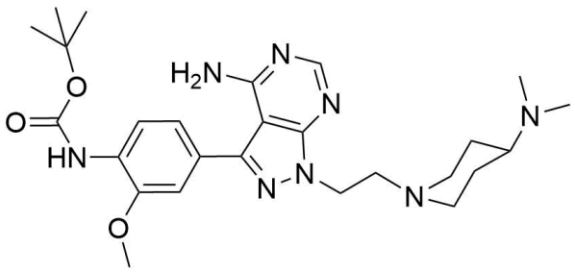

Figure 1.5. Structure of eCF506.

1.4. Aims and hypothesis

The non-receptor tyrosine kinase SRC is a central node in cell signalling pathways and has repeatedly been associated with cancer progression, treatment resistance, angiogenesis and other diseases. While multiple dual SRC/ABL inhibitors are already used in the clinic to treat CML, efforts to repurpose these for their SRC inhibition have so far failed. Indeed, ABL may not be a desirable target in solid tumours such as breast cancer and the promiscuity of current inhibitors may lead to undesirable off-target effects. The recently discovered selective SRC/non-ABL inhibitor eCF506 has the potential to overcome these limitations. It exhibits nanomolar potency, excellent drug-like properties and has achieved target inhibition *in vivo*.

Hypothesis

Based on its potency, selectivity and drug-like properties, eCF506 has the potential be better than current dual SRC/ABL inhibitors in preclinical models of cancer.

Aims

The aim of this thesis is to continue the preclinical investigation of eCF506, with a particular focus on:

- eCF506's potency *in vitro* in comparison to other SRC inhibitors and in different types of cancer.
- Unique properties distinguishing eCF506 from the current best-in-class inhibitor dasatinib.
- eCF506's pharmacokinetic and pharmacodynamic properties and ability to show efficacy *in vivo*.

Chapter 2. Materials and Methods

2.1. Materials

2.1.1. Common buffers and reagents

The compositions of commonly used buffers are listed below in Table 2.1. Buffers were prepared using Milli-Q® water, unless stated otherwise.

Table 2.1. Composition of common buffers and reagents.

Buffer	Composition
Blocking Buffer	5% (w/v) bovine serum albumin (BSA) (Sigma, A9647) added to TBST 0.1%.
Buffer A	20 mM Tris pH 7.5, 1 mM $MgCl_2$, 1 mM EGTA; sterile filtered and stored at 4°C. Add PI directly before use. With detergent: add 0.03% (v/v) NP-40.
Buffer B	10 mM Tris-HCl pH 7.4, 2.5 mM $MgCl_2$, 1.5 mM KCl, 0.2 M LiCl; sterile filtered and stored at 4°C. Add PI, 0.1% (v/v) Triton X100 and 0.1% (w/v) sodium deoxycholate directly before use.
DAPI solution	20 µg/mL DAPI (Sigma, D9542) in PBS; prepare directly before use.
Citrate Buffer	18 mL of 0.1 M citric acid (21 g in 1L water), 82 mL of 0.1 sodium citrate (29.4 g in 1 L water), make up to 1 L with water.
Mammosphere medium	500 mL DMEM/F12 (Gibco, 21041), 10 mL B27 supplement without vitamin A (Invitrogen, 12587), 20 ng/mL rEGF (Gibco, PHG0314).
Lysis Buffer (2X)	40 mM Tris pH 7.5, 300 mM NaCl, 1% (v/v) Triton X100.
Pepsin solution	1 mg / mL pepsin (Sigma, P6887) in 30 mM hydrochloric acid (pH 1.5); freshly prepared.
pHEMA coating	12 g of poly-(2-hydroxyethyl methacrylate) were dissolved in 1 L of 98% ethanol by constant mixing on a heated plate.
Phosphate Buffered Saline (PBS)	137 mM NaCl, 2.7 mM KCl, 10 mM Na_2HPO_4, 1.8 mM KH_2PO_4, pH 7.4.

Table continued on next page

Table continued from previous page

Buffer	Composition
Protease/Phosphatase inhibitors (PI)	1.25 mM PMSF (Sigma, 93482), 0.1% (v/v) aprotinin (Sigma, A6278), 100 µM Na_3VO_4 (Sigma, S6508), 500 µM NaF (Sigma, S7920). Added to RIPA buffer, Buffer A and Buffer B.
Radioimmunoprecipitation assay (RIPA) buffer	50 mM Tris pH 8.0, 150 mM NaCl, 1% (v/v) NP-40, 0.5% (w/v) sodium deoxycholate, 0.1% (v/v) SDS. Sterile filtered, stored at 4°C.
RIPA lysis buffer	PI are added to RIPA buffer directly before use.
Scott's Tap Water	3.5 g sodium bicarbonate, 20 g magnesium sulphate, make up to 1 L with water.
Tris Buffered Saline (TBS)	24.23 g Trizma HCl and 80.06 g NaCl in 1 L water, pH 7.6.
Tris Buffered Saline Tween (TBST 0.1%)	Add 0.1% (v/v) Tween® 20 (Sigma, P1379) to TBS.
Tris Glycine SDS (TGS)	25 mM Tris HCl, 192 mM glycine, 0.1% (w/v) SDS, pH 8.3.
Trypsin	10X Trypsin-EDTA (Sigma, T4174) diluted to 1X in PE (PBS with EDTA) buffer.

2.1.2. Antibodies

Antibodies for Western blots were diluted in blocking buffer to which sodium azide (0.02% w/v) was added and prepared antibody dilutions were stored at 4°C. Antibodies for co-immunoprecipitation were added directly to samples in RIPA lysis buffer. Antibodies for immunohistochemistry were diluted in Dako antibody diluent.

Table 2.2. Antibody list. SCB = Santa Cruz Biotechnology, CST = Cell Signalling Technology.

Target	Host	Company	ID	Dilution
Western blots				
ABL	Mouse	SCB	SC-23	1 / 1000
ABL (Y245)	Rabbit	CST	2861	1 / 1000
α-tubulin	Mouse	CST	3873	1 / 1000
β-actin	Mouse	CST	3700	1 / 1000
β-catenin	Rabbit	CST	9582	1 / 1000
BRCA1	Rabbit	CST	9010	1 / 1000
cdc25A	Mouse	Neomarker	MS-640-P0	1 / 1000
CDK2	Rabbit	CST	2546	1 / 1000
CDK4	Mouse	Neomarker	MS-299-P0	1 / 1000
CDK6	Mouse	Neomarker	MS-451-P0	1 / 1000
c-Myc	Mouse	SCB	SC-40	1 / 1000
CRKL	Mouse	CST	3182	1 / 1000
CRKL (Y207)	Rabbit	CST	3181	1 / 1000
ERα	Rabbit	Abcam	16660	1 / 1000
FAK	Rabbit	CST	3285	1 / 1000
FAK	Mouse	Millipore	05-537	1 / 1000
FAK (Y397)	Rabbit	CST	3283	1 / 1000
FAK (Y861)	Rabbit	Invitrogen	44626	1 / 1000
FAK (Y407)	Rabbit	Invitrogen	44-650	1 / 1000
GAPDH	Rabbit	CST	5174	1 / 1000
GM130	Mouse	BD	610822	1 / 1000
HER3 / ErbB3	Rabbit	CST	4754	1 / 1000
Histone H4	Mouse	CST	2935	1 / 1000
JNK/SAPK1	Rabbit	Upstate	06-748	1 / 1000
mTOR (S2448)	Rabbit	CST	2971	1 / 1000
PI3K (p85 subunit)	Mouse	BD	610045	1 / 1000

Table continued on next page

Table continued from previous page

Target	Host	Company	ID	Dilution
Rb	Mouse	CST	9309	1 / 1000
SRC	Rabbit	CST	2109	1 / 1000
SRC	Mouse	SCB	SC-8056	1 / 1000
SRC (Y416)	Rabbit	CST	2101	1 / 1000
SRC (Y527)	Rabbit	CST	2105	1 / 1000
Anti-Mouse	Horse	CST	7076	1 / 5000
Anti-Rabbit	Goat	CST	7074	1 / 5000
Co-immunoprecipitation				
SRC	Rabbit	CST	2109	2 µg / sample
SRC	Mouse	SCB	SC-8056	2 µg / sample
FAK	Mouse	Millipore	05-537	2 µg / sample
Rabbit IgG	Rabbit	CST	2729	2 µg / sample
Mouse IgG1	Mouse	CST	5415	2 µg / sample
Immunohistochemistry				
Ki67 (Mouse-preferred)	Rabbit	CST	12202	1 / 4000
CD8α (Mouse-specific)	Rabbit	CST	98941	1 / 400
Anti-rabbit	Goat	Dako	K4003	As provided

2.1.3. Primers

Primers sequences are based on previously published papers and all primers were made by Integrated DNA Technologies as ready-formulated solutions (100 µM in IDTE buffer which contains 10 mM Tris and 0.1 mM EDTA, pH 8.0).

Table 2.3. Primer sequences.

Gene	Species	Sequence (5'-3')	Ref
CCL5	Mouse	F - CCCTCACCATCATCCTCACT R - CCTTCGAGTGACAAACACGA	290
CXCL10	Mouse	F - GGATGGCTGTCCTAGCTCTG R - TGAGCTAGGGAGGACAAGGA	291
TGFB2	Mouse	F - GAACCCAAAGGGTACAATGC R - TGGTGTTGTACAGGCTGAGG	292
IGFBP3	Mouse	F - AATGCTGGGAGTGTGGAAAG R - TTCTGGGTGTCTGTGCTTTG	293
B2M	Mouse	F - GGGAAGCCGAACATACTGAA R - TGCTTAACTCTGCAGGCGTAT	290
VEGFR2	Human	F - GAGAGTTGCCCACACCTGTT R - CAACTGCCTCTGCACAATGA	294
GAPDH	Human	F - CAGCCTCAAGATCATCAGCA R - TGTGGTCATGAGTCCTTCCA	294

2.1.4. Compounds

Dasatinib was acquired from Cell Guidance Systems (SM45). Bosutinib (S1014), imatinib (S2475), saracatinib (S1006), sunitinib (S7781) and VS-4718 (S7653) were acquired from Selleck Chemicals.

eCF506 was synthesised in five steps from commercially available starting materials. The method has previously been described by Fraser *et al.* [1] and minor changes made for scale up purposes are highlighted in the following (see also Figure 2.1):

- Step 1 (A to B) and step 2 (B to C): No changes.
- Step 3 (C to D): No changes in synthesis. The solvent mix used for purification of D was changed, as ethyl acetate : hexane (65 : 35) resulted in better separation.

- Step 4 (D to E): Reactant amounts and volumes of solvents were tripled during synthesis. The aldehyde intermediate was suspended in THF instead of DCM to improve solubility. Four batches were combined for purification. The solvent mix used for purification of E was changed to DCM : methanol : triethylamine (89 : 10 : 1) to reduce costs.
- Step 5 (E to eCF506): Reactant amounts and volumes of solvents were tripled during synthesis. Five batches were combined for purification. The solvent mix used for purification of eCF506 was changed to DCM : methanol : 4 M ammonia in methanol (85 : 10 : 5). Scaling up of the last step improved the yield from 38% to 65%.

A total of 3.4 g of eCF506 was synthesised by me and an additional 4 g was synthesised by Dr Rafael Contreras-Montoya.

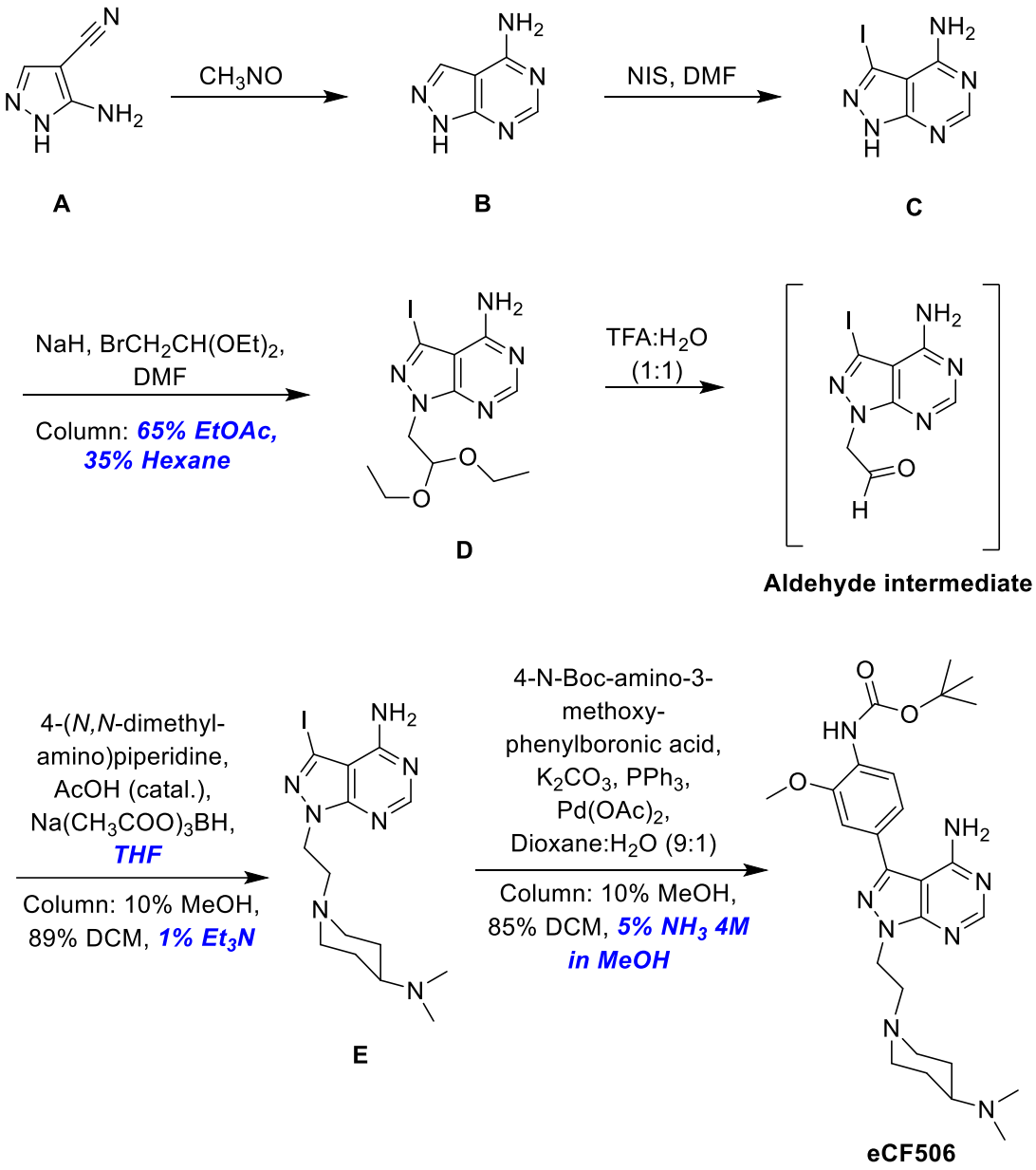

Figure 2.1. Synthetic route of eCF506. Modifications from the method published by Fraser *et al.* are highlighted in blue [1]. DCM - dichloromethane, DMF - dimethylformamide, Et_2N - triethylamine, EtOAc - ethyl acetate, MeOH - methanol, NH_3 - ammonia, NIS - *N*-iodosuccinimide, PPh_3 - triphenylphosphine, TFA - trifluoroacetic acid, THF - tetrahydrofuran.

2.2. Cellular assays

2.2.1. Cell culture methods

The cell lines used were either purchased directly from the European Collection of Authenticated Cell Cultures (MCF-7) or were a kind donation from several research groups at the Institute of Genetics and Molecular Medicine, Edinburgh, UK (all others). Cells are grown in the medium specified in Table 2.4 and maintained in a Heracell 240i tissue culture incubator (37°C, humidified air, 5% CO_2). Cell lines in culture were mycoplasma tested every 2 months.

Table 2.4. Cell culture conditions. DMEM = Dulbecco's Modified Eagle's Medium (Gibco, 21969035); RPMI = RPMI 1640 Medium (Gibco, 31870025); FBS = foetal bovine serum (Gibco, 10270-106); L-glutamine (Gibco, 25030081). Seeding density shown is for 96-well plates (see chapter 2.2.2.1 for protocol).

Cell line	Medium	Supplements	Cells / well
BT-474	RPMI	10% FBS, 2 mM L-glutamine	5,000
BT-549	RPMI	10% FBS, 2 mM L-glutamine	1,000
CAMA-1	DMEM	10% FBS, 2 mM L-glutamine	1,000
ES-2	DMEM	10% FBS, 2 mM L-glutamine	1,000
HCC-1569	DMEM	10% FBS, 2 mM L-glutamine	3,000
HCC-1954	DMEM	10% FBS, 2 mM L-glutamine	2,000
HUVEC	Ham's F-12K	10% FBS, 100 µg/mL heparin (Sigma, H3149-10KU), 30 µg/mL endothelial cell growth supplement (Sigma, E2759)	1,000
IGROV-1	RPMI	10% FBS, 2 mM L-glutamine	1,000
JIMT-1	DMEM	10% FBS, 2 mM L-glutamine	1,000
K-562	RPMI	10% FBS, 2 mM L-glutamine	4,000
KCL-22	RPMI	10% FBS, 2 mM L-glutamine	4,000
KPL-4	DMEM	10% FBS, 2 mM L-glutamine	1,000
LAMA-84	RPMI	10% FBS, 2 mM L-glutamine	4,000
MCF-7	DMEM	10% FBS, 2 mM L-glutamine	1,000
MDA-MB-134VI	RPMI	10% FBS, 2 mM L-glutamine	10,000
MDA-MB-157	DMEM	10% FBS, 2 mM L-glutamine	5,000
MDA-MB-231	DMEM	10% FBS, 2 mM L-glutamine	1,000
MDA-MB-436	DMEM	10% FBS, 2 mM L-glutamine	3,000
Met1	DMEM	10% FBS, 2 mM L-glutamine	1,000

Table continued on next page

Table continued from previous page

Cell line	Medium	Supplements	Cells / well
MetBo2	DMEM	10% FBS, 2 mM L-glutamine	1,000
OVCAR-3	RPMI	20% FBS, 2 mM L-glutamine, 0.01 mg/mL bovine insulin	3,000
OVMANA	RPMI	10% FBS, 2 mM L-glutamine	3,000
OVTOKO	RPMI	10% FBS, 2 mM L-glutamine	1,000
PEO cell lines	RPMI	10% FBS, 2 mM L-glutamine, 2 mM sodium pyruvate	3,000 (PEO4 6,000)
SCC cell lines	MEM	10% FBS, 2 mM L-glutamine, 1X MEM non-essential amino acids, 1X MEM vitamins, 1 mM sodium pyruvate; SCC FAK WT and SCC FAK NLS are maintained in 1% Hygromycin	1,000
SKBR3	DMEM	10% FBS, 2 mM L-glutamine	4,000
SKOV-3	McCoy's 5a	10% FBS, 2 mM L-glutamine	1,000
SUM44PE	Ham's F-12	1 g/L BSA, 5 mM ethanolamine, 10 mM HEPES, 1 µg/mL hydrocortisone, 5 µg/mL insulin, 50 nM sodium selenite, 5 µg/mL apo-transferrin, 10 nM triiodo thyronine; 2% FBS was added when thawing and splitting cells.	5,000
SYF	DMEM	10% FBS, 2 mM L-glutamine	1,000
T47-D	RPMI	10% FBS, 2 mM L-glutamine	2,000
TOV112D	RPMI	10% FBS, 2 mM L-glutamine	1,000
TOV-21G	RPMI	10% FBS, 2 mM L-glutamine, 1X non-essential amino acids, 1 mM sodium pyruvate, 0.01 mg/mL bovine insulin	1,000
ZR75.1	RPMI	10% FBS, 2 mM L-glutamine	4,000

2.2.2. Cell proliferation assays

2.2.2.1. Cell viability assays

On day 0, cells were seeded in 96-well plates at the seeding density specified in Table 2.4. Edge wells are not used due to evaporation effects that can affect cell growth. After 48 hours, the medium was removed and 95 µL of fresh medium was added,

except for suspension cell lines which were seeded and treated on the same day. Dilution plates of the test compounds were prepared in DMSO and diluted 1:50 into medium, of which 5 µL were added to the cell plates (final DMSO concentration 0.1% v/v). Cells were treated for 5 days before cell viability was measured using the resazurin-based PrestoBlue solution (Invitrogen, A13262), which is converted into fluorescent red resorufin in the reducing environment of viable cells. PrestoBlue was added to an untreated plate on day 2 and treated plates on day 7 (1 in 10 dilution) and fluorescence (550 nm excitation, 580 nm emission) was measured after the same incubation time on both days (0.25-6 hours after addition, depending on cell line) using the Perkin Elmer Envision 2101 plate reader. The average fluorescence on day 2 was subtracted from the values on day 7 to distinguish between cytotoxic and cytostatic treatment effects and the data was normalised to DMSO controls. GraphPad Prism 7 was used to fit non-linear regression curves (four-parameter logistic fit or biphasic fit, depending on shape of data points) to determine growth inhibition 50% (GI_{50}), 75% (GI_{75}), 90% (GI_{90}) and total growth inhibition (TGI) concentrations.

2.2.2.2. Oesophageal cancer screen

This work was done by Dr Richard Elliott and Becka Hughes from the Drug Discovery group of Prof Neil Carragher at the University of Edinburgh, UK.

eCF506, dasatinib and imatinib were tested in six oesophageal adenocarcinoma cell lines (FLO-1, OE33, MFD1, SKGT4, OAC-P4C, JHesoAD1) and two non-malignant, tissue matched controls immortalised by hTERT (EPC2 is a human oesophageal squamous epithelial cell line; CP-A is a Barrett's oesophagus epithelial cell line with non-dysplastic metaplasia; both are p53 wild-type).

Cells were seeded in 384-well plates (1000 cells/well, 45 µL/well) and left to attach for 24 hours. Compounds were added (10X dose, 5 µL/well) in a 10-point dose response with half-log serial dilutions from 10 µM to 0.5 nM final concentration with DMSO controls (final DMSO concentration 0.1% v/v). Cells were then incubated for 48 hours prior to fixation with 4% formaldehyde. Fixed cells were stained with Hoechst 33342 (2 µg/mL) for 20 minutes. Total Nuclei per well was quantified automatically using an ImageXpress MicroXl platform (10X objective, DAPI channel, 4 sites per well, average Total Nuclei/site calculated via a built-in 'Count Nuclei' analysis module). Data was normalised to the DMSO controls and presented as '% Cell Survival'.

2.2.2.3. GDSC cell line screen

This work was done by the group of Dr Mathew Garnet, Wellcome Sanger Institute, UK.

eCF506 was screened in the Genomics of Drug Sensitivity in Cancer (GDSC) cell line collection. This collection comprises of 750 cell lines, most of which are commercially available, across a variety of cancer types. All cell lines have been authenticated by STR analysis and are kept in either DMEM/F12 (supplemented with 10% FBS, 1% Pen-Strep) or RPMI (supplemented with 10% FBS, 1% Pen-Strep, 4.5 mg/mL glucose, 1 mM sodium pyruvate). The cell lines were split into two sets and the screen was performed in two stages lasting ca. 4 months each. Cells are seeded at optimal density in 1536-well plates in 7.5 µL medium by automated fluid dispensers and incubated (37°C, 5% CO_2, humidified atmosphere) for 24 hours. Compounds are added (final DMSO concentration 0.1% v/v) using the Echo555 Acoustic Dispenser (Labcyte) and plates were incubated for 72 hours. Cell viability is measured after addition of 2.5 µL Cell Titer Glo 2.0 (Promega) per well and a 10-minute incubation at room temperature. Luminescence is measured on a Paradigm (Molecular Devices) plate reader. An additional untreated plate is read 24 hours after seeding as above to determine cell viability at the time of treatment. Negative controls (untreated, DMSO) and positive controls (MG-132, staurosporine, media only) are included in the screen for quality control and seven cell lines are tested at multiple stages of the screening process to identify inconsistencies and systematic errors. eCF506 dissolved in DMSO was stored in 1536-well source plates at room temperature (low humidity <12%, low oxygen <2.5%, UV protected) for the duration of the screening period. Data analysis was done after normalisation of each plate to negative and positive controls using the R package gdscIC50 (see https://github.com/CancerRxGene/gdscIC50). Dose-response curves were fitted using a non-linear mixed effects model which assumes a classical sigmoidal S-shape dose-response from which IC_{50} and AUC values were calculated.

2.2.2.4. Spheroid assay

Cells were seeded on day 0 in ultra-low adhesion round bottom 96-well plates (Costar, 7007) at the seeding densities shown in Table 2.5 in 200 µL of medium. Plates were centrifuged (1,000 x g, 10 minutes, 4°C, acceleration/deceleration 1/10) and

incubated for 2-3 days as specified in Table 2.5 to allow spheroids to form. Compounds were added to the wells without changing the medium (final DMSO concentration 0.1% v/v) and the plates were incubated for 7 days. Spheroids were imaged on the day of treatment, 4 days post treatment and 7 days post treatment using the ImageXpress MicroXI platform. Eight Z-stack images (40X, brightfield) were taken with 50 µM size step and collapsed into a single image from which the size of the spheroid was measured using CellProlifer. On the final day of treatment, calcein-AM (3.5 µM) and propidium iodide (4 µM) were added to the plates, which were incubated for 1 hour and fluorescence was measured on the ImageXpress to visualise viable and dead cells, respectively. The size of each spheroid was calculated for all time points and expressed as percentage of spheroid size on day of treatment start.

Table 2.5. Seeding densities of 3D spheroid models.

Cell Line	Seeding Density (cells / well)	Treatment start / end (days post seeding)
MDA-MB-231	4,000	3 / 10
MCF-7	2,000	2 / 9
T-47D	2,000	2 / 9
MetBo2	2,000	2 / 9

2.2.2.5. Mammosphere assay

This protocol was adapted from Shaw *et al.* [295]. The mammosphere forming ability in the first generation was assessed as follows: 6-well plates were coated with warm pHEMA solution (1 mL/well) and left to dry at 40°C for 72 hours under sterile conditions. MetBo2 cells were trypsinised, collected in normal medium, centrifuged (580 x g, 2 min) and the cell pellet was resuspended in 2 mL of ice-cold PBS. A single cell suspension was created by syringing the cells with a 25 G needle six times. The cell concentration was determined using a haemocytometer and 4,000 cells were added to each well in 2 mL of mammosphere medium (see Common buffers for composition). Compounds were added to the wells (final DMSO concentration 0.1% v/v) and the plates were incubated for 5 days without any disturbance. Plates were then imaged on the ImageXpress MicroXI platform (40X, brightfield) and the number of mammospheres with a diameter over 50 µM counted using CellProfiler. Mammosphere forming efficiency (MFE) was calculated as follows:

$$\text{MFE}\ (\%) = \frac{\text{number of mammospheres per well}}{\text{4,000 cell seeded per well}} * 100$$

To assess their self-renewal capacity, mammospheres were then passaged and assessed again in a secondary generation as follows: All mammospheres for each condition were collected, centrifuged (115 x g, 5 min), resuspended in 300 µL of trypsin and incubated at 37°C for 3 minutes. A single cell suspension was created by syringing the mammospheres with a 25 G needle six times, after which the trypsin was neutralised with 1 mL of normal medium. The cell suspension was centrifuged (580 x g, 5 min) and the cell pellet was resuspended in 100 µL of ice-cold PBS. The cell concentration was determined using a haemocytometer and for each condition the entire cell suspension was plated out in mammosphere medium in new pHEMA coated 6-well plates as close to the original seeding density as possible. Compounds were added to the wells (final DMSO concentration 0.1% v/v) and the plates were incubated for 5 days without any disturbance. The number of mammospheres in the secondary generation were counted as described for the first generation and the mammosphere self-renewal rate was calculated as follows:

$$\text{Self} - \text{renewal rate} = \frac{\text{total number of second generation mammospheres}}{\text{total number of first generation mammospheres}}$$

2.2.2.6. Cell migration assay

HUVEC cells (20,000 cells / well) were seeded on 96-well ImageLock plates (Essen Bioscience, 4379) and left to attach for 3 hours. Compounds were added to the wells (final DMSO concentration 0.1% v/v) and plates were incubated for 2 hours before homogenous scratch wounds (700-800 µm) were created in all wells using the WoundMaker tool (Essen BioScience, 4563). Wells were washed twice with medium to remove detached cells before plates were incubated in the IncuCyte ZOOM incubator (37°C, humidified air, 5% CO_2). Photos were taken every hour for 24 hours and the relative wound density was determined using the IncuCyte wound cell migration software (Essen BioScience).

2.2.2.7. Cell cycle assay

Cells were seeded (1 million cells / 15 cm plate) and left to attach for 24 hours. Compounds were added (final DMSO concentration 0.1% v/v) and the treated plates were incubated for 48 hours. Cells were trypsinised, resuspended in medium and centrifuged (1,000 rpm, 5 minutes). The cell pellet was resuspended in 50 µL PBS with 2% FBS and cell aggregates were broken up through gentle pipetting. Cells were fixed by adding 1 mL ice-cold 70% ethanol dropwise while vortexing gently and samples were stored at 4°C for up to two weeks. The cell concentration was determined using a haemocytometer and 1.5 million cells were used per sample. Cells were centrifuged (1,000 rpm, 5 minutes) and the cell pellet was resuspended in 2 mL pre-warmed pepsin solution and incubated for 30 minutes in a 37°C water bath with frequent vortexing. The digested samples were centrifuged (4,000 rpm, 4 minutes) and the pellet was resuspended in 0.25 mL HCl and incubated for 15 minutes at room temperature. 12 mL PBS was added and samples were centrifuged (4,000 rpm, 4 minutes), after which the pellet was washed a second time in 5 mL PBS. The pellet was resuspended in 0.5 mL DAPI solution and incubated in the dark for 30 minutes at room temperature. Samples were analysed by flow cytometry using the LSR Fortessa (BD Biosciences) and 30,000 events were recorded per sample.

2.3. Nucleic acid methods

2.3.1. RNA extraction

Cells were seeded (500,000 cells / 10 cm dish) and left to attach for 48 hours. Compounds were added (final DMSO concentration 0.1% v/v) and cells incubated for 24 hours. Cells were lysed and ribonucleic acid (RNA) was extracted using the RNeasy Mini Kit (Qiagen, 74106) according to the manufacturer's instructions.

2.3.2. cDNA synthesis

The RNA concentration was determined and 1 µg of each sample was used to synthesise complementary deoxyribonucleic acid (cDNA) using the qScript cDNA SuperMix (Quanta Biosciences, 95048) according to the manufacturer's instructions.

2.3.3. Real time PCR

100 ng of cDNA was used for each reaction and each sample was assessed in triplicate. Primers were used at a final concentration of 200 nM.
Real Time PCR was performed using SYBR Select Master Mix (Applied Biosystems) according to the manufacturer's instructions and PCR-grade H_2O was used as a control for primer specificity. The cycling conditions used on the StepOnePlus™ Real-Time PCR System (Applied Biosystems) were as follows:

- Pre-incubation: 95°C (10 minutes)
- 40 cycles:
    - Denaturation: 95°C (15 sec)
    - Annealing/Extension: 60°C (1 min)
- Dissociation/Melt Curve analysis:
    - Denaturation: 95°C (15 sec)
    - Annealing: 60°C (1 min)
    - Increasing temperature by 0.3°C every 15 seconds until 95°C

The cycle threshold (CT) was determined by StepOne Real-Time PCR Systems Software v2.3 (Applied Biosystems). CT of the gene of interest was normalised to a

housekeeping gene (B2M for mouse cells, GAPDH for human cells) and compound-treated samples were normalised to DMSO-treated controls.

2.3.4. siRNA

Master mixes were prepared as shows in Table 2.6. On a 12-well plate, 200 µL master mix was added per well and complexes were allowed to form for 20 minutes at room temperature. Cells were trypsinised, counted, centrifuged and resuspended in OptiMEM (80,000 cells / mL) and 1 mL of cell suspension was added to each well. Plates were left at room temperature for 1 hour and then incubated at 37°C. After 24 hours, medium as replaced with standard medium, compounds were added (final DMSO concentration 0.1% v/v) and cells incubated for 4 days. Cells were lysed with RIPA lysis buffer (80 µL / well) and Western blotting was performed as described in methods 2.4.

Table 2.6. siRNA mastermix composition.

Sample	Master mix
Untreated	200 µL OptiMEM
Mock	200 µL OptiMEM, 2 µL Lipofectamine RNAiMAX (Invitrogen, 13778100)
Non-silencing RNA	200 µL OptiMEM, 2 µL Lipofectamine RNAiMAX, 40 nM Non-targeting control siRNA (Dharmacon, D-001206-14)
SRC siRNA	200 µL OptiMEM, 2 µL Lipofectamine RNAiMAX, 40 nM Human SRC siRNA (Dharmacon, M-003175-03)

2.4. Protein methods

2.4.1. Cell lysates

Cells were seeded in 6-well plates or 10 cm dishes, depending on the experiment, and incubated for 48 hours until 70% confluence was reached. Compounds were added (final DMSO concentration 0.1% v/v) and cells incubated for the time specified (3, 6 or 24 hours). Plates were put on ice, the medium was removed and cells were washed twice with ice-cold PBS. RIPA lysis buffer with protease and phosphatase inhibitors was added (100 µL / well or 200 µL / 10cm dish) and the cells were scraped, collected and incubated on ice for 10 minutes with occasional vortexing. Lysates were centrifuged at 4°C (17,000 x g, 10 minutes) and the supernatant was transferred into a new microcentrifuge tube. Lysates were stored at -20°C (short-term) or -70°C (long-term).

The protein concentration of lysates was determined in a bicinchoninic acid (BCA) assay. The Pierce BCA Protein Assay Kit (Thermo Scientific, 23225) was used according to the manufacturer's instructions, with samples being diluted 1 in 4 and set up in duplicate on 96-well plates. Plates were read on a Spark 20M microplate reader (Tecan) and absorbance was measured at 562 nm.

2.4.2. Western blotting

Samples for SDS-PAGE were prepared as follows: 20 µg cell lysate was diluted with RIPA buffer to a final volume of 15 µL, to which 5 µL of 4X Laemmli Sample Buffer (Bio-Rad, 1610747) were added. Samples were heated to 95°C for 5 minutes and then loaded onto Mini-PROTEAN TGX precast gels (12-well or 15 well, 4-15% or 12%, depending on experiment; Bio-Rad). Precision Plus Protein Dual Color Standards (Bio-Rad, 1610374) were loaded alongside the lysates. Gels were run in Mini-PROTEAN Tetra Cell tanks in TGS buffer (pH 8.3) at 150 V for 45 minutes. Proteins were transferred onto Trans-Blot Turbo Nitrocellulose membranes (Bio-Rad, 1704159) using the Trans-Blot Turbo Transfer System (Bio-Rad) for semi-dry blotting at 2.5 A (midi) or 1.3 A (mini) and up to 25 V for 10 minutes. Membranes were cut and blocked with blocking buffer for 1 hour at room temperature before incubation with primary antibodies at 4°C over night. Membranes were washed twice with TBST (0.1%) for 3 minutes before addition of secondary antibodies and incubation for 2

hours at room temperature, before washing another 3 times with TBST (0.1%) for 5 minutes. Antibodies were detected by chemiluminescence by incubating membranes for 2 minutes with the Clarity ECL Western Blotting Substrates (Bio-Rad, 102031309) before imaging in the ChemiDoc XRS+ Imaging System (Bio-Rad). Protein bands were quantified using the ImageLab software v5.2 (Bio-Rad) with automated band detection and background subtraction (disk size 70 mm).

2.4.3. Thermal shift assay

This protocol is adapted from the Nature Protocols publication by Jafari *et al.* [296]. Cells were seeded (3 million cells per 10 cm dish) and left to attach for 24 hours. Compounds were added (final DMSO concentration 0.1% v/v) and cells incubated for 1 hour before being washed with PBS, trypsinised, collected in PBS and centrifuged (300 x g, 3 min). The cell pellet was gently resuspended in 10 mL PBS, centrifuged again (300 x g, 3 min) and resuspended in 1 mL PBS with protease inhibitors (aprotinin and leupeptin, both 1/1,000 dilution). Compounds were added back to samples at the previously used concentrations. Each sample was split into 10 PCR tubes (100 µL) which were heated at different temperatures (40.0°C to 65.0°C) for 3 minutes. Samples were cooled at room temperature for 3 minutes before being put on ice, lysed in 100 µL of a mild detergent lysis buffer prepared at 2X (40 mM Tris HCl pH 7.5, 300 mM NaCl, 1% v/v Triton X100), briefly vortexed and centrifuged at 4°C (17,000 x g, 20 minutes). The supernatant was transferred into a new microcentrifuge tube and stored at -20°C.
Western blots were performed and quantified as described in methods 2.4.2 to assess heat degradation of the compounds' protein targets compared to DMSO controls.

2.4.4. Subcellular fractionation

Cells were seeded in 10 cm or 15 cm dishes and left to attach for 48 hours until 70% confluence was reached. Compounds were added (final DMSO concentration 0.1% v/v) and cells incubated for 6 or 24 hours. Cells were washed twice with ice-cold PBS and 300 µL (10 cm) or 500 µL (15 cm) Buffer A with detergent was added before cells were gently scraped, collected in microcentrifuge tubes and rotated at 4°C for 5 minutes. Samples were centrifuged at 4°C (800 x g, 4 minutes) and both the supernatant and pellet were kept.

The supernatant was transferred into a new tube to which NP-40 was added to a final concentration of 1% v/v, samples vortexed rigorously and centrifuged at 4°C (17,000 x g, 10 minutes). The supernatant was transferred into a new microcentrifuge tube and labelled as 'cytoplasmic fraction'.

The pellet from the previous step was washed once with Buffer A with detergent and once with Buffer A without detergent by flicking the tubes until the pellet is suspended, centrifuging at 4°C (800 x g, 3 minutes) and removing the supernatant. The pellet was resuspended in two volumes of Buffer B (related to pellet size), samples rotated at 4°C for 15 minutes, centrifuged at 4°C (2,000 x g, 5 minutes) and both the supernatant and pellet were kept. The supernatant was transferred into a new tube and centrifuged at 4°C (17,000 x g, 10 minutes). The supernatant was transferred into a new microcentrifuge tube and labelled as 'perinuclear fraction'.

The pellet from the previous step was washed twice with Buffer B by flicking the tubes until the pellet is suspended, centrifuging at 4°C (2,000 x g, 3 minutes) and removing the supernatant. The pellet was resuspended in two volumes of RIPA lysis buffer (related to pellet size), sonicated for five cycles (30 seconds on, 30 seconds off) and centrifuged at 4°C (17,000 x g, 10 minutes). The supernatant was transferred into a new microcentrifuge tube and labelled as 'nuclear fraction'.

All fractions were stored at -20°C (short-term) or -70°C (long-term) and Western blots were performed as described in methods 2.4.2. The following controls were used for the different fractions: cytoplasmic (α-tubulin), perinuclear (GM130), nuclear (Histone H4).

2.4.5. Co-immunoprecipitation

Cell lysates were prepared from 10 cm dishes and the protein concentration determined as described in methods 2.4.1. 1 mg of lysate was diluted with RIPA lysis buffer to 1 mL in a microcentrifuge tube. 20 µL Dynabeads Magnetic Beads (Invitrogen) per sample were washed once in 1 mL RIPA lysis buffer using the DynaMag-2 Magnet (Invitrogen), resuspended in 20 µL RIPA lysis buffer and added to the cell lysate. 2 µg primary antibody or appropriate IgG control was added and samples rotated at 4°C over night. Dynabeads were washed twice with RIPA lysis buffer and three times with PBS before being resuspended in 20 µL of 1X Laemmli sample buffer (4X Laemmli sample buffer diluted to 1X with PBS). Samples were heated to 95°C for 5 minutes and beads were separated using the magnetic rack before lysates were loaded for Western blotting as described in methods 2.4.2.

Dynabeads were matched to the source of the antibody used for co-immunoprecipitation, and primary antibodies used during Western blotting were chosen from a different species to avoid visualisation of the co-immunoprecipitation antibody's heavy (50 kDa) and light (25 kDa) chains (unless otherwise stated), as shown in Table 2.7.

Table 2.7. Co-IP Dynabead and antibody host combination.

Host of co-IP Abs	Dynabeads	Host of primary Abs (Western Blot)
Rabbit	Protein A (10002D)	All mouse
Mouse	Protein G (10004D)	All rabbit

2.4.6. Zeptosens reverse phase protein array

This work was done together with Kenneth Macleod from the Drug Discovery group of Prof Neil Carragher at the University of Edinburgh, UK.

The general procedure for the reverse phase protein array has previously been published by Macleod, Serrels and Carragher [297]. The following section describes the specific method used in this thesis.

Cells were seeded in 6-well plates (MDA-MB-231 400,000 cells/well, MCF-7 600,000 cells/well) and left to attach for 24 hours. Compounds were added (final DMSO concentration 0.1% v/v) and plates incubated for 3 or 24 hours. Cells were washed twice with 3 mL PBS and lysed with 80 µL CLB1 (Bayer Technology Services), scraped and collected in microcentrifuge tubes and incubated at room temperature for 30 minutes with occasional vortexing. Lysates are centrifuged (17,000 x g, 10 minutes) and the supernatant transferred to new microcentrifuge tubes. The protein concentration was determined in a Bradford Assay using the Coomassie Plus Protein Assay (Thermo Scientific) according to the manufacturer's instructions and all samples were adjusted to 2 mg/mL. Samples were stored at -70°C.
20 µL of the samples were diluted 1:10 with spotting buffer CSBL1 (Bayer Technology Services) and a dilution series (0.2, 0.15, 0.1, 0.05 mg/mL) was created with CSBL1 and 10% CLB1. The diluted samples were transferred onto a 384-well plate and printed as single spots onto ZeptoChips using the Nanoplotter 2.1E (GeSim) in a

controlled environment (70% humidity, 14°C). Fluorescently labelled BSA standards were also printed onto the slides. ZeptoChips were blocked for 1.5 hours in blocking buffer BB1 (Bayer Technology Services), washed three times for 2 minutes in distilled water, dried by centrifugation and washed 3 times with 90 µL CAB1 buffer (Bayer Technology Services). Primary antibodies diluted in CAB1 or CAB2 buffer were added and incubated at room temperature overnight, before ZeptoChips were washed three times with CAB1 and 90 µL of appropriate Alexa Fluor conjugated secondary antibodies were added and incubated for 2.5 hours in the dark at room temperature. ZeptoChips were washed three times with CAB1, with the last wash left on, and slides scanned using the ZeptoReader (Zeptosens-Bayer). Exposure times just below saturation of the fluorescent signal were automatically selected for analysis by the ZeptoView 3.1 software and a weighted linear fit through the fourfold dilution series was used to calculate the relative fluorescence intensity (RFI) of each sample. Normalisation to the reference BSA signal was used to compensate for intra- and inter-chip variation. Proteins with very low signal (RFI <0.05) were excluded from analysis. The local normalised RFI values were then normalised to DMSO controls for each cell lines, relative protein abundance plotted and hierarchical clustering performed (Euclidian distance, complete linkage) using the free online Morpheus software (Broad Institute).

2.4.7. Cytokine array

This work was done together with Kenneth Macleod from the Drug Discovery group of Prof Neil Carragher at the University of Edinburgh, UK.

MetBo2 cells were seeded (1.5 million cells / 10 cm dish) and left to attach for 24 hours. Compounds were added (final DMSO concentration 0.1% v/v) and cells pre-treated for 24 hours. Medium was changed and any floating cells were spun down and returned to the dishes. Compounds were added again to 4 mL fresh medium per dish and cells treated for 48 hours. A control sample of medium without cells was incubated for 48 hours. Medium was collected and spun down at 1,000 rpm for 5 minutes, supernatant was transferred into a fresh tube and frozen at -80°C. Cells were washed with PBS, lysed and protein concentration determined as described in methods 2.4.1 for later normalisation.

Oncyte supernova slides (one slide per sample) with 64 sub-arrays are prepared with each subarray being printed with four replicate spots of a different capture antibody

(at 0.2 mg/mL in PBS with 0.05% v/v Tween20) using the Aushon 2470 Arrayer Platform. Slides are blocked with Superblock T20 (Thermo Scientific, 37536) for one hour prior to incubation with sample at 4°C overnight. Slides were washed three times for five minutes in PBST (PBS supplemented with 0.05% v/v Tween20), incubated in Super G blocking buffer (Grace Biolabs, 105101) for 10 minutes and washed again three times in PBST. Slides were incubated with detection antibodies (1:500 in PBST with 5% w/v BSA and 10% v/v Super G blocking buffer) for one hour after which they were washed three times in PBST, incubated for 10 minutes in Super G blocking buffer, washed again three times in PBST and incubated with streptavidin 800 (Li-Cor, 926-32230) diluted 1:500 in PBST with 5% w/v BSA and 10% v/v Super G blocking buffer. Slides were washed three times in PBST, three times in PBS, once with water, centrifuged at 200 x g to dry for five minutes and then air dried in the dark. Slides were imaged and microarray images analysed using Mapix software (Innopsys) by determining the average signal intensity for each spot and subtracting the median background from the adjacent area. The net signal per spot is expressed as relative fluorescence intensity (RFI) and averaged across all four spots per antibody. Proteins with similar RFI as the media only control sample were excluded. RFI value per protein is normalised to the amount of protein present in the respective cell lysate and expressed as percentage of DMSO treated control.

2.5. Other assays

2.5.1. Kinase screening assays

This work was done by Reaction Biology Corporation, USA and the method has previously been described for the same data set by Fraser *et al.* [1].

2.5.2. Hepatocyte stability / Metabolite study

This work was performed by Cyprotex Discovery Limited.

A suspension of cryopreserved human hepatocytes (0.5 x 10^6 viable cells/mL) was incubated with Williams E media (supplemented with 2 mM L-glutamine, 25 mM HEPES) and eCF506 (3 µM, final DMSO concentration 0.25% v/v) at 37°C for 120 minutes. Two control compounds and vehicle controls were included. At six different time points, 50 µL of incubate was transferred to 100 µL acetonitrile and centrifuged at 2500 rpm at 4°C for 30 minutes to remove protein. Supernatants were analysed by LC-MS/MS using Cyprotex generic conditions.
The data was plotted as ln peak area ratio (compound peak area / internal standard peak area) over time, from which the gradient of the line was determined. Half-life ($t_{1/2}$) and intrinsic clearance (CL_{int}) were calculated as follows:

$$\text{Elimination rate constant (k)} = (- \text{gradient})$$
$$\text{Half-life } (t_{1/2}) \text{ (min)} = 0.693 / k$$
$$\text{Intrinsic clearance } (CL_{int}) \text{ (µL / min / million cells)} = V \times 0.693 / t_{1/2}$$
$$\text{with V = incubation volume (µL) / number of cells}$$

Further metabolite profiling of the 60-minute and 120-minute samples was performed using a Q-Tof UPLC-MS/MS platform. This uses a 15-minute gradient where the test compound eludes after 70-80% of the gradient. Samples are compared to a time zero control sample. Analysis is done using the instrument manufacturer's proprietary functions (MS^e) which reports the mass and abundance as percentage of total compound related material of the parent and any metabolites found. Metabolites are identified by searching against a list of expected biotransformations, whilst additional

metabolites are searched for by comparison to time zero control samples. Area percentage will be calculated and may be related to the amount of metabolite based on the assumption that each metabolite is equally as responsive as parent. The combination of fragmentation patterns and internal biotransformation expertise was applied to the data to propose structures for the identified metabolites.

2.5.3. X-ray crystallography

This work was done by Dr Daniel Lietha at the Centro de Investigaciones Biológicas (CIB) in Madrid, Spain.

Expression and purification:

The hSRC kinase domain (residues 254-536) was expressed with an N-terminal 6xHis tag in E.coli (BL21) co-expressed with the YopH phosphatase, as described previously [298]. Pure protein was obtained by Ni-chelate affinity chromatography (HisTrap, GE Healthcare), ion exchange chromatography (Source 15Q column, GE Healthcare) and size exclusion chromatography (Superdex200, GE Healthcare). After the Ni-chelating column, the 6xHis tag was removed by incubation with TEV protease.

Crystallisation:

Purified SRC kinase was concentrated to 6.3 mg/ml (193uM) and incubated with 10 mM eCF506 for 30 min on ice. Crystallisation was performed using the hanging drop, vapor diffusion method. Crystallisation conditions were optimised from [299] with final crystals grown by mixing the protein with equal volume of 6% PEG3350, 300mM ammonium acetate, 0.1M HEPES pH7.5, 10mM TCEP. Crystals were flash frozen in liquid nitrogen after soaking in growth condition with 25% ethylene glycol.

Data collection and structure solution:

Diffraction data collection was carried out at the XALOC beamline of the ALBA synchrotron facility (Barcelona, Spain). Data was integrated to 1.5 Å using XDS [300], scaled with AIMLESS [301] and an initial structure obtained by molecular replacement with PHASER [302] using the SRC kinase domain (pdb:4MXO) as search probe. The structure was refined using Refmac5 [303] and manual rebuilding with Coot [304]. Final R-factors are 18.9/21.4 (R_{work}/R_{free}).

2.5.4. Ames test

This work was done by Sequani Limited, UK.

The mutagenic potential of eCF506 was assessed in four 4 Salmonella typhimurium strains (TA1535, TA1537, TA98, TA100) and 1 Escherichia coli strain (WP2 uvrA), in the presence and absence of a metabolic activation system (S-9 mix). A range of six concentrations of eCF506 up to 5,000 µg / plate were tested in triplicate alongside negative and positive controls (see Table 2.8).

The following components were mixed in an Eppendorf tube:

- 2 mL of L-histidine: D-biotin solution (Salmonella) or tryptophan (Escherichia) supplemented top agar
- 0.1 mL bacterial culture
- 0.5 mL of S-9 mix *or* 0.2 M phosphate buffer
- 0.1 mL solvent (negative control) *or* eCF506 dilution *or* positive control

The mixtures were added to a Petri dish containing minimal agar, which were inverted when set and incubated at 37±3°C. The integrity of the background lawns was assessed and revertant colonies were scored after approx. 66±1 hours using an image analyser. Statistical analysis was carried out using Dunnett's t-test.

Table 2.8. Ames test positive controls.

Strain	Without S-9 mix	With S-9 mix
Salmonella typhimurium		
TA1535	Sodium azide (1 µg / plate)	2-aminoanthracene (2 µg / plate)
TA1537	9-aminoacridine (50 µg / plate)	2-aminoanthracene (4 µg / plate)
TA98	2-nitrofluorence (1 µg / plate)	2-aminoanthracene (2 µg / plate)
TA100	Sodium azide (1 µg / plate)	2-aminoanthracene (4 µg / plate)
Escherichia coli		
WP2 uvrA	4-nitroquinoline-N-oxide (1 µg / plate)	2-aminoanthracene (10 µg / plate)

2.5.5. *Ex vivo* murine choroidal angiogenesis model

This work was done by Oxurion (formerly Thrombogenics), Belgium.

This method was adapted from Shao et al. [305]. Briefly, the choroid attached to the sclera is dissected from mice and embedded in Matrigel™. Compounds were added to the explant culture media and explants treated for 4 days. Explants were imaged, the vessel outgrowth area annotated and calculated and treated samples normalised to vehicle treated control.

2.5.6. Human retinal microvascular endothelial cell cytotoxicity assay

This work was done by Oxurion (formerly Thrombogenics), Belgium.

Primary human retinal microvascular endothelial cells (hRMVEC) were seeded in 96-well plates and left to attach. Compounds were added at different concentrations and cells treated for 24 hours. Cytotoxicity was determined using CellTox™ Green Cytotoxicity assay (Promega) according to the manufacturer's instructions, with higher fluorescence indicating the presence of nonviable cells with permeable cell membranes. Background fluorescence was measured in cell-free wells and subtracted from the final results. Hydrogen peroxide was used as a positive control. Cell morphology was also assessed by microscopy.

2.6. Animal models

2.6.1. Efficacy models

Experiments involving animals were carried out in accordance with the UK Coordinating Committee on Cancer Research guidelines by approved protocol. Animal models assessing the efficacy of eCF506 were done at the Institute of Genetics and Molecular Medicine by Morwenna Muir and Dr John Dawson (MDA-MB-231 xenograft, MetBo2 mammary fat pad) or at the Queen's Medical Research Institute by Dr Xue-Feng Li (MetBo2 bone metastasis), both of which are part of the University of Edinburgh, UK.

2.6.1.1. MDA-MB-231 xenograft model

This work was done by Dr John Dawson and Morwenna Muir of the groups of Prof Valerie Brunton and Prof Margaret Frame at the University of Edinburgh, UK.

MDA-MB-231 tumour fragments were created by injecting MDA-MB-231 cells into each flank of CD1 nude mice (50 million cells / flank). Tumours were allowed to develop up to 8 mm in diameter and were collected before ulceration or necrosis had occurred. Tumours were dissected into 1 mm^3 pieces for transplantation into recipient mice.

Fifteen CD1 nude mice were implanted subcutaneously with MDA-MB-231 fragments bilaterally on both flanks using a 12G trochar with local anaesthesia (ethyl chloride). Tumour growth was monitored by calliper measurements and treatment started after 24 days when average tumour volume reached 20 mm^3. Mice were randomised into three groups and received daily treatment by oral gavage (100 µL per 10 g mouse weight) with vehicle (saline), eCF506 (25 mg/kg) or dasatinib (25 mg/kg). Mice were weighed and tumours measured twice a week for 25 days. Mice were dosed 2 hours prior to culling by cervical dislocation after which tumours were removed and fixed in formalin for paraffin embedding.

2.6.1.2. MetBo2 bone metastasis model

This work was done by Dr Xue-Feng Li in the group of Dr Bin-Zhi Qian at the University of Edinburgh, UK.

FVB mice were anesthetised by isoflurane and injected with 100,000 MetBo2 cells into the left ventricle. Tumour growth was monitored by bioluminescence imaging on the Optima imager (Biospace). Bone metastasis tumours were allowed to grow for 7 days until the signals of bone metastasis were clearly detected by Optima imager. 11 mice that developed tumours in the hind legs or jaw were included in the study. Mice were randomized and put into control (5 mice) or treatment (6 mice) groups. Treated mice received daily eCF506 by oral gavage (40 mg/kg in ultrapure water, dissolved at 8 mg/mL) and control group mice received vehicle only. Mice were imaged twice a week and the bioluminescence intensity of tumours in the hind legs or jaw was quantified by M3 software. Mice were culled when the tumour burden became too great.

2.6.1.3. MetBo2 mammary fat pad model

This work was done by Dr John Dawson and Morwenna Muir of the groups of Prof Valerie Brunton and Prof Margaret Frame at the University of Edinburgh, UK.

Eleven FVB mice and twelve CD1 nude mice were anesthetised by isoflurane and implanted in the left 4th mammary fat pad with one million MetBo2 cells. Tumours were allowed to grow until they reached around 50 mm^3 (FVB) or 40 mm^3 (CD1) in size after which mice were randomly allocated into two groups. Mice were treated with vehicle (3 mM sodium citrate buffer pH 3.0) or eCF506 (40 mg/kg, dissolved at 4 mg/mL in vehicle) once daily by oral gavage (100 µL per 10 g mouse weight) for 28 days. Tumour size was measured by calliper and mice weighed twice a week. Mice were culled by cervical dislocation once tumour size reached 15 mm in diameter. After the initial treatment phase, surviving mice were monitored until tumours relapsed and treatment restarted once average tumour size reached 280 mm^3 (FVB) or 250 mm^3 (CD1), except for one mouse that showed no tumour regrowth. Mice were dosed 2 hours prior to culling by cervical dislocation after which tumours were removed and fixed in neutral buffered formalin for immunohistochemistry and H&E staining.

2.6.1.4. Immunohistochemistry

Formalin-fixed tissues were embedded in paraffin wax blocks from which sections were cut for haemotoxylin and eosin (H&E) staining and immunohistochemical analysis. H&E staining was performed according to standard procedures by the Pathology Technical Services team at the Institute of Genetics and Molecular Medicine, University of Edinburgh, UK. Immunohistochemistry was performed by me as described in the following.

Paraffin embedded tumours were cut into 5 µm thick sections using a microtome, placed on SuperFrost Plus™ (Thermo Scientific) slides and dried at 40°C for 24 hours. Paraffin was removed by immersion of slides in xylene for 5 minutes, followed by rehydration in decreasing ethanol baths (100%, 100%, 80%, 50%) for 3 minutes each and rinsing in water. Antigens were retrieved by boiling in citrate buffer pH 6.0 in a pressure cooker (121°C) for 8 minutes. Slides were left to cool and endogenous peroxidases were blocked using Dako REAL Peroxidase-Blocking solution (Agilent, S2023) for 5 minutes. After washing in water, slides were incubated with Dako Serum-free Protein Block (Agilent, X0909) for 30 minutes before primary antibodies diluted in Dako Background Reducing Antibody Diluent (Agilent, S3022) were added and slides incubated in a humid chamber at 4°C overnight. Following two washes in TBST (0.025%) for 5 minutes, slides were incubated with Dako Goat Anti-Rabbit HRP-linked secondary antibody (Agilent, K4003) for 1 hour at room temperature. Slides were washed twice in TBST (0.025%) for 5 minutes followed by staining with Dako Envision DAB+ kit (Agilent, K3468) for 5 minutes, rinsing in water for 2 minutes and immersion in haematoxylin for 100 seconds. Slides were rinsed in water and immersed in Scott's tap water for 4-8 minutes until tissue appeared blue, before being dehydrated in increasing ethanol baths (50%, 80%, 100%, 100%) and xylene for 2 minutes each. Dry slides were mounted onto coverslips using DPX, left to dry for 36 hours and imaged using the Nanozoomer (Hamamatsu).

Images were analysed using the free QuPath software tool by automatically counting the number of positively stained cells as percentage of all cells in the tumour area [306].

2.6.2. Acute toxicity model

This work was done by Evotec, France.

The aim of this study was to determine the maximum tolerated dose (MTD) of eCF506 following a single oral administration by gavage to male and female Sprague-Dawley rats.

6 to 8 week-old Sprague-Dawley rats were obtained from Janvier Labs, France. After an acclimatisation period of at least 5 days, the 9 male and 9 female rats were split randomly into five groups depending on their weight (Table 2.9). eCF506 was formulated in citrate buffer as shown in Table 2.9 and administered once by oral gavage, with the quantity being adjusted for the respective weight of the rat and received dose being within ±10% of the theoretical dose.

The doses of groups 3 and 4 were chosen based on results from groups 2 and 3, respectively. The dose volume of group 3 was changed to maintain the same formulation as group 2, and the formulation of group 4 was changed to maintain the same pH and solubility as groups 2 and 3. The changed dose volume and formulation of the vehicle was tested on rats in group 5.

Table 2.9. Treatment groups of acute toxicity study.

Group	No. of rats / group / sex	eCF506 dose (mg/kg)	Dose volume (mL/kg)	Formulation
1	2	-	10	50 mM citrate buffer pH 3.0
2	2	200	10	50 mM citrate buffer pH 3.0
3	2	400	20	50 mM citrate buffer pH 3.0
4	2	700	20	100 mM citrate buffer pH 3.0
5	1	-	20	100 mM citrate buffer pH 3.0

Animal observations for adverse clinical signs or premature death were recorded pre-dosing and 1, 2, 4, 6, 8 and 24 hours post-dosing and scored as described in Table 2.10. Body temperatures were measured pre-dosing and 4, 8 and 24 hours post-dosing and body weights were measured pre- and post-dosing. Blood samples were collected 24 hours after dosing from the vena cava and analysed on a VetScan HM5 haematology analyser (Abaxis) for white blood cell count (10^9/L), lymphocyte count (10^9/L), monocyte count (10^9/L), neutrophil count (10^9/L), red blood cell count (10^{12}/L), haemoglobin concentration (g/dL), haematocrit (%), mean globular volume (fL) and

platelets (10^9/L). Post-mortem examinations were performed 24 hours after dosing. Rats were anaesthetised by isoflurane inhalation and exsanguinated prior to cervical dislocation. Necropsy was performed with animals being examined visually for external abnormalities and palpable masses; abnormalities in the abdominal, thoracic and cranial cavities and contents; and gross abnormalities on organs after their removal. No statistical analysis was performed due to the low number of animals per groups (n = 1 or 2).

Table 2.10. Clinical scores. HEP = humane end point; - = no criteria defined. Total scoring >2 = additional care considered (e.g. extra fluid), >4 = veterinarian consulted, >6 = HEP implemented.

Score	Coat Condition	Environment	Face	Motor activity	Respiratory	Neurological signs	Provoked behaviour	Mucous	Body weight
0	Normal	Normal	Normal	Normal	Normal	No clinical signs	Normal	Normal	<5 % weight loss
1	Coat slightly unkempt / alopecia	Faecal soiling	Grimace / half closed eyes	Slightly abnormal gait / posture	Tachypnoea (fast breathing) or nasal discharge	Falling over / cycling / stereotypy	Tense and nervous on handling	Pallor / redness	5-10 % weight loss
2	Coat wound or swelling or slight piloerection	Loose stools or diarrhoea	-	Markedly abnormal gait / posture	Coughing	Myoclonia / seizures	-	-	11-15 % weight loss
3	Marked piloerection	-	-	Hunched posture	Dyspnea (difficulty breathing)	-	Markedly distressed on handling (e.g. shaking, vocalising, aggressive)	Icterus / cyanosis	16-20 % weight loss
HEP	-	Blood in diarrhoea	-	Ataxia	Asphyxia	Convulsions / paralysis	-	-	>20 % weight loss

2.6.3. Pharmacokinetic models

2.6.3.1. Bioavailability and pharmacokinetics parameters assessment in rats

This work was done by Evotec, France.

Pharmacokinetic parameters were tested in 7-week-old male Sprague-Dawley rats, with three rats per dose and per route, which were treated as follows: intravenous (IV) injection (1 mg/kg eCF506 in 50 mM acetate buffer saline, pH 4.6, given at 2 mL/kg), oral (PO) gavage (10 mg/kg or 200 mg/kg in 50 mM citrate buffer, pH 3.0, given at 5 mL/kg). Blood was collected from a cannula previously implanted under isoflurane anaesthesia in the jugular vein; serial blood micro-sampling (200 µL) was performed at the following time points:

- IV dosing: 2 min, 7 min, 15 min, 30 min, 1 hr, 2 hrs, 4 hrs, 6 hrs, 7 hrs, 24 hrs
- PO dosing: pre-dose, 15 min, 30 min, 45min, 1 hr, 2 hrs, 4 hrs, 6 hrs, 7 hrs, 24 hrs

Blood was centrifuged (10,000 x g, 3-4 minutes, 4°C) and two aliquots of plasma (at least 50 µL) were collected per time point in 2 mL Safelock tubes and immediately snap frozen. Plasma samples were analysed by LC-MS/MS, with a lower limit of quantification of 10 ng/mL.

2.6.3.2. Blood-brain-barrier penetration in mice

This work was done by Dr Alaide Morcavallo and Nikita Locket (group of Prof Louis Chesler) and Louise D Johnson and Ruth R Ruddle (group of Dr Florence I Raynaud) at the Institute of Cancer Research, London, UK.

17 NSG mice (highly immunodeficient; lack T-cells, B-cells, natural killer cells, some cytokine signalling pathways) were randomised into two groups and received intraperitoneal injections of either vehicle (3 mice) or 40 mg/kg eCF506 (14 mice). Mice in the treatment group were culled after 0.5, 1, 2, 4 or 8 hours at which point plasma samples and brain tissue samples were taken and frozen.

Calibration standards

Calibration and quality control solutions were prepared in DMSO from 1 mM stocks for eCF560. Calibration standards used for spiking were prepared on the Hamilton robot over the dynamic range 50 nM to 100 µM in DMSO. Quality control standards were also prepared at 150, 4000, and 75000 nM on the Hamilton robot. A stock solution of Olomoucine internal standard was prepared in DMSO at a concentration of 1 mM. A working internal standard solution was prepared at a concentration of 250 nM in methanol.

Plasma and tissues sample preparation

Plasma and tissue samples were thawed on ice. All tissues were homogenised in 3 mL/g PBS and kept on ice. 100 µL aliquots of untreated mouse plasma or tissue homogenates were spiked with 10 µL of the appropriate calibration or quality control standard solutions. 100 µL aliquots of the unknown samples were spiked with 10 µL DMSO. Where appropriate, unknown plasma samples were diluted with untreated plasma.

Protein precipitation

Spiked calibration standards, quality control standards and unknown samples were protein precipitated with 300 µL methanol containing 250 nM internal standard. Blank samples were prepared by spiking 100 µL untreated plasma/tissue with 10 µL DMSO and protein precipitated with 300 µL methanol. All samples were centrifuged at 3700 rpm for 20 minutes at 4°C. Supernatants were transferred into a new 96-well plate and subsequently analysed by LC-MS/MS.

LC-MS/MS Method

Extracted plasma and tissue samples were analysed by LC-MS/MS for the quantification of eCF560 and Olomoucine (Sigma) as internal standard using an Acquity H Class LC system coupled with a Waters TQS triple mass spectrometer (Waters). Compounds were separated on a Kinetex C18, 2.6 µ 50x2.1 mm analytical column (Phenomenex) with a 2 µL injection volume. The mobile phase consisted of methanol and 0.1% formic acid with a constant flow rate of 0.6 mL/min at 55°C. A linear gradient was initiated from the 5% methanol/95% formic acid starting conditions over 3 minutes before sustaining at 100% organic for 1 minute. The column was then re-equilibrated with the original mobile phase for a further 1 minutes.

Analytes were ionised by electrospray interface in positive mode and detected by multiple reaction monitoring. The characteristic ion transitions monitored were m/z 511.25-410.17 for eCF560, and 299.1-176.2 for Olomoucine. Ionisation was optimised with a desolvation gas temperature of 600°C and flow rate of 1000 L/hr. The nebulizer gas flow was set to 7 bar with the capillary charge at 3 kV. Fragmentation in the presence of argon was achieved using a collision energy of 32 V for eCF560 and 26 V for Olomoucine. Data acquisition was performed using Targetlynx V4.1 SCN876. The assay was linear over the range 5-1000 nM in plasma and 5-5000 nM in brain homogenate.

2.6.3.3. Retinal phospho-SRC inhibition in mice

This work was done by Oxurion (formerly Thrombogenics), Belgium.

8-10-week-old male C57BL/6J mice received intraperitoneal injections of vehicle (PBS) or eCF506 (10 mg/kg). One hour later, mice received intravitreal injections of VEGF. After 30 minutes, mice were euthanized by an overdose of Nembutal and retinas were isolated after enucleation, stored at -80°C and analysed by Western blot for phospho-SRC and total SRC.

2.7. Data analysis

Graphs were plotted and statistical analysis was performed using GraphPad Prism 7.0 software, unless stated otherwise. Details of statistical tests performed are provided in figure or table legends.

Chapter 3. *In vitro* assessment of eCF506

Fraser *et al.* developed eCF506 as an inhibitor with high potency in breast cancer cells by using a ligand-based design approach coupled with phenotypic screening [1]. In reiterative steps of design, synthesis and screening, they developed several new compounds that improved on the scaffold PP1's anti-proliferative activity against two breast cancer cell lines (MCF-7, MDA-MB-231). This led to the discovery of the selective SRC/non-ABL inhibitor eCF506 with similar potency in cell viability and migration assays as the dual SRC/ABL inhibitor dasatinib.

This chapter continues from these findings by screening eCF506 across many different cell lines to determine its potential use across various types and subtypes of cancer. Some of these cell lines were re-tested in a spheroid assay to determine the consistency between 2D and 3D models. *In vitro* models of angiogenesis were also assessed due to the established role of SRC in this hallmark of cancer. Furthermore, eCF506's cytostatic properties were confirmed in a cell cycle assay and stratification of cell line response based on phospho-SRC levels was attempted.

In vitro testing of eCF506 was done in comparison to dasatinib and other SRC and/or ABL inhibitors to identify the best-in-class inhibitor and establish eCF506's relative potency. The outstanding selectivity of eCF506 in comparison to these clinically approved inhibitors is highlighted in a side-by-side comparison of their full kinome screening data. Further experiments were performed to confirm the unique selectivity for SRC over ABL in cellular models.

This chapter explores the following aims:

- Assessment of eCF506's anti-proliferative properties in different cancers and comparison to other dual SRC/ABL inhibitors.
- Comparison of eCF506's anti-proliferative effects in a 3D spheroid model.
- Validation of eCF506's cytostatic effect in a cell cycle assay.
- Exploration of the anti-angiogenic properties of eCF506.
- Comparison of eCF506's selectivity and potency for SRC kinase inhibition.

3.1. eCF506 has anti-proliferative and anti-angiogenic properties *in vitro*

3.1.1. eCF506 is as potent as dasatinib at inhibiting proliferation in 2D cell viability assays

In order to get an overview of which cancers show sensitivity to eCF506 treatment, it was screened against a genetically-characterised panel of hundreds of cell lines representing many different cancers at the Wellcome Sanger Institute, UK (see chapter 3.1.1.1). Based on these results, as well as the previous focus on breast cancer, eCF506 was then tested in more detail in 29 breast and ovarian cancer cell lines that were available in-house. The aim of this second screen was to establish the potency of eCF506 in comparison to four other SRC and/or ABL kinase inhibitors (dasatinib, bosutinib, saracatinib, imatinib) that are already used in the clinic or are in late stage development (see chapter 3.1.1.2). Last, eCF506 was included in a high-throughput screen of oesophageal cancer cell lines that was performed by the Drug Discovery group of Prof Neil Carragher at the University of Edinburgh, in which dasatinib had previously been identified as a hit (see chapter 3.1.1.3).

The testing of eCF506 in these three different screens and the comparison to other inhibitors with a similar target profile gives a better understanding of eCF506's potential in different types of cancer.

3.1.1.1. Genomics of Drug Sensitivity in Cancer (GDSC) cell line panel

This work was done by the group of Dr Mathew Garnett at the Wellcome Sanger Institute, UK.

eCF506 was screened against 750 cell lines across a variety of cancers from the Genomics of Drug Sensitivity in Cancer (GDSC) cell line collection at the Sanger Institute, UK. Cells were treated for 72 hours and cell viability determined using Cell Titer Glo 2.0® (Promega). Dose-response curves were fitted automatically to determine the IC_{50} values. After excluding cell lines that did not match quality control criteria, the IC_{50} values of 739 cell lines for eCF506 were included in the analysis.

40 of 739 cell lines were classified as being sensitive to eCF506 by having an IC_{50} value below 1 µM (Table 3.1); in comparison, dasatinib, which was previously screened by the Sanger Institute, inhibits 188 of 761 cell lines at the same cut-off [307]. Only one breast cancer cell line (HDQ-P1) of the 43 tested was sensitive to eCF506; this set included MDA-MB-231 and MCF-7, which had IC_{50} values of 13.1 µM and 81.9 µM, respectively. These concentrations were around one thousand-fold higher than those previously reported by Fraser *et al.* in the same cell lines (authenticated by STR analysis) [1]. The lack of sensitivity is surprising and the previous screening of dasatinib also showed much higher IC_{50} values of 1.33 µM (MDA-MB-231) and 273 µM (MCF-7). However, another study found dasatinib had similar potency in both cell lines as reported by Fraser *et al.* and thus supports the values reported in the paper [308]. A possible reason for the discrepancy could be the different screening set up used in the GDSC screen (1536-well plates, 3-day treatment, Cell Titer Glo® readout) compared to the previous experiments in the group (96-well plates, 5-day treatment, PrestoBlue™ readout), with the GDSC set up likely to favour the discovery of cytotoxic rather than cytostatic drug effects. Nevertheless, the third study showed similar results with dasatinib to Fraser *et al.* after only 48 hours of treatment (96-well plates, MTT assay readout). This unexplained loss of activity in the GDSC screen cautions against overinterpreting the results from this high-throughput screening.

Seven of the 40 cell lines sensitive to eCF506 are classified as chronic myeloid leukaemia (CML), which is mostly caused by a mutant form of ABL kinase (see Table 3.1). As only ten CML cell lines were tested in total, this suggests that eCF506 is still a potent inhibitor of ABL signalling with potential applications in CML, despite its superior selectivity for SRC kinase.

A promising new finding was the apparent sensitivity of ovarian cancer; six of 24 ovarian cancer cell lines responded at nanomolar levels to eCF506, three of which were among the top five results from the screen. The role of SRC in ovarian cancer has been studied by multiple groups who identified SRC as a potential target for ovarian cancer growth and stem cell survival; SRC inhibitors are also being tested in clinical trials of ovarian cancer [153,309–311].

Several cancer subtypes appear to be mainly resistant to eCF506. While one acute myeloid leukaemia cell line was very sensitive, all other 17 cell lines had IC_{50} values over 40 µM. Of the 37 small-cell lung cancer cell lines included in the screen, only

nine had values below 100 µM. Unexpectedly, all 43 colorectal cancer cell lines had IC_{50} values of 3.5 µM or higher, even though this cancer type has repeatedly been associated with SRC hyperactivation [312]. It is likely that the observed discrepancy between IC_{50} values from the GDSC screen and independent studies means that some of these cell lines could be found more sensitive in other assays.

Analysis of the dataset by the Sanger Institute showed a correlation between sensitivity to eCF506 and the BCR-ABL fusion protein as well as mutations in BRAF, NRAS or KRAS. While the link to BCR-ABL is likely due to eCF506's ability to inhibit ABL signalling, other studies have shown that SRC inhibition is indeed able to overcome acquired BRAF and NRAF mutations *in vitro* and can be useful in KRAS mutant pancreatic cancer [238,313–315]. However, due to the discrepancy between sensitivity seen in the GDSC screen and in cell viability assays in our group, care should be taken not to overinterpret these results. Nevertheless, they served as a good starting point to investigate eCF506 in other cancers, such as ovarian cancer, and further investigation into the particular sensitivity of ovarian cancer cell lines will be discussed in the following chapter 3.1.1.2.

Table 3.1. List of cell lines from GDSC screen of eCF506 with IC_{50} values <1 μM.

Cell line	Cancer	IC50 (μM)
SU-DHL-6	lymphoid neoplasm diffuse large B-cell lymphoma	0.04838
CTV-1	acute myeloid leukemia	0.07673
OVMIU	ovarian serous cystadenocarcinoma	0.10090
IGROV-1	ovarian serous cystadenocarcinoma	0.10237
DOV13	ovarian serous cystadenocarcinoma	0.13629
NCI-H322M	lung adenocarcinoma	0.17467
JURL-MK1	chronic myelogenous leukemia	0.26472
SW982	unclassified (Soft tissue)	0.33618
NB69	brain neuroblastoma	0.35232
HDQ-P1	breast invasive carcinoma	0.38067
CAL-39	cervical squamous cell carcinoma and endocervical adenocarcinoma	0.38743
ALL-SIL	acute lymphoblastic leukaemia	0.39530
KU812	chronic myelogenous leukemia	0.40916
NCI-H1755	lung adenocarcinoma	0.42715
CAL-54	kidney renal clear cell carcinoma	0.44364
NCI-H2795	mesothelioma	0.44421
SU-DHL-5	lymphoid neoplasm diffuse large B-cell lymphoma	0.45453
PA-1	unclassified (Ovary)	0.46028
BPH-1	unclassified (Prostate)	0.50062
LAMA-84	chronic myelogenous leukemia	0.51507
FLO-1	oesophageal carcinoma	0.61079
HCC1806	Unclassified (Breast)	0.61954
LOXIMVI	skin cutaneous melanoma	0.63853
A704	kidney renal clear cell carcinoma	0.67268
OVTOKO	ovarian serous cystadenocarcinoma	0.69597
BV-173	chronic myelogenous leukemia	0.71934
CML-T1	chronic myelogenous leukemia	0.72407
TOV-21G	ovarian serous cystadenocarcinoma	0.73398
CHP-212	brain neuroblastoma	0.73961
PSN1	pancreatic adenocarcinoma	0.75017
KARPAS-1106P	lymphoid neoplasm diffuse large B-cell lymphoma	0.75290
SW1710	bladder urothelial carcinoma	0.79980
TE-8	oesophageal carcinoma	0.81202
SAT	head and neck squamous cell carcinoma	0.87338
EM-2	chronic myelogenous leukemia	0.88603
CAPAN-2	pancreatic adenocarcinom	0.89426
OC-314	ovarian serous cystadenocarcinoma	0.90952
MOG-G-CCM	brain lower grade glioma	0.91521
LXF-289	lung adenocarcinoma	0.94356
MEG-01	chronic myelogenous leukemia	0.95140

3.1.1.2. Breast and Ovarian cancer cell line panel

Part of the work with ovarian cancer cells was done by Anna Wijngaard as part of her honours project under my supervision.

The anti-proliferative properties of eCF506 were tested alongside a panel of three approved or late stage dual SRC/ABL kinase inhibitors (dasatinib, bosutinib, saracatinib) and one ABL kinase inhibitor (imatinib) in 16 breast cancer and 13 ovarian cancer cell lines. Cells were seeded in 96-well plates with compounds being added two days later and plates were treated for a total of five days. Cell viability was assessed before and after treatment using the resazurin-based PrestoBlue™ (Invitrogen) reagent that measures metabolic activity. By taking into account the cell viability before treatment it is possible to distinguish between cytotoxic and cytostatic effects, which allows the calculation of the concentration needed to inhibit cell proliferation by 50% (growth inhibition 50%, GI_{50}) or 100% (total growth inhibition, TGI). The GI_{50} and TGI values were determined for all 29 cells lines from three biological repeats, ranked by sensitivity to eCF506 and plotted in Figure 3.1; exact values are shown in Table 3.2. The data shows that the five tested SRC and ABL kinase inhibitors have mainly anti-proliferative but not cytotoxic effects in breast and ovarian cancer cell lines at sub-micromolar concentrations. While cytotoxic effects can be observed in the micromolar range (see Appendix A.1), those are likely due to off-target effects that commonly occur at high concentrations with kinase inhibitors that target the ATP-binding pocket [12].

eCF506 and dasatinib exhibited the lowest GI_{50} values of all five inhibitors. Values were often similar for both compounds in the same cell line, with larger differences (e.g. MCF-7, ZR-75.1) often due to smaller shifts in the biphasic dose-response curves (see Appendix A.1). However, GI_{50} values for eCF506 and dasatinib also showed the greatest variability between the cell lines tested; while 50% growth inhibition was observed in some at low double-digit nanomolar concentrations, other cell lines required concentrations up to one thousand-fold higher. Bosutinib and saracatinib generally had less variability in their GI_{50} values between cell lines, as they were overall less potent, while imatinib consistently showed low potency with concentrations of at least 4 µM and in some cases more than 100 µM required to halve cell proliferation. In the subset of cell lines that can be classified as sensitive to eCF506 and dasatinib (GI_{50} <500 nM), bosutinib and saracatinib always performed

worse in comparison and their GI_{50} values do not appear to correlate with sensitivity to eCF506 or dasatinib.

Total growth inhibition is generally only observed at micromolar concentrations in most cell lines, with bosutinib often being more potent than the other inhibitors. One reason for this is that cell lines often exhibit a biphasic dose-response curve when treated with eCF506 and dasatinib, while bosutinib usually exhibits a normal nonlinear curve with a steep slope, albeit at higher concentrations (see Appendix A.1). Consequently, eCF506 and dasatinib are more potent at partially inhibiting cell proliferation but require much higher concentrations to stop cell growth completely. A possible explanation for this is that eCF506 and dasatinib are more potent SRC kinase inhibitors, as suggested by their IC_{50} values obtained in isolated kinase screens, while bosutinib is less potent but inhibits several targets at once, eliciting a stronger cellular effect at higher concentrations (see Table 1.3 in chapter 1.3.1).

Seven of the 16 breast cancer cell lines tested are sensitive to eCF506 (GI_{50} <500 nM) (see Figure 3.1). All of them are classified as either triple negative or oestrogen receptor positive breast cancer, with the exception of JIMT-1, which was derived from a HER2-positive patient with trastuzumab resistance. Source and type of the breast cancer cell lines does not appear to correlate with sensitivity (see Table 3.2).
Of the 13 ovarian cancer cell lines tested, 8 were sensitive to eCF506 and half of these have been classified as clear cell carcinoma (see Figure 3.1 and Table 3.2). The PEO cell lines tested were taken from two high-grade serous ovarian cancer patients before and after diagnosis of clinical cisplatin resistance. While these cells often gave variable results, dasatinib was generally more potent than eCF506 in all five cell lines. Opposite trends were observed in the matched sets, with cisplatin-resistant cells being less sensitive to kinase inhibitors in one set but showing higher sensitivity in the other one.

(a)

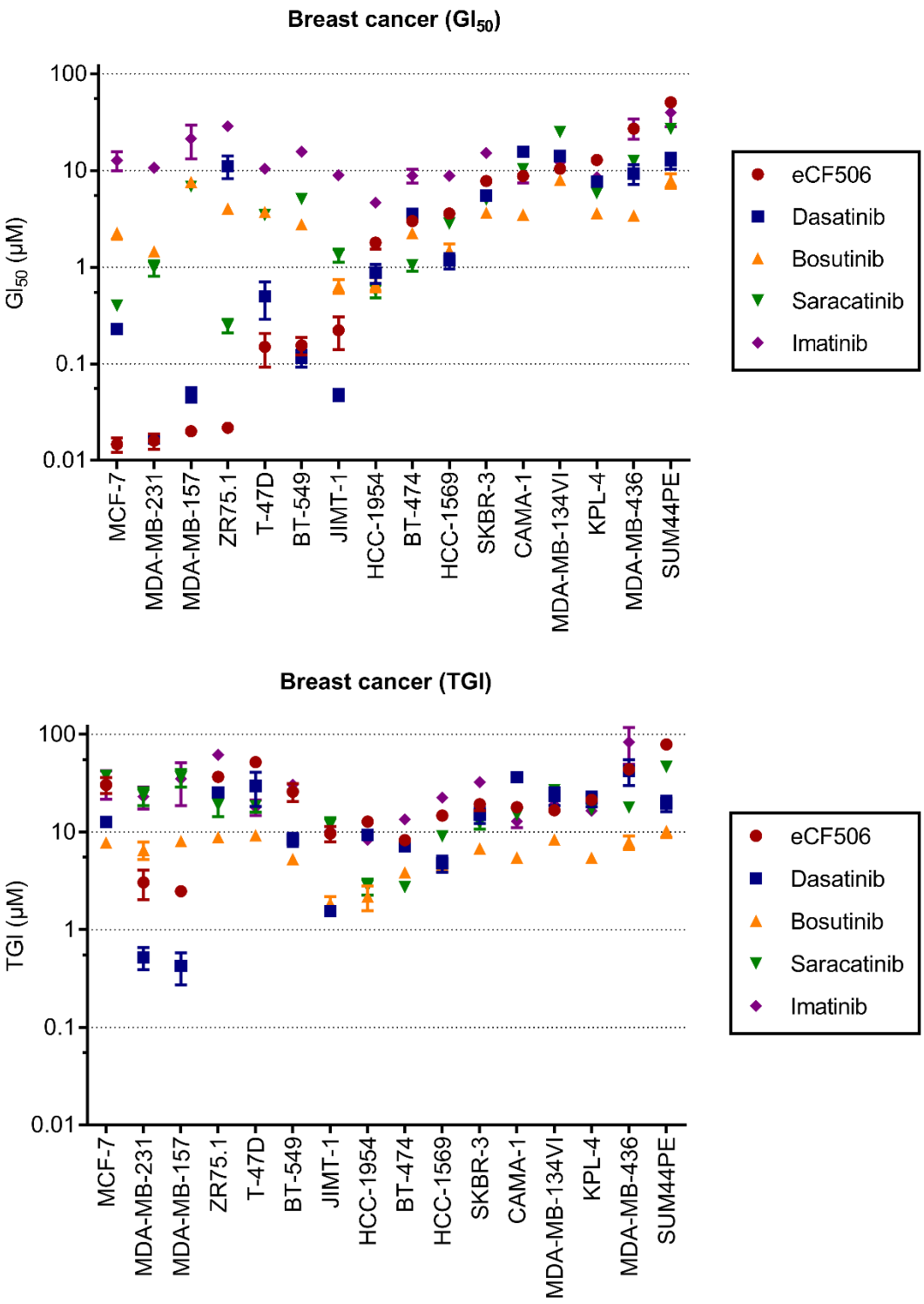

Figure continued on next page

Figure continued from previous page

(b)

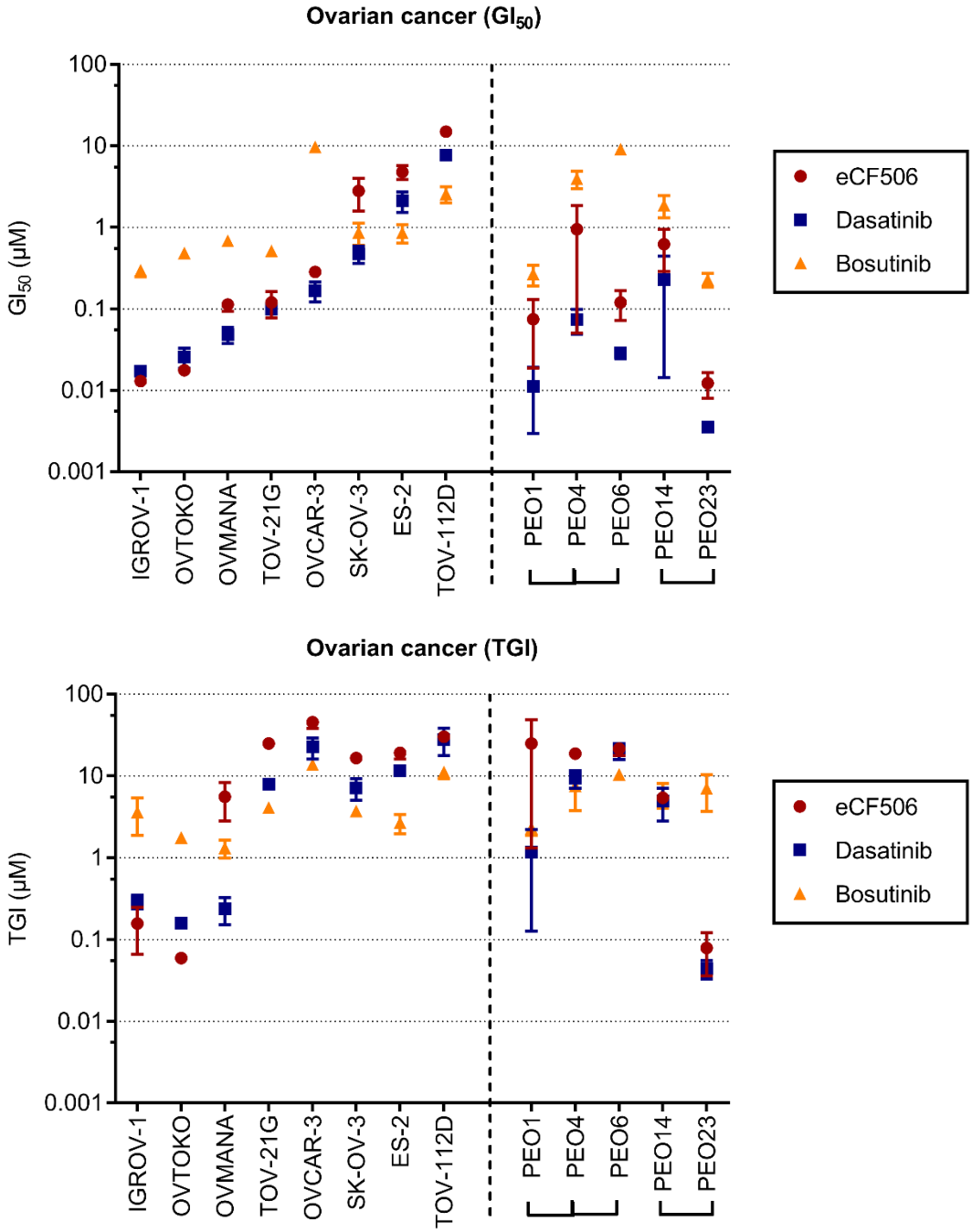

Figure 3.1. Anti-proliferative effects of SRC/ABL kinase inhibitors in breast and ovarian cancer cell lines. (a) Panel of 16 human breast cancer cell lines tested and ranked by sensitivity to eCF506. (b) Panel of 13 human ovarian cancer cell lines tested and ranked by sensitivity to eCF506; PEO cell lines represent two patients before and after clinical cisplatin resistance. Effects on cell proliferation were measured after 5 days of treatment using PrestoBlue™ reagent and curves were fitted using GraphPad Prism 7. GI_{50} and TGI values represent the average of three biological replicates with standard error.

Table 3.2. GI_{50} and TGI values. (a) Ovarian cancer cell lines. (b) Breast cancer cell lines. GI_{50} (white) and TGI values (grey) values represent the average of three biological replicates rounded to three significant figures with standard deviation shown in brackets (in µM). Ovarian cancer subtypes: HGSOC = high-grade serous ovarian cancer, CCC = clear cell carcinoma, EC = endometrioid adenocarcinoma. Breast cancer sources: PBr = primary breast, PE = pleural effusion, A = ascites. Breast cancer type: AC = adenocarcinoma, DC = ductal carcinoma, MC = metaplastic carcinoma, M = medullary carcinoma, LC = lobular carcinoma. Breast cancer subtypes: HER2+ = HER2 amplified, ER+ = oestrogen receptor expressing, TNBC = triple negative breast cancer lacking ER, PrR and HER2. Breast cancer subgroups: Luminal A (ER+, PR±, HER2-, Ki67 low), Luminal B (ER+, PR±, HER2+, Ki67 high), Basal A (luminal-like), Basal B (basal-like, claudin-low), HER2 (ER-, PR-, HER2 amplified).

(a) Ovarian cancer

	Subtype		eCF506	Dasatinib	Bosutinib
Ovarian					
ES-2	CCC / HGSOC		4.80 (1.61)	2.12 (1.03)	0.856 (0.375)
			19.2 (5.47)	11.7 (1.92)	2.68 (1.24)
IGROV-1	EC / CCC		0.0130 (0.00128)	0.0173 (0.00267)	0.298 (0.0861)
			0.157 (0.158)	0.294 (0.0962)	3.64 (3.05)
OVCAR-3	HGSOC		0.285 (0.0606)	0.168 (0.0791)	9.74 (0.914)
			45.5 (12.4)	22.7 (11.3)	13.8 (2.32)
OVMANA	CCC		0.113 (0.0337)	0.0485 (0.0190)	0.682 (0.181)
			5.58 (4.75)	0.239 (0.152)	1.32 (0.565)
OVTOKO	CCC		0.0177 (0.00451)	0.0258 (0.0125)	0.486 (0.0234)
			0.0596 (0.00207)	0.159 (0.0118)	1.78 (0.225)
PEO1	HGSOC patient (Cisplatin / 5-fluorouracil / Chlorambucil)	Post-treatment	0.0744 (0.0964)	0.0111 (0.0142)	0.268 (0.133)
			25.1 (41.1)	1.17 (1.81)	2.32 (0.731)
PEO4		Clinical resistance	0.950 (1.56)	0.0735 (0.0430)	3.95 (1.64)
			18.8 (4.79)	9.35 (3.92)	7.54 (6.49)
PEO6		Prior to death	0.120 (0.0830)	0.0291 (0.00815)	9.14 (0.704)
			21.7 (6.61)	20.4 (7.77)	10.5 (1.79)
PEO14	HGSOC patient (Cisplatin / Chlorambucil)	Chemo-naive	0.621 (0.575)	0.229 (0.371)	1.88 (0.985)
			5.41 (1.12)	4.95 (3.72)	6.07 (3.52)
PEO23		Relapse	0.0123 (0.00731)	0.00353 (0.000673)	0.228 (0.0757)
			0.0789 (0.0746)	0.0442 (0.0195)	7.06 (5.81)
SK-OV-3	Unclassified		2.80 (2.10)	0.474 (0.195)	0.864 (0.449)
			16.6 (2.49)	7.18 (3.72)	3.73 (0.898)
TOV-112D	EC		15.0 (3.12)	7.75 (0.660)	2.58 (0.994)
			30.1 (3.74)	28.1 (17.9)	11.2 (3.42)
TOV-21G	CCC		0.120 (0.0740)	0.0998 (0.0193)	0.515 (0.0785)
			25.1 (6.62)	7.98 (1.56)	4.11 (0.949)

Table continued on next page

Table continued from previous page

(b) Breast cancer

	Source	Type	Subtype (Subgroup)	eCF506	Dasatinib	Bosutinib	Saracatinib	Imatinib
Breast Cancer								
BT-474	PBr	DC	HER2+ (HER2)	2.99 (0.287)	3.56 (0.430)	2.25 (0.187)	1.05 (0.250)	8.80 (2.46)
				8.28 (0.900)	7.15 (1.34)	3.86 (0.272)	2.72 (0.359)	13.4 (1.92)
BT-549	PBr	DC	TNBC (Basal B)	0.155 (0.0564)	0.115 (0.0406)	2.78 (0.159)	5.07 (1.07)	15.7 (2.41)
				25.9 (9.30)	8.40 (2.26)	5.29 (0.737)	24.2 (2.00)	30.5 (7.61)
CAMA-1	PE	AC	ER+ (Luminal A)	8.75 (0.464)	15.6 (0.938)	3.49 (0.103)	10.3 (0.831)	8.64 (2.16)
				18.0 (1.90)	36.6 (5.27)	5.46 (0.0786)	15.0 (2.93)	12.8 (3.04)
HCC-1569	PBr	MC	HER2+ (Basal A-HER2)	3.59 (0.352)	1.17 (0.378)	1.49 (0.422)	2.81 (0.392)	8.84 (1.17)
				14.7 (2.45)	4.78 (1.57)	4.59 (1.11)	9.06 (1.90)	22.5 (4.72)
HCC-1954	PBr	DC	HER2+ (Basal A-HER2)	1.79 (0.446)	0.879 (0.341)	0.665 (0.196)	0.568 (0.149)	4.65 (0.204)
				12.8 (0.521)	9.34 (1.23)	2.19 (1.08)	2.78 (0.903)	8.30 (0.811)
JIMT-1	PE	DC	HER2+ (HER2)	0.222 (0.141)	0.0484 (0.0119)	0.638 (0.180)	1.33 (0.368)	8.92 (0.929)
				9.65 (2.99)	1.56 (0.150)	1.85 (0.562)	11.7 (3.81)	10.3 (1.00)
KPL-4	PE	DC	HER2+ (HER2)	12.8 (1.07)	7.66 (0.643)	3.60 (0.516)	5.79 (0.911)	8.52 (1.64)
				21.4 (1.33)	21.9 (6.50)	5.43 (0.770)	17.0 (1.52)	16.5 (2.12)
MCF-7	PE	AC	ER+ (Luminal A)	0.0147 (0.00431)	0.229 (0.0156)	2.26 (0.572)	0.398 (0.0504)	12.7 (4.85)
				30.3 (9.73)	12.7 (2.10)	7.76 (0.483)	37.5 (7.55)	32.0 (18.1)
MDA-MB-134VI	PE	LC	ER+ (Luminal A)	10.4 (0.323)	14.1 (2.39)	7.97 (0.148)	24.9 (0.673)	12.1 (2.03)
				16.7 (1.99)	23.5 (8.50)	8.37 (0.140)	26.9 (0.478)	19.0 (4.58)
MDA-MB-157	PE	M	TNBC (Basal B)	0.0200 (0.00281)	0.0486 (0.0143)	7.61 (0.189)	6.83 (1.38)	21.3 (14.1)
				2.47 (0.542)	0.426 (0.267)	8.05 (0.184)	36.2 (13.0)	34.9 (28.3)
MDA-MB-231	PE	AC	TNBC (Basal B)	0.0160 (0.00498)	0.0169 (0.00350)	1.45 (0.206)	0.983 (0.307)	10.7 (0.284)
				3.04 (1.74)	0.522 (0.232)	6.54 (2.28)	23.4 (8.46)	23.0 (10.2)
MDA-MB-436	PE	AC	TNBC (Basal B)	27.0 (3.13)	9.33 (3.67)	3.42 (0.428)	12.6 (1.35)	27.5 (11.2)
				43.9 (6.83)	42.3 (21.5)	7.86 (2.14)	17.8 (2.90)	83.4 (58.8)
SKBR-3	PE	AC	HER2+ (HER2)	7.80 (1.21)	5.49 (0.366)	3.65 (0.382)	4.99 (0.402)	15.2 (2.61)
				19.3 (4.67)	15.0 (4.73)	6.77 (0.127)	12.3 (2.82)	32.3 (3.42)
SUM44PE	PE	LC	HER2+ (Luminal B)	50.8 (7.66)	12.7 (4.15)	7.87 (2.28)	26.9 (5.81)	39.8 (20.0)
				78.8 (3.17)	20.0 (6.13)	10.2 (2.60)	46.4 (9.09)	>100
T-47D	PE	DC	ER+ (Luminal A)	0.149 (0.0983)	0.497 (0.363)	3.70 (0.500)	3.46 (0.729)	10.4 (1.40)
				52.0 (7.59)	29.6 (19.5)	9.26 (1.79)	18.5 (4.51)	18.0 (5.53)
ZR75.1	A	DC	ER+ (Luminal A)	0.0218 (0.00223)	11.2 (5.09)	4.04 (0.693)	0.248 (0.0687)	28.7 (3.90)
				36.6 (4.81)	25.3 (5.65)	8.83 (1.27)	18.9 (7.93)	61.7 (5.53)

3.1.1.3. Oesophageal cancer cell line panel

Work done by Dr Richard Elliott and Becka Hughes in the Drug Discovery group of Prof Neil Carragher at the University of Edinburgh, UK.

From the GDSC screen at the Sanger Institute, only two of 31 oesophageal cancer cell lines in the GDSC screen were found to be sensitive to eCF506 (FLO-1, TE-8) (see Table 3.1). However, dasatinib was identified as a hit in an in-house high-throughput screen of several thousand compounds against a panel of oesophageal cancer cell lines performed by Prof Carragher's lab (unpublished data). Therefore, eCF506 was included in this screen and compared against dasatinib and imatinib to determine whether dasatinib's efficacy was due to its SRC or ABL inhibition.

Cells were treated 24 hours after seeding for a total of 2 days, after which they were fixed, stained with DAPI and the total number of cell nuclei counted automatically using the ImageXpress MicroXl platform. Of the eight cell lines used, six represent oesophageal cancer (FLO-1, OE33, MFD1, SKGT4, OAC-P4C, JHesoAD1) and two were included as non-malignant controls (normal oesophageal epithelial cell line, EPC2; Barrett's cell line with non-dysplastic metaplasia, CP-A).

eCF506 was found to be superior to dasatinib and imatinib at inhibiting oesophageal cancer cell viability (see Table 3.3 and Appendix A.2). It showed good potency in three of the six cancer cell lines and selectivity for cancer over untransformed oesophageal cells. These results suggest that dasatinib's potency in the oesophageal screen was not due to its ABL inhibition and that the selective SRC inhibitor eCF506 could have potential applications in a subset of oesophageal cancers.

Table 3.3. Absolute EC_{50} values of eCF506, dasatinib and imatinib in oesophageal cancer screen. Absolute EC_{50} is the concentration at which 50% nuclei remained compared to DMSO control (in µM) and was calculated using GraphPad Prism 7 (blue = low EC_{50}, red = high EC_{50}). Data represent average of three technical repeats.

	Cancer						*Non-cancer*	
	FLO-1	OE33	MFD1	SKGT4	OAC-P4C	JHesoAD1	EPC2	CP-A
eCF506	0.02	0.28	0.6	1.05	10	10	10	10
Dasatinib	0.99	0.79	1.02	0.96	10	10	10	1.98
Imatinib	10	10	10	10	10	10	10	10

3.1.2. eCF506 induces cell cycle arrest in the G1 phase

Previous studies have shown that SRC inhibition can induce cell cycle arrest in the G1 phase due to stabilisation of the CDK inhibitor p27, which inhibits progression into S phase (see chapter 1.2.3.2) [52,71]. In agreement with this, the 2D cell viability experiments in this thesis found that the tested SRC kinase inhibitors generally have cytostatic rather than cytotoxic effects (see chapter 3.1.1.2). To confirm that the observed reduction in cell viability is due to changes in cell cycle progression rather than metabolic changes affecting PrestoBlue™ readout, eCF506 and dasatinib were tested in a cell cycle assay. Cells were treated at two different concentrations for 48 hours, fixed and treated with pepsin to extract the cell nuclei. These were stained with DAPI and the DNA content was analysed by flow cytometry.

The data shows that both eCF506 and dasatinib induce arrest in the G1 phase of the cell cycle (see Figure 3.2). In MDA-MB-231 cells, dasatinib was more potent at increasing the percentage of cells in the G1 phase (from 64% in untreated cells to 90% and 91% at 100 nM and 1 µM, respectively), while eCF506 was less potent at both concentrations (82% and 84%, respectively). This agrees with data from previous cell viability assays, where dasatinib also had stronger anti-proliferative effects than eCF506 at both concentrations in this cell line (see Figure 3.2c).

In MCF-7 cells, eCF506 is superior to dasatinib at inducing cell cycle arrest, as the latter only increased the G1 population by 3% at 100 nM but had no effect at 1 µM. While eCF506 does reduce cell viability considerably more than dasatinib in this cell line, it is interesting that no effect was observed for dasatinib at 1 µM in the cell cycle assay, as cell viability is reduced to 39% at this concentration. One possibility is that the different treatment times between the cell cycle assay and cell viability assay (48 hours vs. 5 days, respectively) are responsible for this discrepancy. A longer treatment time of 5 days should be tested in the cell cycle assay to assess whether this leads to different results. The high heterogeneity of the MCF-7 cell line and changes over time in culture are likely also contributing factors, as these assays were performed at different time points. Nonetheless, another study reported the same results for dasatinib after 48 hours treatment: a dose-dependent increase in G1 arrest in MDA-MB-231 cells but only a slight increase in MCF-7 at 100 nM and none at 1 µM [172]. Therefore, it is a possibility that dasatinib's antiproliferative mode of action in this cell line is different (e.g. apoptosis).

(a)

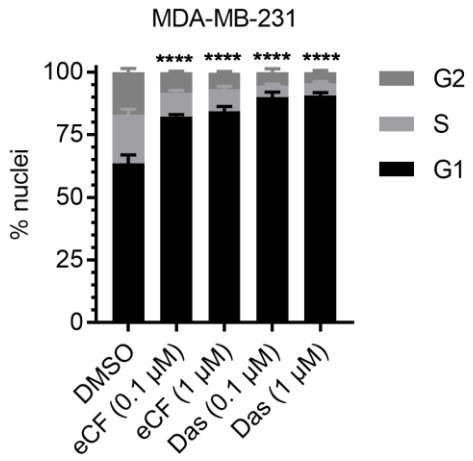

(b)

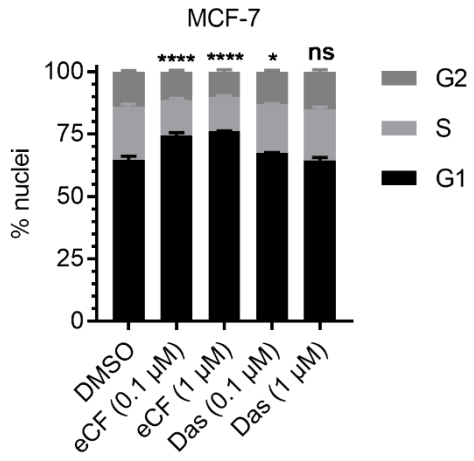

(c)

	48 hours			*5 days*
	G1	**M**	**G2**	**Viability**
MDA-MB-231				
DMSO	63.5	19.6	16.9	100.0
eCF506 (0.1 µM)	82.2	9.4	8.3	20.3
eCF506 (1 µM)	84.4	8.8	6.7	7.6
Dasatinib (0.1 µM)	89.9	4.7	5.4	5.0
Dasatinib (1 µM)	90.6	4.9	4.5	0.7
MCF-7				
DMSO	64.6	21.4	13.9	100.0
eCF506 (0.1 µM)	74.4	14.2	11.4	26.9
eCF506 (1 µM)	76.1	13.7	10.2	19.1
Dasatinib (0.1 µM)	67.4	19.5	13.1	70.1
Dasatinib (1 µM)	64.5	20.4	15.0	38.7

Figure 3.2. eCF506 and dasatinib induce G1 cell cycle arrest and reduce proliferation. Cell cycle assay of (a) MDA-MB-231 and (b) MCF-7 cells treated with eCF506 or dasatinib for 48 hours and analysed by flow cytometry. Changes in G1 phase were compared to DMSO treated control samples using one-way ANOVA with Dunnett correction for multiple comparison; $p>0.05$ (ns), $p<0.05$ (*), $p<0.0001$ (****). Data represents three biological replicates with standard deviation. (c) Comparison of data from cell cycle and cell viability assays.

3.1.3. Phospho-SRC (Y416) is not a reliable biomarker to predict cell line sensitivity to eCF506

Elevated SRC activity has been found in many solid tumours and drug resistance mechanisms but the challenge remains to find reliable biomarkers that can predict (patient) response to SRC inhibition (see chapter 1.2.4). A thorough screening for and testing of several candidates in different *in vitro*, *in vivo* and patient-derived models would be necessary to identify reliable and novel biomarkers, which was beyond the scope of this PhD project. However, in order to check whether the anti-proliferative effects of eCF506 observed in chapter 3.1.1.2 can be linked to quantity or activity of the target, the amount of total and phosphorylated SRC kinase was quantified in all cell lines by Western blotting. The protein amounts relative to a reference cell line (MDA-MB-231) were plotted against the respective growth inhibition values (GI_{25}, GI_{50}, GI_{75}, GI_{90}, TGI) for eCF506 and analysed for correlation between the two.

In general, using GI_{25} values, GI_{50} values or total SRC levels in the analysis did not give statistically significant results (see Figure 3.3a and Appendix A.3). When comparing phospho-SRC levels or the ratio of phospho-SRC to SRC (pSRC/SRC) with their respective GI_{75}, GI_{90} or TGI values of the cell lines, all analyses showed statistically significant correlations ($p<0.05$). Phospho-SRC levels plotted against GI_{90} values correlated the strongest ($p=0.0045$, $r=-0.512$; $R^2=0.262$) (see Figure 3.3b). As cell lines with a biphasic dose-response curve are those for which GI_{25}, GI_{50}, GI_{90} and TGI values would differ the most, this suggests that the relative amount of phospho-SRC only gives information on near total growth inhibition by eCF506 rather than partial response. However, when looking at the plotted data and the low coefficient of determination (R^2), it becomes clear that even the strongest correlation found still has large variability between cell lines. While it is notable that those cell lines with relatively low amounts of phospho-SRC (<100% compared to MDA-MB-231) all have high GI_{90} values, the large variability in eCF506 sensitivity between cell lines with higher amounts of phospho-SRC (e.g. HCC-1954 vs. IGROV-1) limits the use of this approach to predict cell line sensitivity with a good degree of certainty. It is possible that this analysis could be improved by including a second biomarker, yet the key question remains of how well these findings from 2D cell line assays can ever translate into other models and the clinic. One improvement would be to use primary

patient samples for testing the response to eCF506 and presence of biomarkers and this would be an interesting follow-up experiment to do.

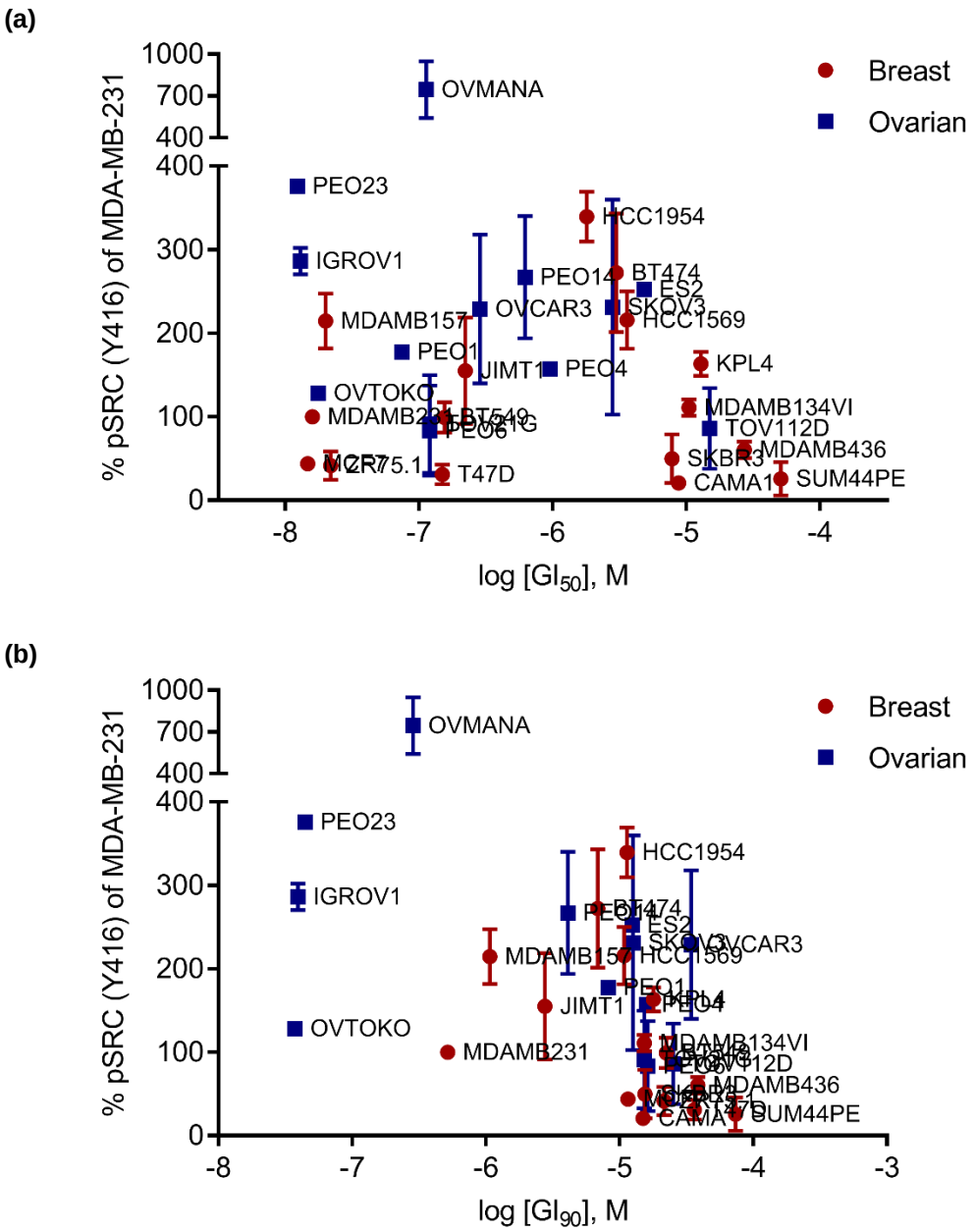

Figure 3.3. Correlation between cell line sensitivity to eCF506 and (phospho)-SRC levels. SRC protein and phosphorylation levels were determined for all cell lines from Western blots and are plotted against eCF506 sensitivity from 2D cell viability assays (see Appendix A.3). Protein levels were determined from two biological replicates, normalised to MDA-MB-231 and are shown with standard error. Correlation analysis of combined breast and ovarian data shows (a) no correlation for GI_{50} and pSRC (R^2 = 0.0351, p>0.05) and some correlation for GI_{90} and pSRC (R^2 = 0.262, p=0.0045 **).

3.1.4. eCF506 is less potent than dasatinib at inhibiting 3D spheroid growth

2D assays, such as the cell viability assays performed in chapter 3.1.1, are commonly used in high-throughput screens to reduce labour, cost and variability in drug discovery. However, results from these assays do not always translate into 3D models or animal experiments. In order to determine whether eCF506's potency in the tested cell lines is assay-dependent, a 3D spheroid assay was performed in three cell lines classified as being sensitive in chapter 3.1.1.2 (MDA-MB-231, MCF-7, T-47D). Cells were seeded in ultra-low adherent U-bottom plates, spun down and left for two to three days to form spheroids. Compounds were added to the wells and cells treated for a total of seven days. Spheroids were imaged before, during and after treatment and spheroid area was measured using CellProfiler. Graphs of spheroid size and representative images are shown in Figure 3.4 with the full dataset in Appendix A.4.

Spheroid growth patterns differed between the cell lines over the treatment period. MDA-MB-231 cells formed very loose spheroids which shrank to half the size over time. MCF-7 spheroids did not change in size during the seven days, whereas T-47D spheroids grew by two thirds over the same period.

Concentrations in the micromolar range are necessary for eCF506 to have a significant effect on spheroid size in any of the three cell lines tested (see Figure 3.4). Dasatinib has similar low potency to eCF506 in MCF-7 cells, with both compounds reducing spheroid size by only 21% at 10 µM compared to DMSO. Dasatinib is more potent in T-47D cells than eCF506 (44% and 23% size reduction at 10 µM, respectively), although only the highest concentration was able to fully stop spheroid growth during the treatment period. In MDA-MB-231 cells, dasatinib is able to reduce spheroid size at sub-micromolar concentrations, with a 25% reduction in size at 30 nM and a 55% reduction at 3 µM. In contrast, eCF506 only achieves a maximum 17% reduction in spheroid size in this cell line. Longer treatment (7 days instead of 4 days) generally increased the effect of both compounds slightly.

Spheroids were stained with calcein-AM and propidium iodide on the final day of treatment to visualise live and dead cells, respectively (see Figure 3.4). Increased propidium iodide staining could only be observed in MDA-MB-231 cells at very high concentrations, which suggests that the compounds did not have cytotoxic effects even at 10 µM in MCF-7 and T-47D cells.

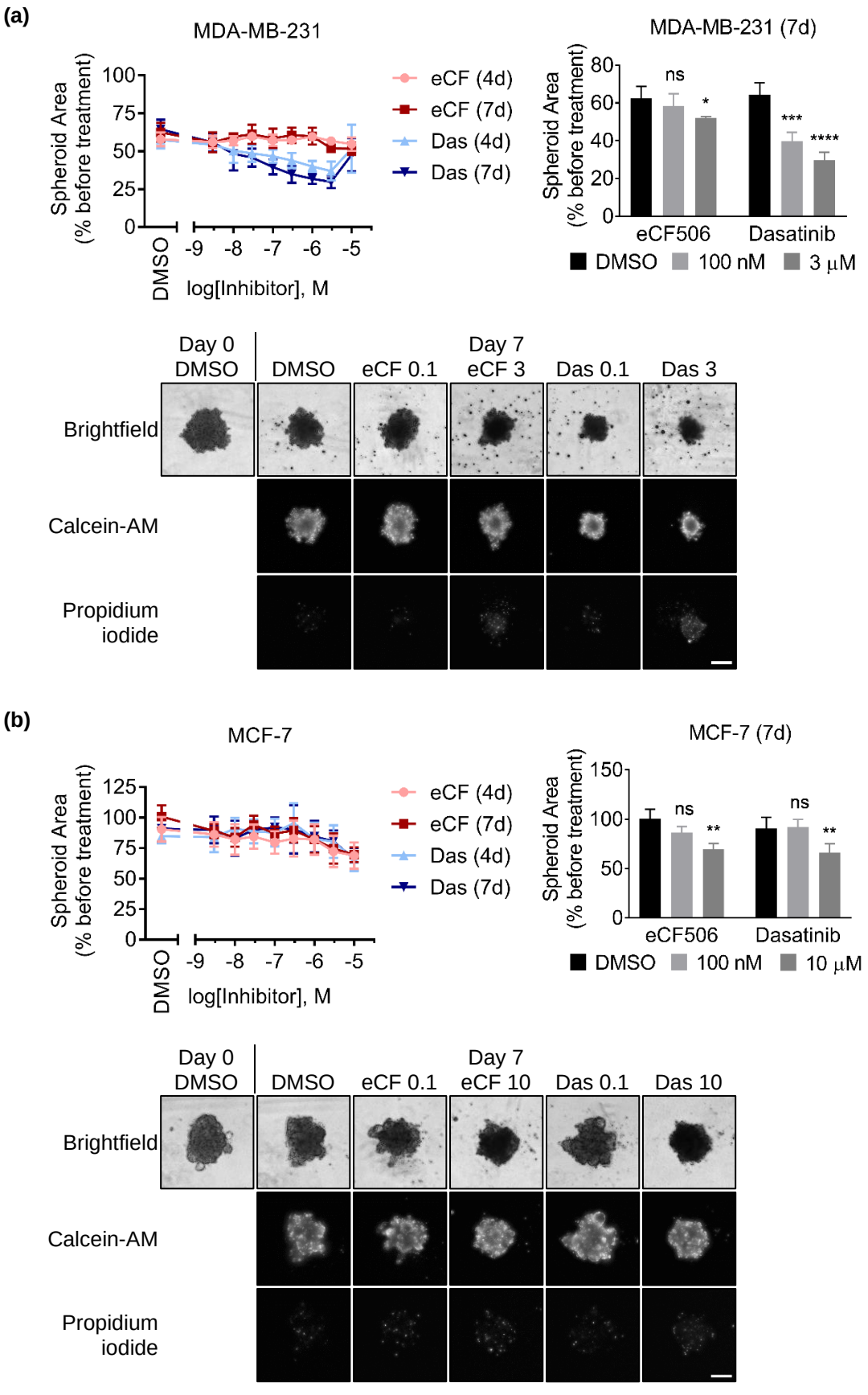

Figure continued on next page

Figure continued from previous page

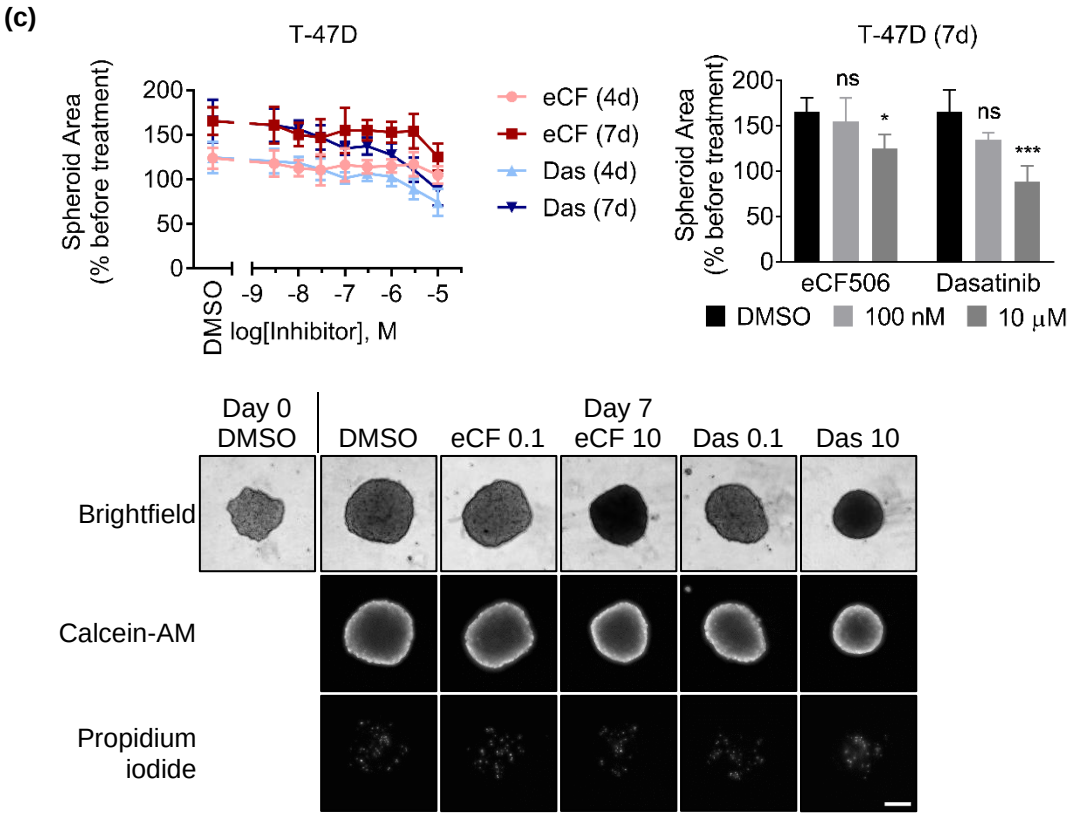

Figure 3.4. Breast cancer spheroids treated with eCF506 or dasatinib. (a) MDA-MB-231, (b) MCF-7 and (c) T-47D cells were grown as spheroids and imaged prior to and after four or seven days of treatment using ImageXpress. Spheroid size was measured from a collapsed Z-stack image using CellProfiler software. Data was normalised to spheroid size prior to treatment start. Data represents average of three biological replicates with standard deviation. Statistical analysis was done using two-way ANOVA with Dunnett correction for multiple comparison; $p<0.05$ *, $p<0.01$ **, $p<0.001$ ***, $p<0.0001$ ****. Images show representative spheroids using brightfield microscopy or fluorescent microscopy after staining with calcein AM (live cells) or propidium iodide (dead cells). Scale bar = 200 µm.

3.1.5. eCF506 has anti-angiogenic properties

Part of this work was done by Oxurion (formerly Thrombogenics), Belgium.

As SRC kinase and its downstream target FAK have been found to play important roles in angiogenesis (see chapter 1.2.3.4), eCF506 has potential anti-angiogenic properties that could lead to applications in cancer and other diseases involving abnormal blood vessel growth.

Primary human umbilical vein endothelial cells (HUVEC) were used as a model for endothelial cells in angiogenesis. eCF506 was tested alongside four other SRC/ABL kinase inhibitors (dasatinib, bosutinib, saracatinib, imatinib), the FAK inhibitor VS-4718 (which has previously been tested in phase 1 clinical trials for cancer), and the approved VEGFR inhibitor sunitinib. The effects of all seven compounds on cell proliferation were assessed in a 2D cell viability assay, as described previously in chapter 3.1.1.2, and the results are shown in Figure 3.5a. eCF506 was the most potent inhibitor of HUVEC cell growth with a GI_{50} of 35.6 nM; it was slightly better than dasatinib (GI_{50} 49.8 nM) and more potent than both sunitinib and VS-4718 (GI_{50} 0.852 µM and 2.45 µM, respectively). Similar results in the low micromolar range have been reported previously with sunitinib in HUVEC cell proliferation and cytotoxicity assays [316,317].

As endothelial cell migration is equally as important as proliferation for blood vessel formation, a scratch wound assay was performed with HUVEC cells to determine the anti-migratory effects of eCF506, VS-4718 and sunitinib. Only eCF506 slightly reduced HUVEC migration in this assay at concentrations between 0.1 to 1 µM, while the other two compounds had no significant effects (see Figure 3.5b). These results and the nearly 20-fold lower potency of sunitinib in the cell viability assays compared to eCF506 are surprising as it is an approved angiogenesis inhibitor; however, a previous study reports slightly stronger activity of 1 µM sunitinib in a HUVEC wound healing assay than found here [318].

A collaboration with the Belgian research company Thrombogenics was established to further test the anti-angiogenic properties of eCF506 in their standardised *in vitro* and *in vivo* assays for non-cancer applications. The *in vitro* cytotoxicity of eCF506, dasatinib and saracatinib was assessed in primary human retinal microvascular endothelial cells and all three compounds were found to have no toxic effects after 24

hours at concentrations up to 10 µM (see Figure 3.6). A second assay tested the efficacy of eCF506 at inhibiting the vessel outgrowth from *ex vivo* murine choroid explants; eCF506 was as good as dasatinib (IC_{50} 4.85 nM and 6.72 nM, respectively) and clearly superior to saracatinib (IC_{50} 396 nM) (see Figure 3.7). These results suggest that eCF506 could have potential applications in angiogenesis-related disorders, both in cancer and non-cancer indications.

(a)

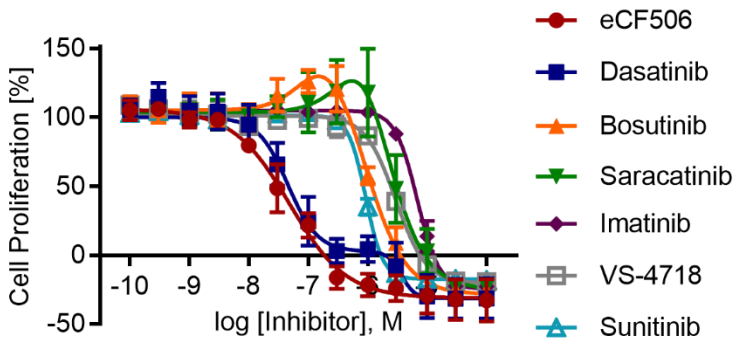

	eCF506	Dasatinib	Bosutinib	Saracatinib	Imatinib	VS-4718	Sunitinib
GI_{50}	0.0356 (0.0130)	0.0498 (0.0252)	1.18 (0.184)	3.29 (1.55)	6.30 (0.484)	2.45 (0.120)	0.852 (0.0608)
TGI	0.187 (±0.0655)	2.17 (2.16)	3.51 (0.706)	8.87 (4.15)	12.6 (2.43)	7.66 (1.65)	1.63 (0.0940)

(b)

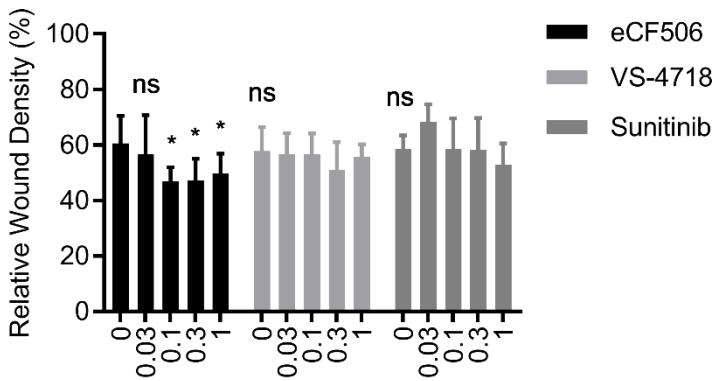

Figure 3.5. Effects of different kinase inhibitors on HUVEC proliferation and migration. (a) HUVEC cell viability after 5 days of treatment with different kinase inhibitors was determined with PrestoBlue™ reagent. Table shows the GI_{50} and TGI values from three biological repeats with standard deviation in brackets. (b) Migration of HUVEC cells treated with eCF506, VS-4718 or sunitinib. Cells were pre-treated for 2 hours prior to wounding and treated again post-wounding. Data shows relative wound density 6 hours after wounding and represents the average of three experiments with standard deviation. Analysis was done using two-way ANOVA with Dunnett's post-hoc test; $p>0.05$ (ns), $p<0.05$ (*).

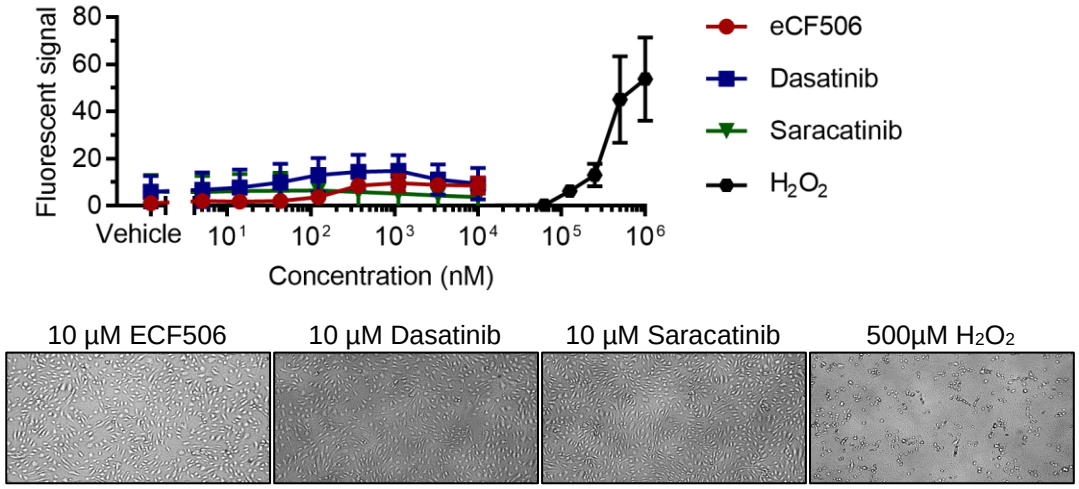

Figure 3.6. Cytotoxicity of kinase inhibitors in primary human retinal microvascular endothelial cells (hRMVEC). Cells were treated with compounds for 24 hours and analysed using the CellTox™ Green Cytotoxicity assay (Promega). Higher fluorescent signal indicates dead cells. Data shows fluorescent signal minus background fluorescence from cell-free wells from three biological replicates with standard deviation. Bottom shows representative images of hRMVECs.

(a)

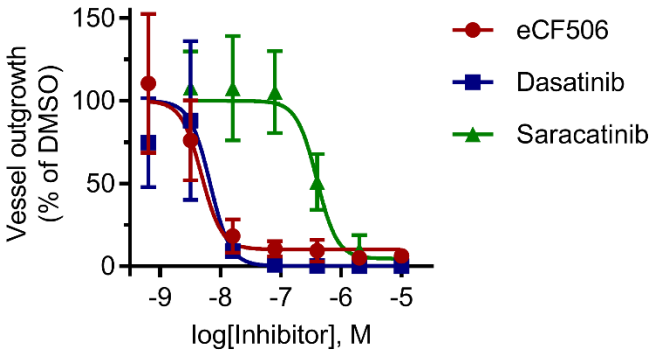

Inhibitor	IC_{50} (nM)
eCF506	4.85
Dasatinib	6.72
Saracatinib	396

(b)

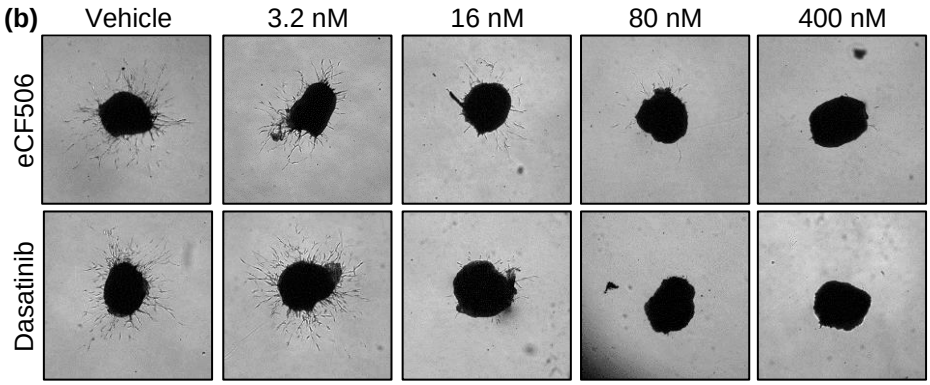

Figure 3.7. Vessel outgrowth from *ex vivo* murine choroid explants. (a) The vessel outgrowth area of murine choroid explants was calculated and normalised to DMSO treated control. Data represents three biological replicates with standard deviation from which IC_{50} was calculated using GraphPad Prism 7. (b) Representative images of vessel outgrowth of untreated and treated murine choroid explants.

3.2. eCF506 selectively inhibits SRC kinase over ABL kinase

3.2.1. eCF506 has superior potency and selectivity for SRC kinase

3.2.1.1. Comparison of kinome screen data

eCF506 and dasatinib have previously been tested by Reaction Biology against 14 wild-type kinases to determine their IC_{50} values in cell-free assays [1]. This revealed approximately thousand-fold selectivity of eCF506 for SRC kinase over ABL kinase (IC_{50} <0.5 nM vs 479). In order to test for potential "off-targets" in the rest of the human kinome, which currently includes 538 identified kinases, eCF506 was screened in a panel of 340 wild-type kinases by Reaction Biology, which constituted the biggest commercially available panel at the time [9]. Percentage inhibition of kinase activity was determined in duplicate at a single dose of eCF506 (1 µM) in the presence of 10 µM ATP and compared to DMSO. Part of the results were previously published in the thesis of Dr Craig Fraser and the full dataset is shown in Appendix A.6 [319].

In Figure 3.8a, the full results for eCF506 have been plotted in a kinome map using the free TREEspot™ Software Tool from DiscoveRx Corporation. All kinase targets that were inhibited more than 65% by eCF506 are also listed in Table 3.4. In addition, the results of a kinome screen with dasatinib and bosutinib, which were previously tested in the same assay as part of a large scale kinase inhibitor screen [221], are plotted in Figure 3.8b,c. No kinome screening data could be found for saracatinib. In the study by Reaction Biology Corporation, dasatinib and bosutinib were tested at 500 nM in a panel of 300 wild-type human kinases at 10 µM ATP. In Figure 3.8, red dots denote kinases that are inhibited by 65% or more, with SRC and ABL coloured in blue, and green dots show all other tested kinases that fall below this threshold.

eCF506 is more than twice as selective in comparison to dasatinib and bosutinib. It inhibited 23 of 340 kinases at 65% or more, while the other two compounds targeted 46 and 66 out of 300 kinases, respectively, at the same cut-off. Since eCF506 was screened at double the concentration, it would likely be even more selective when compared under the same conditions. eCF506 also inhibited SRC more strongly than any other kinase (0.1% activity remaining) closely followed by other SRC family kinases, with its main off-target being ARAF (see Table 3.4). Dasatinib and bosutinib's primary targets, on the other hand, include many kinases unrelated to SFKs, such as

EphB2, DDR2, MAP4K4 and MINK, and they inhibited SRC to a lesser degree (3.5% and 6.0% activity remaining). Both inhibited other SRC family kinases as well as ABL (ABL1) and ARG (ABL2) more strongly than SRC kinase. This comparison highlights eCF506's superior selectivity for SRC kinase in particular, and SFKs in general across the human kinome.

(a)

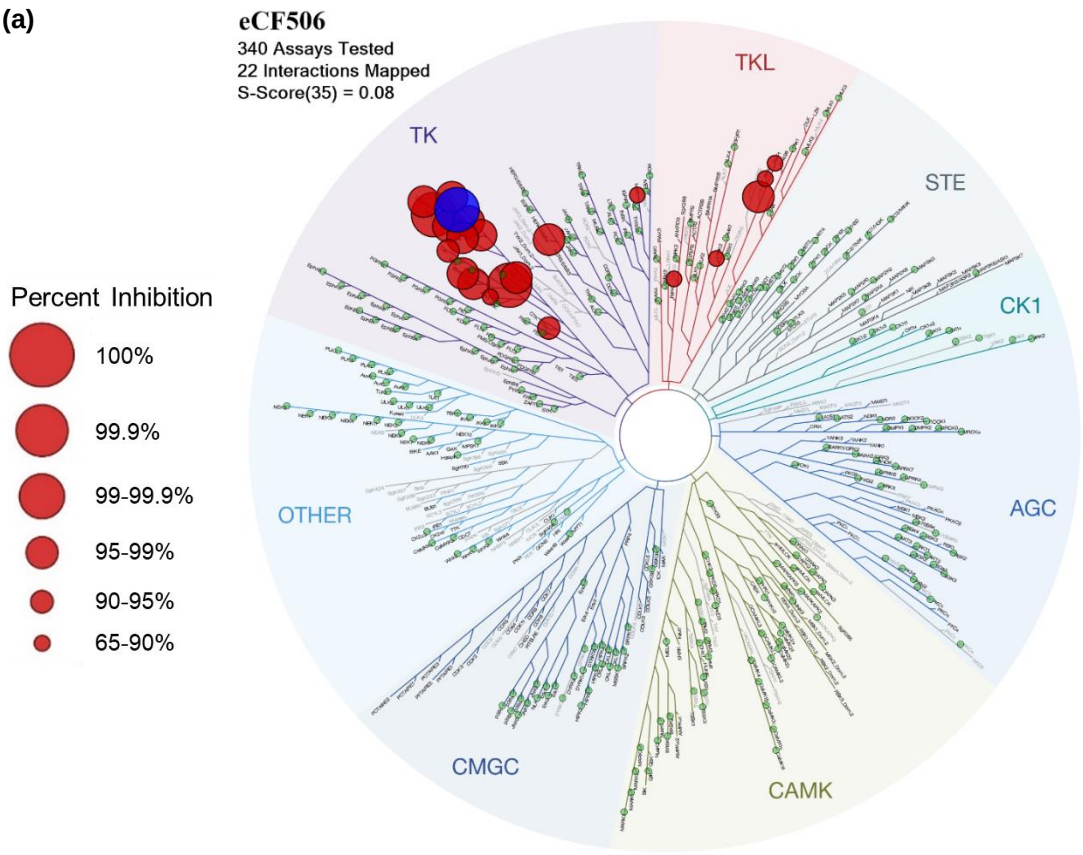

(b)

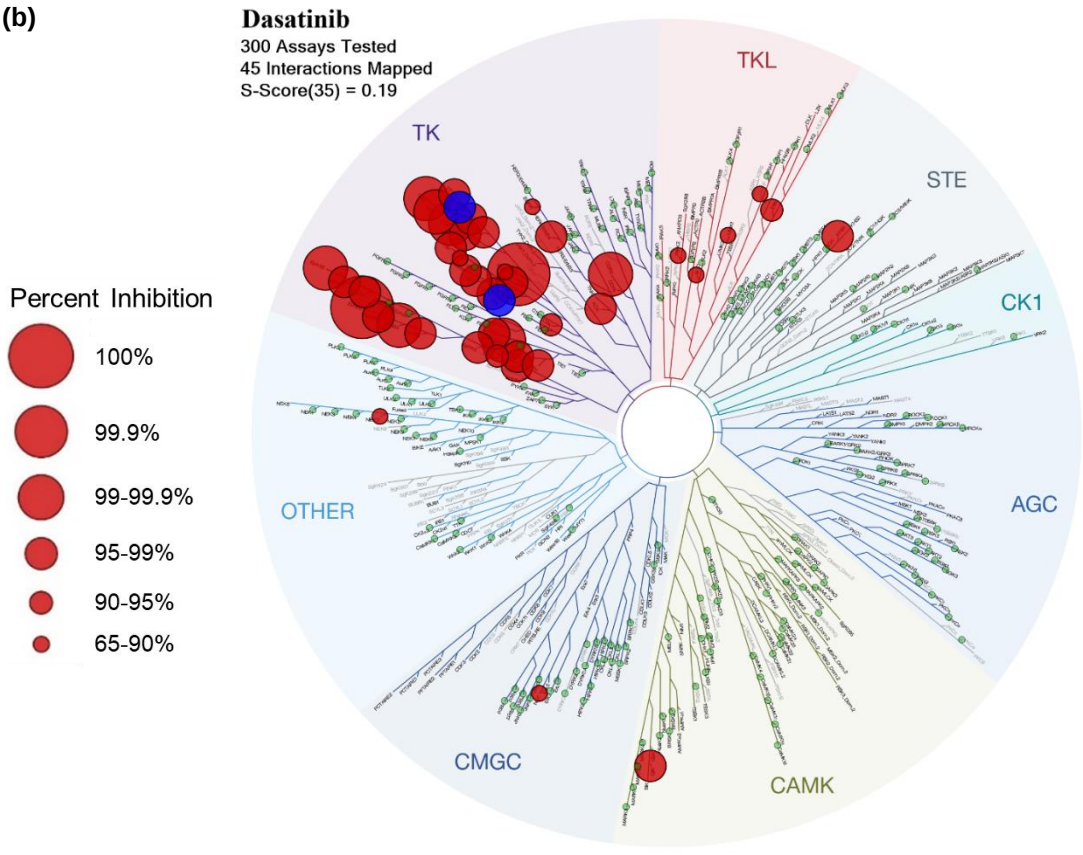

Figure continued on next page

Figure continued from previous page

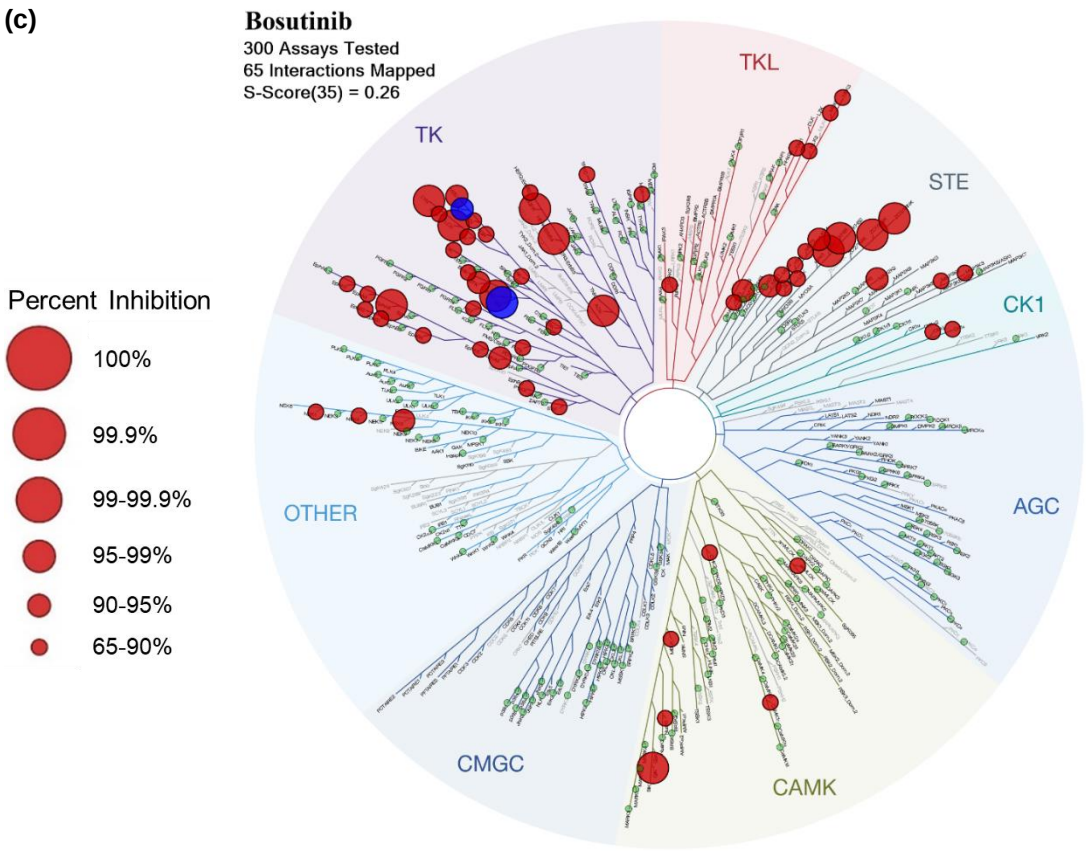

Figure 3.8. Map of the protein kinome showing the selectivity of eCF506, dasatinib and bosutinib. (a) eCF506 was tested at double the concentration (1 µM) than (b) dasatinib (500 nM) or (c) bosutinib (500 nM). Tested kinases are shown as circles in the map, with green indicating inhibition below threshold and red denoting inhibition of kinase activity by more than 65%, depending on size of the circle. SRC and ABL1 are highlighted in blue. Atypical, mutant, lipid and pathogen kinases are not shown. The S-score denotes the selectivity of the compound at 35% cut-off. LYN B kinase could not be mapped. eCF506 was tested by Reaction Biology Corporation and the data for dasatinib and bosutinib stems from a published inhibitor screen by Anastassiadis *et al.* in the same assay [221]. All compounds were tested at 10 µM ATP. Images generated using TREEspot™ Software Tool and reprinted with permission from KINOMEscan®, a division of ©DiscoveRx Corporation, 2010.

Table 3.4. Kinase targets of eCF506, dasatinib and bosutinib. All targets with less than 35% activity remaining after compound addition are shown. SFKs are highlighted in red, ABL kinases in blue. Data for dasatinib and bosutinib comes from Anastassiadis *et al.* assay [221]. eCF506 was screened at 1 µM, while dasatinib and bosutinib were tested at 500 nM. Full results for eCF506 are shown in Appendix A.6.

	eCF506		Dasatinib		Bosutinib	
No.	*Kinase*	*% Activity*	*Kinase*	*% Activity*	*Kinase*	*% Activity*
1	SRC	0.1	FRK	-0.9	MAP4K4	1.0
2	BRK	0.2	EPHB2	-0.2	MINK	1.2
3	HCK	0.8	DDR2	0.2	ERBB4	1.5
4	FGR	1.3	EPHA5	0.2	MAP4K5	1.7
5	LYN	1.3	LCK	0.3	ABL1	1.8
6	LCK	1.4	LYN	0.4	LCK	1.9
7	ARAF	1.7	CSF1R	0.8	SIK2	1.9
8	YES	1.8	HCK	0.8	LYN	2.1
9	LYN B	2.0	EPHB3	1.0	ABL2	2.2
10	FYN	2.3	EPHB4	1.2	MAP4K2	3.2
11	FRK	2.4	TXK	1.4	ACK1	3.5
12	BMX	2.8	LYN B	1.6	EGFR	3.8
13	BTK	3.8	EPHA4	1.6	EPHA6	4.4
14	ERBB4	4.5	FGR	1.7	BTK	5.7
15	BLK	4.8	PDGFRa	1.8	MST4	5.9
16	CSK	5.0	SIK2	1.9	LYN B	6.0
17	TXK	9.1	YES	1.9	SRC	6.0
18	RIPK3	12.1	FYN	2.0	YES	7.3
19	RAF1	19.6	BTK	2.1	MST1	7.4
20	ABL2	28.7	PDGFRb	2.5	MEK2	8.4
21	LIMK2	30.0	BMX	2.5	NEK2	8.6
22	MER	30.1	ACK1	2.6	EPHA2	9.6
23	BRAF	34.5	EPHA1	2.7	PAK3	9.9
24			ABL2	2.7	YSK1	10.1
25			ABL1	2.8	EPHA8	10.5
26			BLK	3.0	CK1d	10.9
27			MAP4K5	3.1	MST3	11.0
28			pdg	3.3	ARK5	11.4
29			EPHA3	3.5	CK1e	11.4
30			SRC	3.5	FGR	11.5
31			ERBB4	4.0	PAK1	11.7
32			EPHA8	4.1	MAP3K3	11.8
33			BRK	4.6	EPHB1	11.8
34			EPHB1	4.8	HCK	11.9
35			EPHA2	6.8	CSK	12.3
36			CSK	7.1	EPHB4	12.5
37			ZAK	8.6	LOK	12.6
38			TEC	11.3	MLK3	13.5
39			ALK1	15.9	MST2	13.9
40			LIMK1	16.7	BMX	14.5
41			SRMS	17.0	NEK1	15.2
42			EGFR	21.1	TRKC	15.2
43			NEK11	21.7	MLK1	16.5
44			RIPK2	25.2	CAMK1d	16.6
45			NLK	27.5	EPHB2	17.4
46			ARAF	33.8	RET	18.9
47					BLK	20.7
48					SYK	21.1
49					SLK	21.6
50					CHK2	21.7
51					MLK2	22.9
52					MAP3K2	23.5
53					MELK	25.8
54					EPHA4	27.0
55					TXK	27.5
56					TAK1	28.3
57					MER	28.9
58					FRK	29.2
59					FYN	29.4
60					LRRK2	30.1
61					FLT3	30.3
62					EPHA3	31.7
63					MYLK2	32.1
64					PYK2	32.6
65					NEK4	32.6
66					ERBB2	32.9

3.2.1.2. Comparison of SRC activity in Western blots

Previous Western blot experiments have shown that eCF506 can inhibit SRC phosphorylation at tyrosine 416, its autophosphorylation site necessary for full kinase activity, as much as or even better than dasatinib [1,319]. These experiments were done after cells were serum starved for 24 hours, followed by compounds being added for 1.5 hours and serum stimulation for 1 hour. While serum starvation is useful to assess downstream effects in signalling pathways, it does not give information on whether the compounds would also be able to inhibit SRC phosphorylation and downstream pathways in a serum-containing environment, which is relevant for mimicking *in vivo* conditions. Therefore, Western blots were performed in the same two breast cancer cell lines used previously, MDA-MB-231 and MCF-7, in normal serum conditions (10% FBS). Cells were treated with all four SRC/ABL inhibitors (eCF506, dasatinib, bosutinib, saracatinib) for 3 or 24 hours prior to cell lysis and Western blots were performed as described in methods 2.4.2.

The results are similar to those obtained previously with serum starvation and stimulation (see Figure 3.9). eCF506 and dasatinib give almost complete inhibition of SRC phosphorylation at 100 nM in MDA-MB-231 cells, with little difference between 3 and 24 hours of treatment. In contrast, dasatinib is less potent than eCF506 at inhibiting phospho-SRC (Y416) in MCF-7 cells, with >100 nM needed for complete inhibition compared to eCF506's 30 nM after 24 hours of treatment.
Bosutinib and saracatinib both appear to be weak inhibitors of SRC autophosphorylation at tyrosine 416, with concentrations in the micromolar range needed to see significant changes. Slightly stronger inhibition was observed after longer incubation, although 10 µM bosutinib and 30 µM saracatinib was necessary to achieve near full inhibition of SRC autophosphorylation.

Dasatinib seems to be slightly less potent in MCF-7 cells than eCF506, both at inhibiting SRC phosphorylation as well as at inhibiting cell proliferation (see chapter 3.1.1.2). In order to test whether differences in the cell viability assays could be due to variable potency of the inhibitors against SRC, five other cell lines with little (CAMA-1, MDA-MB-436), biphasic (T-47D, ZR-75.1) and high (JIMT-1) anti-proliferative response were assessed in Western blots (see Figure 3.10). In all five, eCF506 achieves maximum inhibition around 100 - 300 nM, although some residual signal remained in CAMA-1 cells. Dasatinib's potency was similar, except in T-47D and

ZR75.1 cells where it was slightly weaker, which again correlates with reduced anti-proliferative properties in these cell lines compared to eCF506 (see Figure 3.1). Full phospho-SRC (Y416) inhibition at 100 nM eCF506 or dasatinib was also found by collaborators at McGill University who tested eCF506 in two HER2-positive murine breast cancer cell lines [77].

Activated SRC kinase phosphorylates FAK on several tyrosine residues, one of which is tyrosine 861. Phosphorylation at this position can therefore act as a marker of pathway activation downstream of SRC. Previous Western blots using serum starvation showed that phospho-FAK (Y861) inhibition mimicked the response of phospho-SRC (Y416) in both cell lines, with full inhibition at 100 nM. Similar results were obtained when FAK phosphorylation was assessed again in the presence of serum (see Figure 3.9). Bosutinib and saracatinib showed efficacy at similar concentrations as for SRC autophosphorylation, which confirms that high concentrations of both are needed to inhibit SRC activity.

The results of these Western blots agree with the findings from the kinome screen in the previous section (chapter 3.2.1.1) and confirm that eCF506 is the most potent inhibitor of SRC kinase both in cell-free and cellular assays. It has similar and at times slightly superior potency compared to the current best-in-class SRC inhibitor dasatinib and both are better than bosutinib and saracatinib.

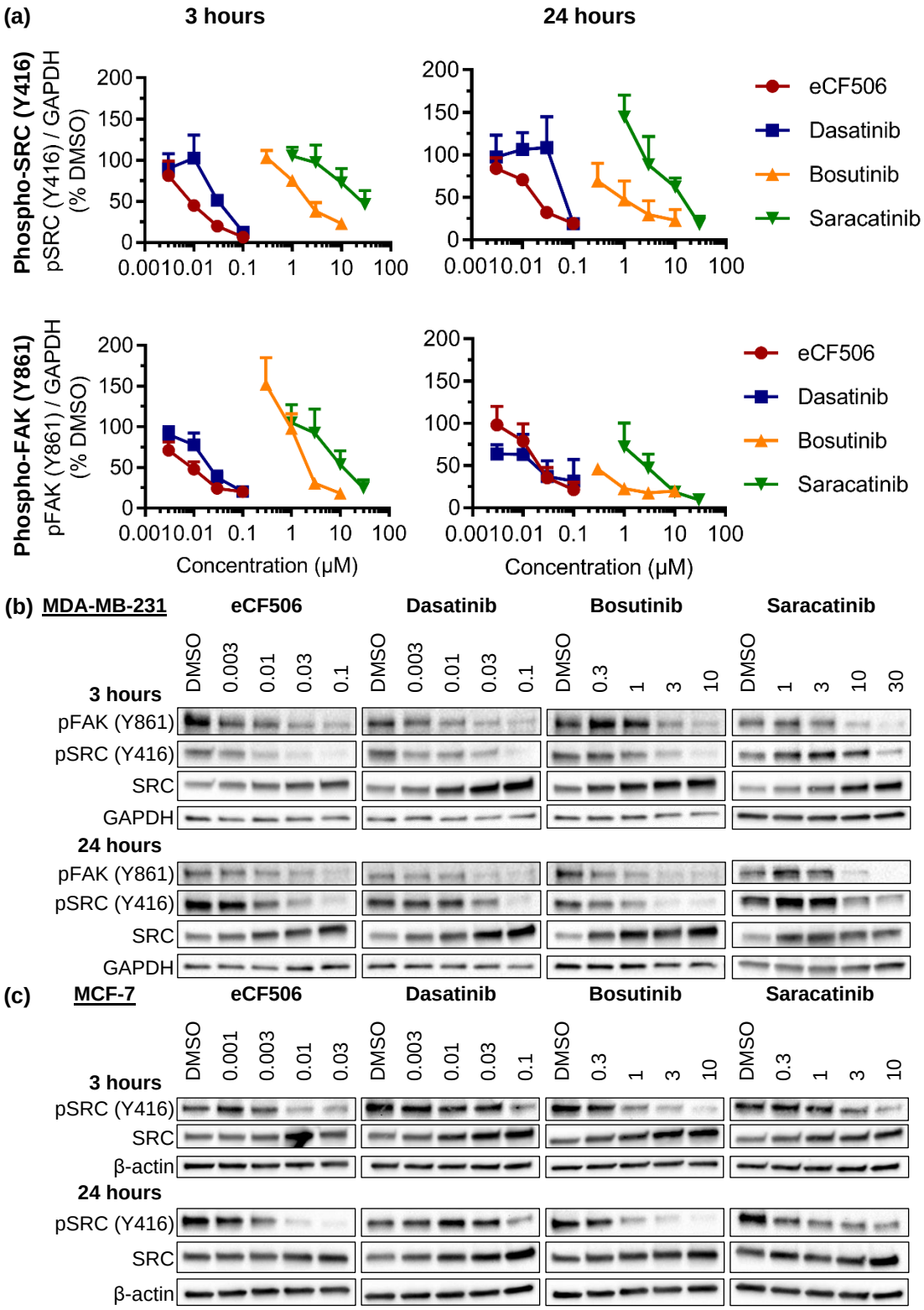

Figure 3.9. Western blot analysis of eCF506, dasatinib, bosutinib and saracatinib for phospho-SRC (Y416) and phospho-FAK (Y861). (a) MDA-MB-231 cells were treated for 3 or 24 hours prior to cell lysis and analysis by Western blot. Protein levels were normalised to GAPDH. Graphs show average of three biological replicates with standard error. (b) Representative Western blot of MDA-MB-231 cells. (c) Western blot of MCF-7 cells treated for 3 or 24 hours. Concentrations are in μM.

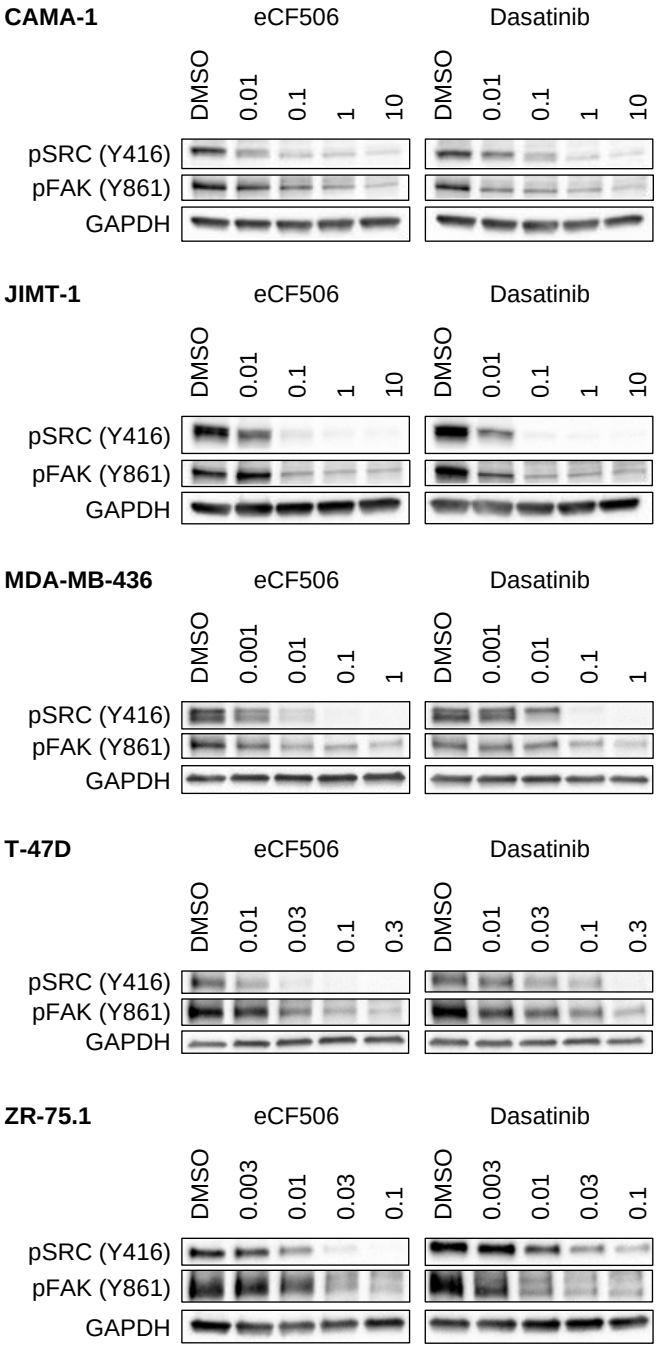

Figure 3.10. Western blot analysis of eCF506 and dasatinib in different breast cancer cell lines. Five different cell lines were treated for 24 hours prior to cell lysis and analysis by Western blot. Concentrations are in μM.

3.2.2. eCF506 is one thousand-fold less potent at inhibiting ABL kinase than dasatinib

One distinguishing property of eCF506 is its approx. 1000-fold selectivity for SRC kinase over ABL kinase, as identified in cell-free kinase assays [1]. This is unique among all currently available small molecule SRC inhibitors (see chapter 1.3.1). While its high potency against SRC kinase was confirmed *in vitro* by Western blots, the comparatively lower potency against ABL kinase has not yet been confirmed in cells.

One challenge when trying to assess ABL activity by Western blot is its lack of sites that are exclusively autophosphorylated to determine ABL kinase activity, as is the case for SRC tyrosine 416. Two residues have been identified that contribute to ABL's activity, tyrosine 245 and tyrosine 412 [320]. Importantly, there is evidence that both of these sites are phosphorylated by the SFKs HCK, LYN and FYN [321]. Assessment of phospho-ABL Y245 after treatment with eCF506 and dasatinib showed only minor differences between both compounds, which correlates well with the similar effect of these compounds on HCK, LYN and FYN activity (see Figure 3.11a and Table 3.4). Assessment of phospho-ABL Y412 by Western blot was unsuccessful (data not shown).

Studies in CML have frequently used the SH2/SH3 adapter protein CRKL as a surrogate for BCR-ABL activity. CRKL is a kinase that is directly phosphorylated by BCR-ABL at tyrosine 207 and can therefore act as an indirect measure of BCR-ABL or ABL activity [322]. The effects of eCF506 and dasatinib on CRKL phosphorylation in MDA-MB-231 cells were assessed by Western blot and the results are shown in Figure 3.11b. As eCF506 has approx. one thousand-fold less activity against ABL than dasatinib in cell-free assays, the assumption would be that eCF506 inhibits CRKL phosphorylation at nearly one thousand-fold lower potency than dasatinib. The results in Figure 3.11b show that dasatinib is indeed superior at reducing phospho-CRKL (Y207) levels, although eCF506 is only around 10-fold less potent, much lower than expected. However, the reliability of CRKL as a readout of ABL activity depends on whether its phosphorylation status is largely independent of other kinases and especially SRC. To test whether phospho-CRKL (Y207) can be affected by eCF506's actions on non-ABL kinases, an ABL1 knockout strain of the MDA-MB-231 cell line and a second strain re-expressing ABL1, both created by Dr Henry Beetham at The University of Edinburgh, were tested by Western blot (see Figure 3.12). The results

show that eCF506 and dasatinib maintain their 10-fold potency difference and reduce CRKL phosphorylation to the same degree in the presence and absence of ABL kinase; this suggests that CRKL phosphorylation is not a specific marker of ABL activity. However, one limitation of this experiment is that only ABL1 but not ABL2 was knocked out in these cell lines and the latter might have compensated for ABL1 loss. MDA-MB-231 cells show very similar sensitivity to eCF506 and dasatinib in cell viability assays with or without ABL1, indicating that ABL1 inhibition does not contribute to potency in this cell line (see Appendix A.7).

Another way of measuring whether a compound binds to a target is to assess the thermal stability of the protein in the presence and absence of the potential inhibitor. This method is based on the finding that proteins bound to an inhibitor are more resistant to heat-induced unfolding [323]. Jafari *et al.* published an adapted method that uses this principle in live cells and therefore assesses not only whether the compound binds the target protein but also whether it reaches its subcellular localisation [296].
To assess whether eCF506 binds ABL kinase in the cell, a thermal shift assay was performed based on the method by Jafari *et al.* and as described in methods 2.4.3. Dasatinib was used as a positive control and both compounds were tested at 300 nM, as it is expected that ABL would be strongly inhibited by dasatinib but not eCF506 at this concentration based on their IC_{50} values in isolated kinase assays (<0.5 and 479 nM, respectively). Protein levels were assessed by Western blot after unfolded proteins, which form aggregates, were removed from the heat-treated cell lysates by centrifugation. The results of three biological replicates are plotted in Figure 3.13. Neither dasatinib nor eCF506 significantly shifted the apparent melting temperature (T_m) of ABL kinase. This was unexpected, as dasatinib is a well-established ABL inhibitor. However, a literature search revealed that dasatinib had previously been tested in a large screen of kinase inhibitors by thermal profiling of the proteome in living cells where it also failed to stabilise BCR-ABL [324]. It appears that (BCR-)ABL's heat stability, unlike other proteins tested such as p38α, is unaffected by the binding of at least some inhibitors, which renders this method unsuitable to show that eCF506 does not significantly inhibit ABL at the tested concentration.

As the attempts to confirm eCF506's potency gap between SRC and ABL in cells by Western blot or thermal profiling fell short, chronic myeloid leukaemia (CML) cells were used in a third experiment as a model for ABL-dependent cell growth. CML is

driven by the Philadelphia chromosome, in which a chromosomal translocation fuses the BCR and ABL gene together, giving rise to the hyperactive BCR-ABL protein that drives abnormal proliferation. The potency of eCF506 in comparison to other dual SRC/ABL inhibitors at reducing cell viability in this model is therefore an indirect measure of the degree of BCR-ABL inhibition. Three different CML cell lines were tested in the same assay as discussed in chapter 3.1.1.2 and the results are plotted in Figure 3.14.

Dasatinib is by far the most potent inhibitor of CML cell proliferation in this assay, with GI_{50} and TGI values in the high picomolar range, followed by bosutinib, which is more than 50 times less potent. Notably, eCF506 is one to two thousand-fold less potent than dasatinib in all three cell lines, which is very similar to the difference in IC_{50} values between both compounds in cell-free ABL kinase assays. Moreover, the range of their GI_{50} values in the cell assays is the same order of magnitude as their IC_{50} values, with dasatinib ranging from 98-384 pM (IC_{50} <500 pM) and eCF506 from 93-902 nM (IC_{50} 479 nM). Notably, the first approved ABL inhibitor for CML, imatinib, performed comparatively poorly in this assay, with similar efficacy to eCF506; however, imatinib does indeed have low potency (IC_{50} 25-200 nM against ABL in isolated kinase assays) so these results are expected and in line with previous experiments in these cells [325,326]. The results of this cell viability experiment suggest that CML cell proliferation can be used as a surrogate readout for ABL inhibition and support eCF506's thousand-fold selectivity.

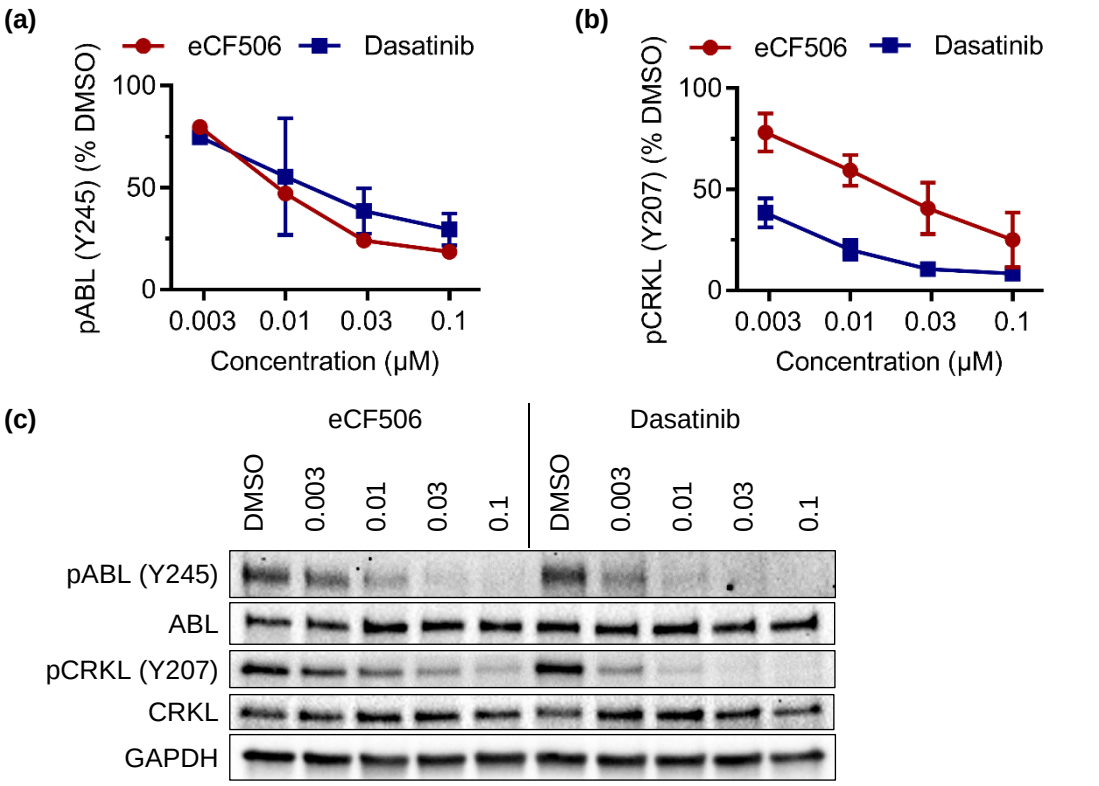

Figure 3.11. Effects of eCF506 and dasatinib on markers of ABL kinase activity. MDA-MB-231 cells were treated with eCF506 or dasatinib for 3 hours prior to cell lysis and analysis by Western blot. (a) Phospho-ABL (Y245) was normalised to GAPDH and is shown as percent of DMSO. Graph shows average of two biological repeats with standard deviation. (b) Phospho-CRKL (Y207) was normalised to GAPDH and is shown as percent of DMSO. Graph shows average of three biological repeats with standard deviation. (c) Representative Western blot of MDA-MB-231 cells treated for 3 hours.

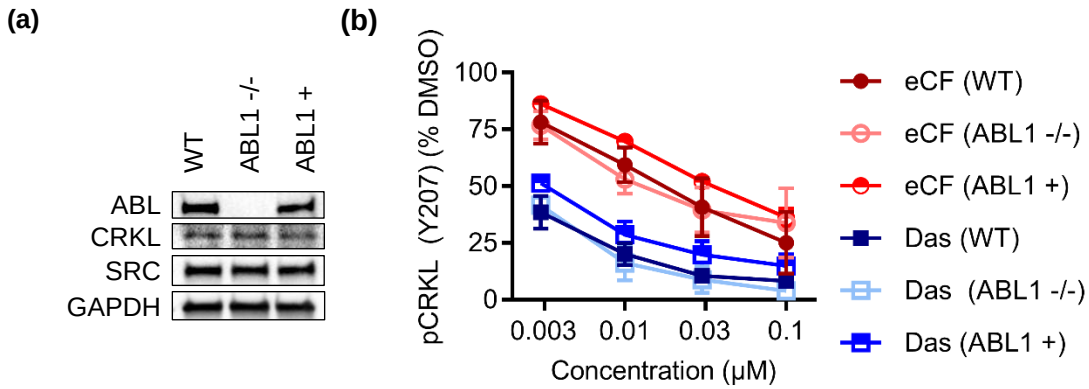

Figure 3.12. CRKL phosphorylation in MDA-MB-231 cells with and without ABL1. Three MDA-MB-231 cell lines (wild-type, ABL1 knockout, ABL1 re-expressed) were treated for 3 hours with eCF506 or dasatinib and phospho-CRKL (Y207) levels were analysed by Western blot. (a) Control Western blot to confirm ABL knockout and re-expression. (b) Graph shows average of three (WT) or two (ABL1 -/-, ABL1 +) biological repeats with standard deviation. Phospho-CRKL (Y207) levels were normalised to GAPDH.

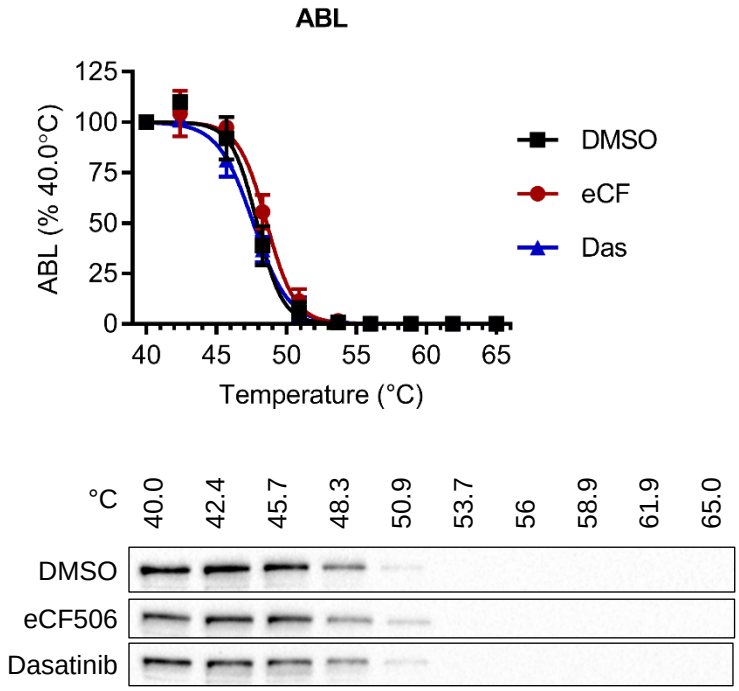

Inhibitor	T_m
DMSO	47.9
eCF506	48.6 (p>0.05)
Dasatinib	47.6 (p>0.05)

Figure 3.13. Thermal shift assay of ABL kinase after treatment with eCF506 and dasatinib. MDA-MB-231 cells were treated with eCF506 (300 nM), dasatinib (300 nM) or DMSO for one hour prior to heating, cell lysis and analysis by Western blot. Band intensities were quantified using Bio-Rad ImageLab® software and normalised to the lowest temperature band for each condition. The top graph shows the average of three biological repeats with standard deviation. The table shows average T_m values calculated by GraphPad Prism 7 and compared to DMSO by one-way ANOVA with Dunnett correction for multiple comparison. The bottom figure shows a representative Western blot.

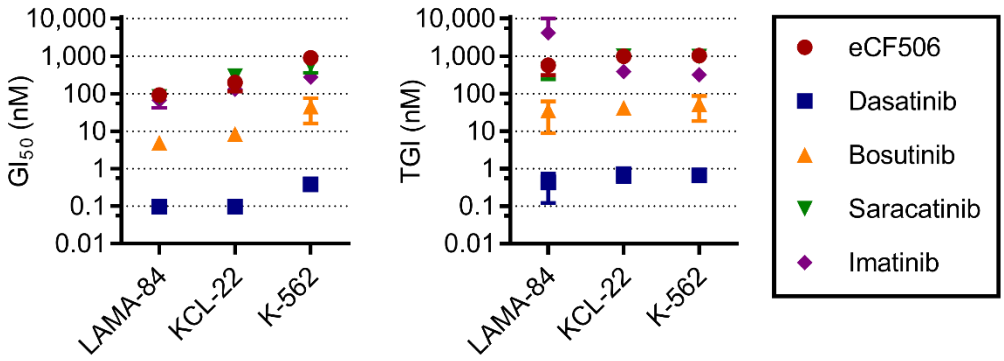

		eCF506	Dasatinib	Bosutinib	Saracatinib	Imatinib	**Ratio eCF / Das**
K-562	GI_{50}	0.902 (0.0434)	0.000384 (0.0000699)	0.0457 (0.0298)	0.567 (0.207)	0.277 (0.0146)	2345
	TGI	1.03 (0.0241)	0.000657 (0.000145)	0.0525 (0.0336)	0.974 (0.260)	0.316 (0.00920)	1571
KCL-22	GI_{50}	0.199 (0.0861)	0.0000981 (0.00000702)	0.00843 (0.000804)	0.292 (0.00866)	0.132 (0.0217)	2031
	TGI	0.993 (0.0460)	0.000717 (0.000276)	0.0419 (0.0151)	1.00 (0.136)	0.388 (0.0873)	1385
LAMA-84	GI_{50}	0.0927 (0.00484)	0.0000974 (0.0000145)	0.00492 (0.000656)	0.0818 (0.00988)	0.0676 (0.0256)	951
	TGI	0.567 (0.257)	0.000432 (0.000308)	0.0357 (0.0269)	0.446 (0.205)	4.16 (5.95)	1315

Figure 3.14. Anti-proliferative effects of SRC/ABL kinase inhibitors in CML cell lines. A panel of three CML cell lines was tested against five kinase inhibitors. Effects on cell proliferation were measured after 5 days of treatment using PrestoBlue™ reagent and curves were fitted using GraphPad Prism 7. GI_{50} (left) and TGI (right) values represent the average of three biological replicates with standard error and values are summarised in table below. Concentrations in µM.

3.3. Discussion

Previous work by Dr Craig Fraser in the Innovative Therapeutics group identified eCF506 as a potent SRC kinase inhibitor with selectivity over ABL kinase in cell-free kinase assays and anti-proliferative properties similar to dasatinib in two breast cancer cell lines [1]. Further *in vitro* analysis and comparison to three other dual SRC/ABL inhibitors reveals that eCF506 is the most potent and selective inhibitor of SRC signalling. It has similar anti-proliferative properties to the current gold-standard SRC inhibitor dasatinib in various cancer types, with ovarian cancer being especially sensitive, and exhibits anti-angiogenic properties in non-cancer models.

3.3.1. eCF506 is the most selective and potent SRC kinase inhibitor

Western blot analysis of different breast cancer cell lines shows that eCF506 is able to potently inhibit SRC kinase autophosphorylation and signalling via downstream pathways such as FAK at nanomolar concentrations (see Figure 3.9 and Figure 3.10). It has similar potency to dasatinib in cells and was slightly better in Western blots of three cell lines (MCF-7, T-47D, ZR-75.1). In these, eCF506 is also somewhat more potent than dasatinib at inhibiting cell proliferation at lower concentrations (see chapter 3.1.1.2), suggesting that these two findings might be linked.

It was surprising that bosutinib and saracatinib only achieved potent SRC inhibition at micromolar concentrations. Both have been studied extensively for their activity against SRC kinase *in vitro*, *in vivo* and in clinical trials [261,262,327,328]. Previous papers report much higher efficacy of saracatinib against SRC autophosphorylation, with full inhibition at 0.25 µM in two prostate cancer cell lines after 30 minutes and at 0.1 µM after 24 hours in a lung cancer cell model; near full inhibition was also seen at 0.5 µM in gemcitabine resistant breast cancer cells after 48 hours [328–330]. However, another study shows that phospho-SRC (Y416) inhibition differs between three gastric cancer cell lines, depending on their levels of phospho-SRC, and full inhibition was not achieved at saracatinib concentrations up to 5 µM; a study in breast cancer cells also showed only partial phospho-SRC inhibition at 1 µM in MCF-7 and T-47D cells, similar to what is shown in Figure 3.9 [175,331]. Bosutinib, on the other hand, has similar potency reported in the literature as found in this thesis, with SRC inhibition around 1 µM reported in the breast cancer cell line MDA-MB-436 and three biliary tract cancer cell lines after 48 hours of treatment [327,332].

While, interestingly, saracatinib is slightly better at inhibiting downstream signalling via FAK than SRC autophosphorylation itself (see Figure 3.9), it is still considerably less potent than eCF506 or dasatinib. Taken together, the data shows that eCF506 is the most consistently potent SRC activity inhibitor in 2D cell models out of the four tested.

The screening of eCF506 against the kinase panel and comparison to previous data sets for dasatinib and bosutinib highlights its superior selectivity for SRC kinase and SRC family kinases across the whole kinome (see chapter 3.2.1.1). Not only do dasatinib and bosutinib have two- and three-fold more off-targets at half the concentration, respectively, they also inhibit several kinases much more potently than SRC or ABL (see Table 3.4). These off-targets likely affect their potency and/or toxicity, which renders their general labelling as dual SRC/ABL inhibitors inadequate and highlights the importance of comprehensive target-deconvolution studies as discussed in a recent paper by Lin *et al*. [333]. In contrast, eCF506's primary kinase target is SRC kinase followed by other SFKs, although no information is available yet about possible non-kinase targets. Its superior selectivity profile and thousand-fold selectivity for SRC over ABL kinase clearly distinguishes eCF506 from dual SRC/ABL inhibitors and can address the concerns of ABL-inhibition linked cardiotoxicity and the emerging role of ABL as a tumour suppressor in certain cancers (see chapter 1.3.3) [282,288].

In order to confirm this key finding again in a cell model, several experiments have been attempted to test for the selectivity gap. It was found that measuring of phospho-CRKL (Y207) levels is not a specific readout of wild-type ABL1 kinase activity, despite its repeated use in the literature, as it was still inhibited by eCF506 and dasatinib in ABL1 knockout cell lines (see Figure 3.12). While it is possible that ABL2 (ARG) somewhat compensates for ABL1 loss in this model, it is likely that SRC inhibition alone also affects CRKL phosphorylation; studies have found that SRC activity can trigger translocation of the adapter protein to focal adhesions where it interacts with the SRC substrate p130Cas [334]. Since SRC inhibition affects focal adhesion formation and turnover (see chapter 1.2.3.1), it is likely that a SRC inhibitor would affect CRKL activity in the cell.

Measuring phosphorylation of tyrosine 245 on ABL kinase, which was found to increase ABL activity, showed similar potency for eCF506 and dasatinib (see Figure 3.11). Several papers found that SRC kinase and other SFKs can interact with ABL

and affect its kinase activity; HCK, FYN and LYN in particular were found to phosphorylate tyrosine 245 and other residues on ABL [320,321,335,336]. The finding that SFKs can phosphorylate and activate ABL could explain the difficulty in trying to assess eCF506's distinct inhibitory effects on each kinase. However, since the effect of SFKs on ABL activation is additive to the autophosphorylation of ABL, it is unlikely that SFK inhibition would fully inhibit ABL functions; for example, the Zebrafish assay by Fraser *et al.* showed that the SRC/ABL inhibitor dasatinib but not the SRC inhibitor eCF506 induces cardiac hyperplasia, an observation closely linked to ABL activity [1,287]. However, it is possible that SFK inhibition and consequent effects on ABL signalling contribute to eCF506's potency in CML cell lines (see chapter 3.1.1.1).
A thermal stability assay was unable to confirm binding of eCF506 or dasatinib to ABL kinase (see Figure 3.13). However, using three CML cell lines as an indirect measure of BCR-ABL inhibition successfully confirmed a more than thousand-fold potency difference between eCF506 and dasatinib. GI_{50} values for CML cells were in the same range as the IC_{50} data for wild-type ABL from the kinase panel, which makes a strong case for this model as a readout of ABL inhibition; yet it is important to point out that this assay has drawbacks, such as the assumption that cell viability fully depends on BCR-ABL activity and that compounds would bind ABL kinase the same as BCR-ABL. All the same, the CML data gives confidence that the findings from isolated kinase assays can translate into cellular models and that eCF506 is indeed a thousand-fold more selective for SRC over ABL than dasatinib; this strengthens its unique status among the small molecule SRC inhibitors (see Table 1.3).

3.3.2. eCF506 inhibits cell proliferation by inducing cell cycle arrest in the G1 phase

The testing of eCF506 in several different screens showed that it is similar to dasatinib and much better than bosutinib, saracatinib and imatinib at inhibiting the proliferation of solid cancer cell lines in 2D models. The screen of oesophageal cell lines also showed selectivity of SRC inhibitors for cancer cell lines over normal tissue. eCF506's potency varied considerably between cell lines over a 3 log-fold range (GI_{50} range: 14.7 nM to 50.8 µM); breast cancer cell lines with HER2 amplification were generally more resistant than those classified as triple negative or ER positive, while ovarian clear cell carcinoma were more sensitive than other ovarian subtypes.

The shape of the dose-response curves was often biphasic (see Appendix A.1). One possible explanation for this is that SRC, unlike v-Src, is not the only driver of proliferation in cancer but rather a contributing factor; therefore, treatment with lower concentrations would only cause a drop in cell proliferation to the degree of SRC's contribution, while the second drop in the dose-response curve is likely due to off-target effects that occur at higher concentrations (see chapter 3.2.1.1).

The degree to which eCF506's anti-proliferative effects are due to changes in the cell cycle or cell death was only partially assessed by Fraser *et al.* and required further investigation. It has previously been shown that the compound was able to increase caspase 3/7 activity, a measure of apoptosis, after 5 days in MCF-7 cells; however, the ratio of apoptotic to non-apoptotic cells only doubled at 100 nM compared to DMSO, which cannot explain the potent effects seen in cell viability assays at this concentration [1]. In this thesis, a cell cycle assay in the same cell line as well as MDA-MB-231 cells showed that eCF506 significantly increases the proportion of cells in the G1 phase at 100 nM after 48 hours (see Figure 3.2); the proportion of MDA-MB-231 cells in the M and G2 phase of the cell cycle was more than halved, although lesser effects were seen in MCF-7 cells. Consequently, eCF506 appears to have mainly cytostatic rather than apoptotic or cytotoxic effects at sub-micromolar concentrations by triggering cell cycle arrest in the G1 phase. Other studies have also found G1 cell cycle arrest for the SRC inhibitors dasatinib, bosutinib and saracatinib in solid tumours [331,332,337]. SRC activity can promote cell cycle progression by phosphorylating and thus destabilising the CDK inhibitor p27 and its inhibition was shown to increase p27 stability and reduce G1 to S phase progression (see chapter 1.2.3.211) [52,71]. It is therefore likely that the eCF506-induced arrest in G1 phase is linked to stabilisation of p27 but further studies should be done to confirm this.

While eCF506 and dasatinib had potent anti-proliferative effects in the 2D screens, their ability to reduce the size of 3D spheroids of the same cell lines was much lower. 3D models such as spheroids more closely mimic the features of tumours than 2D models, for example structural organisation, cell-cell adhesion and gradients of oxygen and nutrients which allow the formation of a necrotic core [338].
Micromolar concentrations of eCF506 were needed to significantly reduce spheroid size in comparison to DMSO treated controls in most cases. Dasatinib was more potent than eCF506, with the biggest effect seen in MDA-MB-231 cells, where it

reduced spheroid size by 44% at 300 nM and even more at higher doses. The effects of both compounds were stronger after 7 days than 4 days of treatment, confirming that they remain stable and active in solution for at least one week and that cells are not able to overcome their effects during this time.

Staining with calcein-AM and propidium iodide showed only some treatment-induced cell death in MDA-MB-231 cells at high concentrations. This suggests that eCF506 and dasatinib have mainly cytostatic effects in MCF-7 and T-47D cells, as seen in the 2D assays of chapter 3.1.1.2. However, the variability of spheroid growth between cell lines (T-47D grew in size, while MCF-7 did not, and MDA-MB-231 shrank) means their antiproliferative effects may be hidden in this assay when measuring only spheroid size; yet, even in the growing T-47D spheroids eCF506 had only little effects at nanomolar concentrations (see Figure 3.4). Future Western blots and cell cycle analysis of the spheroids will be able to show whether eCF506 is still able to inhibit SRC phosphorylation and induce G1 cell cycle arrest at similar concentrations as in the 2D assays or whether it does not achieve sufficient target inhibition in 3D, for example due to the drug gradient across the spheroid. Another possible explanation for the low potency is that 3D features, such as increased cell-cell adhesion and lack of adhesion to the microenvironment via focal adhesions in 2D assays, might reduce the cells' dependency on SRC kinase and consequently the effects of SRC inhibition. A preliminary comparison of the amounts of phospho-SRC and total SRC between cells grown in 2D or 3D shows different trends between cell lines, with significantly more SRC phosphorylation in 3D than 2D in MDA-MB-231 cells, but little difference in MCF-7 cells (see Appendix A.5). Further assays are needed to clarify the effects of eCF506 and dasatinib in 3D models with endpoints other than spheroid size and live/dead cell staining. Nevertheless, current results suggest that high concentrations of eCF506 might be needed to reduce tumours of these three cell lines in *in vivo* models when given as monotherapy. Future studies should also look at bosutinib and saracatinib to assess whether they are similarly less potent in 3D spheroids compared to 2D models.

Several previous studies have tried to identify a biomarker that can predict sensitivity to SRC inhibition. The obvious place to start is to assess the relative quantity and activity of SRC kinase; two studies found that gastric and colorectal cancer cell lines sensitive to saracatinib had higher levels of phospho-SRC (Y416) compared to resistant cells and another one showed higher SRC expression in colorectal cancer

cell lines that were sensitive to dasatinib [331,337,339]. An analysis of the phospho-SRC (Y416) and total SRC levels by Western blot in a panel of 29 breast and ovarian cancer cell lines showed a significant correlation between sensitivity to eCF506 and phospho-SRC Y416 status, but not total SRC amounts (see Figure 3.3 and Appendix A.3). However, this link does not appear to be strong enough to reliably predict cell line response and so far no clinical trial with SRC inhibitors was successful enough in stratifying patient response to gain regulatory approval (see chapter 1.3.2). Further in-depth analysis of the GDSC screening data could help identify better biomarkers for sensitivity to eCF506 by using the sequencing and gene expression data available for all the cell lines; however, comparison between the GDSC and in-house and other published results suggests that the GDSC methodology is tailored to identify cytotoxic effects, which explains why the majority of BCR-ABL-dependent CML cell lines were found to be sensitive but breast cancer ones were not. It might be possible to identify cytostatic effects better through improved curve fitting (e.g. biphasic curves) and taking into account pre-treatment cell viability. Proper analysis of this dataset with advanced bioinformatics and gene expression analysis could therefore provide potential candidate biomarkers. One possible biomarker for SRC sensitivity is *ARID1A* status in a subset of ovarian cancer, which is further explained in the next chapter 3.3.3.

3.3.3. *ARID1A* mutant ovarian clear cell carcinoma are especially sensitive to SRC inhibition

The GDSC panel revealed that ovarian cancer cell lines appear to be especially sensitive to eCF506 compared to other solid cancer types. Several papers and clinical trials have previously investigated SRC inhibitors in ovarian cancer, often in combination with chemotherapy such as paclitaxel [167,257,309]. Konecny *et al.* has previously tested a panel of 34 ovarian cancer cell lines against dasatinib with similar results as reported here (see chapter 3.1.1.2) [310]. Both this thesis as well as Konecny *et al.* found that ovarian cancer cell lines classified as clear cell carcinoma (CCC) tend to be more sensitive to eCF506 or dasatinib than other subtypes. CCC generally respond poorly to standard platinum-based chemotherapy and new treatment options are needed [340]. A previous study analysed hundreds of primary ovarian cancer tissues and found that phospho-SRC (Y416) expression was significantly higher in CCC

compared to other subtypes, with nearly 60% expressing the phospho-protein [341]; however, no such trend was found in the analysis of phospho-SRC levels in this thesis (see Figure 3.3). Phospho-SRC expression in CCC was further linked to sensitivity to SRC inhibition and associated with shorter overall survival in patients [341].

Several potential driver mutations have been identified in endometriosis-associated ovarian cancers, to which both CCC and endometrioid carcinoma (EC) belong. One is the tumour suppressor and epigenetic regulator *ARID1A*, which was mutated in 46% of 119 tested CCC and 30% of 33 EC tumours, but in none of the 76 high-grade serous ovarian cancers (HGSOC) tested in one study [342]. Another study found mutations in 57% of 42 tested CCC samples [343]. Miller *et al.* showed that *ARID1A* mutant CCC cell lines are more sensitive to dasatinib than those with a wild-type copy [344]. This finding matches the results obtained in this study, with all *ARID1A* mutant CCC and EC cell lines (OVTOKO, TOV-21G, OVMANA, IGROV-1, OC-314) exhibiting much higher sensitivity to eCF506 and dasatinib than those with *ARID1A* wild-type copies (ES-2, TOV-112D). CCC as well as one breast and colorectal cancer cell line with wild-type *ARID1A* were also found to become more sensitive to dasatinib when *ARID1A* was knocked down by siRNA [344]. Further analysis found that *ARID1A* mutant cells are addicted to the SRC family kinase YES1 and that SFK inhibition can thus result in synthetic lethal effects [344]. These findings suggest that *ARID1A* could be a potential biomarker, along with phospho-SRC status, for sensitivity of endometriosis-associated ovarian cancer cell lines to eCF506 and dasatinib. A recently completed phase II clinical trial that tested dasatinib in ovarian cancer (NCT02059265) determined *ARID1A* mutation status in patients, although this data was not correlated to patient response; overall the trial results were negative, with an ORR of only 3.6%, PFS of 2.14 months and overall survival of 16.9 months [246].
Several other synthetic lethal targets have also been identified in *ARID1A* mutant CCC, such as PARP, ATR and BET inhibitors, which are linked to *ARID1A*'s role in the DNA damage checkpoint [345,346]. Comparative testing is needed to identify the best treatment option or combination therapy for *ARID1A* mutant CCC patients.

ARID1A mutations were also found in pancreatic (8-47%), gastric (8-29%) and breast cancer samples (4-35%) [347]. No link can be made about the *ARID1A* mutation status in the breast cancer cell lines used in chapter 3.1.1.2 and sensitivity to eCF506, as only T-47D cells are known to have a mutation [348]. However, several papers have

investigated the expression levels of *ARID1A* in breast cancer, which correlated with sensitivity to inhibitors of CDK4/6, mTOR 1/2, SHP 1/2 [349], PI3K, AKT [350] as well as trastuzumab [351] and paclitaxel [352]. The publicly available data of the GDSC screening project also shows that AKT inhibitors especially seem to be more potent across cell lines with *ARID1A* mutations [307]. Interestingly, the unclassified ovarian cancer cell line SKOV-3 has a mutation in *ARID1A* but was only moderately sensitive to SRC inhibitors, while the non-CCC ovarian cancer cell line OC-314 is also mutated and was a hit in the GDSC screen (see Table 3.1 and Figure 3.1). Future assessment of *ARID1A* expression in the cell lines tested in this thesis could reveal whether this tumour suppressor gene is also linked to sensitivity to SRC inhibition in other cancers or whether the unique biology of CCC makes it especially sensitive.

3.3.4. eCF506 has anti-angiogenic properties in non-cancer models

SRC activity has been strongly linked to endothelial cell proliferation and migration which is essential in angiogenesis, as described in detail in chapter 1.2.3.4. An *in vitro* comparison of five SRC/ABL inhibitors, the FAK inhibitor VS-4718 and the FDA-approved VEGFR inhibitor sunitinib showed that eCF506 was superior at inhibiting proliferation of human umbilical vein endothelial cells (HUVEC), which are a model of angiogenesis (see Figure 3.5). eCF506 also slightly inhibited HUVEC migration in a scratch wound assay, unlike VS-4718 and sunitinib. However, as seen in chapter 3.1.2, 2D cell viability assays do not always translate into 3D models. Therefore, the blood vessel outgrowth from *ex vivo* murine choroid explants treated with eCF506, dasatinib or saracatinib was tested in collaboration with the company Thrombogenics. Both eCF506 and dasatinib but not saracatinib potently inhibited vessel outgrowth at low nanomolar concentrations (see Figure 3.7).

These results are promising and suggest that eCF506 could be used to prevent tumour vascularisation as well as other angiogenesis-associated diseases. Pathological blood vessel growth is found in many diseases, such as arthritis, psoriasis and retinopathies [353]. One common complication of diabetes is retinal damage caused by high glucose levels in the blood [354]. Diabetic retinopathy develops in three stages and over the course of several years; the last stage, proliferative retinopathy, involves the formation of new blood vessels and can lead to loss of vision. At this stage, intervention becomes necessary, which currently includes laser

treatment, eye surgery or injections of anti-VEGF compounds or antibodies [354,355]. A previous study found that dasatinib can reduce diabetes-induced and VEGF-mediated retinal vascular leakage [186]. eCF506 might be similarly potent and its superior solubility could allow for easier formulation for topical application [1]. Therefore, further investigations into the anti-angiogenic properties of eCF506 are warranted.

Chapter 4. Differences between eCF506 and dasatinib

eCF506 was developed in a phenotypic screening approach that used the kinase inhibitor PP1 as a scaffold [1]. While PP1 is often described as a selective SRC inhibitor in the literature, it also inhibits KIT, ABL, EGFR and other kinases, making it similarly promiscuous as dasatinib but with much lower potency (see Table 1.3) [356]. Sequential ligand-based design coupled to cell viability assays resulted in the discovery of eCF506, a molecule which shows high selectivity for SRC over the other kinase targets of PP1 and dasatinib. The results of Chapter 3 and Fraser *et al.* confirm its potency in *in vitro* assays of target inhibition, cell proliferation, migration and angiogenesis [1]. While it was clearly superior to the SRC/ABL inhibitors bosutinib and saracatinib or the ABL inhibitor imatinib, it performed similarly well to dasatinib, the current gold standard SRC inhibitor. This raises the question in which ways other than its selectivity profile eCF506 distinguishes itself from dasatinib.

This chapter identifies important differences between eCF506 and dasatinib in their binding mode to SRC kinase and their impact on overall kinase confirmation. This revelation allowed the interpretation of results from a reverse-phase protein array that was done in order to compare both compounds' effects on downstream cell signalling pathways. As a result, inferences can be made on the role of the inhibitor-induced conformation of SRC's αC helix and the kinase's ability to bind its downstream target FAK.
Another difference between eCF506 and dasatinib that has been identified in this thesis is the subcellular localisation of FAK and SRC kinase. Further investigations are needed to determine whether this is linked to the inhibitor's differential effects on SRC-FAK interactions or to their selectivity profiles.

This chapter explores the following aims:

- Determination of eCF506's binding mode to SRC kinase.

- Screening of differential effects of eCF506 and dasatinib on downstream cell signalling pathways.

- Comparison of the subcellular localisation of FAK and SRC with eCF506 and dasatinib and exploration of potential impacts on gene expression.

4.1. eCF506 and dasatinib have opposite effects on SRC conformation

4.1.1. Thermal shift assay suggests eCF506 and dasatinib bind SRC differently

In chapter 3.2.2 a thermal shift assay was performed to confirm the differential engagement of ABL kinase by eCF506 and dasatinib. This assay is based on the published methodology for thermal shift assays in live cells by Jafari *et al.* and used MDA-MB-231 cells treated with eCF506 (300 nM), dasatinib (300 nM) or control (DMSO) [296]. While the assay did not show a significant shift in ABL stability, which was in line with previous findings, assessment of the same samples for SRC kinase stability yielded surprising results [324]. eCF506 and dasatinib appeared to have significant but opposite effects on the apparent melting temperature (T_m) of SRC compared to DMSO, with the former stabilising but the latter destabilising the kinase (see Figure 4.1).

One hypothesis for these results is that the compounds force SRC to take on different conformations that are either more or less likely to form insoluble aggregates when heated, as protein aggregates are subsequently removed from cell lysates by centrifugation. Previous studies report that SRC's thermal stability is reduced in the presence of ATP or a peptide that binds its SH3 domain and forces SRC into an active conformation [357,358]. Dasatinib is known to bind the active conformation of SRC kinase and taken together these findings indicate that binding of eCF506 to SRC kinase might induce a different conformation from dasatinib [218,359,360].

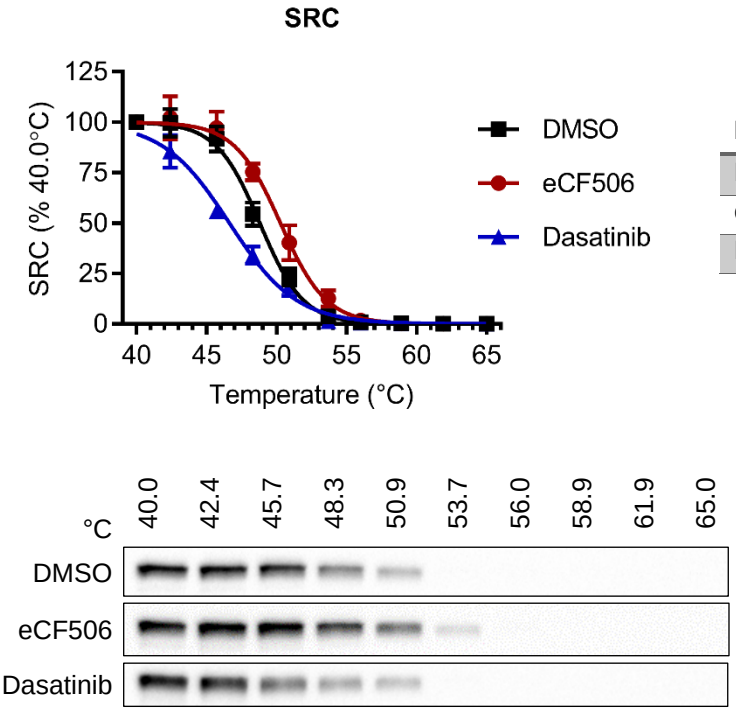

Inhibitor	T_m
DMSO	48.8
eCF506	50.3 (p<0.01)
Dasatinib	46.6 (p<0.001)

Figure 4.1. Thermal shift assay of SRC kinase after treatment with eCF506 and dasatinib. MDA-MB-231 cells were treated with eCF506 (300 nM), dasatinib (300 nM) or DMSO for one hour prior to heating, cell lysis and analysis by Western blot. Band intensities were quantified using Bio-Rad ImageLab® software and normalised to the lowest temperature band for each condition. The top graph shows the average of three biological repeats with standard deviation. The table shows average T_m values calculated by GraphPad Prism 7 and compared to DMSO by one-way ANOVA with Dunnett correction for multiple comparison. The bottom figure shows a representative Western blot.

4.1.2. eCF506 binds SRC kinase in its closed and autoinhibited state

4.1.2.1. X-ray crystallography of the SRC kinase domain reveals a TypeI1/2A binding mode for eCF506

This work was done by Dr Daniel Lietha at the Centro de Investigaciones Biológicas (CIB) in Madrid, Spain.

The observations made in the thermal shift assay in chapter 4.1.1 suggest that eCF506 is potentially inducing a different conformation in SRC kinase upon binding than dasatinib. This was further investigated by determining the crystal structure of eCF506 bound to SRC by X-ray crystallography.
Dr Daniel Lietha generated a co-crystal structure with excellent resolution (1.5 Å) of eCF506 complexed with the kinase domain of SRC (see Figure 4.2). It shows that eCF506 binds strongly to SRC via numerous hydrogen bonds as well as hydrophobic interactions, which are highlighted in Figure 4.2b. The adenine-mimicking pyrazolopyrimidine core of the molecule perfectly overlays with the location of the purine ring of ATP bound to SRC, as previously predicted in *in silico* studies [1]. The highly conserved DFG motif in the activation loop, which is involved in the catalysis of phosphate transfer, is in an "in" conformation, with the aspartate residue 404/407 (chicken/human numbering) pointing inward as seen in the active SRC conformation. The *tert*-butyl group of the carbamate extends deep into the protein to reach a back-pocket beyond the so-called gatekeeper residue (T338/341) (see Figure 4.2b). This distinguishes the binding mode of eCF506 from that of dasatinib, as binding to the back-pocket stabilises an inactive SRC confirmation with the αC helix in an "out" position (see Figure 4.3). eCF506's induction of a "DFG-in" and "αC helix-out" conformation is also called "SRC-like inactive", as it was first observed in the autoinhibited conformation of SRC kinase, in which the phosphorylated Y527/530 residue in the C-terminus binds to the SH2 domain, forcing the whole kinase into a "closed" and inactive conformation (see Figure 4.4) [361,362].

eCF506's binding mode is classified as TypeI1/2A based on Roskoski's classification system, which places it between the Type I inhibitors that bind the active DFG-in state and the Type II inhibitors that bind an inactive DFG-out conformation (see Table 4.1) [360]. The most potent SRC inhibitors currently available, dasatinib, bosutinib, ruxolitinib and AP23464 (see Table 1.3), are all Type I inhibitors that bind SRC in an active

"DFG-in" and "αC helix-in" conformation (see Figure 4.3) [360]. Saracatinib has been described as a Type II inhibitor but papers differentially report its binding mode either as both motifs in an "in" position or as "DFG-in", "αC helix-out"; the X-ray crystal structure available on PDB supports the latter and suggests that it might be a Type I1/2 inhibitor like eCF506 (see Figure 4.3g) [230,363,364]. The dasatinib-derivative UM-164 is a Type II inhibitor that induces a clear flip of the aspartate and phenylalanine of the DFG motif (see Figure 4.3h) and it binds to the protein in an "αC helix-in" conformation, opposite to eCF506; two other dasatinib derivatives were developed to bind an "αC helix-out" and "DFG-out" conformation [230,231,363].

The only other inhibitor that has been reported to bind a similar SRC-like inactive conformation (i.e. DFG-in, αC helix-out) as eCF506 and likely saracatinib is the promiscuous inhibitor PP1, although this binding mode was found in HCK kinase and not investigated in SRC itself (see Figure 4.3c) [360]. Given that eCF506 has been developed in a ligand-based phenotypic screening approach based on PP1, it is perhaps not surprising that it would bind in a similar way. However, it is important to note that PP1 appears to induce an "αC helix-out" confirmation in HCK without occupying the back pocket and its selectivity profile is very poor [360].

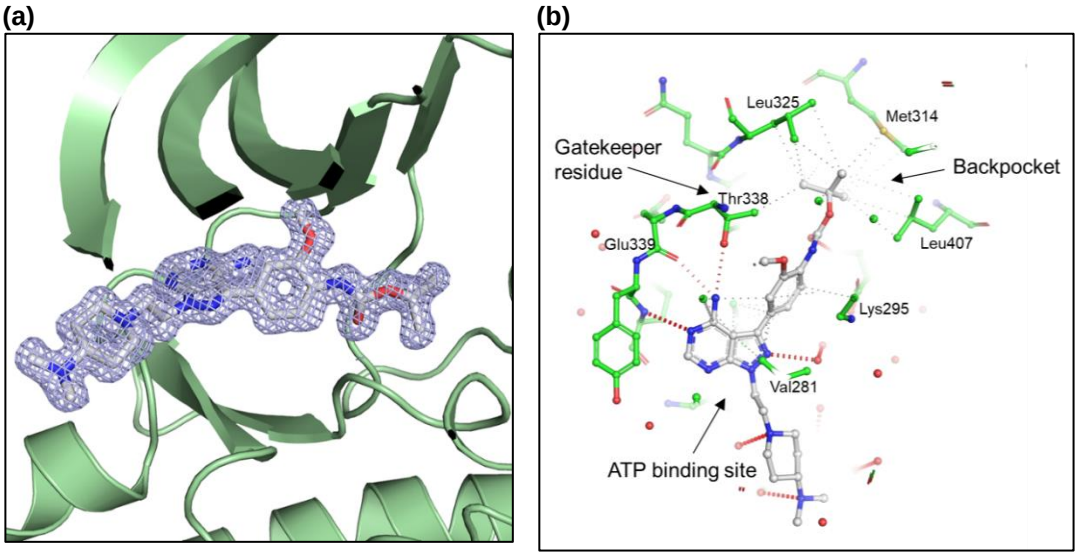

Figure 4.2. eCF506 bound to the ATP binding site of the SRC kinase domain. (a) Electron density map and (b) main interactions of eCF506 bound to SRC kinase domain. Red dotted lines = hydrogen bonds, grey dotted lines = hydrophobic interactions. Figures created by Dr Daniel Lietha, 2018.

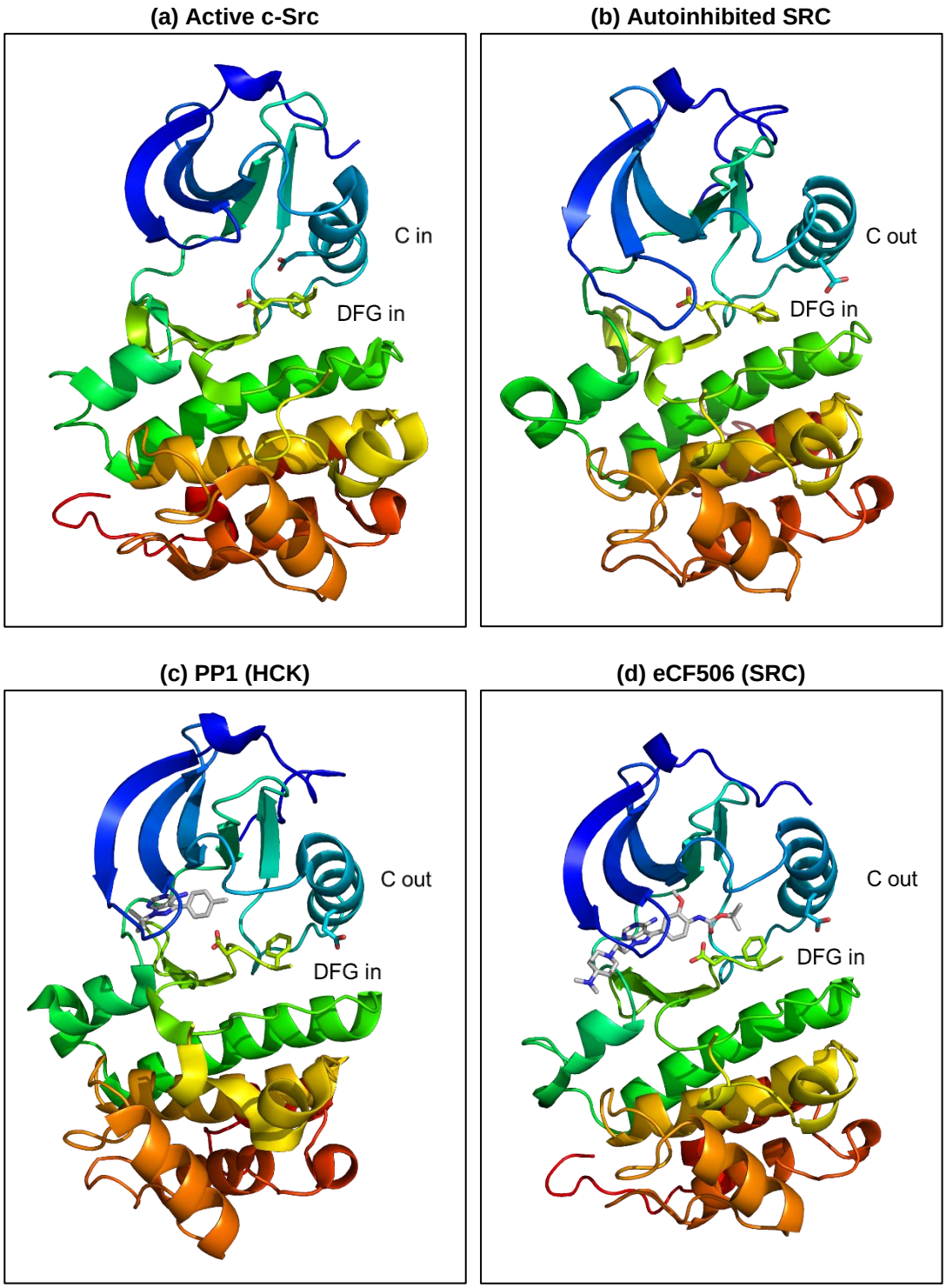

Figure continued on next page

Figure continued from previous page

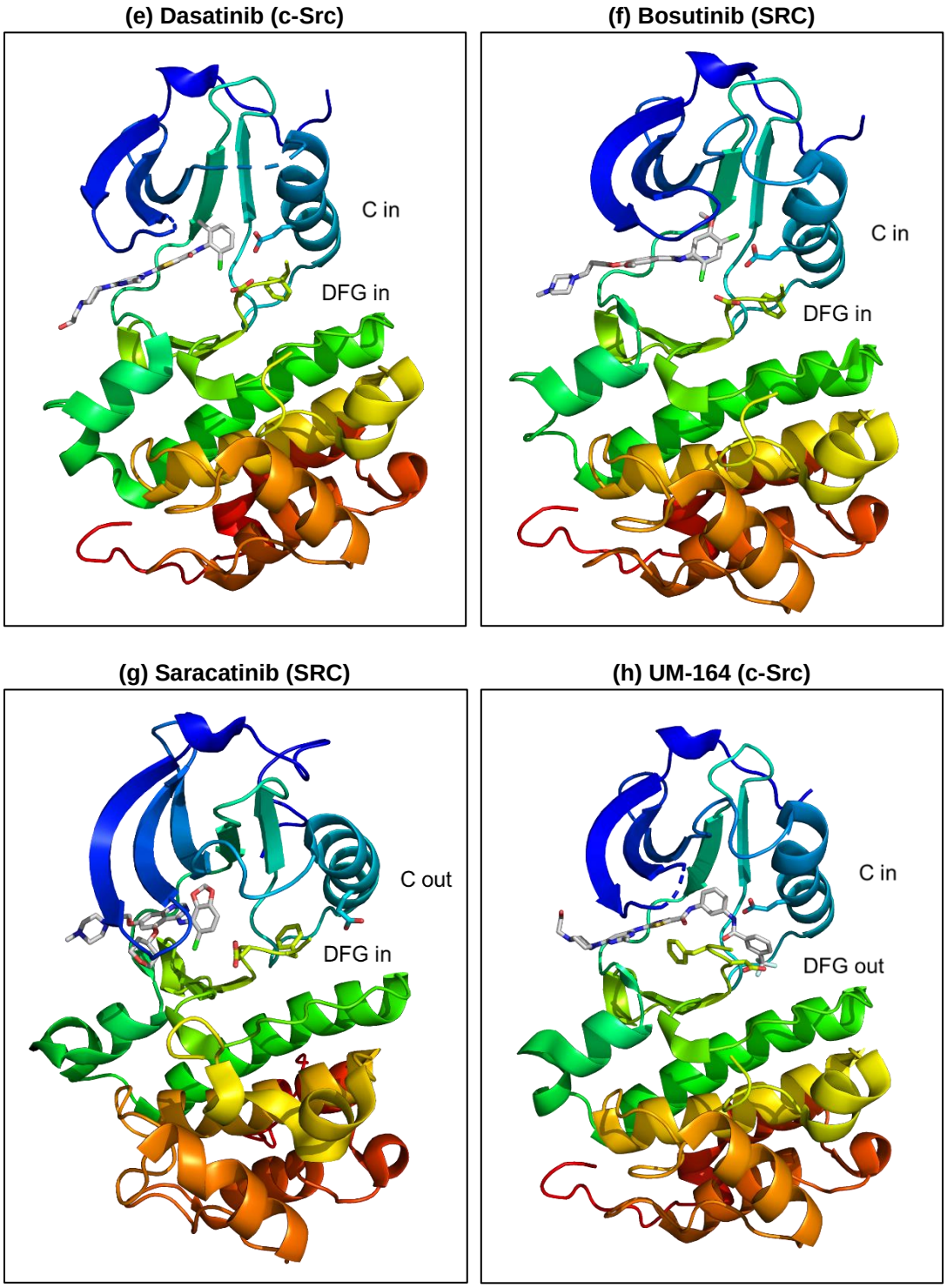

Figure 4.3. Binding modes of SFK inhibitors. Figures show SRC in its (a) active or (b) autoinhibited state or (c-h) SRC or HCK bound to different inhibitors. Residues highlighted are D404 and F405 of the DFG motif in the activation loop and E310 in the αC helix. Figures were created with PyMOL using structures published on the PDB (see Table 4.1 for ID). SRC/HCK = human protein, c-Src = chicken protein.

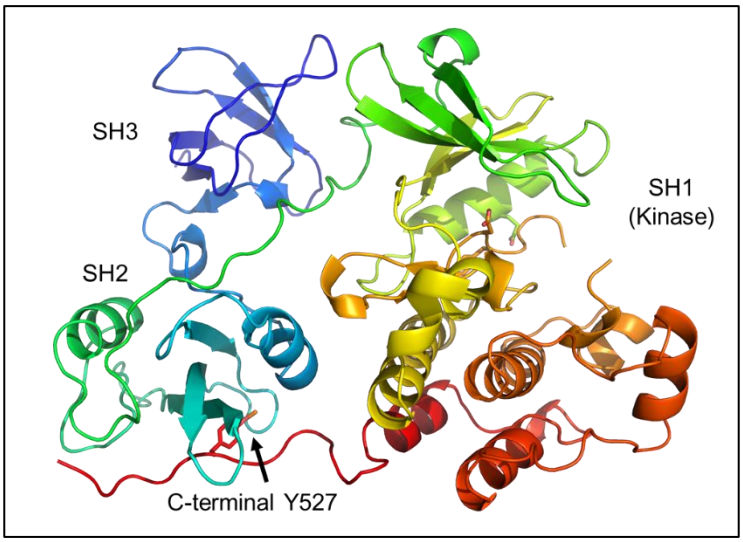

Figure 4.4. Autoinhibited conformation of SRC kinase. Phosphorylation of the Y527 residue in the C-terminus allows binding to the SH2 domain, which locks the protein in an inactive, closed conformation. Residues highlighted are D404 and F405 of the DFG motif in the activation loop, E310 in the αC helix and Y527 in the C-terminus. Figure created with PyMOL using crystal structure published on the PDB (ID: 1FMK).

Table 4.1. Binding mode of different SRC/ABL inhibitors to SRC and ABL kinase. Classification is based on Roskoski (2016) [360]: Type I = DFG-in, αC helix-in; Type I1/2 = DFG-in, αC helix-out; Type II = DFG-out, αC helix-in; A = extends into back pocket; B = does not extend into back pocket; SRC/HCK/ABL = human, c-Src = chicken, c-Abl = mouse.

Inhibitor / State	PDB ID	Protein	DFG	C-helix	Class
Active c-Src kinase	3DQX	c-Src	In	In	-
Autoinhibited SRC kinase	1FMK	SRC	In	Out	-
eCF506	-	SRC	In	Out	I1/2A
Dasatinib	3G5D	c-Src	In	In	I
Bosutinib	4MXO	SRC	In	In	I
Ruxolitinib	4U5J	c-Src	In	In	I
AP23464	2BDJ	SRC	In	In	I
Saracatinib	2H8H	SRC	In or Out	Out	I1/2 or II
Dasatinib-analogue CHO	4YBK	c-Src	Out	Out	II
Dasatinib-analogue DFG-out (UM-164)	4YBJ	c-Src	Out	In	II
PP1	1QCF	HCK	In	Out	I1/2B
Imatinib	1IEP	c-Abl	Out	In	IIA
Dasatinib	2GQG	ABL	In	In	I
Bosutinib	3UE4	ABL	Out	In	IIB

4.1.2.2. SRC (Y527) is differentially phosphorylated by eCF506 compared to other SRC/ABL inhibitors

The X-ray crystallography data revealed that binding of eCF506 to the SRC kinase domain is classified as Type I1/2A, different from the active Type I conformation seen with dasatinib and bosutinib or the previously reported Type II binding of saracatinib, although the latter may bind similarly to eCF506 (see chapter 4.1.2.1). However, as not the full-length protein was crystallised, it remained unclear whether eCF506 only induced a "SRC-like inactive" motif in the kinase domain or whether it had the capacity to induce a closed conformation of the whole kinase as seen in the autoinhibited state (see Figure 4.4). The closed SRC conformation is characterised by the phosphorylation of the tyrosine 527 residue in the C-terminus, which enables it to bind to the SH2 domain. Therefore, phospho-SRC (Y527) phosphorylation was assessed by Western blot for MDA-MB-231 and MCF-7 cells treated with eCF506, dasatinib, bosutinib or saracatinib for 3 or 24 hours.

The Western blots show that eCF506 maintains phosphorylation of SRC (Y527) at similar levels to untreated control, while dasatinib induces a dose-dependent decrease in phosphorylation at the autoinhibition site (see Figure 4.5 and Appendix A.8). These findings are consistent with the hypothesis that eCF506 maintains SRC in a closed, autoinhibited state, whereas dasatinib forces the whole kinase into an open conformation. Consequently, while both compounds can potently inhibit kinase activity (see chapter 3.2.1.2), only eCF506 also inhibits the "scaffolding" functions of the open SRC conformation, such as binding of other proteins via its SH2 domain [130]. Similar results were seen with bosutinib and saracatinib, albeit at higher concentrations due to their lower potency against SRC in cells (see chapter 3.2.1.2); bosutinib treatment caused consistent dephosphorylation of SRC (Y527), while saracatinib's effects differed between biological repeats but generally reduced the levels of Y527 phosphorylation (see Figure 4.5).

In conclusion, the results indicate that eCF506 not only binds a SRC-like inactive conformation in the kinase domain but also maintains the whole protein in a closed conformation that resembles the natural autoinhibited state of SRC. The different SRC structures induced upon binding of eCF506 or dasatinib could explain the opposite effects on the thermal stability of the kinase seen in chapter 4.1.1, as an open and flexible conformation might be more likely to form protein aggregates that precipitate out of solution upon heating than a closed and globular structure.

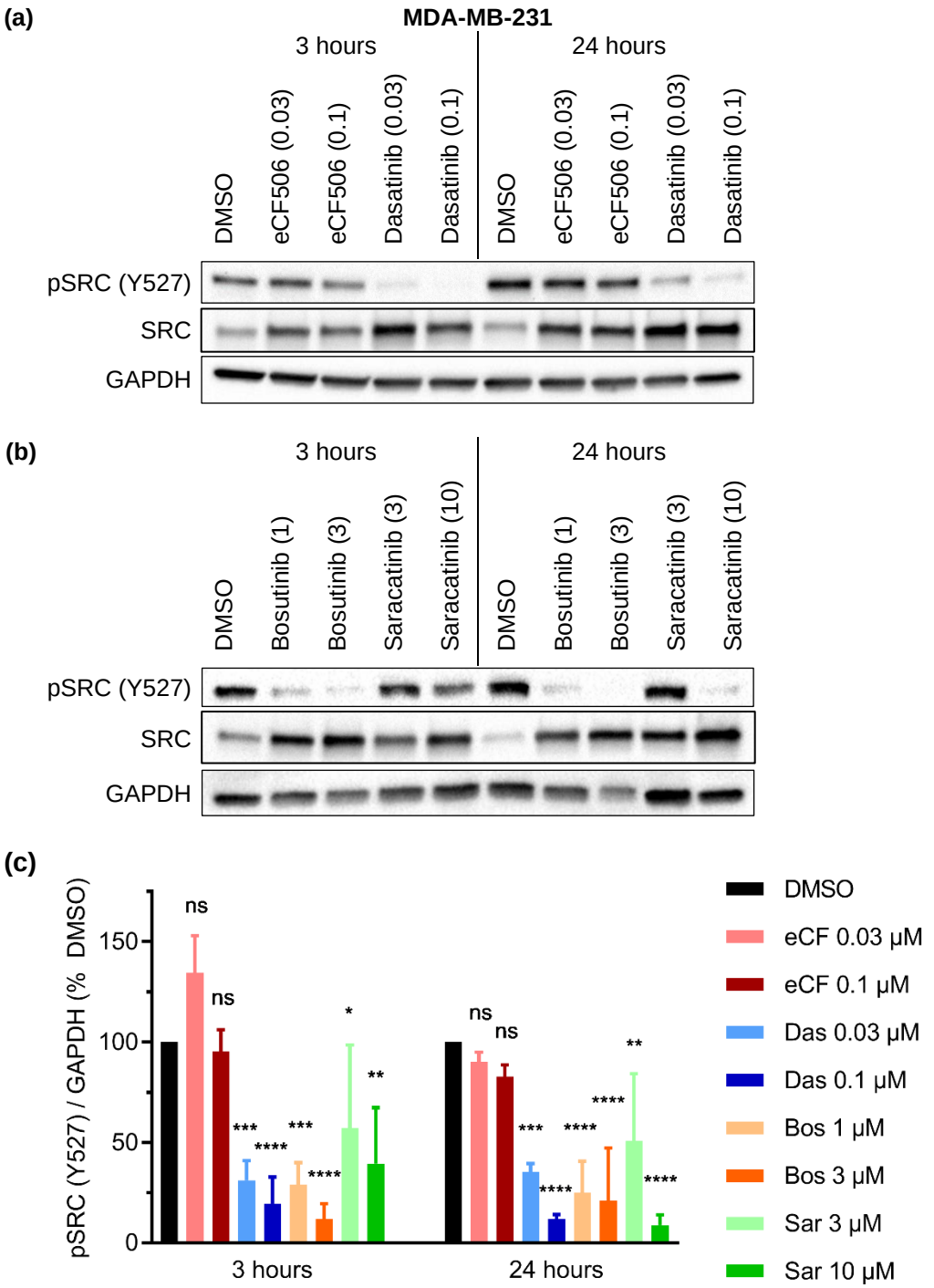

Figure 4.5. Western Blot analysis of phospho-SRC (Y527) in MDA-MB-231. MDA-MB-231 cells were treated for 3 or 24 hours with (a) eCF506 and dasatinib or (b) bosutinib and saracatinib at the concentrations specified. Representative Western blots of three biological replicates. Concentrations in µM. (c) Summary of MDA-MB-231 phospho-SRC (Y527) Western blots showing average of three biological replicates with standard deviation. Band intensities were quantified using Bio-Rad ImageLab® software, adjusted for loading using GAPDH and normalised to DMSO. Statistical analysis was performed comparing treated against DMSO using two-way ANOVA with Dunnett's correction for multiple comparison; p>0.05 (ns), p<0.05 (*), p<0.01 (**), p<0.001 (***), p<0.0001 (****).

4.2. SRC conformation differentially affects downstream FAK with unclear functional consequences

Structural investigation of eCF506 bound to SRC revealed opposite effects compared to dasatinib, with the former maintaining the kinase in a closed conformation similar to the natural autoinhibited state, while the latter forces it into an active-like open conformation (see chapter 4.1). While both compounds still potently inhibit SRC's kinase function, the question remained whether eCF506 inhibited scaffolding functions that are involved in downstream signalling. In order to compare eCF506 and dasatinib's effects, changes in the levels of downstream proteins were investigated in a reverse phase protein array (see chapter 4.2.1). The screening revealed that, although most signalling pathways were similarly affected by both compounds, they had opposite effects on the FAK autophosphorylation site. This can be linked to the different SRC conformations, which either enable or inhibit binding of SRC to FAK (see chapter 4.2.2). Further investigations were made into the potential impact of these findings on protein localisation and gene expression (chapter 4.3).

4.2.1. Reverse phase protein array shows FAK (Y397) is differentially phosphorylated by eCF506 and dasatinib

This work was done together with Kenneth Macleod from the Drug Discovery group of Prof Neil Carragher at the University of Edinburgh, UK.

A reverse phase protein array (RPPA) was performed to identify differences in cell signalling between eCF506 and dasatinib treatment. MDA-MB-231 and MCF-7 cells were treated with either compound for 3 or 24 hours, after which samples were analysed by RPPA on the Zeptosens platform. Results are shown as heat maps (see Figure 4.6) with protein levels expressed in units of relative fluorescence intensity (RFI) normalised to the respective DMSO control. After the exclusion of proteins with low signal (RFI <0.05), a total of 95 (MDA-MB-231) and 93 (MCF-7) proteins were included in the analysis.

Cell line and SRC-specific proteins

The cell lines exhibited characteristic differences in protein expression, with no Caspase 3 present in MCF-7 cells and no E-cadherin in MDA-MB-231 cells. As expected, a strong upregulation of total SRC and downregulation of SRC-phosphorylation sites on FAK (Y576/577, Y861, Y925) was observed with both compounds (Figure 4.6). Both SRC inhibitors also induced further characteristic changes in proteins associated with SRC signalling pathways; these include reduced phosphorylation of MET (Y1349) and JNK (Y185) as well as compensatory upregulation of proteins like total MET, the MAPK pathway (ERK1/2, p38 MAPK, MAPKAPK-2) and other downstream targets such as c-Jun, FRA1, STAT3, PI3K and NFkB (see chapter 1.2.3).

Apoptotis and cell cycle proteins

An overall increase in pro-apoptotic proteins (BAK, BAX, BID, BIM) and decrease in anti-apoptotic proteins (BCL-2, Survivin, XIAP) could be observed for both compounds (Figure 4.6) [365]. Although apoptotic cells can be washed off during the experiment, which can affect signal intensity of these proteins, the general trend of increased apoptosis signalling ties into the results of the caspase 3/7 apoptosis assay performed by Fraser *et al.* [1]. The upregulation of PTEN and downregulation of CDK2 indicates increased cell cycle arrest, which was confirmed in the cell cycle assay done in chapter 3.1.2 [366].

Other confirmed and refuted changes

The levels of several other proteins were found to be changed in response to eCF506 or dasatinib treatment in the RPPA, but this could not always be confirmed by Western blot. Both inhibitors seem to influence mTOR signalling by decreasing mTOR (Y2481) and increasing total mTOR protein. mTOR (Y2448) also seems to increase but Western blot analysis could not confirm this and indeed found levels to be reduced using the same antibody (see Appendix A.9). Similarly, β-catenin appears to be highly upregulated in both cell lines, but this was not found in Western blots, and the upregulation of JNK and downregulation of the oncogene c-Myc could also not be confirmed (see Appendix A.9). However, different antibodies were used for these Western blots than in the RPPA and the quality of the c-Myc and JNK Western blots in particular was poor. Nevertheless, these discrepancies highlight the need for verifying RPPA results.

The dramatic decrease of BRCA1 and Rb protein in MDA-MB-231 cells after 24 hours of treatment with both compounds could be confirmed by Western blot (see Figure 4.6 and Appendix A.9). Tau protein is also dramatically downregulated in this cell line, although none of these three proteins showed a big change in MCF-7 cells. An increase in E-cadherin levels in MCF-7 cells and decrease in the E-cadherin downregulating protein Slug in MDA-MB-231 cells suggests greater cell-cell adhesion with SRC inhibition, which ties into the role of SRC in the turnover of adherens junctions (see chapter 1.2.3.1) [367]. eCF506 and dasatinib increase H2AX, ATM and p53 in the cells and reduce the amount of phospho-Chk, which indicates DNA damage, although Western blot confirmation for this is still outstanding [368].

Phospho-FAK (Y397)

The only consistent and clear difference between eCF506 and dasatinib found in the RPPA screening was the differential phosphorylation of tyrosine 397 on FAK; dasatinib increased and eCF506 decreased phosphorylation of this residue in a dose-dependent manner. This was observed after short (3 hours) and longer (24 hours) treatment times in both MDA-MB-231 and MCF-7 cells and confirmed by Western blot (see Figure 4.7a,b and Appendix A.8). FAK (Y397) is autophosphorylated in response to integrin signalling and allows SRC to bind via its SH2 domain (see chapter 1.2.3.1). SRC kinase then phosphorylates multiple tyrosine residues on FAK (Y576, Y577, Y861, Y925), all of which were found to be downregulated by both eCF506 and dasatinib in the RPPA (see Figure 4.6). A previous paper reports a negative regulation of FAK (Y397) by phosphorylation of FAK (Y407), a site which has been suggested but not conclusively shown to be phosphorylated by SRC [369,370]. Phospho-FAK (Y407) was not investigated in the RPPA but assessment by Western blot shows that both eCF506 and dasatinib reduce phosphorylation of this site, suggesting that this is not the cause of FAK's differential autophosphorylation (see Figure 4.7c).

A likely explanation is that the different inhibitor-induced SRC conformations either enable or prevent binding to phospho-FAK (Y397); the open SRC conformation upon binding of dasatinib frees the kinase's SH2 domain to bind phospho-FAK (Y397), which could then protect this site from dephosphorylation by phosphatases. This hypothesis is supported by the inverse correlation between SRC (Y527) and FAK (Y397) phosphorylation with eCF506 and dasatinib treatment (see Figure 4.7b).

Another Type I inhibitor, bosutinib, had the same effect as dasatinib, while the reported Type II but possible Type I1/2 inhibitor saracatinib showed variable results with phospho-FAK (Y397) (see Figure 4.5). SYF cells, which are murine embryonic fibroblasts deficient for SRC, YES and FYN kinase, exhibited no dose-dependent changes in phospho-FAK (Y397) levels when treated with eCF506 or dasatinib (see Figure 4.9a). Knockdown of SRC kinase in MDA-MB-231 cells by siRNA found no reduction in FAK autophosphorylation, but large variability was observed between repeats (see Figure 4.9b). This data suggests that SRC kinase conformation might affect FAK autophosphorylation status and that this can be augmented through specific inhibitors, but further experiments are needed to confirm this.

(a)

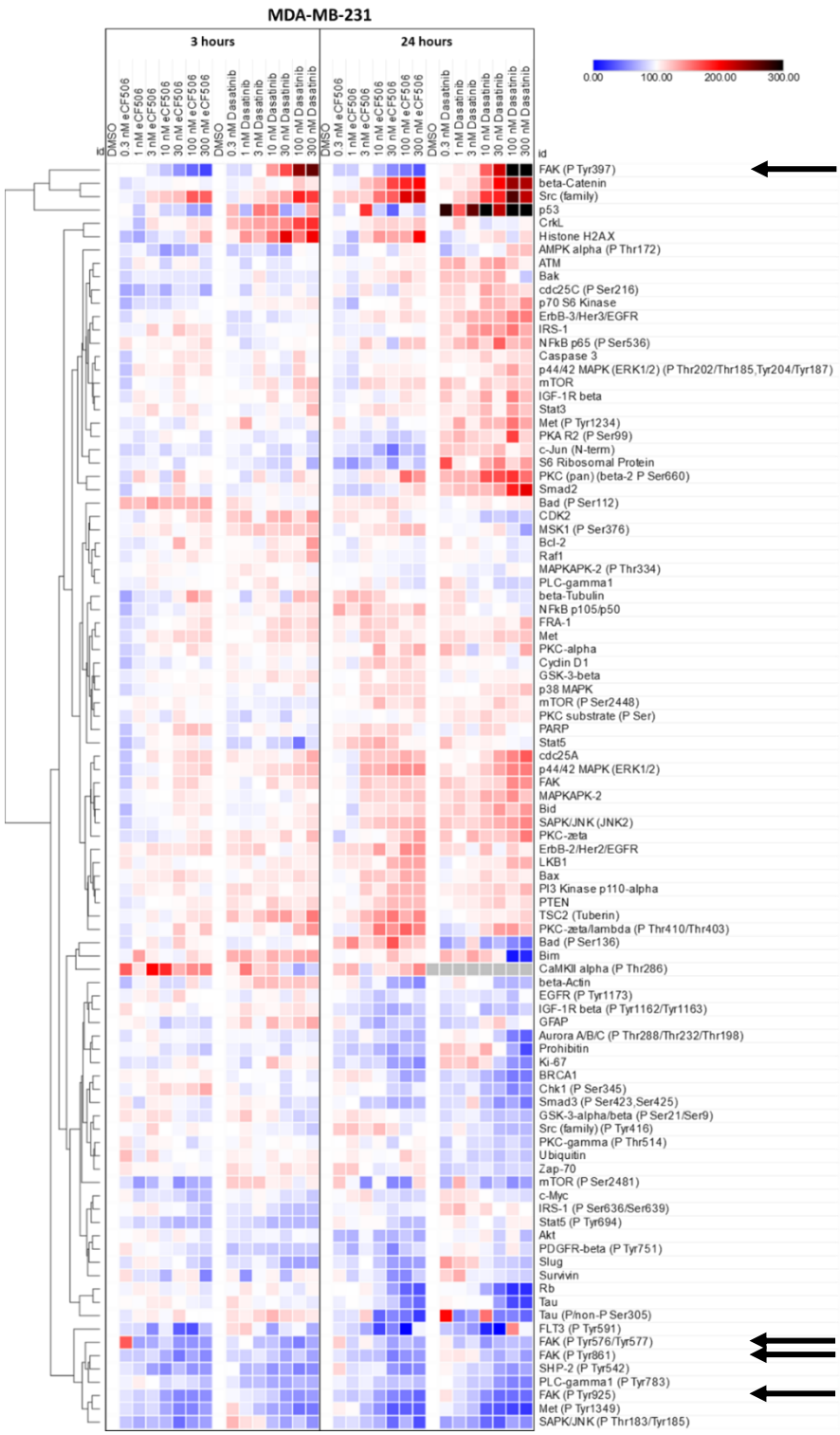

Figure continued on next page

Figure continued from previous page

(b)

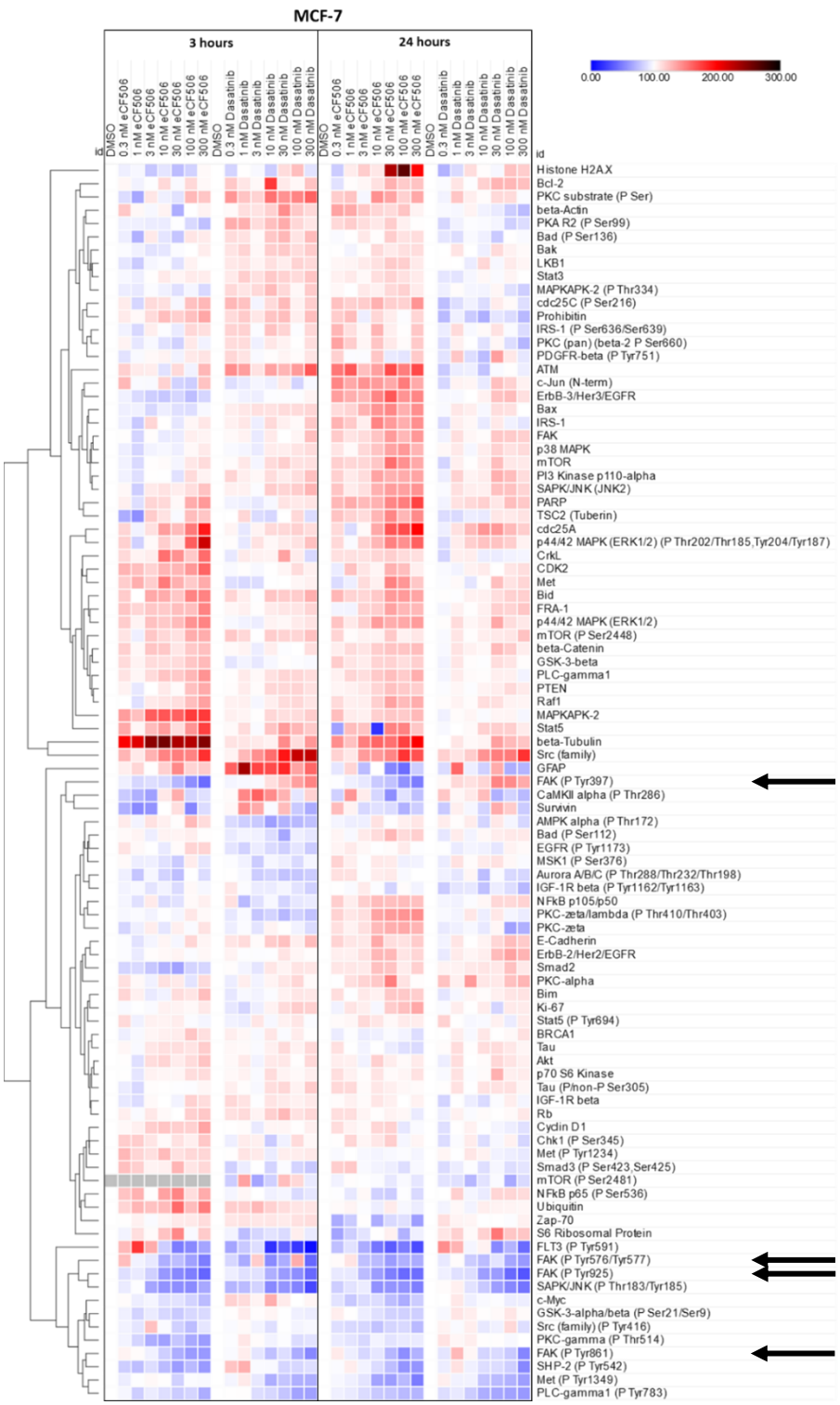

Figure 4.6. Hierarchical clustering analysis of the RPPA results. (a) MDA-MB-231 and (b) MCF-7 cells were treated with eCF506 or dasatinib for 3 or 24 hours, lysed and analysed by reverse-phase protein array on the Zeptosens platform. RFI values were normalised globally and are expressed as percentage of the respective DMSO control. Arrows indicate phospho-FAK proteins. Hierarchical clustering was done with the free Morpheus software by the Broad Institute using Euclidian distance and complete linkage.

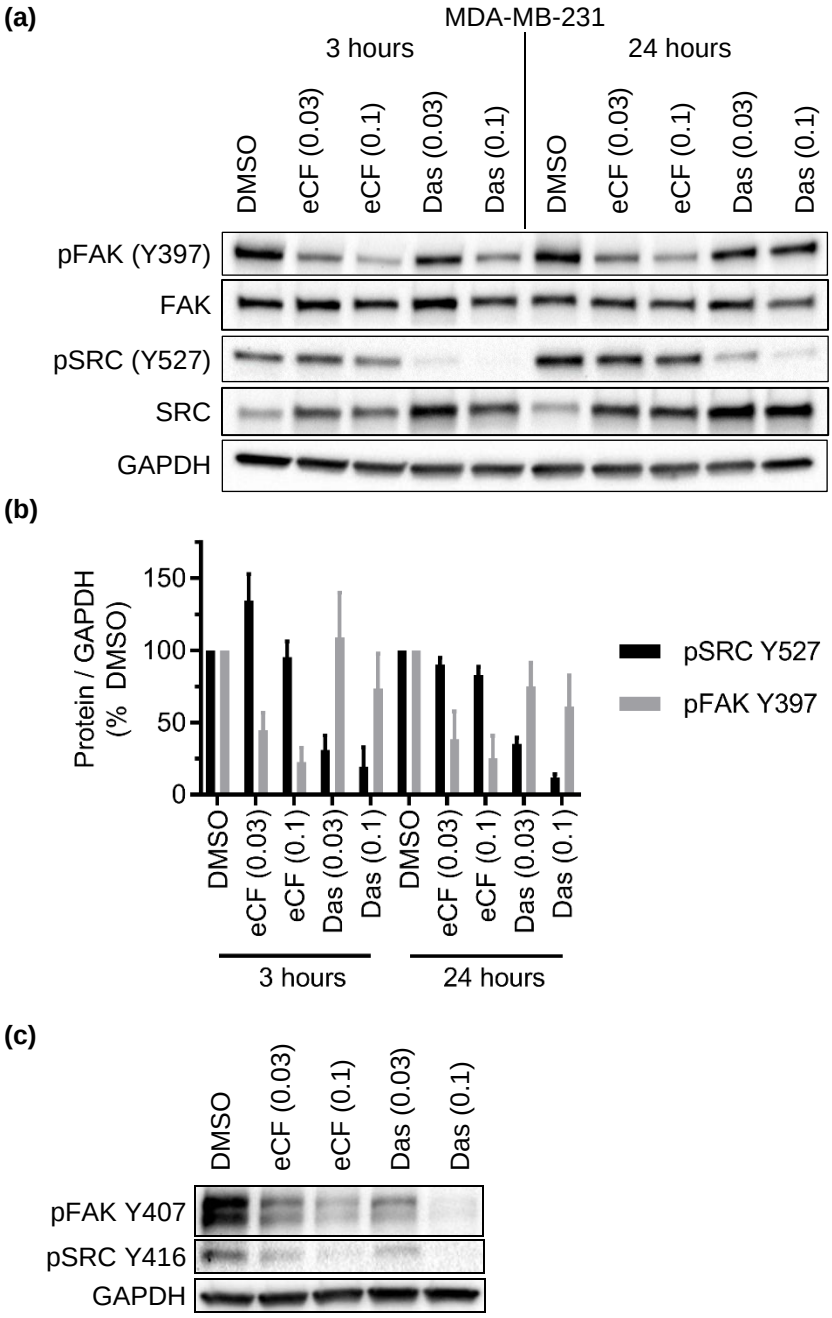

Figure 4.7. Western blot analysis of phospho-FAK in MDA-MB-231 cells treated with eCF506 or dasatinib. (a) Phospho-FAK (Y397) and phospho-SRC (Y527) Western blot analysis after treatment of MDA-MB-231 cells for 3 or 24 hours. Representative Western blot from three biological replicates. (b) Summary of phospho-SRC (Y527) and phospho-FAK (Y397) Western blots of MDA-MB-231 cells showing average of three biological replicates with standard deviation. Band intensities were quantified using Bio-Rad ImageLab® software, adjusted for loading using GAPDH and normalised to DMSO. (c) Western blot of the effect of eCF506 and dasatinib on phospho-FAK (Y407) in MDA-MB-231 cells after 24 hours of treatment. Western blot represents one biological replicate. Concentrations given in μM.

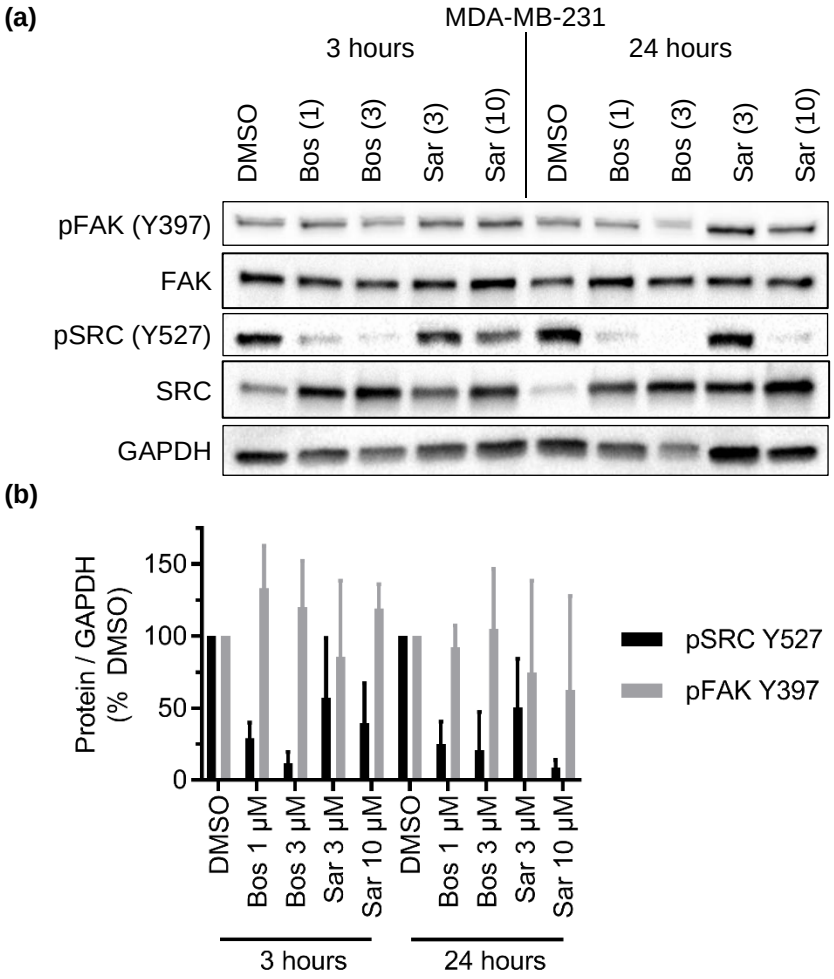

Figure 4.8. Western blot analysis of phospho-FAK in MDA-MB-231 cells treated with bosutinib or saracatinib. (a) Phospho-FAK (Y397) and phospho-SRC (Y527) Western blot analysis after treatment of MDA-MB-231 cells for 3 or 24 hours. Representative Western blot from three biological replicates. (b) Summary of phospho-SRC (Y527) and phospho-FAK (Y397) Western blots of MDA-MB-231 cells showing average of three biological replicates with standard deviation. Band intensities were quantified using Bio-Rad ImageLab® software, adjusted for loading using GAPDH and normalised to DMSO. Concentrations given in µM.

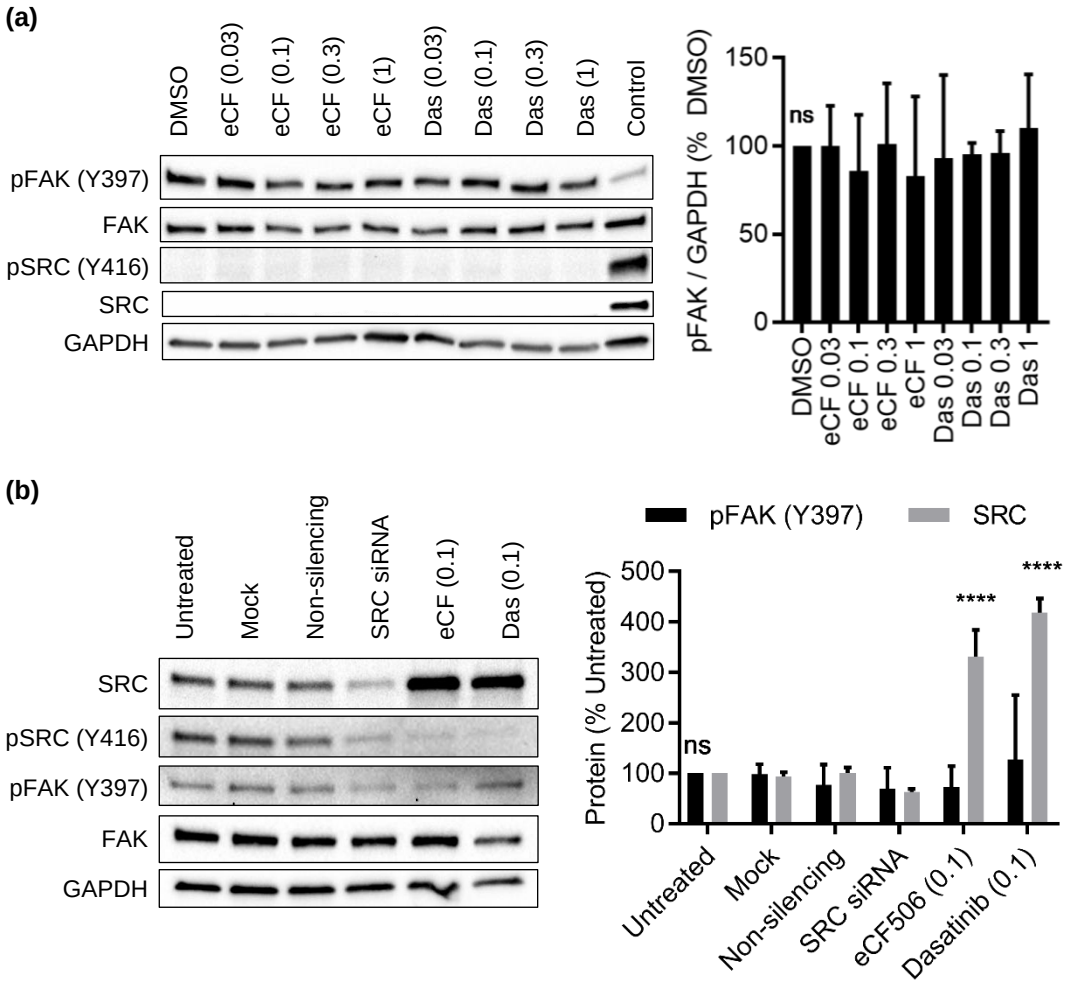

Figure 4.9. Western Blot analysis of pFAK (Y397) in SYF$^{SRC-/-, YES-/-, FYN-/-}$ cells and SRC knockdown in MDA-MB-231 cells. (a) SYF cells were treated with eCF506 or dasatinib for 24 hours prior to cell lysis and Western blot. DMSO-treated MDA-MB-231 cells were used as a control. Left: Representative Western blot. Right: Summary of phospho-FAK (Y397) data showing average of three biological replicates with standard deviation. Statistical analysis was performed against untreated cells using one-way ANOVA with Dunnett's correction for multiple comparison; $p>0.05$ (ns). (b) siRNA knockdown of SRC kinase. Mock (lipofectamine), non-silencing RNA (40 nM) and SRC siRNA (40 nM) were added for 24 hours prior to medium change and cells were lysed 96 hours later. Compounds were added to non-silencing RNA wells after medium change and treated for 96 hours prior to cell lysis and Western blot. Band intensities were quantified using Bio-Rad ImageLab® software, adjusted for loading by calculating pFAK (Y397)/FAK and SRC/GAPDH and normalised to DMSO. Left: Representative Western blot. Right: Summary graph of three biological replicates with standard deviation. Statistical analysis was performed against untreated cells using two-way ANOVA with Dunnett's correction for multiple comparison; $p>0.05$ (ns), $p<0.0001$ (****). All concentrations given in µM.

4.2.2. Dasatinib but not eCF506 forces a stable SRC-FAK interaction

The results of chapter 4.2.1 suggest that binding of SRC kinase to phospho-FAK (Y397) protects this site from dephosphorylation by phosphatases. Dasatinib appears to support binding of SRC to FAK, as suggested by FAK's autophosphorylation status, but assessment of the actual protein-protein interaction is necessary to prove this hypothesis. Therefore, binding of FAK to SRC in MDA-MB-231 cells was tested in a co-immunoprecipitation experiment. Cells were treated for 6 hours with eCF506 (100 nM), dasatinib (100 nM), bosutinib (1 µM) or saracatinib (1 µM) prior to lysis. SRC was immunoprecipitated by magnetic beads and bound proteins visualised by Western blot. As SRC inhibitors typically increase the amount of total SRC, FAK levels were normalised to the amount of immunoprecipitated SRC.
The results show that bosutinib and dasatinib treatment significantly increase binding of FAK to SRC by two- to three-fold, respectively, compared to DMSO (see Figure 4.10). Saracatinib also increased binding of SRC to FAK, whereas eCF506 decreased binding on average by 50%, although neither was significant when compared to DMSO. These findings support the hypothesis that the dasatinib- and bosutinib-induced open SRC conformation enables stable binding of its SH2 domain to FAK via its tyrosine 397 residue, while eCF506 inhibits these interactions. A recent paper has made similar observations by showing that dasatinib and bosutinib treatment causes localisation of SRC to focal adhesions, while saracatinib does not affect localisation of SRC in the cell [363].

SRC kinase has been shown to interact with other proteins in the cell via its SH2 and SH3 domains. It is therefore possible that its different conformations with eCF506 and dasatinib would also differentially affect targets other than FAK. Co-immunoprecipitation experiments with other targets were attempted but either failed (oestrogen receptor α, paxillin) or limited results showed no changes in protein binding (p85 subunit of PI3K) (see Appendix A.10). Further optimisation of the method may be necessary to assess less stable or common SRC binding interactions than FAK, as bound proteins were potentially removed during washing steps or escaped detection due to low concentrations. Many SRC interactions are also formed in response to external signals, such as oestrogen inducing binding of SRC to the oestrogen receptor or PI3K, which might explain why these were not observed with the unstimulated conditions that are sufficient for FAK co-immunoprecipitation [371,372].

In conclusion, the data presented in this chapter shows that dasatinib and bosutinib bind SRC in an active-like, open conformation that can stably bind to FAK and potentially other target proteins *(= only catalytic activity is inhibited*). Saracatinib may have similar effects on SRC-FAK binding but its effects are variable. In contrast, eCF506 inhibits both the catalytic activity of SRC and forces the protein into an inactive, closed conformation that is unable to interact with FAK *(= both catalytic activity and scaffolding properties of active conformation are inhibited*).

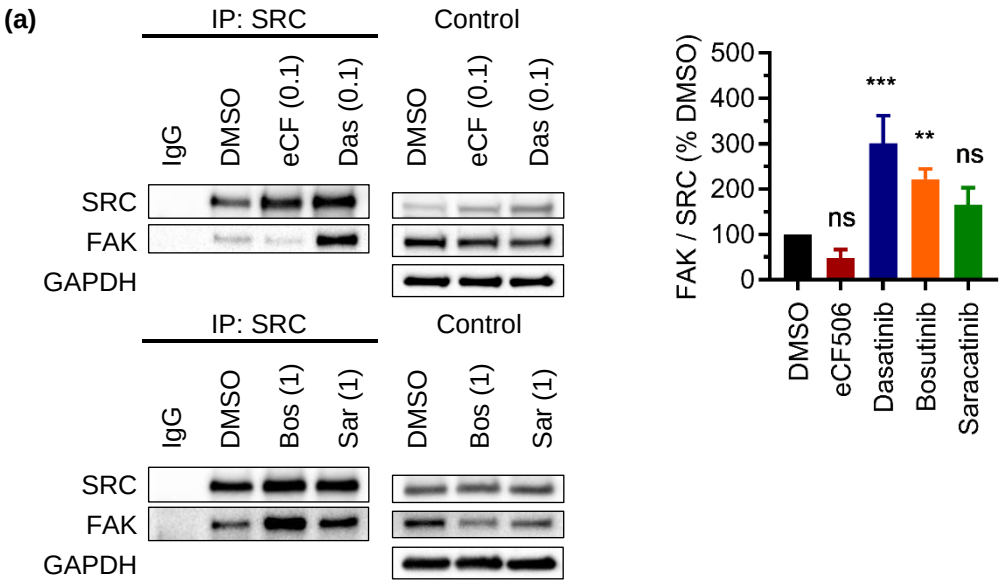

Figure 4.10. Co-immunoprecipitation of SRC and FAK after drug treatment. MDA-MB-231 cells were treated with eCF506 (0.1 µM), dasatinib (0.1 µM), bosutinib (1 µM) or saracatinib (1 µM) for 6 hours prior to cell lysis and co-immunoprecipitation using SRC antibody overnight. Bound proteins were eluted and analysed using Western blot with total cell lysates as control. Band intensities were quantified using Bio-Rad ImageLab® software, adjusted for loading by calculating FAK/SRC ratio and normalised to DMSO. Left: Representative Western blots. Right: Summary graph of three biological replicates with standard deviation. Statistical analysis was done using one-way ANOVA with Dunnett's correction for multiple comparison; $p>0.05$ (ns), $p<0.01$ (**), $p<0.001$ (***). All concentrations given in µM.

4.3. Dasatinib and eCF506 differentially affect localisation of FAK with unclear consequences

4.3.1. Dasatinib causes nuclear translocation of FAK

The X-ray crystallography data combined with the co-immunoprecipitation and phosphorylation results show clearly that eCF506 and dasatinib differ in their binding to SRC and its subsequent binding to FAK. The question remains whether the opposite effects on FAK (Y397) phosphorylation of both compounds would have different effects on FAK function.

Integrin clusters form focal adhesions which recruit FAK to the cell membrane and trigger its autophosphorylation on tyrosine 397 that enables SRC binding (see chapter 1.2.3.1). However, FAK has also been found in the cell nucleus and studies have shown that reduced cell adhesion or FAK inhibition can increase the amount of nuclear FAK [373]. SRC inhibition affects focal adhesion turnover and eCF506 inhibits FAK autophosphorylation similar to the effects seen with FAK inhibitors. It was therefore investigated whether eCF506 and dasatinib have differential effects on the localisation of FAK in the cell. This was done by performing subcellular fractionations of treated breast cancer cells as described in methods 2.4.4; murine squamous cancer cells were included as they have previously been used to test the effects of nuclear FAK on gene expression [290,293].

The results of the subcellular fractionations show that SRC kinase is mainly located in the perinuclear fraction, as described previously, while FAK is mostly in the cytoplasmic and perinuclear fractions (see Figure 4.11 and Appendix A.11) [34,373]. Both eCF506 and dasatinib increase the amount of SRC in all fractions, which has also been seen in total cell lysates and is likely due to reduced degradation.

Dasatinib but not eCF506 increases the amount of nuclear FAK in a human breast cancer (MDA-MB-231), murine breast cancer (MetBo2) and murine squamous cell carcinoma cell line (SCC) but not in three other human breast cancer cell lines (MCF-7, T-47D, ZR-75.1) (see Figure 4.11 and Appendix A.11). The amount of cytoplasmic FAK slightly decreases and/or perinuclear FAK increases in MDA-MB-231 cells and there is more nuclear FAK after 24 hours than after 6 hours, which suggests that FAK

is shuttled from the cytoplasm to the nucleus upon dasatinib treatment (see Figure 4.11b,c). Nuclear translocation of FAK does not seem to be linked to general cell line sensitivity to eCF506 or dasatinib, as MDA-MB-231, MetBo-2 and MCF-7 cells are much more sensitive than SCC cells in cell viability assays (see Appendix A.12).

Genetically modified SCC cells that were previously generated and validated by Serrels *et al.* were used next to investigate whether the increase in nuclear SRC with dasatinib treatment could be due to shuttling of FAK-bound SRC into the nucleus rather than reduced degradation [290]. SCC cells deficient for FAK (SCC FAK -/-), with re-expressed wild-type FAK (SCC FAK WT) or with re-expressed mutant FAK lacking the nuclear localisation sequence (SCC FAK NLS) were treated with eCF506 or dasatinib and the amount of nuclear FAK and SRC was quantified (Figure 4.12a,b). SCC FAK WT and SCC FAK NLS had higher overall levels of FAK than unmodified SCC cells (see Figure 4.12c). However, less nuclear FAK was observed in SCC FAK NLS cells than in SCC FAK WT cells after dasatinib treatment, which suggests that the NLS sequence is at least partially necessary for the dasatinib-induced nuclear translocation of FAK (see Figure 4.12a,b). Moreover, the increase of nuclear SRC with dasatinib that is observed in SCC FAK WT cells is attenuated in SCC FAK NLS cells and reduced even further in SCC FAK -/- cells, even though all have similar amounts of total SRC. This indicates that at least some SRC is brought to the nucleus by FAK (see Figure 4.12a,b). FAK is still autophosphorylated in the nucleus and co-immunoprecipitation of the nuclear fraction confirms that it is bound to SRC with dasatinib treatment but not with eCF506 or DMSO (see Figure 4.12a,d). Overall, the findings suggest that dasatinib induces nuclear translocation of the FAK-SRC complex in SCC cells. With the data available, it cannot be confirmed whether this is caused by the dasatinib-induced open conformation of SRC and its stable binding to FAK and studies in SRC knockout cells should be done to assess this in the future.

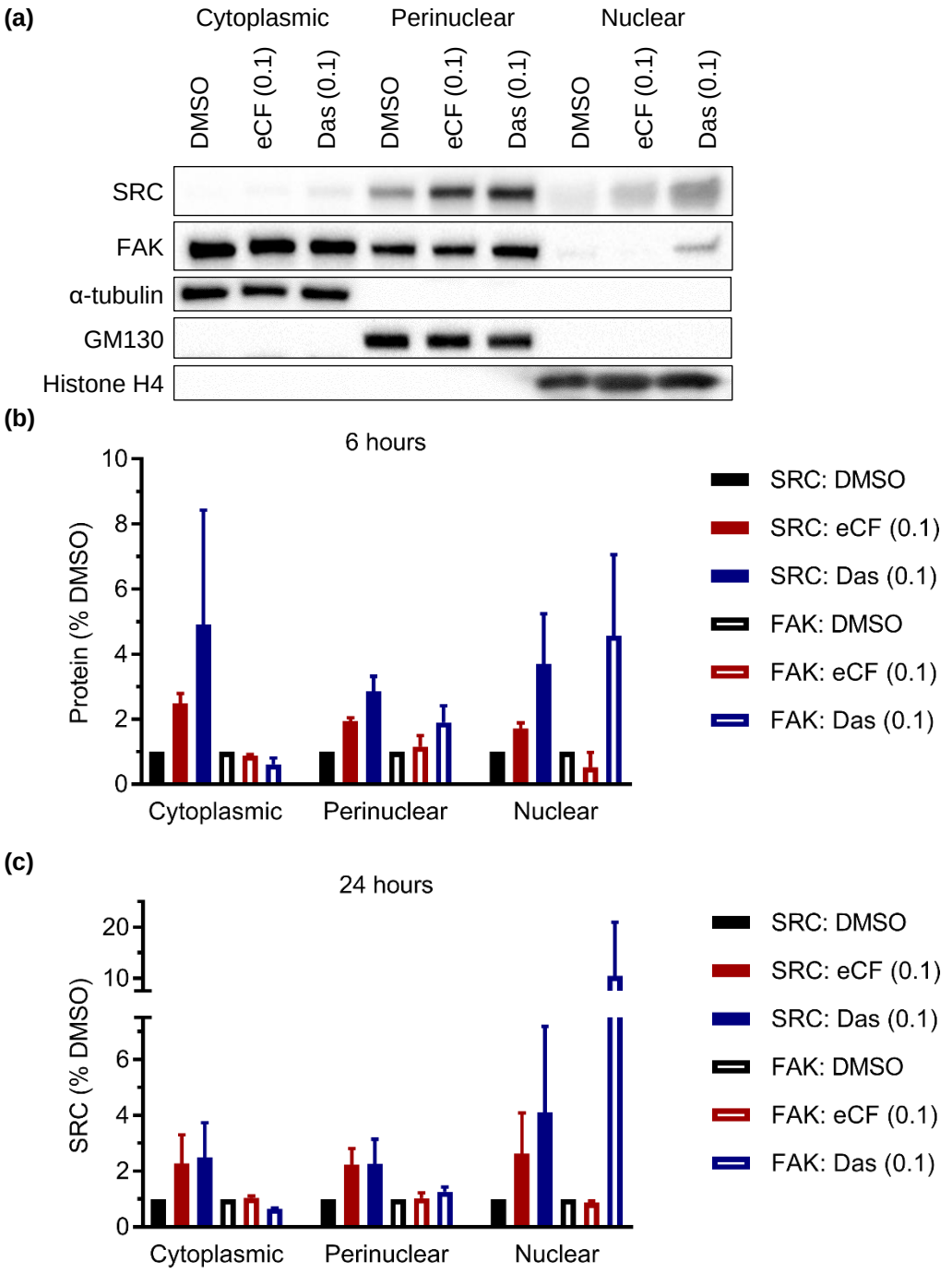

Figure 4.11. Subcellular fractionation of MDA-MB-231 cells. Subcellular fractionation of MDA-MB-231 cells treated with eCF506 or dasatinib (both 0.1 μM) for 6 or 24 hours prior to subcellular fractionation and analysis by Western blot. (a) Representative Western blot of cells treated for 6 hours and summary table of three biological replicates with standard deviation of cells treated for (b) 6 hours of (c) 24 hours. Band intensities were quantified using Bio-Rad ImageLab® software and normalised to DMSO for each fraction. All concentrations given in μM.

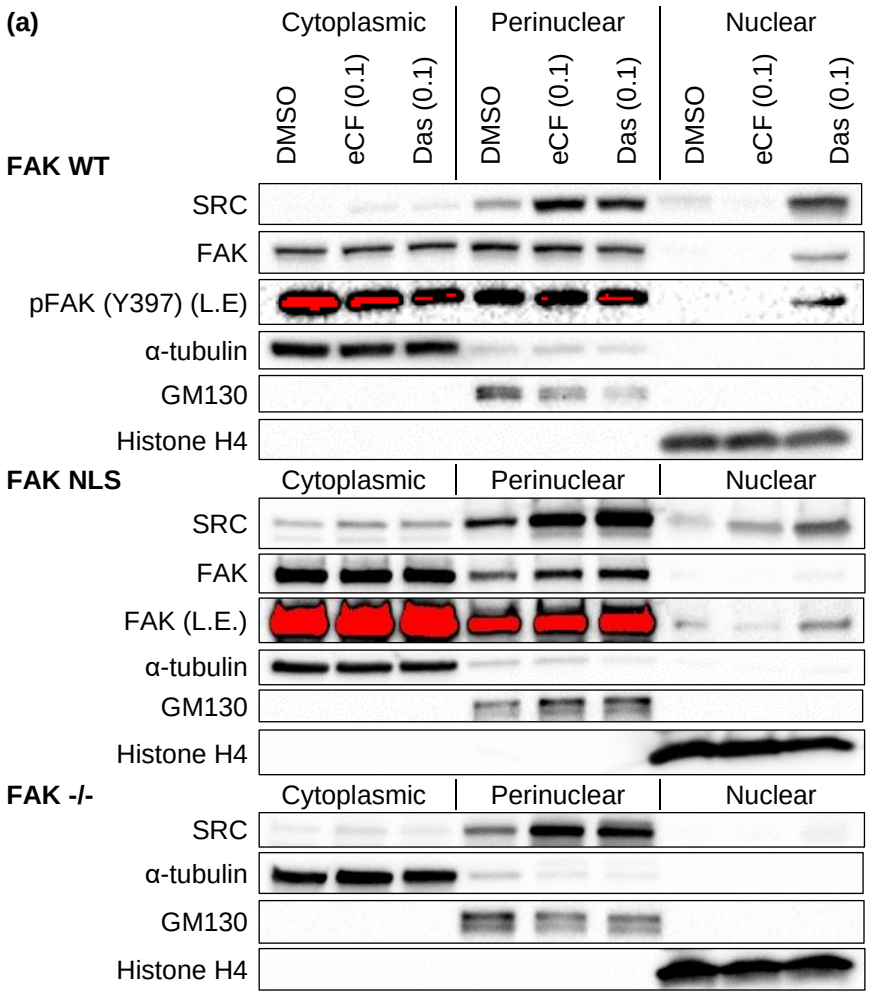

(b)

		Cytoplasmic			Perinuclear			Nuclear		
		DMSO	eCF (0.1)	Das (0.1)	DMSO	eCF (0.1)	Das (0.1)	DMSO	eCF (0.1)	Das (0.1)
SRC	WT	100	304	325	100	416	295	100	128	791
	NLS	100	230	300	100	227	272	100	158	407
	-/-	100	271	206	100	330	317	100	102	356
FAK	WT	100	95	80	100	117	95	100	162	1071
	NLS	100	101	97	100	111	167	100	70	221
	-/-									

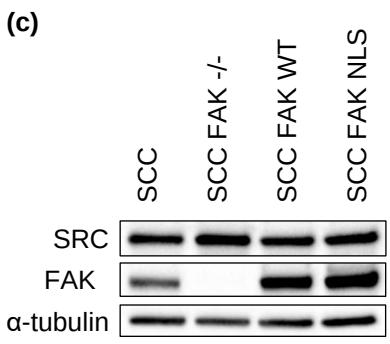

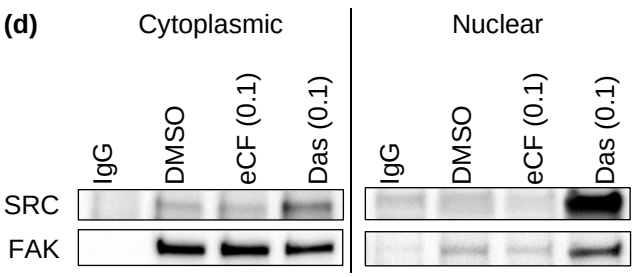

Figure continued on next page

Figure continued from previous page

Figure 4.12. Subcellular fractionation and co-immunoprecipitation of SCC cells. (a, b) Subcellular fractionation of SCC cells treated with eCF506 or dasatinib (both 0.1 µM) for 6 hours prior to subcellular fractionation and analysis by Western blot. Representative Western blots and summary table of three biological replicates with standard deviation. Band intensities were quantified using Bio-Rad ImageLab® software and normalised to DMSO for each fraction. L.E. = longer exposure. (c) Western blot of untreated SCC cells. Representative Western blot of three biological replicates. (d) Co-immunoprecipitation of FAK in cytoplasmic and nuclear fraction. SCC FAK WT cells were treated with eCF506 or dasatinib (both 0.1 µM) for 6 hours prior to subcellular fractionation followed by co-immunoprecipitation using FAK antibody overnight. Representative Western blot of three biological repeats. All concentrations given in µM.

4.3.2. The effects of dasatinib-induced nuclear FAK on gene expression are inconclusive

The results of chapter 4.3.1 show that dasatinib but not eCF506 induces nuclear translocation of FAK. It is not clear whether this difference is related to their SRC activity or their off-target effects and further experiments are needed to determine the cause of FAK shuttling. Moreover, the functional consequences of dasatinib-induced nuclear FAK, if any, have not been determined. Serrels *et al.* have reported that nuclear FAK regulates the expression of cytokines and IGFBP3 in SCC cells and another study found it affects the expression of VEGFR2; the results of these studies are summarised in Table 4.2 [290,293,374]. The hypothesis is that dasatinib but not eCF506 might induce similar changes. Thus, expression of these genes was determined by real-time PCR in SCC, MetBo2 and HUVEC cells and preliminary results are summarised in Figure 4.13. These experiments were only performed once and results are thus only indicative.

Table 4.2. Summary of effects of nuclear FAK.

Gene	Proposed nuclear FAK effect	Cells	Ref
CCL5	↑	SCC	290
CXCL10	↑	SCC	290
TGFB2	↑	SCC	290
IGFBP3	↓	SCC	293
VEGFR2	↑	MS1	374

Analysis of gene expression changes of known nuclear FAK targets shows that eCF506 and dasatinib generally have similar effects (see Figure 4.13). It is very likely that their common SRC inhibitory effects have a much greater impact on gene expression than differential presence of nuclear FAK. Moreover, the SCC cell lines used here exhibited different expression levels of IGFBP3 from what has previously been reported and VEGFR2 expression in HUVEC cells, which were used instead of mouse endothelial cells (MS1), was very low [293,374]. In conclusion, no convincing changes consistent with nuclear FAK were observed in the preliminary gene expression data.

(a)	SCC		
	FAK WT	FAK -/-	FAK NLS
CCL5	1.00	0.17	-
CXCL10	1.00	0.36	-
TGFB2	1.00	0.41	-
IGFBP3	1.00	0.13	0.23

(b)	SCC FAK WT			SCC FAK NLS			SCC FAK -/-		
	DMSO	eCF (0.1)	Das (0.1)	DMSO	eCF (0.1)	Das (0.1)	DMSO	eCF (0.1)	Das (0.1)
CCL5	1.00	0.74	0.7	1.00	1.17	1.45	1.00	0.88	0.78
CXCL10	1.00	0.59	0.29	1.00	0.38	0.68	1.00	0.20	0.50
TGFB2	1.00	1.10	1.06	1.00	0.89	0.88	1.00	0.94	0.91
IGFBP3	1.00	0.94	0.94	1.00	0.93	1.73	1.00	0.57	1.05

(c)	MetBo2		
	DMSO	eCF (0.1)	Das (0.1)
CCL5	1.00	2.67	2.38
CXCL10	1.00	0.92	0.91
TGFB2	1.00	1.23	1.94
IGFBP3	1.00 ± 0.00	1.50 ± 0.67	0.81 ± 0.40

(d)	HUVEC		
	DMSO	eCF (0.1)	Das (0.1)
VEGFR2	1.01	3.60	2.08

Figure 4.13. Gene expression changes with eCF506 and dasatinib. SCC, MetBo2 and HUVEC cells were treated for 24 hours prior to cDNA extraction and real-time PCR analysis. Data represents one average of three technical replicates and was normalised to DMSO (except IGFBP3 in MetBo2 for which n = 3 is shown with standard deviation); red = increase, blue = decrease relative to DMSO. (a) Relative expression of untreated SCC cell lines. (b) Relative gene expression in treated SCC cell lines. (c) Relative gene expression in treated MetBo2 cells. (d) Relative gene expression in treated HUVEC. All concentrations given in µM.

4.4. Discussion

4.4.1. eCF506 is a TypeI1/2A inhibitor which might contribute to its selectivity

eCF506 and dasatinib exhibited opposite effects on SRC heat stability in a thermal shift assay, giving rise to the hypothesis that they induce different SRC conformations (see chapter 4.1.1). This was confirmed by Dr Daniel Lietha who crystallised eCF506 bound to the SRC kinase domain, revealing its TypeI1/2A binding mode; this makes eCF506 the first confirmed compound to potently inhibit SRC in its natural autoinhibited state, although PP1 was found to bind HCK in a similar way and the reported Type II inhibitor saracatinib appears to actually bind a DFG-in conformation (see chapter 4.1.2.1). It is possible that this uncommon binding mode contributes to eCF506's high selectivity across the kinome.

Most kinase inhibitors identified to date are ATP-competitive and bind the ATP-binding site between the N-lobe and C-lobe of the kinase domain [9,220]. This site is highly conserved across the human kinome, which makes it difficult to develop highly selective inhibitors, and many promiscuous ones such as dasatinib and sunitinib interact with several kinases [221]. The majority of kinase inhibitors developed to date are Type I, a subclass of ATP-competitive inhibitors that bind to the active conformation of the kinase. Nevertheless, utilisation of differences in the gatekeeper residues between kinases can improve selectivity, for example by enabling binding to adjacent hydrophobic pockets [9]. X-ray crystallography of eCF506 bound to the SRC kinase domain has revealed that its *tert*-butyl group extends deep into the hydrophobic pocket present near the active site, which disrupts a key salt bridge between the catalytic lysine and a glutamate residue in the αC-helix (see Figure 4.2). As a result, SRC is in a "DFG-in" but "αC helix-out" conformation that resembles its natural autoinhibited state, causing eCF506 to be classified as a TypeI1/2A inhibitor [9,360]. This is a similar binding mode as its scaffold PP1 bound to the SFK HCK, which is classified as TypeI1/2B binding; however, PP1 is much more promiscuous than eCF506 and also inhibits ABL and KIT (see Table 1.3), which suggests that PP1 can adopt multiple binding modes. It is possible that this is in part because it does not extend beyond the gatekeeper residue and thus lacks additional interactions with residues in the hydrophobic pocket.

A study with matched analogues of dasatinib compared the kinome selectivity of (i) dasatinib (DFG-in, αC helix-in), (ii) two analogues inducing “DFG-out”, “αC helix-in” conformations, and (iii) two analogues inducing “DFG-out”, “αC helix-out” conformations [231]. It found that the DFG-out motif alone did not make dasatinib more selective and indeed was slightly more promiscuous by also binding kinases with non-threonine gatekeepers; this contradicts previous assumptions that Type II inhibitors such as imatinib are generally more selective than Type I inhibitors [375,376]. In contrast, the αC helix-out analogues were much more selective than αC helix-in analogues or dasatinib; in particular, these analogues were unable to bind the entire Ephrin receptor family. Notably, eCF506 is also unable to inhibit any of the 12 Ephrin kinases tested in the kinome screen (see Appendix A.6). The study of dasatinib analogues and their selectivity supports the theory that the αC helix-out conformation and binding in the hydrophobic pocket can improve inhibitor selectivity.

While eCF506’s Type I1/2A binding mode might contribute to its superior selectivity profile observed in chapter 3.2.1.1, it does not explain its selectivity for SRC over ABL, as PP1 and the dasatinib αC helix-out analogues remain equipotent against both kinases [231]. ABL has also been found to be able to adopt a SRC-like inactive conformation as induced by eCF506 in SRC [377]. Fraser *et al.* have previously performed *in silico* docking studies with eCF506 which suggested that its large dimethylamino-piperidine group clashes with the tyrosine 253 located in the catalytic ATP-binding loop of ABL kinase. However, these studies also assumed that eCF506 binds the active conformation of SRC; this highlights the fallibility of *in silico* studies and the need to determine eCF506’s binding mode to ABL kinase by X-ray crystallography to reliably determine the cause of its selectivity.

A recent paper by Koudelkova *et al.* assessed several SRC kinase inhibitors in a fluorescence resonance energy transfer (FRET) based assay and found a similar correlation between binding type and SRC tyrosine 527 phosphorylation as done in chapter 4.1.2.2 [363]. Surprisingly, it showed differences between the two reported Type II inhibitors saracatinib and UM-164, with the former inducing a closed autoinhibited conformation, while the latter decreased SRC Y527 phosphorylation resulting in an open SRC structure that accumulated at focal adhesions. This shows that the general kinase inhibitor classification system, in which Type II inhibitors are described as binding an inactive kinase conformation, is confusing in the case of SRC kinase, as

its “DFG-inactive” and “autoinhibited-inactive” states are not based on the same conformations in the kinase domain. The autoinhibited conformation of SRC kinase appears to be defined by an αC helix-out conformation alone, independent of the orientation of the DFG motif in the activation loop. This is a likely reason for the mislabelling of saracatinib as a Type II inhibitor in the literature, when it actually appears to be a Type I1/2 based on its crystal structure.

As kinases undergo switching between different conformations during their catalytic cycle, it is unclear whether eCF506 and saracatinib bind the closed, autoinhibited SRC kinase and dasatinib and bosutinib only bind the active conformation and stabilise these, or whether they can actively force SRC into their preferred conformations. The paper by Koudelkova *et al.* employed a FRET-based SRC biosensor and found that dasatinib decreases FRET in WT and constitutively activated Y527F SRC, indicating a less compact structure of the kinase; conversely, SKI-1, which maintains SRC in an autoinhibited state like saracatinib, increased FRET signalling in the constitutively active kinase [363]. This indicates that binding of SKI-1 can partially close SRC even in the absence of the stabilising SH2-binding residue tyrosine 527. The authors conclude that inhibitors can have a direct effect on SRC opening or closing, based on their induced αC helix orientation, with the conformation likely determining the liability of tyrosine 527 to be dephosphorylated by phosphatases [363]. It would be interesting to assess eCF506 in this model to determine whether it can also close the constitutively active Y527F SRC kinase or even v-SRC, which lacks the inhibitory C-terminus altogether.

4.4.2. Inhibitor-induced SRC conformation affects its scaffolding functions

Western blot analysis of tyrosine 527 phosphorylation confirmed that eCF506 and to some degree saracatinib maintain SRC kinase in its closed, autoinhibited state, whereas dasatinib and bosutinib force it into an open and active conformation. In the latter, the SH2 domain is no longer bound by the C-terminus, allowing it to bind other proteins and kinases. This means that while all four compounds inhibit the catalytic activity of SRC, only eCF506 and possibly saracatinib also inhibit its kinase-

independent scaffolding functions, with eCF506 showing much higher potency against SRC than saracatinib.

In order to determine whether eCF506 and dasatinib differ in their effects on downstream signalling pathways, they were tested in a reverse phase protein array of two different breast cancer cell lines. The results showed largely similar effects of both inhibitors, which agrees with assumptions that most of SRC's functions are dependent on its kinase function. However, contrasting effects on the phosphorylation of FAK's tyrosine 397 residue were observed, which is autophosphorylated upon integrin accumulation and forms the SRC binding site. Previous papers have reported that dasatinib increases FAK (Y397) phosphorylation but no convincing explanation has been offered to this date, although a recent publication suggests that this effect limits dasatinib's potency in liver cancer [158,378,379]. Co-immunoprecipitation experiments confirmed that this observation correlates with the formation of a stable SRC-FAK complex with dasatinib or bosutinib treatment, while eCF506 tends to decrease SRC-FAK binding to varying degrees (see Figure 4.10). Brunton *et al.* have previously shown that FAK is more phosphorylated in colon cancer cells with kinase-defect SRC than with wild-type SRC; only mutation of SRC's SH2 domain was able to reduce FAK tyrosine phosphorylation, while mutation of its SH3 domain or a SRC kinase inhibitor showed no changes [135]. Addition of kinase-defect SRC to cells with kinase-defect FAK also increased FAK tyrosine 397 phosphorylation, proving that SRC can affect phosphorylation at this site but not by phosphorylating it directly. This agrees with our hypothesis that binding of SRC via its SH2 domain to phospho-FAK (Y397) protects this site from dephosphorylation; consequently, compound-induced changes of the SRC conformation that affect the SRC-FAK interaction can modulate FAK phosphorylation at this site.

While the SRC-FAK complex is the best characterised interaction of SRC in the literature, other proteins have previously been found to interact with SRC, such as p85 subunit of PI3K and ERα [371,372]. While co-immunoprecipitation experiments largely failed in non-optimised conditions, limited results indicate that binding of the PI3K subunit p85 to SRC's SH3 domains is not affected by eCF506 or dasatinib (see Appendix A.10) [380]. Further experiments should assess protein-protein interactions after specific stimulation of cell signalling events which are known to induce binding of target proteins to SRC.

Several studies have tried to characterise the non-catalytic functions of SRC by re-expressing kinase-defective SRC in SRC-deficient cells (see chapter 1.2.3.8). The scaffolding roles identified for SRC include the migration of fibroblasts on fibronectin, cytoskeletal organisation in osteoclasts, partial rescue of an osteopetrosis phenotype in SRC-deficient mice and prolactin receptor signalling via JAK2/STAT5 and JAK2/ERK1/2; other kinase-defective SFKs have been implicated in CD4 T-cell activation and B cell stimulation [130]. Especially the former examples suggest that SRC kinase might have a kinase-independent scaffolding role in the cytoskeleton, which might be mediated through its interaction with FAK. eCF506, dasatinib and kinase-defect SRC should be compared in these models to see whether the different inhibitor-induced SRC conformations have distinct effects. One major limitation in such experiments is the promiscuity of kinase inhibitors such as dasatinib, which likely confound any differential effects of SRC scaffolding functions with off-target effects. Moreover, the limited number of studies on SRC's kinase-independent roles have so far not taken into account protein conformation; while it is likely that cytoskeletal scaffolding functions that involve FAK would require the open and active conformation, little is known about any potential scaffolding roles of the closed, autoinhibited state that is induced by eCF506.

4.4.3. Dasatinib but not eCF506 causes nuclear translocation of the FAK-SRC complex with unclear functional consequences

Western blot and co-immunoprecipitation studies revealed differential effects of eCF506 and dasatinib on the SRC-FAK interaction and FAK (Y397) phosphorylation but the functional consequences of this are not yet clear. A paper utilising a FRET-based SRC biosensor showed that dasatinib causes translocation of SRC to focal adhesions, whereas αC helix-out inhibitors did not, and Lim *et al.* found that kinase-defect FAK or FAK inhibition increases FAK nuclear localisation [363,373]. Since eCF506 can decrease FAK (Y397) phosphorylation similar to a FAK inhibitor or kinase-defect FAK, and dasatinib induces the opposite effect, subcellular translocation of FAK after treatment with both compounds was studied. Subcellular fractionations were performed which, interestingly, revealed a big increase in nuclear FAK after dasatinib treatment but not with eCF506. Further experiments in SCC cells, previously used by Serrels *et al.* to study nuclear FAK, showed that this translocation seemed to be

partially dependent on the presence of FAK's nuclear localisation sequence, with a five-times smaller increase after dasatinib treatment in FAK NLS mutant SCC cells compared to wild-type FAK (see Figure 4.12) [290]. eCF506 and dasatinib both increased the amount of SRC in the cytoplasmic and perinuclear fraction, although a big increase in nuclear SRC was only seen with dasatinib, which was attenuated in FAK NLS and FAK KO cells. Further studies confirmed that the nuclear FAK seen with dasatinib is phosphorylated on tyrosine 397 and bound to SRC.

Taken together, this suggests that dasatinib treatment induces FAK translocation from the cytoplasm to the nucleus, bringing SRC with it. This observation is opposite from what would have been expected based on the observations with FAK inhibitors and kinase-defect FAK. It could be that, rather than simply FAK (Y397) phosphorylation, the overall conformation of FAK protein plays a role in its subcellular localisation. The nuclear localisation sequence is located in the FAK FERM domain, which is bound to the kinase domain in autoinhibited FAK[381,382]; SRC binds to the phosphorylated tyrosine 397 residue in the active, open FAK conformation, so it is possible that the stable SRC-FAK interaction induced by dasatinib exposes the nuclear localisation sequence to cause translocation of the complex [381,382]. It is important to note that the previous study by Koudelkova *et al.* showed SRC localises to focal adhesions with Type I inhibitors (i.e. dasatinib, bosutinib) and did not report a subsequent localisation to the nucleus [363]; however, not all cell lines tested in this thesis exhibited nuclear translocation of FAK (e.g. MCF-7, ZR-75). Furthermore, several studies have found that FAK translocates to the nucleus in response to non-specific cellular stress, such as treatment with the highly promiscuous kinase inhibitor staurosporine or hydrogen peroxide or after detachment from the substratum [373]. It is a possibility that dasatinib's promiscuity exerts more cellular stress than eCF506, even though no inhibition of SCC cell proliferation was seen at the 100 nM used (see Appendix A.12). A recent conference report associates the presence of nuclear FAK with resistance to dasatinib treatment, indicating that the translocation might be a cellular resistance mechanism [383]. Further experiments are needed to determine whether FAK translocates in response to stable SRC binding or due to off-target effects of dasatinib on other kinases or proteins. This could be done by assessing FAK translocation in SRC knockout cells treated with dasatinib, such as SYF fibroblasts, or by comparing the amount of nuclear FAK in cells with open versus closed kinase-defect SRC.

Irrespective of the cause of FAK's nuclear translocation with dasatinib, the question remains whether this has any functional consequences. Several studies have linked nuclear FAK to p53-degradation leading to increased cell proliferation and survival as well as gene expression changes linked to immune evasion [290,293,373]. This thesis briefly explored the expression of several chemokines that have previously been linked to nuclear FAK (CCL5, CXCL10, TGFB2, IGFBP3) in the same SCC model as used by Serrels *et al.*; however, preliminary results identified no changes that could consistently be linked to dasatinib-induced nuclear translocation (see Figure 4.13). It is likely that any effects of nuclear FAK would be hidden by the potent inhibition of SRC kinase and other direct or downstream targets, as SRC activity is known to affect the expression of many genes, for example through its activation of STAT3 [57]. It is also possible that the stable dasatinib-induced SRC-FAK interaction that can be observed in the nucleus (see Figure 4.12) prevents FAK from interacting with and participating in transcription factor complexes, thus inhibiting its nuclear functions.

Chapter 5. *In vivo* assessment of eCF506

Guidelines by the International Council for Harmonisation of Technical Requirements for Registration of Pharmaceuticals for Human Use (ICH) state three aims for the nonclinical evaluation of novel anticancer pharmaceuticals: (i) identification of the pharmacological properties, (ii) determination of a safe initial dose for humans, and (iii) understanding of toxicological profile of the pharmaceutical [384]. The first two chapters of this thesis focus mainly on the pharmacological aspect by establishing eCF506's *in vitro* potency in comparison to other inhibitors and investigating its binding mode. This chapter will focus on the *in vivo* properties of eCF506 by assessing its pharmacokinetic properties, toxicities and efficacy in different rodent models.

The experiments presented in this chapter expand on the previous results published by Fraser *et al.*, which included several key *in vitro* assays (cytochrome P450 enzyme inhibition profile; hERG channel inhibition; plasma protein binding; stability in microsomes, plasma and hepatocytes) and *in vivo* models (single dose pharmacokinetics in mice; SRC inhibition in a mouse xenograft; developmental effects in Zebrafish embryos) [1]. The additional studies presented in this thesis provide a more comprehensive understanding of eCF506's genotoxicity (Ames test), acute toxicity (single dose toxicity in rats), ADME profile (metabolite study; rat PK study) and *in vivo* anti-tumour properties. While more PK and toxicology studies, especially in non-rodent species, are necessary prior to entry of the compound into clinical trials, the current pre-clinical profile of eCF506 shows a generally safe and well tolerated compound with some species-dependent variability in PK properties which exhibits high potency in certain murine breast cancer models.

This chapter explores the following aims:

- Evaluation of the mutagenicity and acute toxicity of eCF506.

- Further testing of the pharmacokinetic properties of eCF506 in specific body compartments and a second rodent species.

- Assessment of the efficacy of eCF506 in *in vivo* models of metastatic breast cancer.

5.1. eCF506's *in vivo* pharmacokinetic and safety profile

5.1.1. eCF506 is not mutagenic and has a high maximum tolerated dose in rats

5.1.1.1. Ames test

This work was done by Sequani Limited, UK.

The mutagenic potential of eCF506 was assessed in an Ames test by the company Sequani Limited. The Ames test is commonly used in drug development to detect potential carcinogenic effects of novel compounds during the lead identification and optimisation phase. It is therefore a critical hurdle that eCF506 needs to pass in order to move further into pre-clinical development.

The Ames test determines whether a chemical compound causes mutations in the DNA of bacteria. It is performed in auxotrophic bacterial strains that cannot grow in the absence of histidine or tryptophan, as they have a genetic mutation in the biosynthesis pathway of this amino acid. Exposure to a mutagenic compound can reverse this mutation, allowing the growth of revertant bacterial colonies on minimal agar. An increased revertant rate compared to a control usually correlates with carcinogenicity in animals, with 80-90% accuracy [385]. By including mammalian liver homogenates this test also detects pro-mutagens that require metabolic activation.
The battery of strains used in the test of eCF506 included four Salmonella typhimurium strains (TA1535, TA1537, TA98, TA100) and one Escherichia coli strain (WP2 uvrA), in the presence and absence of a metabolic activation system (S-9 mix). This choice allows sensitive detection of both point and frame shift mutations caused by the test compound. The test produced no significant increase in the number of revertant colonies for any of the five strains over the expected normal variation found in the negative control number of revertants (see Figure 5.1). Bacteriotoxic effects were seen at the highest concentrations of eCF506 (≥ 1500 µg/plate); these are frequently observed at high doses and have also been reported for dasatinib (≥400 µg/plate) and bosutinib (≥333 µg/plate) at even lower concentrations [386,387]. Consequently, the Ames test was considered negative and eCF506 was found to be non-mutagenic.

5.1.1.2. Acute toxicity study of oral eCF506 in rats

This work was done by Evotec, France.

The general toxicity of novel small molecule compounds needs to be assessed in several repeat-dose toxicology experiments in both a rodent (e.g. mouse, rat) and non-rodent species (e.g. dog, pig) to fulfil regulatory requirements for progression into clinical trials [384]. These involve maximum tolerated dose studies with a single dose or treatment for 7 days to determine a suitable dose-range and assess acute toxicity. After that, 14 or 28-day toxicity studies are required to determine side effects and toxicokinetics of repeated administration.

The first of these studies has now been completed. The single-dose acute toxicity of eCF506 was assessed in Sprague-Dawley rats by Evotec (Reference: EVT06968). The aim of this study was to determine the maximum tolerated dose (MTD) of eCF506 after oral administration by gavage of a single dose to male and female rats. 18 Sprague-Dawley rats were split into five groups, dosed once, observed for 24 hours and examined post-mortem. Two different control groups were needed as the vehicle concentration had to be doubled to maintain solubility and pH at the highest dose tested (700 mg/kg).

No clinical signs were observed for rats treated with 200 or 400 mg/kg eCF506 (see Table 5.1). In the group treated with 700 mg/kg, all four rats exhibited clinical signs, including faecal soiling, soft faeces, half closed eyes, drop in body temperature, tachypnoea and abnormal posture (see Table 5.1 and Figure 5.2a). These started 2 hours post-dosing, with a peak at 4 hours, and then subsided without disappearing fully at 24 hours. Body weight pre- and post-dosing did not differ (Figure 5.2a).
Haematological analysis found no changes in red blood cell count, haemoglobin concentration, haematocrit fraction and mean globular volume (see Figure 5.2b). However, a dose-dependent increase in white blood cells and a sharp drop in platelet count were observed, especially in female rats. Further analysis of the white blood cells showed no dose-dependent changes in lymphocyte numbers, whereas monocyte and neutrophil counts more than doubled and tripled, respectively, at most tested doses compared to vehicle. It is important to note that both male rats in vehicle group 1 had much lower platelet counts and higher white blood cell counts than

expected and observed in the male rat of vehicle group 2 or both female vehicle groups; they were therefore disregarded in the comparison of haematology results.
A necropsy was performed 24 hours post-dosing. The main observations were done on the digestive tract, with induration and dilation of the stomach, haemorrhagic areas and petechiae observed in all treated animals, and intensity of these signs increased in a dose-dependent manner. 11 of 12 treated rats also exhibited slight hyperaemia of the digestive tract. Reactive Peyer's patches were observed on all four rats treated with 700 mg/kg. Some discoloured areas, petechiae or haemorrhagic areas were found on the lungs as well as petechiae on the thymus; however, these lesions are likely unrelated to the compound as some were also observed in vehicle animals. Granulomatous spleens were found in some treated animals at different doses. No notable observations were made on the brain or cranial cavity.

The MTD was determined to be 700 mg/kg for both male and female Sprague Dawley rats after a single oral administration. While a lethal dose could not be determined in the dose range tested (200-700 mg/kg), clinical symptoms were observed at the highest dose tested and suggest that higher doses would have severe side effects or cause lethality.
In comparison, the MTD of dasatinib in the same rat strain and route of administration was 30 mg/kg; severe renal and cardiac toxicities and lethality were observed at the next highest dose of 100 mg/kg (see Table 5.2) [388]. The MTD reported for bosutinib in this model was the same as for eCF506 at 700 mg/kg [387]. Reversible dose-dependent gastrointestinal changes, as seen with eCF506, were observed for both compounds and dasatinib also caused dose-related bone marrow and lymphoid organ toxicities [387,388]. No publicly available results have been found for the acute toxicity of saracatinib in rats.

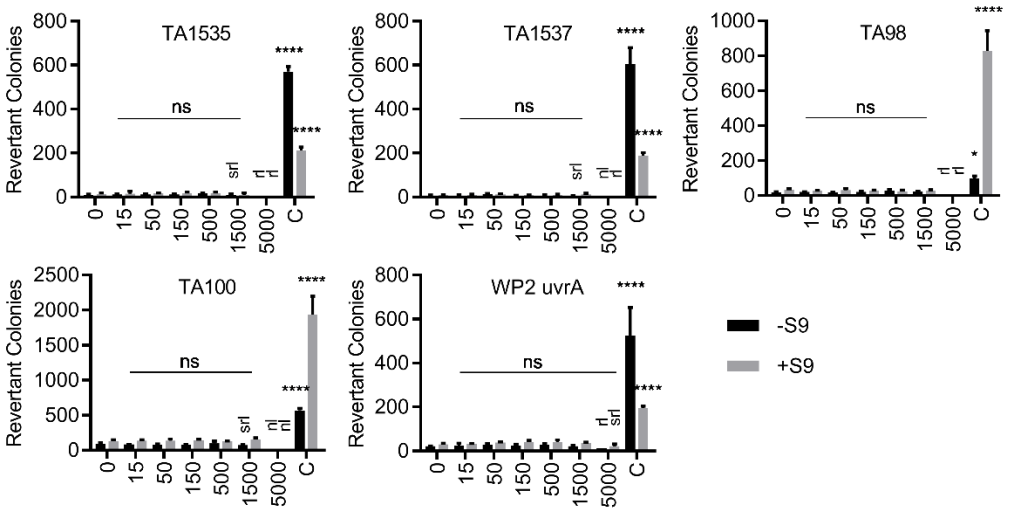

Figure 5.1. Ames test of eCF506. The mutagenicity of eCF506 was tested in five different auxotrophic bacterial strains. Graphs show average of three biological repeats with standard deviation. Bacteriotoxic effects: srl = slightly reduced lawn, rl = reduced lawn, nl = no lawn. Statistical analysis was done by two-way ANOVA with Dunnett's correction for multiple comparison showed no significant ($p>0.05$) changes for eCF506, while the controls all significantly increased the number of revertant colonies compared to the respective untreated control; $p>0.05$ (ns), $p<0.05$ (*), $p<0.0001$ (****).

Table 5.1. Sum of clinical scores. Clinical scores describe the sum and severity of adverse effects observed in Sprague-Dawley rats at different time points as described in methods chapter 2.6.2. Vehicle group 1 received the same vehicle concentration as mice treated with 200 mg/kg or 400 mg/kg eCF506, while vehicle group 2 received the same vehicle concentration as mice treated with 700 mg/kg eCF506.

Group	Sex	Female										Male									
	Dose (mg/kg)	Vehicle 1		Vehicle 2		200		400		700		Vehicle 1		Vehicle 2		200		400		700	
Time (h)	0	0	0	0	0	0	0	0	0	0	0	0	0	0	0	0	0	0	0	0	0
	1	0	0	0	0	0	0	0	0	0	0	0	0	0	0	0	0	0	0	0	0
	2	0	0	0	0	0	0	0	4	3	0	0	0	0	0	0	0	0	2	0	
	4	0	0	0	0	0	0	0	4	5	0	0	0	0	0	0	0	0	3	4	
	6	0	0	0	0	0	0	0	1	1	0	0	0	0	0	0	0	0	1	0	
	8	0	0	0	0	0	0	0	1	1	0	0	0	0	0	0	0	0	2	0	
	24	0	0	0	0	0	0	0	1	1	0	0	0	0	0	0	0	0	1	1	

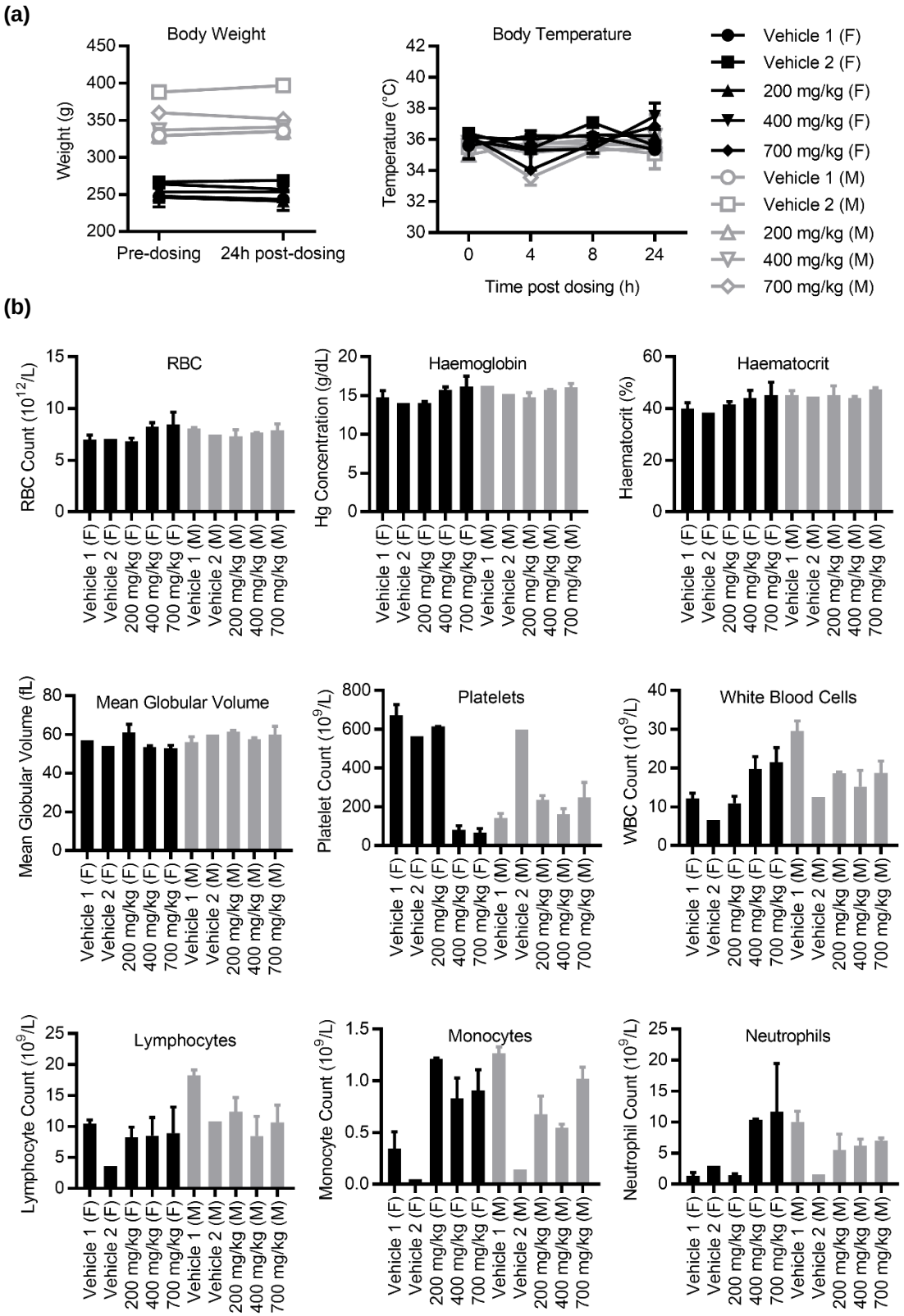

Figure 5.2. Individual results of acute toxicity study. (a) Body weight and temperature and (b) haematology results of individual Sprague-Dawley rats treated with eCF506 in an acute toxicity study. No statistical comparison was performed due to small sample size (1-2 rats/group).

Table 5.2. MTD or highest reported doses of eCF506, dasatinib and bosutinib in rodents. Summary of MTD as determined in toxicity studies (white background) or the highest dose used in published *in vivo* efficacy studies (grey background). Length of study shown in brackets. BID = twice daily. Doses given in mg/kg.

Dose	Route	eCF506	Dasatinib	Bosutinib
Mice				
Single	Oral	50	-	2,000 [387]
	IP	20	-	20 [387]
Repeat	Oral	40 (3 months)	50 (8 weeks, 5-on 2-off) [389]	100 (21 days, BID) [390]
Rats				
Single	Oral	700	30 (<100) [388]	700 [387]
	IP	-	-	70 [387]
Repeat	Oral	-	15 (2 weeks, daily), 15 (1 month, 5-on 2-off), 4 (6 months, daily) [388]	100 (7 days, daily), 70 (1 month, daily), 10-30 (6 months, daily) [387]

5.1.2. Pharmacokinetic and metabolite profile of eCF506

5.1.2.1. Pharmacokinetic evaluation in Sprague-Dawley rats

This work was done by Evotec, France.

The pharmacokinetic properties of eCF506 have previously been evaluated by Fraser *et al.* in a mouse model [1]. In order to confirm that the high MTD of the acute toxicity study (see chapter 5.1.1.2) is not due inadequate exposure to eCF506, additional pharmacokinetic testing in Sprague-Dawley rats was performed by Evotec, France.

Pharmacokinetic parameters were measured in male Sprague-Dawley rats after single intravenous (1 mg/kg) or oral dose (10 mg/kg, 200 mg/kg) for 24 hours. The plasma concentration time profile is shown in Figure 5.3 and the full dataset is shown in Appendix A.13. The systemic pharmacokinetic parameters for this study as well as previous reported studies with eCF506, dasatinib and bosutinib in mice and rats are shown in Table 5.3 for comparison.

While eCF506 had a generally favourable pharmacokinetic profile in mice in comparison to dasatinib, it was unable to achieve comparable exposure times and concentrations in rats at the same dose. In mice, the maximum plasma concentration (C_{max}) of eCF506 (oral gavage, 10 mg/kg) was nearly 200 nM, with dasatinib achieving half this concentration at half the dose (see Table 5.3) [391,392]. However, in rats treated the same way, eCF506 only achieved a concentration of 32 nM in plasma, which was over 15 times lower than the reported value for dasatinib (490 nM) at the same dose [391]. Dasatinib was also able to sustain concentrations over 100 nM for the whole duration of the study (10 hours), while eCF506 was only detectable in the rats from 2-7 hours post-dosing (see Figure 5.3) [391]. Bosutinib also had a much lower exposure in male rats than dasatinib, with a similar C_{max} and area under curve (AUC) reported at 50 mg/kg as for dasatinib at a fifth of the concentration; however, exposure was higher in female rats [393].

The half-life ($t_{1/2}$) of intravenous eCF506 was also significantly reduced in rats compared to mice (0.5 hours and 2.9 hours, respectively) as well as in comparison to dasatinib (3.3-6.7 hours), although it is important to note that eCF506 was tested at a ten-fold lower dose than dasatinib in rats (1 mg/kg vs 10 mg/kg). eCF506 showed a very large volume of distribution (Vd_{ss}) in both rats (14.2 L/kg) and mice (11.8 L/kg),

which indicates that it passes rapidly from blood to tissues; this could be a reason for its low plasma half-life in rats. However, bosutinib still achieved a better half-life with similar Vd_{ss} values in both rodent species and dasatinib had a much shorter half-life in mice than eCF506 despite a comparatively lower volume of distribution. Therefore, it currently remains unclear why eCF506 performed worse in rats than in mice when given via intravenous injection.

After administration of eCF506 to male rats by oral gavage at 10 mg/kg, the compound only had an oral bioavailability of 13%, which was half that found in mice and of dasatinib in rats. The comparatively poor performance of eCF506 in rats when given orally could be due to a higher first pass metabolism than in mice. The sex-specific differences seen with bosutinib indicate that eCF506 could perform differently in female rats.

The results of treating Sprague-Dawley rats orally with 10 mg/kg were suggesting that the toxicology study done in chapter 5.1.1.2 might have yielded good results due to low exposure of the test animals to the compound. However, the doses used in the toxicology study were more than 20-fold higher than in the pharmacokinetic one. As higher doses can saturate metabolic clearance pathways and can be absorbed in the gastrointestinal tract over a longer period, it was likely that higher exposure was achieved than could be predicted from using 10 mg/kg. Therefore, eCF506 was tested again in the rat pharmacokinetic model at a single dose of 200 mg/kg (see Table 5.3 and Figure 5.3). Oral bioavailability was much improved at the higher dose (45%) and the plasma concentration was greater than 95 nM throughout the whole study; it even increased with time to over 700 nM at 24 hours and a longer study is needed to definitively determine the C_{max} and T_{max} at this dose. Even though the compound had not been cleared from the system after 24 hours, the AUC was 3.5-fold higher than expected based on results from the 10 mg/kg oral dose, demonstrating much higher exposure.

This study gives confidence in the findings of the toxicology study by showing that high and sustained exposure to eCF506 was achieved in rats at the doses tested. However, it also highlights the fact that animals should have been observed for longer, even though clinical symptoms were subsiding over time, as plasma concentrations were likely still increasing at the time of necropsy.

Table 5.3. *In vivo* pharmacokinetic data of eCF506, dasatinib and bosutinib. Data based on PK studies performed with eCF506 by Evotec or as reported in the literature. IV = intravenous administration, IA = intraarterial administration, IPT = intraportal administration, PO = oral administration, AUC = area under curve, $t_{1/2}$ = half-life, C_{max} = maximum plasma concentration, T_{max} = time to reach maximum concentration, CL = clearance, Vd_{ss} = volume of distribution (steady-state), F = bioavailability. Diluent: [a] saline solution; [b] propylene glycol:water (1:1); [c] nanopure water; [d] 50 mM sodium acetate buffer, pH 4.6; [e] 50mM citrate buffer, pH 3.0.

Species / Strain	Route	Compound	Dose (mg/kg)	Duration (h)	Sex/Group	AUC (µg hr/mL)	$t_{1/2}$ (h)	C_{max} (µM)	T_{max} (h)	CL (mL/min/kg)	Vd_{ss} (L/kg)	F (%)	Reference
Mouse / nude	IV	eCF506	10 [a]	8	F/3	2.07	2.9	-	-	72.3	11.8	-	[1]
		Dasatinib	10 [b]	6	F/3	2.86	0.9	-	-	61.7	4.2	-	[391]
			5 [b]	24	F/3	0.92	0.8	-	-	98	6.1	-	[392]
		Bosutinib	5	-	-	2.22	4.8	-	-	37.5	11.5	-	[393]
	PO	eCF506	10 [c]	8	F/3	0.53	-	0.196	2	-	-	25.3	[1]
		Dasatinib	5 [b]	8	F/3	0.22	2.5	0.104	2	-	-	17	[391]
			15 [b]	8	F/3	0.58	2.0	0.320	2	-	-	14	[391]
			5 [b]	24	F/3	0.42	-	0.119	1	-	-	45	[392]
			2.5 [b]	24	F/3	0.24	-	0.99	1	-	-	51	[392]
			1.25 [b]	24	F/3	0.11	-	0.050	1	-	-	48	[392]
		Bosutinib	50	-	-	11.7	4.2	2.845	4	-	-	52.6	[393]
Rat / Sprague-Dawley	IV	eCF506	1 [d]	24	M/3	0.06	0.5	0.484	-	252	14.2	-	
	IA	Dasatinib	10 [b]	10	M/3	6.78	3.3	13.2	-	26.4	6.3	-	[391]
	IPT		10 [d]	10	M/3	7.66	6.7	7.5	0.5	-	-	-	[391]
	IV	Bosutinib	5	-	M	0.66	2.5	1.218	-	128	15.2	-	[393]
					F	0.72	4.3	1.363	-	70.3	17.1	-	
	PO	eCF506	10 [e]	24	M/3	0.08	-	0.032	-	-	-	13	
			200 [e]	24	M/3	5.53	>24	0.806	2	621	-	45	
		Dasatinib	10 [b]	10	M/3	1.85	3.1	0.49	2.3	-	-	27	[391]
		Bosutinib	50	-	M	1.51	3.7	0.422	3	-	-	23	[393]
					F	7.10	5.4	1.571	5.5	-	-	59.5	

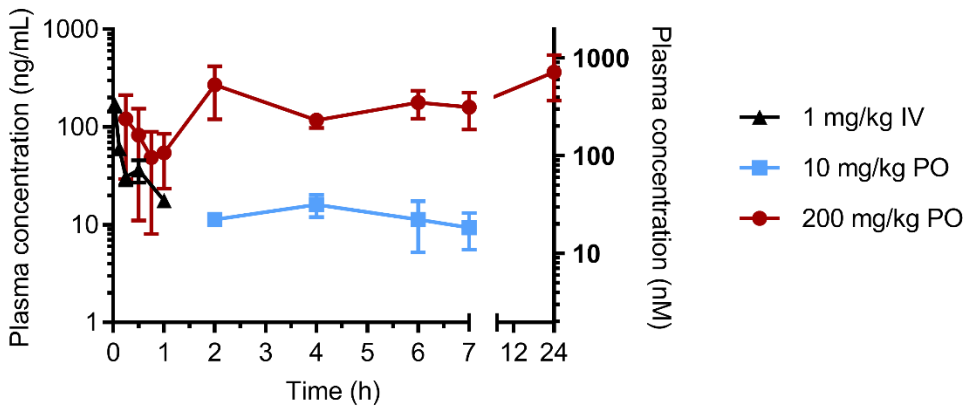

Figure 5.3. Pharmacokinetics of single dose eCF506 in Sprague-Dawley rats. Graph shows average of three rats per experiment with standard deviation. Calculated parameters are included in Table 5.2 above.

5.1.2.2. Metabolite study

This work was done by Cyprotex, UK.

eCF506 has previously been tested for its *in vitro* metabolic stability in human and mouse hepatocytes [1]. However, it has not yet been determined what its main metabolites are after breakdown in the liver. This is important as metabolites that retain potency against the target can contribute to the overall efficacy of a drug. Conversely, other metabolites have been found to cause toxicity, one example being the paracetamol metabolite N-acetyl-p-benzoquinone imine that can damage the liver when not cleared fast enough [394]. Therefore, it is important to determine the metabolite profile of a novel compound early on during drug development.
In order to get a better understanding of how eCF506 is broken down by hepatocytes, it was tested in a second human hepatocyte stability assay that was followed by metabolite profiling (performed by Cyprotex, UK). Cryopreserved human hepatocytes were treated with eCF506 (3 µM) and samples analysed using a Q-Tof UPLC-MS/MS platform at different time points over the course of the 120-minute experiment (see Figure 5.4 and Appendix A.14). Metabolites are identified by comparison against a time zero control and quantified using the area percentage of the LC-MS chromatogram. The fragmentation patterns were used for structural elucidation of the metabolites which are shown in Figure 5.5.

The calculated half-life of eCF506 in human hepatocytes was less than a third of that reported previously (212 and 751 minutes, respectively, see Figure 5.4b,c). Due to the expected differences between donors of primary hepatocytes, variability between experiments is expected and can be seen in the slower breakdown of the control compound umbelliferone and the faster clearance of verapamil in the second assay. In this experiment, approx. 70% of eCF506 remained after 2 hours of incubation, which is slightly lower than the 78% of dasatinib after 3 hours measured in a previous experiment with human hepatocytes [395]. However, these two compounds should be tested head-to-head to properly compare them due to the high assay variability.

Metabolite profiling revealed four major metabolites of eCF506 after 2 hours (see Figure 5.5). The main metabolite, making up 19% of the drug-related components, is a demethylation of the dimethylamino-piperidine of eCF506. The other three

metabolites are oxidations of different parts of the molecule and make up 1-7% of the drug-related components.

Based on structure activity relationships found by the Innovative Therapeutics Lab for this scaffold, it is likely that the N-demethylated metabolite retains some activity against SRC kinase; this is currently being investigated further [1]. A possible O-demethylation of the methoxy-group on the benzene ring was not found in this assay, which is positive as this molecule has previously been found to have no activity in cell viability assays (EC_{50} = 9.71 µM in MDA-MB-231 cells, see compound 12s in Fraser *et al.* [1]). No information is available on the activity of the oxidised metabolites.

(a)

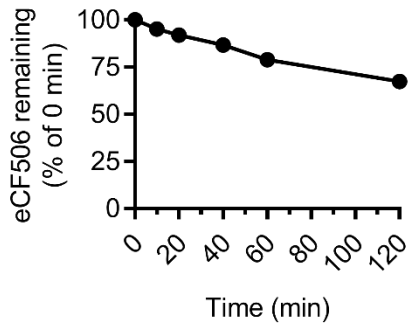

Time (min)	eCF506 remaining (% of 0 min)
0	100
10	95.1
20	92.0
40	86.7
60	78.9
120	67.3

(b)

Species	Compound	CL_{int} (µL/min/10^6 cells)	SE CL_{int}	$t_{1/2}$ (min)
Human	eCF506	6.55	0.334	212
	Verapamil	88.8	3.13	15.6
	Umbelliferone	77.9	1.71	17.8

(c)

Species	Compound	CL_{int} (µL/min/10^6 cells)	Standard error CL_{int}	$t_{1/2}$ (min)
Human	eCF506	1.84	0.989	751
	Verapamil	60.8	1.3	22.8
	Umbelliferone	150	0.8	9.7
Mouse	eCF506	12.5	0.447	110
	Verapamil	317	21.6	4.4
	Umbelliferone	983	135	1.4

Figure 5.4. Hepatocyte stability of eCF506. (a, b) Human hepatocytes were incubated for 120 minutes prior to analysis of drug metabolites in the medium by liquid chromatography and mass spectrometry. The average of six biological repeats was used to calculate intrinsic clearance (CL_{int}) with standard error and half-life ($t_{1/2}$). (c) Results of a previous study of eCF506 in human and mouse hepatocytes as reported by Fraser *et al.* [1].

(a)

Metabolite	Formula	[M + H]$^+$	Time	Peak area %		
				0 min	60 min	120 min
eCF506	$C_{26}H_{38}N_8O_3$	511.31	6.98	100	84.66	69.64
Demethylation	$C_{25}H_{36}N_8O_3$	497.30	6.84	0	10.33	19.10
Oxidation 1	$C_{26}H_{38}N_8O_4$	527.31	5.16	0	1.66	7.05
Oxidation 2	$C_{26}H_{38}N_8O_4$	527.31	5.37	0	2.29	1.14
Oxidation 3	$C_{26}H_{38}N_8O_4$	527.31	7.08	0	1.06	3.07

(b)

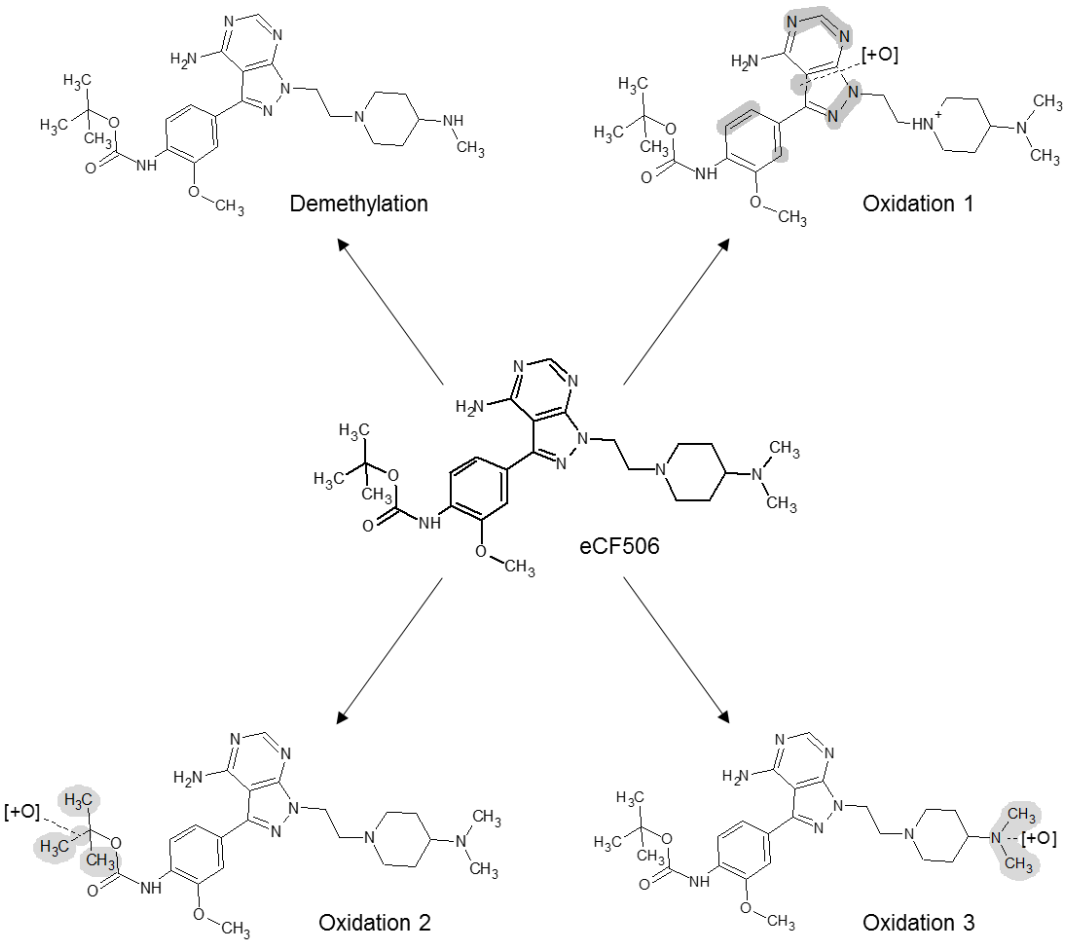

Figure 5.5. Metabolite profile of eCF506. (a) Summary table of results. (b) Structures of identified metabolites. Metabolites were analysed from their fragmentation patterns in the LC-MS chromatogram after incubation of human hepatocytes with eCF506 for 60 or 120 minutes. Percentage area under the chromatogram was used to determine relative quantities.

5.1.3. eCF506 can reach the brain and retina in mouse models at efficacious concentrations

5.1.3.1. eCF506 can cross the blood brain barrier in mice

This work was done by Dr Alaide Morcavallo and Nikita Locket (group of Prof Louis Chesler) and Louise D Johnson and Ruth R Ruddle (group of Dr Florence I Raynaud) at the Institute of Cancer Research, London, UK.

Elevated SRC signalling has recently been identified as a key hallmark in type 4 medulloblastoma, the most common malignant brain tumour in children [162]. A SRC inhibitor could therefore have potential efficacy in this setting. The group of Prof Louis Chesler at the Institute of Cancer Research in London is currently investigating the use of eCF506 in *in vitro* and *in vivo* medulloblastoma models. One important factor to consider in this disease setting is the ability of a SRC inhibitor to penetrate the blood brain barrier. This was assessed for eCF506 by Dr Alaide Morcavallo in a pharmacokinetic study done in highly immunodeficient NSG mice.

eCF506 (40 mg/kg) was injected intraperitoneally and mice were sacrificed at different time points over an 8-hour period to collect blood and brain samples, from which the eCF506 concentration was determined by LC-MS/MS (see method 2.6.3.2). Plasma concentrations dropped over the course of the study from 4.2 to 1.8 µM (see Figure 5.6). The concentration measured in the brain was more consistent and increased with time from 498 nM (0.5 hours) to 763 nM (8 hours). The brain to plasma ratio ranged from 12-43%, which is much higher than previously reported for dasatinib in a SCID mouse model with intracranial CML tumours (3.2-8.6%) [396].

Both plasma and brain concentrations far exceeded those needed for effective phospho-SRC inhibition *in vitro* over the 8-hour period. This suggests that eCF506 could potentially be used to treat SRC-related diseases in the brain or central nervous system, such as type 4 medulloblastoma or Alzheimer's disease (see chapter 1.2.3.7).

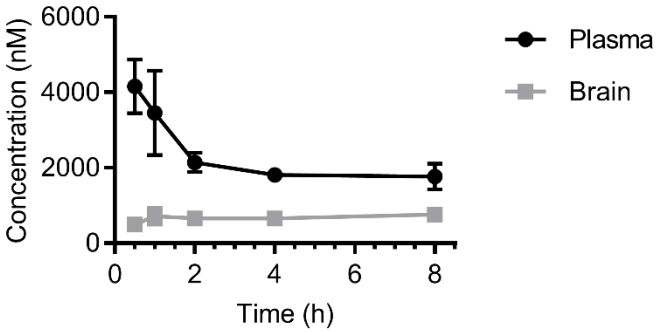

Time (h)	Average Concentration (nM)		Brain:Plasma ratio
	Plasma	Brain	
0.5	4158 (±714, n=3)	498 (±17, n=3)	0.12
1	3455 (±1121, n=3)	714 (±225, n=3)	0.21
2	2136 (±257, n=3)	655 (±127, n=3)	0.31
4	1806 (±17, n=3)	657 (±101, n=3)	0.36
8	1764 (±341, n=2)	763 (±152, n=3)	0.43

Figure 5.6. Pharmacokinetic study of eCF506 in the brain. Analysis of concentration versus time in blood and brain samples from NSG mice after intraperitoneal administration of 40 mg/kg eCF506. Table shows average with standard deviation and number of mice per group shown in brackets.

5.1.3.2. eCF506 can inhibit SRC activity in the retina of mice

This work was done by Oxurion (formerly Thrombogenics), Belgium.

Retinopathies have been linked to aberrant angiogenesis and eCF506 has been found to inhibit blood vessel outgrowth in an *ex vivo* murine choroid transplant (see chapter 3.1.5). As it was not clear whether eCF506 can reach the retina at biologically relevant concentrations, an *in vivo* experiment was done by Thrombogenics, Belgium, to assess target inhibition in mouse retinas.

Male C57BL/6J mice received one intraperitoneal injection of eCF506 (10 mg/kg) one hour prior to stimulation of SRC phosphorylation by intravitreal injection of murine VEGF. Mice were culled after 30 minutes, enucleated and retinas isolated. Western blot analysis was performed to assess levels of total and autophosphorylated SRC kinase (see Figure 5.7). eCF506 was able to significantly reduce the amount of phospho-SRC (Y416) by more than 50% compared to control. This suggests that eCF506 is present and functionally active in the retina for at least 90 minutes and is able to inhibit SRC phosphorylation induced by VEGF pulse. It is likely that higher doses or topical application would result in even higher levels of inhibition.

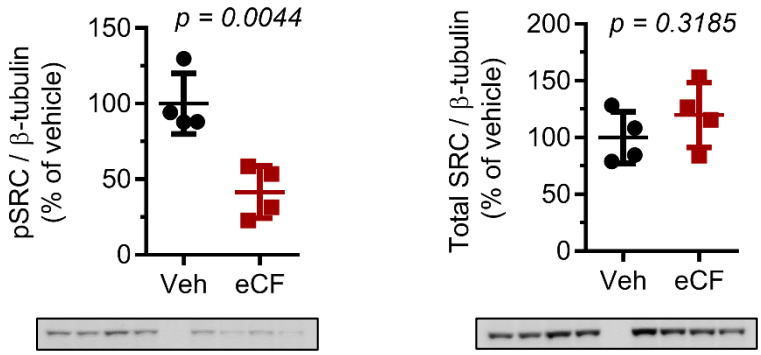

Figure 5.7. SRC levels and activation in mouse retinas after eCF506 treatment and VEGF stimulation. Phospho-SRC Y416 (left) and total SRC (right) were assessed by Western blot and signal normalised to loading control (β-actin). Graphs show average of four retina samples per group with standard deviation. Statistical analysis by unpaired t-test.

5.2. eCF506 shows model-dependent efficacy *in vivo*

5.2.1. eCF506 and dasatinib were not potent in an MDA-MB-231 mouse xenograft model

This work was done by Dr John Dawson and Morwenna Muir at the Institute of Genetics and Molecular Medicine, University of Edinburgh, UK.

The human breast cancer cell line MDA-MB-231 has been shown to be highly sensitive to eCF506, with inhibition of proliferation and migration seen at nanomolar concentrations *in vitro* (see chapter 3.1.1.2) [1]. It was therefore further investigated in a murine xenograft to compare eCF506's potency against dasatinib *in vivo*.

CD-1 nude mice received subcutaneous bilateral implantations of MDA-MB-231 fragments and tumours were allowed to grow until they reached 20 mm^3 in size. Mice were treated with eCF506, dasatinib (both 25 mg/kg) or vehicle (saline) once daily by oral gavage for 25 days and the measured tumour sizes are plotted in Figure 5.8. Both eCF506 and dasatinib were unable to prevent the growth of MDA-MB-231 xenografts, although the latter showed some significant effect towards the end of the treatment period. Tumours treated with eCF506 were slightly but not significantly bigger than controls throughout the study, while those treated with dasatinib were smaller; this correlates with corresponding slight differences in tumour size between the groups at the start of the study. On the final day of the study, a small decline in tumour size was observed for 3 of the 4 remaining tumours treated with eCF506 and 8 of the 10 dasatinib treated ones. However, this was only found to be significant for dasatinib ($p = 0.0002$) when compared to control; notably 5 of the 9 remaining vehicle-treated tumours also slightly reduced in size.

The results of this study suggest that the treatment with daily doses of eCF506 at 25 mg/kg does not have antiproliferative effects in a murine xenograft of MDA-MB-231 breast cancer cells, while dasatinib only showed limited potency after three weeks. A longer study would be needed to determine whether the reduction in tumour size on the final day is treatment-related and whether eCF506 could produce significant results with longer treatment or higher doses.

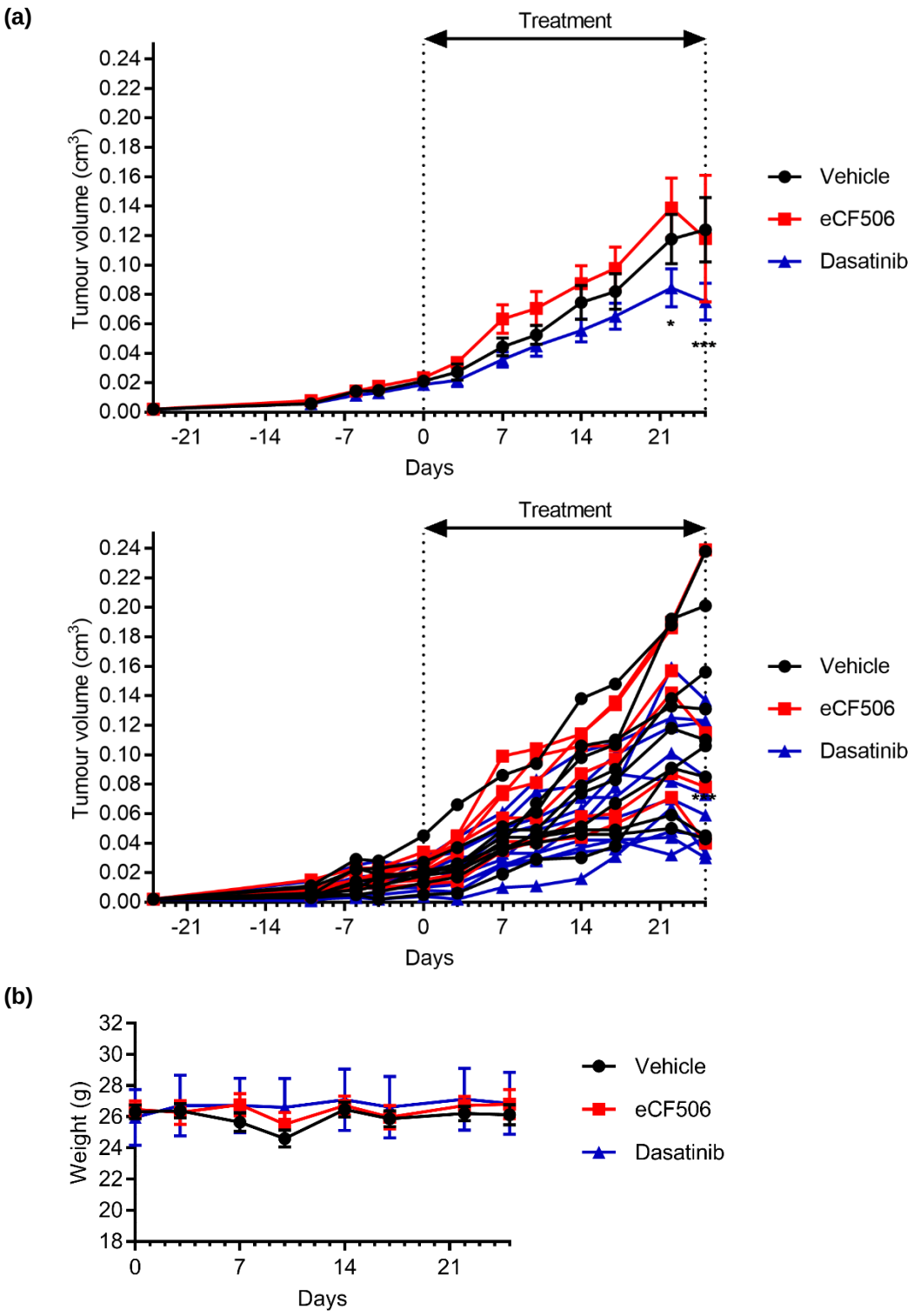

Figure 5.8. MDA-MB-231 xenograft in mice treated with eCF506 or dasatinib. (a) Graphs show average tumour volume with standard error (top) and individual tumour volumes (bottom) of CD-1 nude mice treated with saline, eCF506 or dasatinib (both 25 mg/kg). eCF506 and dasatinib were compared to vehicle group by two-way ANOVA with Dunnett's correction for multiple comparison; eCF506 did not differ significantly from vehicle at any point, while dasatinib was significantly more potent at the last two measurements, with $p<0.05$ (*), $p<0.001$ (***). (b) Average weight of mice during treatment period with standard error.

5.2.2. eCF506 potently reduces tumour growth in syngeneic mouse models of metastatic breast cancer

5.2.2.1. MetBo2 cells as a murine model of metastatic breast cancer

Due to the role of SRC kinase in cell migration and the bone environment, SRC inhibitors have frequently been tested in models of cancer metastasis and in particular in patients with breast cancer bone metastases (see chapters 1.2.3.1, 1.2.3.5, 1.3.2). Therefore, the *in vivo* potency of eCF506 was tested in the murine breast cancer cell line MetBo2 which has similar characteristics to human triple negative breast cancer and preferentially metastasises to the bone.
This cell line was created by the group of Dr Bin-Zhi Qian at the University of Edinburgh, UK, by cardiac injection of the murine breast cancer cell line Met1 into syngeneic mice and selection of metastatic lesions in the bone; the selection process was repeated in a second round to obtain the bone-tropic cell line MetBo2.

Prior to testing this cell line *in vivo*, it was assessed in several *in vitro* assays for its sensitivity to eCF506. Western blot analysis of the parental Met1 and derived MetBo2 cell line revealed a doubling of SRC activation in the latter but only minor changes in downstream FAK activity between the two (see Figure 5.9a). This was expected, as Zhang *et al.* have previously shown that bone metastatic MDA-MB-231-derived cells have increased levels of SRC autophosphorylation [92]. However, when both cell lines were tested in a 2D cell viability assay, they did not exhibit differences in their sensitivity to eCF506 (see Figure 5.9b). When MetBo2 sensitivity was tested in a panel of five SRC/ABL inhibitors, it was found that they were nearly ten-fold more sensitive to dasatinib than eCF506 (GI_{50} of 41 nM and 297 nM, respectively) (see Figure 5.9c,d and Appendix A.15).

However, previous experiments have shown that results obtained in this 2D cell viability assay do not necessarily translate into 3D (see chapter 3.1.4); therefore, MetBo2 cells were further assessed in a 3D spheroid assay as performed previously (see methods 2.2.2.4). The results from this experiment differed strongly from those obtained previously in three other human breast cancer cell lines, as MetBo2 cells remained highly sensitive to treatment in the spheroid assay (see Figure 5.10 and Figure 3.4). While untreated MetBo2 spheroids doubled in size during the seven days, the lowest concentration of eCF506 tested (3 nM) was able to shrink spheroids by

50% compared to pre-treatment size. This is opposite from what has been observed for human breast cancer spheroids, where only high concentrations of eCF506 or dasatinib were able to reduce spheroid size significantly. Furthermore, eCF506 was significantly more potent at reducing spheroid size at 10 nM than at one thousand-fold higher concentration and it appeared slightly better than dasatinib at lower concentrations, which is opposite from what would have been expected from the 2D cell viability assays (see Figure 5.9 and Figure 5.10). However, staining with calcein-AM and propidium iodide for live and dead cells, respectively, shows more dead cells after treatment with dasatinib than with eCF506 and at higher concentrations of both compounds; this suggests that spheroid size does not directly reflect cytotoxicity in this cell line.

Based on the potent results of the spheroid assay, a second 3D mammosphere assay was performed to assess the effects of eCF506 and dasatinib on the MetBo2 stem-like cell subpopulation. Cancer stem cells have the capacity to self-renew and have been reported to be especially resistant to treatment; targeting them effectively is therefore essential to prevent relapse [397]. Previous studies have found that SRC and FAK inhibitors can target cancer stem cells, which highlights the potential benefit of combining standard therapy with SRC inhibitors [398,399]. The mammosphere assay performed in this thesis is based on the protocol published by Shaw *et al.* and modified as described in methods 2.2.2.5 [295]. A single cell suspension was seeded sparsely in serum-free mammosphere medium in non-adherent plates, treated with eCF506 or dasatinib (both 100 nM) and allowed to form mammospheres for 5 days. These were disaggregated, re-seeded as single cells and treated again for 5 days in a second generation. Only mammospheres with a diameter over 50 µm were counted after each generation and the mammosphere forming efficiency (MFE) and self-renewal rate were calculated as described by Shaw *et al.* [295]. The results of three biological repeats, plotted in Figure 5.11, show that both eCF506 and dasatinib were able to significantly decrease the MFE and self-renewal rate of MetBo2 cells. As seen previously in the spheroid assay, eCF506 was slightly but not significantly more potent than dasatinib. Shaw *et al.* have previously assessed the mammosphere forming ability of several breast cancer cell lines in their assay and found a maximum MFE of around 2.5% [295]. MetBo2 cells have a MFE nearly twice as high, which suggests they have a high proportion of stem-like cells; this is in line with unpublished findings by the group of Dr Bin-Zhi Qian that found MetBo2 cells to be resistant to standard chemotherapy.

The self-renewal rate is a measure of the ability of one cell from a primary mammosphere to self-renew and form another mammosphere in the second generation. Shaw *et al.* found that mammospheres undergo asymmetric self-renewal, while other groups found symmetric self-renewal based on an increase in mammosphere number in later generations [295,400]. MetBo2 had a self-renewal rate of around 2, with twice as many mammospheres observed in the second generation; this suggests symmetric self-renewal and combined with high MFE it supports the hypothesis of high stem cell activity in this cell line.

One limitation of this study is the pre-defined mammosphere size cut-off of 50 µM, which excludes detection of stem cells with reduced proliferative ability that result in smaller spheroids. eCF506 and dasatinib are both potent inhibitors of cell proliferation and 3D spheroid size which likely could have skewed the MFE results in the primary generation. However, by comparing mammospheres between the second and first generation, it is possible to distinguish between inhibition of proliferation or self-renewal [295]. Therefore, eCF506 appears to be a potent inhibitor of both cell proliferation and self-renewal of MetBo2 stem cells *in vitro*. Further experiments should be done to confirm the stem cell-targeting properties of eCF506, for example an *in vivo* assay with serial transplantation, which is the gold-standard for assessing self-renewal capacity.

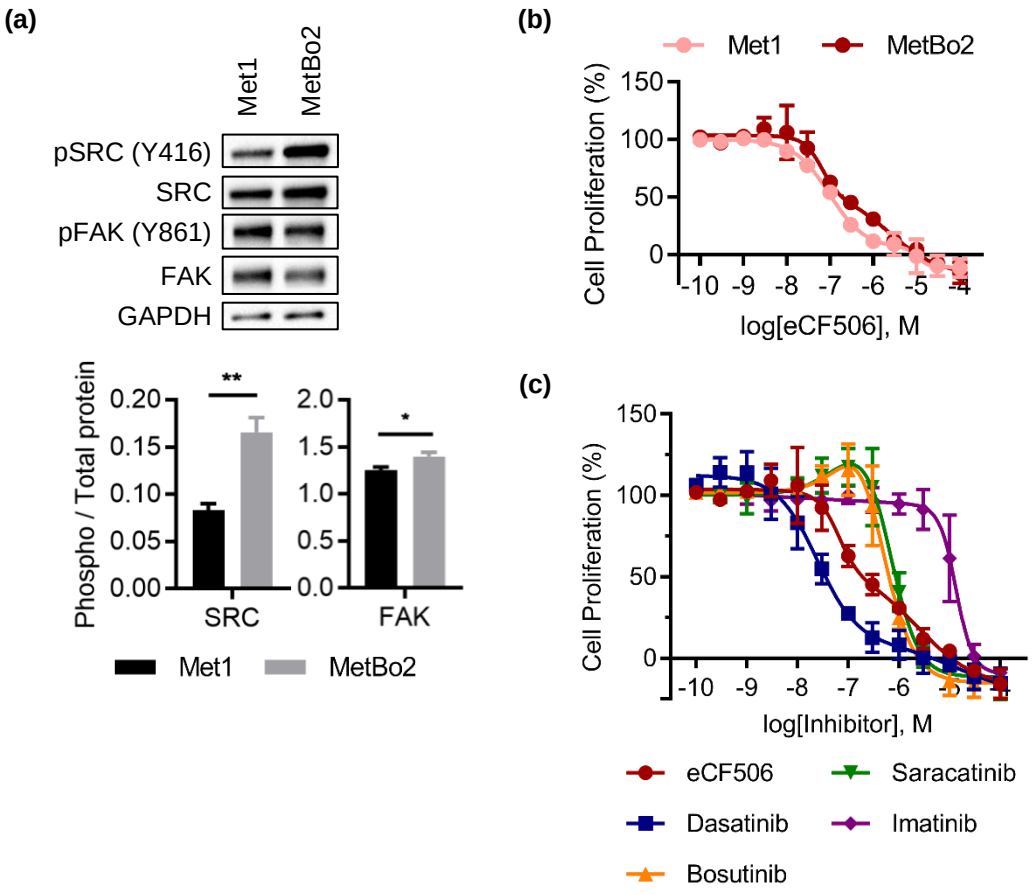

(d)

	eCF506	Dasatinib	Bosutinib	Saracatinib	Imatinib
Met1	0.108 (0.0184)	0.0408 (0.0188)	0.597 (0.200)	0.429 (0.0853)	7.80 (1.74)
MetBo2	0.297 (0.0955)	0.0406 (0.0112)	0.729 (0.244)	0.854 (0.184)	12.5 (5.82)

Figure 5.9. *In vitro* sensitivity and SRC signature of Met1 and MetBo2 cells. (a) The amount of phospho-SRC (Y416) and phospho-FAK (Y861) was quantified relative to the amount of total protein in both Met1 and MetBo2 cells. Statistical analysis by unpaired t-test; $p<0.05$ (*), $p<0.01$ (**). (b) Cell proliferation of Met1 and MetBo2 cells treated for 5 days with eCF506. Viability was measured using PrestoBlue™ reagent and adjusted to viability prior to treatment. Graph shows average of three biological repeats with standard deviation. (c) Cell proliferation of MetBo2 cells treated for 5 days with different kinase inhibitors. Viability was measured using PrestoBlue™ reagent and adjusted to viability prior to treatment. Graph shows average of three biological repeats with standard deviation. (d) Summary of GI_{50} values of Met1 and MetBo2 cells treated with different kinase inhibitors. Values were calculated from three biological repeats with standard deviation shown in brackets.

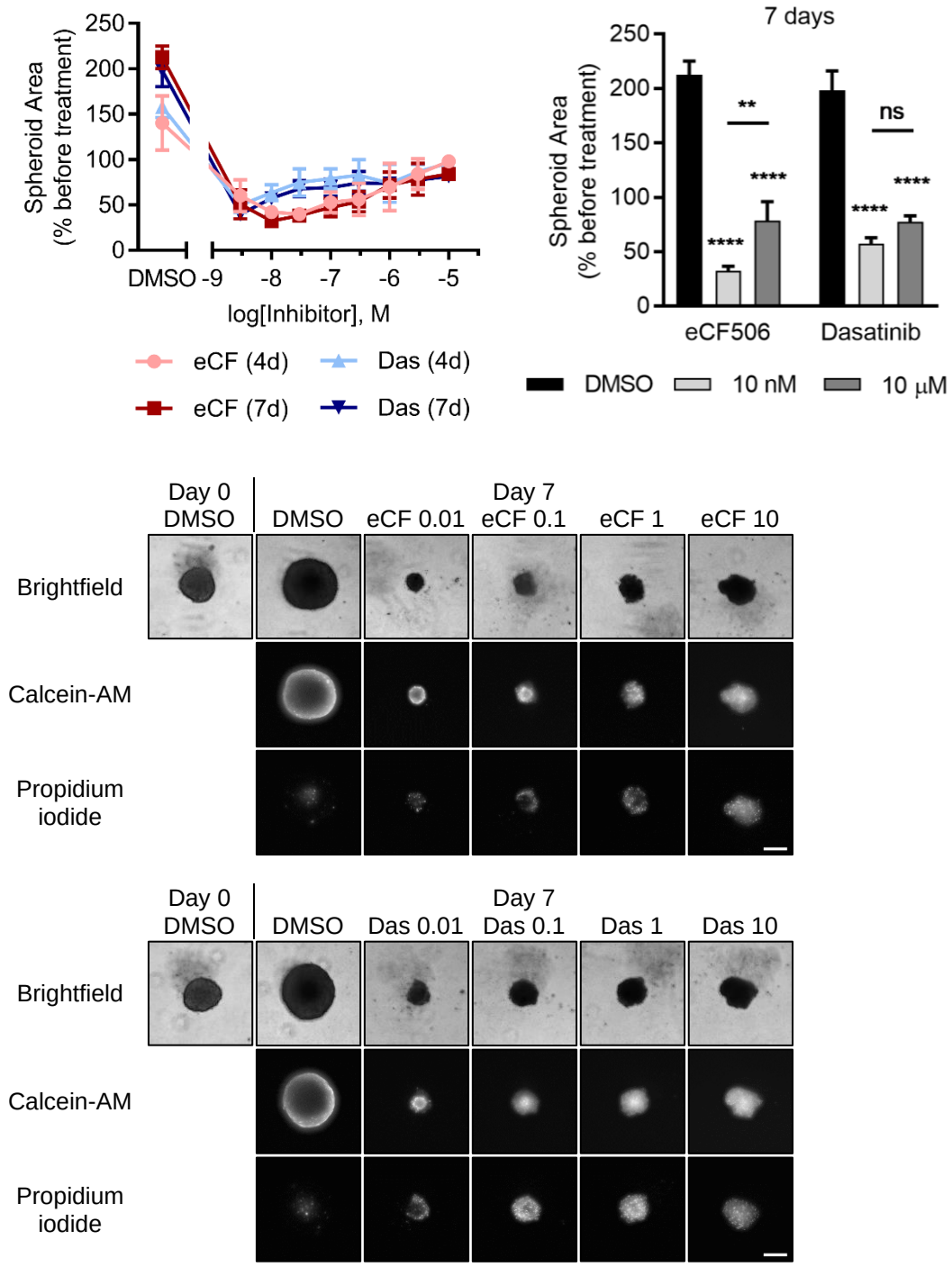

Figure 5.10. MetBo2 spheroids treated with eCF506 or dasatinib. Spheroids size was measured before and after four or seven days of treatment from a collapsed Z-stack image using CellProfiler software. Data was normalised to spheroid size prior to treatment start. Data represents average of three biological replicates with standard deviation. Top left: Graph showing spheroids size as percentage of size prior to treatment start. Top right: Comparison of spheroid size after seven days of treatment. Statistical analysis was done using two-way ANOVA with Tukey correction; $p>0.05$ (ns), $p<0.01$ (**), $p<0.0001$ (****). Images show representative spheroids using brightfield microscopy or fluorescent microscopy after staining with calcein (live cells) or propidium iodide (dead cells). Scale bar = 200 µm.

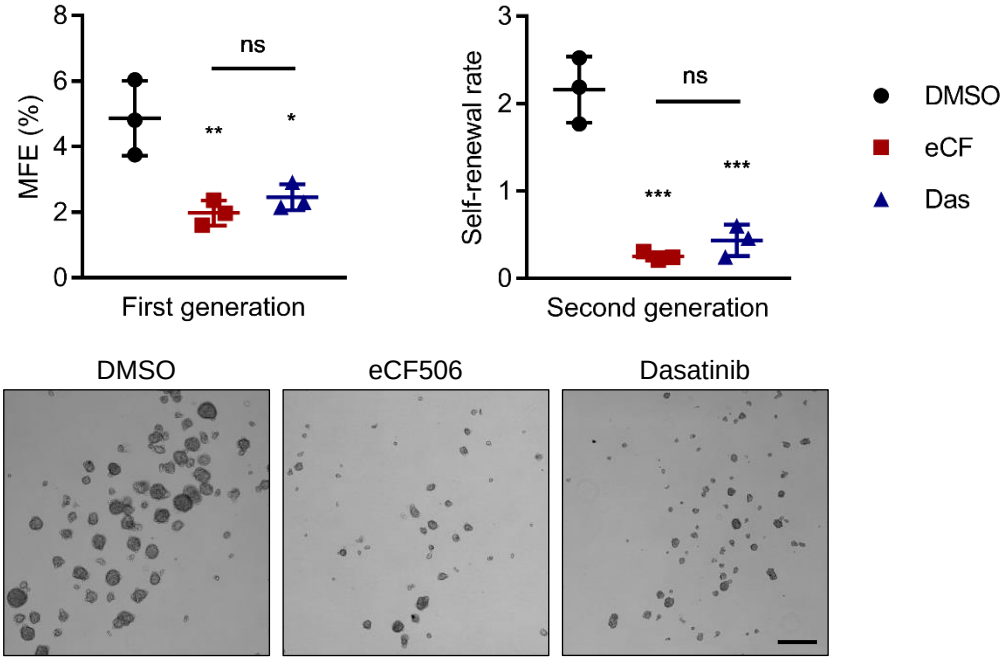

Figure 5.11. MetBo2 mammosphere assay. A single cell suspension of MetBo2 cells in non-adherent plates was treated for five days with eCF506 or dasatinib (both 100 nM). First generation mammospheres were disaggregated, re-seeded at the same density and treated again for five days. First and second generation mammospheres were imaged using the ImageXpress platform and quantified using CellProfiler, with only mammospheres with a diameter over 50 µm being included. Graphs show mammosphere forming efficiency (MFE) and self-renewal rate calculated as described by Shaw *et al.* from three biological repeats with standard deviation [295]. Photos show representative second generation mammospheres. Scale bar = 200 µm.

5.2.2.2. eCF506 and dasatinib affect MetBo2 cytokine signalling

The cytokine array was done by Kenneth Macleod from the Drug Discovery group of Prof Neil Carragher at the University of Edinburgh, UK.

Several papers have previously shown that nuclear FAK and FAK inhibitors affect cytokine expression and secretion by murine squamous cell carcinoma (SCC) cells [290,293]. eCF506 and dasatinib have different effects on nuclear FAK (see chapter 4.3.1) but no consistent changes in gene expression could be identified in SCC cells (see chapter 4.3.2). Nonetheless, it is possible that eCF506 and dasatinib differ in their effects on cytokine secretion, whether due to their differences in nuclear FAK or selectivity across the kinome. As eCF506 is tested in multiple *in vivo* models of MetBo2 cells that show high potency and might involve immune system activation (see following chapter), its effect on cytokine secretion was tested in this cell line and compared to dasatinib in a cytokine array. Cells were treated with four concentrations of each compound (3 nM, 10 nM, 30 nM, 100 nM) for 48 hours prior to collection of the supernatant and analysis using capture antibodies in a microarray. Cytokine levels were adjusted for protein concentration of cell lysates. 22 of 64 antibodies tested gave a signal that was significantly above background and their results are plotted in Figure 5.12 as percent secretion of DMSO control.
In general, eCF506 and dasatinib had very similar effects, although dasatinib appeared to be more potent than eCF506 at upregulating cytokine secretion; this is affected by normalisation to protein concentration, as dasatinib is a stronger inhibitor of MetBo2 cell viability (see Figure 5.9c). While dasatinib but not eCF506 treatment caused nuclear translocation of FAK in MetBo2 cells (see Appendix A.11), this did not seem to differentially affect cytokine secretion and results could thus not be linked to previous findings in SCC cells [290,293].

Both eCF506 and dasatinib upregulated secretion of several cytokines, especially at high concentrations (e.g. amphiregulin, CCL2, CCL3, CCL5, CXCL1, G-CSF, IGFBP5, IL-6, IL-1RA, lipocalin-2, osteopontin, pentraxin-3, PIGF2). Most notably, IL-1RA was 6.5- and 30-fold increased and IGFBP5 was increased 3- and 4.5-fold by 100 nM eCF506 and dasatinib, respectively. IL-6 and CCL11 were mostly decreased by eCF506 and lower concentrations of dasatinib, but increased 12-fold (IL-6) and 3-fold (CCL11) by higher concentrations of dasatinib.

Several cytokines were downregulated by eCF506 and dasatinib. In particular, levels of VEGF and CXCL2 were reduced by 70-90% and moderate inhibition (<50%) was seen for TNF-alpha, IL-12, MMP-3 and GM-CSF.

Overall, both compounds affected secretion of several cytokines, with IL1-RA, IL-6, IGFBP5, CXCL2 and VEGF showing the biggest changes. While the question remains to which degree these signalling changes would also be observed in an *in vivo* model with this cell line, they provide valuable guidance on which pathways to investigate first.

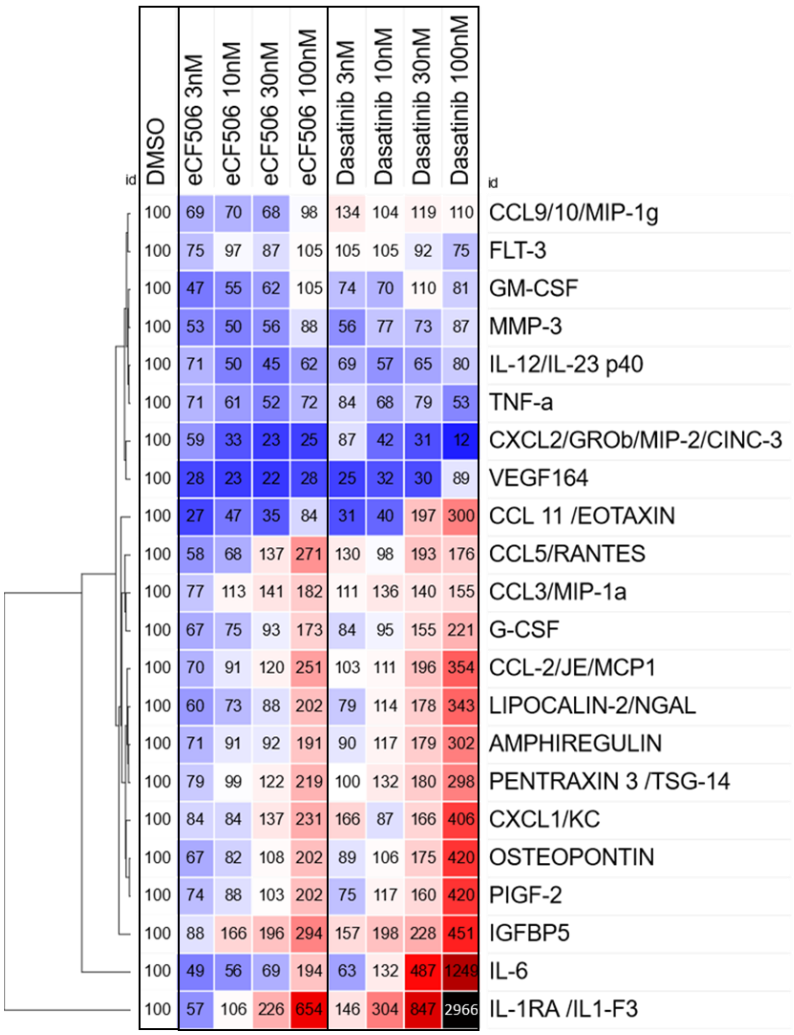

Figure 5.12. Cytokine array of MetBo2 cells. MetBo2 cells were treated with eCF506 or dasatinib for 48 hours prior to analysis of the medium by capture antibodies. Concentration of secreted proteins was adjusted for protein concentration of lysed cells and normalised to DMSO control (blue = decreased, red = increased secretion relative to DMSO). Clustering was performed using Morpheus software by the Broad Institute using Euclidian distance and average linkage.

5.2.2.3. eCF506 reduces bone metastases in a murine breast cancer model

This work was done by Dr Xue-Feng Li in the group of Dr Bin-Zhi Qian at the University of Edinburgh, UK.

After *in vitro* assessment of eCF506 in the bone-tropic murine breast cancer cell line MetBo2 indicated high sensitivity (see chapter 5.2.2.1), an *in vivo* experiment in a syngeneic bone metastasis model was performed by the group of Dr Bin-Zhi Qian at the QMRI, University of Edinburgh, UK.

Immunocompetent FVB mice received intracardiac injections of MetBo2 cells, which leads to metastasis formation in the hind legs and jaw bones. As MetBo2 cells were engineered to express luciferase, metastasis growth was monitored via bioluminescence imaging twice a week. Metastases were allowed to develop until bioluminescence intensity (BLI) in the hind legs was greater than 2000 for each group, before treatment with daily eCF506 (40 mg/kg) or vehicle by oral gavage was started for 28 days. No obvious toxicity was observed in the treatment group during the duration of the study and the mice exhibited normal behaviour and slight weight gain.

BLI of hind leg bone metastases were quantified and plotted in Figure 5.13a. This model is highly aggressive with bone metastases progressing quickly and control mice having to be sacrificed after one to three weeks. eCF506 was able to significantly reduce BLI after four days of treatment compared to vehicle-treated mice (see Figure 5.13b). Four of the six eCF506 treated mice showed significant regression of hind leg metastases (see Figure 5.13c), while the other two exhibited slower growth than control mice. Treatment was stopped after 28 days and the residual BLI in the hind legs of the surviving treated mice remained stable during the following five weeks. However, two mice developed metastasis in the thoracic cavity during this time and their treatment was resumed at day 63 to establish whether these tumours would still respond (see Figure 5.13d). The relapsed metastases of both mice differed vastly in size but both regressed during 7 days of re-treatment (see Figure 5.13), after which the experiment was ended.

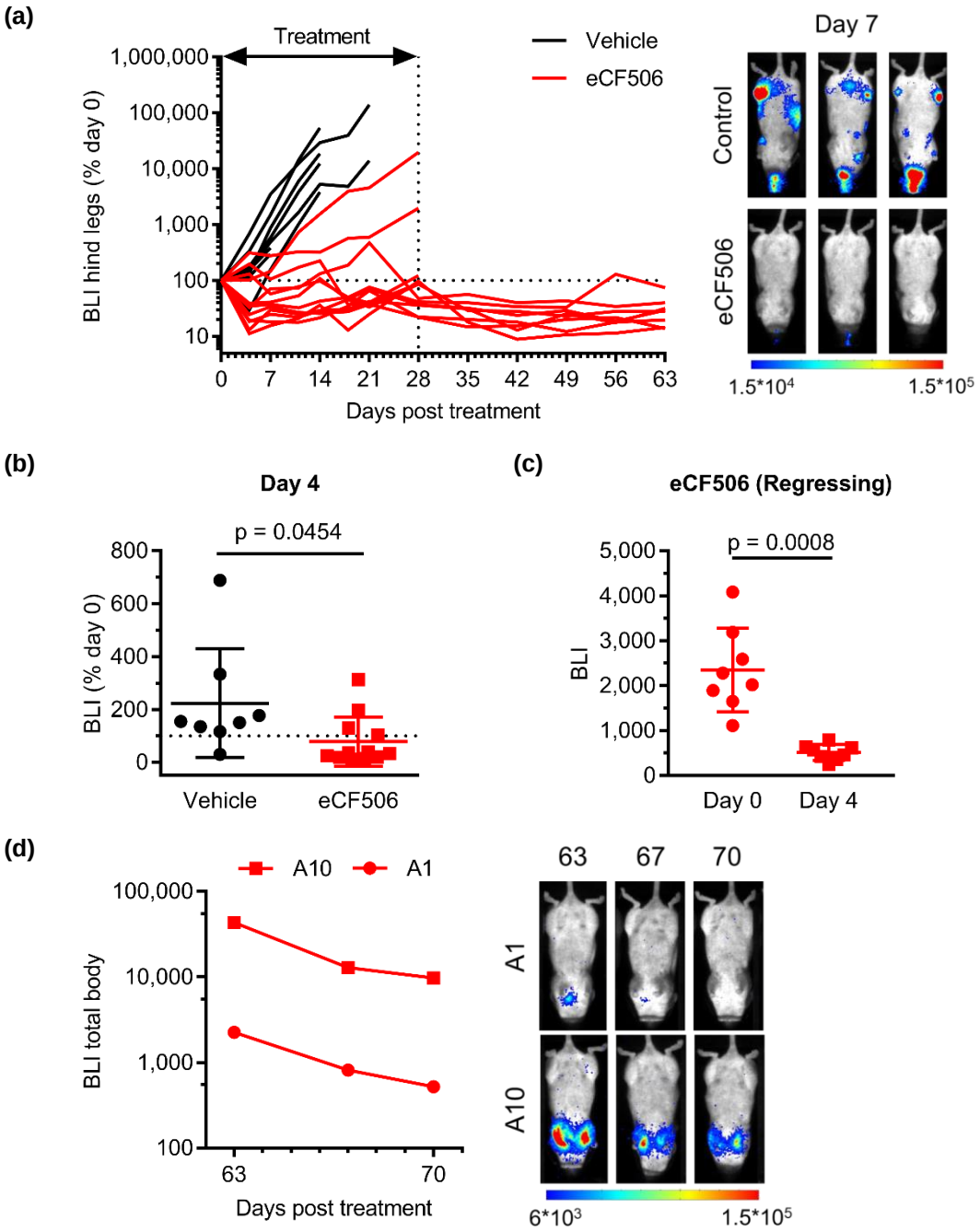

Figure 5.13. eCF506 in a syngeneic murine breast cancer bone metastasis model. (a) Left: % BLI in hind legs of vehicle- and eCF506-treated mice relative to day 0. Each hind limb is shown separately. Treatment was continued for 28 days and then stopped. Right: Representative images of mice 7 days after treatment start. (b) Comparison of % BLI between vehicle- and eCF506 treated mice 4 days post treatment. Each hind limb was quantified separately. Statistical analysis by unpaired t-test. (c) Comparison of absolute BLI signals of the four eCF506-treated mice that exhibited regression. Statistical analysis by paired t-test. (d) Left: Absolute BLI in total body of the two relapsed eCF506-treated mice. Treatment was re-started on day 64 for 7 days. Right: Images of both mice before, during and after re-treatment.

5.2.2.4. eCF506 triggers regression of MetBo2 mammary fat pad tumours but resistance develops during second round treatment

This work was done by Dr John Dawson and Morwenna Muir of the groups of Profs Valerie Brunton and Margaret Frame at the University of Edinburgh, UK.

The *in vivo* testing of eCF506 in a breast cancer bone metastasis model showed high potency of the compound (see previous chapter 5.2.2.3). However, it was unclear whether this was due to eCF506's effects on MetBo2 cancer cells or on the bone microenvironment. Several papers have shown that SRC kinase plays an important role in bone resorption by osteoclasts and this has been implicated in the formation of bone metastatic lesions (see chapter 1.2.3.5).

In order to determine the potency of eCF506 independent of the bone microenvironment, it was tested in a second *in vivo* model in which MetBo2 cells were injected into the mammary fat pad of immunocompetent (FVB) or nude (CD-1) mice. Tumours were allowed to grow for 8-9 days to 40-50 mm^3 prior to treatment with daily eCF506 (40 mg/kg) by oral gavage. Treatment was stopped after 28 days and tumours allowed to regrow to a bigger size, after which eCF506 treatment was re-started for another 28 days. Tumour measurements are plotted in Figure 5.14 and Figure 5.16.

The first experiment was done in immunocompetent mice and eCF506 was found to have potent anti-tumour effects (see Figure 5.14a). It was able to significantly inhibit the growth of MetBo2 mammary fat pad tumours compared to control as early as 4 days after start of treatment (see Figure 5.14b). After 11 days, eCF506-treated tumours had significantly regressed by an average of 50% compared to pre-treatment size and maintained this level throughout the initial treatment phase (see Figure 5.14c). One mouse in the treatment group, which had the smallest tumour at the start of treatment, was completely cleared and remained tumour free until the end of the study. Treatment was stopped after 28 days to see whether residual tumours would regrow, which they did after an initial lag phase of 1.5 weeks. Second round treatment was started once tumours had regrown to 0.3 cm^3, six-fold bigger than at the start of the previous round. After a 3-day lag phase, tumour size reduced drastically by an average of 35% in all four mice for 10 days, after which tumours started to grow again at a similar rate as seen in the control group. This shows that despite initial regression,

tumours appear to become resistant to eCF506 during round two treatment; nevertheless, eCF506 was able to significantly prolong survival without obvious side effects (see Figure 5.14d,e).

The strong anti-tumour response observed in FVB mice was surprising, as previous studies have found SRC inhibitors to only slow growth but not trigger regression in solid tumours [337,390,401,402]. One possible explanation could be the involvement of the immune system in clearing of treated MetBo2 tumours. Therefore, immunohistochemical analysis of the tumour samples was performed to assess cell proliferation and cytotoxic T-cell infiltration. Staining with Ki67 and CD8 antibodies was performed as described in methods 2.6.1.4. Both control and treated tumours exhibited large necrotic cores and proliferating patches around the edges (see Appendix A.16). A significant difference between both groups was seen with CD8 staining; only very few positive cells were found in the control mice, while high infiltration of CD8 positive cells was found in all five mice treated with eCF506, both in proliferating and non-proliferating areas of the tumour (see Figure 5.15). This could suggest that eCF506 induces infiltration of CD8 positive cytotoxic T-cells. However, control and treatment mice were sacrificed at different times of the experiment, with all control mice being culled within the first four weeks of treatment and treated mice up to 9 weeks later. Cytotoxic T-cell infiltration could therefore be related to time rather than treatment and a properly controlled experiment is needed in which mice are culled at the same time to be able to draw any definitive conclusions.

After the initial *in vivo* experiments in FVB mice saw strong tumour responses to eCF506 treatment, it was hypothesized that these could be in part due to the involvement of the immune system. Therefore, the experiment was repeated in immunocompromised CD1 mice (see Figure 5.16a). A very similar pattern of response was observed in these nude mice, with initial treatment significantly reducing tumour growth after 4 days compared to control and triggering regression (see Figure 5.16b,c). Tumour size was stable during the 28-day treatment phase, but regrowth occurred immediately after treatment stop, which was much quicker than in FVB mice. Re-treatment was started at a slightly smaller tumour size than in FVB (0.25 cm^3) and again triggered a strong reduction in size by 42% on average. This was followed by a quick relapse and regrowth after 10 days as seen before. Notably, tumour growth in CD1 mice seemed to slow down again somewhat toward the end of the study,

although some mice had to be culled as maximum tumour size was reached. Again, eCF506 treatment significantly prolonged survival and only some treatment-related side effects such as ruffled fur were observed (see Figure 5.16d,e).

The results of these two studies show that eCF506 is able to trigger and maintain tumour regression for at least four weeks in MetBo2 mammary fat pad models. While the similar response between FVB and CD1 nude mice initially suggests that the immune system was not involved, the longer delay until relapse that was seen only in FVB mice could suggest that an immune response might be activated during the initial treatment phase. Treatment of relapsed tumours still elicits regression in both models, although resistance mechanisms are activated quickly, and tumours regrow similarly fast as in the control groups. CD1 tumours may respond again later on in round two treatment and it is unclear whether FVB mouse tumours could also have been stabilised at a later point.

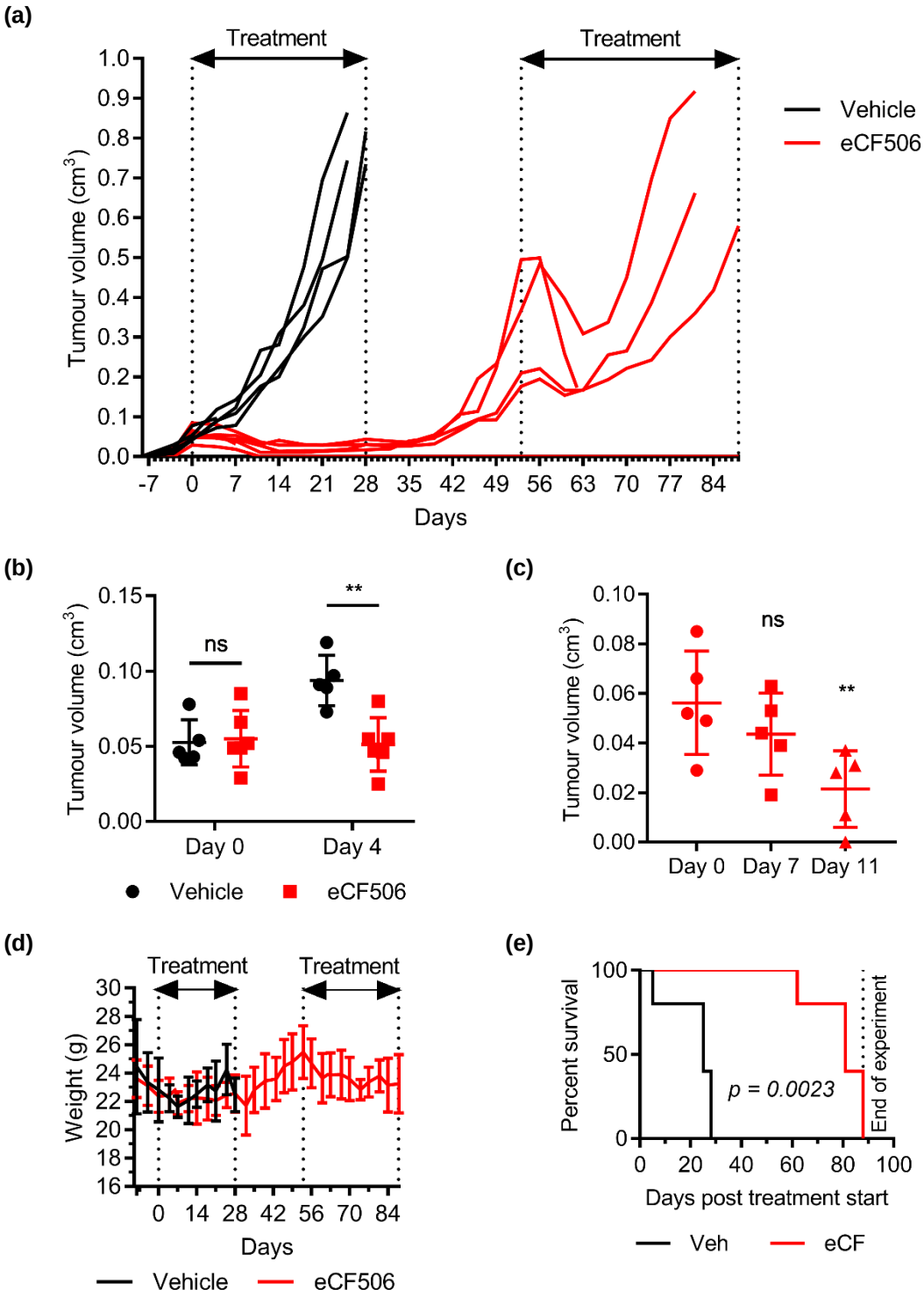

Figure 5.14. eCF506 in MetBo2 mammary fat pad tumours in immunocompetent FVB mice. (a) Tumour size of vehicle- and eCF506-treated mice. (b) Comparison of tumour size between groups at day 0 and day 4. Statistical analysis by two-way ANOVA with Sidak correction. (c) Comparison of tumour size in eCF506-treated mice between different days. Statistical analysis by repeated measures one-way ANOVA with Greenhouse-Geisser and Dunnett correction. (d) Weight of mice over the course of the study. $p>0.05$ (ns), $p<0.01$ (**). (d) Kaplan-Meyer survival plot showing deaths due to tumour size or sickness. Statistical analysis by log-rank (Mantel-Cox) test.

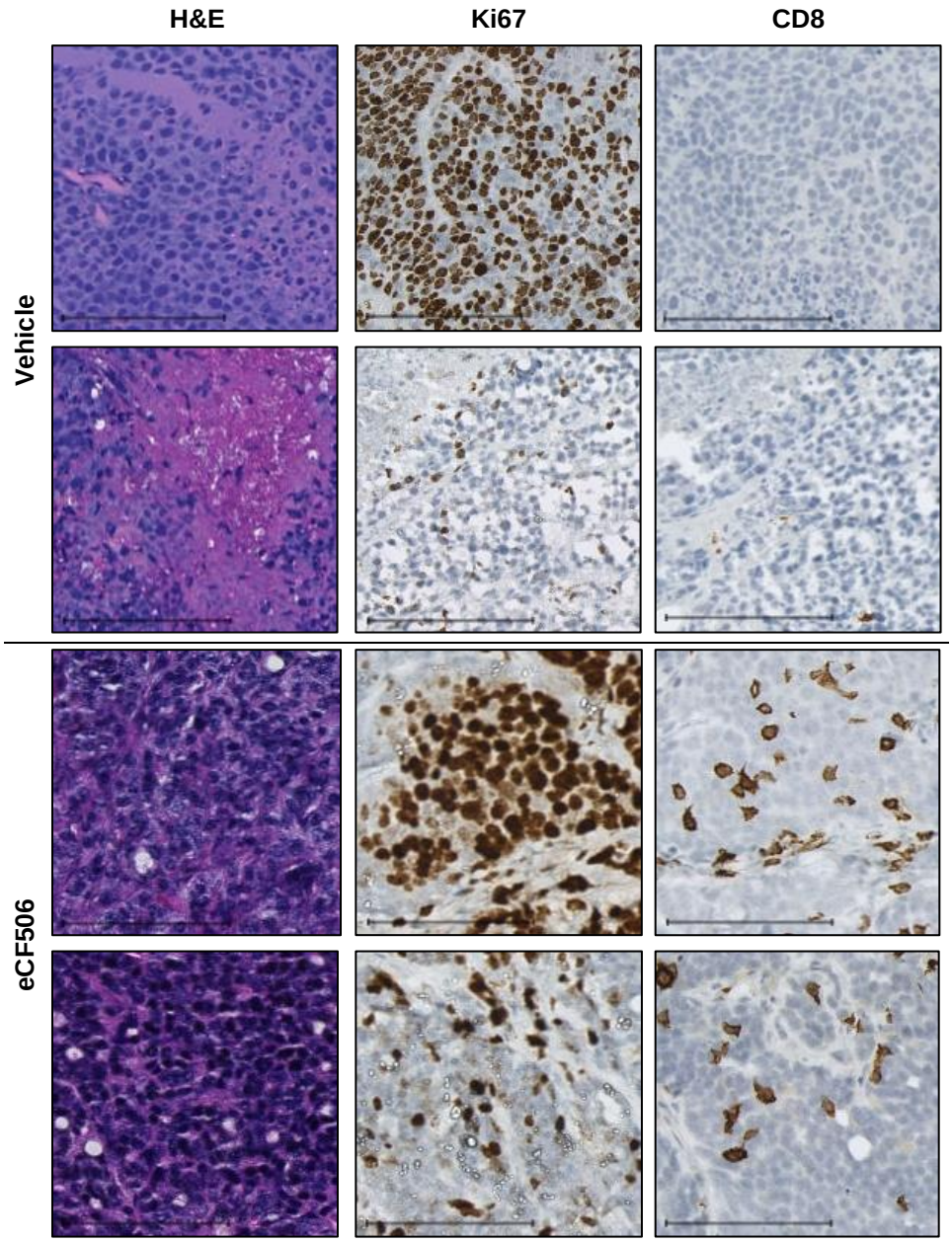

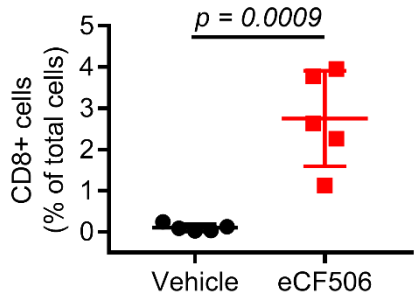

% CD8+ cells of total cells		
Mouse	Vehicle	Treated
1	0.021	2.634
2	0.122	2.262
3	0.090	1.127
4	0.242	3.775
5	0.032	3.957

Figure 5.15. Immunohistochemical analysis of MetBo2 mammary fat pad tumours in FVB mice. Images were quantified using QuPath and the percentage of CD8+ cells of total cell number was plotted with exact numbers shown in the table on the right. Statistical analysis by unpaired t-test. Scale bar represents 100 µm.

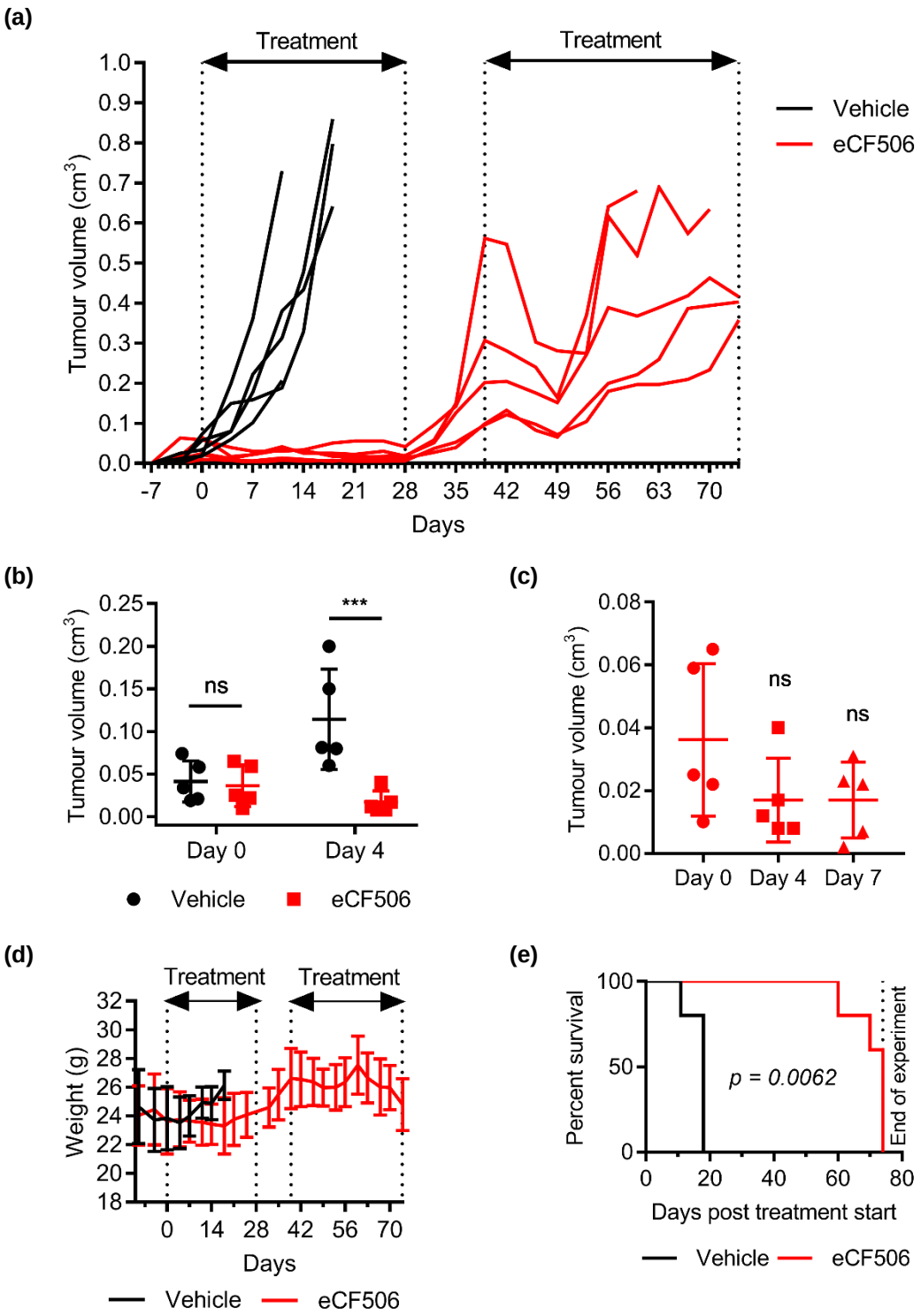

Figure 5.16. eCF506 in MetBo2 mammary fat pad tumours in immunodeficient CD1 nude mice. (a) Tumour size of vehicle- and eCF506-treated mice. (b) Comparison of tumour size between groups at day 0 and day 4. Statistical analysis by two-way ANOVA with Sidak correction. (c) Comparison of tumour size in eCF506-treated mice between different days. Statistical analysis by repeated measures one-way ANOVA with Greenhouse-Geisser and Dunnett correction. (d) Weight of mice over the course of the study. $p>0.05$ (ns), $p<0.001$ (***). (d) Kaplan-Meyer survival plot showing deaths due to tumour size or sickness. Statistical analysis by log-rank (Mantel-Cox) test.

5.3. Discussion

5.3.1. eCF506's pharmacokinetic and safety profile differs from dasatinib in rat models

The assessment of eCF506's pharmacokinetic properties shows that it has a favourable PK profile in mice but appears to be metabolised faster than dasatinib in rats. At the same dose of 10 mg/kg by oral gavage, eCF506 had a 15-fold lower maximum concentration and 23-fold lower AUC (concentration per hour) in comparison to previously reported values for dasatinib in Sprague-Dawley rats (see Table 5.3). Stability of eCF506 in rat plasma remains near 100% over 2 hours according to a previous study but it has not yet been tested in rat hepatocytes; future tests could confirm whether the PK results are due to a faster first-pass metabolism for eCF506 than dasatinib in rats [1]. eCF506's half-life in rats was also less than a sixth of that reported for dasatinib when administered directly into the circulation (0.5 hours and 3.3-6.7 hours, respectively), although this could have been affected by the very low dose used and the high volume of distribution of eCF506 in this species. In contrast, previous testing revealed similar C_{max} and AUC values in mice and a three-fold increased half-life for eCF506 compared to dasatinib in this species (see Table 5.3) [1]. One conclusion that can be drawn from the observed variability in exposure is that anti-tumour effects of eCF506 and dasatinib should only be compared to each other at the same dose in mouse but not rat models. Further, 10 mg/kg of eCF506 daily by oral gavage is unlikely to achieve significant levels of SRC inhibition in rats, so much higher doses should be used in any potential efficacy studies in this species. Overall, the differences between mice and rats, two closely related species, highlight the need for further pharmacokinetic testing of eCF506 in other non-rodent species, such as dogs, in order to be able to predict a safe but efficacious starting dose for first use in humans. Testing eCF506 in *in vitro* hepatocyte stability assays using cells from different species prior to the next *in vivo* PK study can help in choosing an appropriate species with similar first-pass metabolism as humans.

The comparatively poor performance of low dose eCF506 in the rat pharmacokinetic study led to the re-testing of the compound at the starting dose used in the acute toxicity study to determine whether adequate exposure had been achieved. At 200 mg/kg, eCF506 exhibited more than 45% bioavailability in rats and achieved sustained high plasma concentrations throughout the 24-hour study period (>95 nM)

that are likely sufficient for strong SRC inhibition based on *in vitro* findings. These values indicate adequate exposure of eCF506 is obtained in rats at higher doses (>200 mg/kg), providing confidence in the toxicology results from chapter 5.1.1.2. It is important to note that the plasma concentration of eCF506 was still increasing at the end of the high dose PK study, which makes it likely that repeat dosing of daily 200 mg/kg could lead to an accumulation of the compound (as suggested by its large volume of distribution) and possible toxicities over time; this should be considered when planning repeat dose toxicity studies.

Based on the results of the pharmacokinetic studies, the big gap between the MTD in single dose toxicity studies of eCF506 and dasatinib in Sprague-Dawley rats (700 mg/kg and 30 mg/kg, respectively) is likely due to their exposure differences in this species. Even though 200 mg/kg eCF506 was able to achieve concentrations of over 95 nM and up to 806 nM for 24 hours, dasatinib was able to achieve comparable concentrations between 100 to 500 nM over at least 10 hours at a twentieth of the dose [391]. This suggests that dasatinib's lower MTD is at least in part related to much higher exposure and cannot be directly attributed to higher toxicity of the compound. Similar observations were made for the comparative exposure and safety of dasatinib and bosutinib in male rats, with the latter having a higher MTD of 700 mg/kg but also lower exposure (see Table 5.3) [387]. It would be necessary to determine the therapeutic window of both eCF506 and dasatinib in order to state with confidence which drug is safer. However, due to already observed species-dependent differences, it is not until eCF506 has undergone pharmacokinetic and pharmacodynamic assessment in humans that definite and useful comparisons can be drawn to the safety profile of dasatinib.

One aspect that was not taken into account in the pharmacokinetic studies is the potential activity of drug metabolites. eCF506 was found to be 30% metabolised by human hepatocytes after 2 hours and the main metabolite, an N-demethylated derivative representing two thirds of all metabolites, could retain activity against SRC kinase based on previous structure-activity studies (see chapter 5.1.2.2). This is currently being investigated further by synthesising the N-demethylated derivative of eCF506 and testing it *in vitro* in comparison to eCF506. The results of this study will indicate whether treatment with eCF506 might produce greater results than expected based on non-metabolised eCF506 levels measured in the PK studies.

A previous study found several metabolites of dasatinib with pharmacological activity in humans (called M4, M5, M6, M20, M24 in publications) [395,403]. The metabolite M4, result of a N-dealkylation of the hydroxyethyl moiety, had equipotency to dasatinib against SRC and ABL in cellular studies, with the other four exhibiting at least 10-fold less activity [403]. However, only low levels of these active metabolites were found in a hepatocyte study and human plasma levels in a clinical trial, with M4 making up less than 5% of dasatinib's AUC, which suggests they do not contribute significantly towards *in vivo* anti-tumour effects [395,403].
It is important to add that even if eCF506's main metabolite retains activity against SRC kinase *in vitro*, it has to be determined first whether it is present at relevant levels in the blood instead of being excreted or metabolised further, in order to determine its potential contribution towards eCF506's *in vivo* efficacy.

5.3.2. eCF506 can inhibit SRC activity in the brain, retina and subcutaneous tumours in mouse models

Fraser *et al.* have previously shown that 50 mg/kg oral eCF506 can achieve *in vivo* phospho-SRC Y416 inhibition in a mouse colorectal cancer xenograft model [1]. Further studies by collaborators (*data not shown*) found that eCF506 achieved similarly potent levels of SRC inhibition in an orthotopic murine breast cancer model when given orally (50 mg/kg) or intraperitoneally (10 or 20 mg/kg). These findings guided the dosing levels used in later efficacy studies; based on an oral bioavailability of 25% in mice and good target inhibition at 10 mg/kg via IP, 40 mg/kg given once daily by oral gavage was chosen as a suitable dosing regimen for mouse *in vivo* studies (see chapter 5.3.4). Nevertheless, a comprehensive dose range study is still outstanding to determine the optimal dose level and schedule for sustained SRC inhibition.

As SRC kinase plays a role in a specific type of brain cancer as well as diseases other than cancer, eCF506's ability to reach organs and tissue sites needs to be evaluated alongside its potency in those settings. Two mouse studies have been performed to assess eCF506's ability to cross the blood brain barrier and its anti-SRC activity in the retina of the eye (chapter 5.1.3.1 and 5.1.3.2). Both have found positive results, with eCF506 reaching the brain compartment at efficacious concentrations (≥500 nM)

sustained for at least 8 hours and potent inhibition of VEGF-induced SRC activation in mouse retinas.

Dasatinib has previously been evaluated for its ability to penetrate the blood brain barrier in SCID mice with intracranial CML tumours [396]. Daily doses of oral dasatinib (50 mg/kg) achieved brain concentrations of >10 nM over 24 hours in this model, but peak concentration was more than 7-fold lower than for eCF506 at 40 mg/kg via IP administration (763 nM for eCF506 and <100 nM for dasatinib); it is important to note the difference in administration route between both studies, with the oral administration of dasatinib and its low bioavailability resulting in an overall lower exposure. Nevertheless, the brain:plasma ratio of dasatinib ranged between 0.032 to 0.086 over 24 hours, much lower than the 0.12 to 0.43 of eCF506 over an 8-hour period. This discrepancy may be explained by the active removal of dasatinib from the brain, as several papers have found it to be a substrate for the multidrug efflux pumps P-glycoprotein (Pgp) and breast cancer resistance protein (BCRP) [404,405]. These are expressed at the blood-brain barrier or in tumour cells to reduce exposure to harmful substances. Dasatinib is able to reach a brain:plasma ratio of 0.93 in a mouse Pgp and BCRP knockout model, 7-fold higher than in wild-type mice [404]. Another study found a similar brain:plasma ratio for knockout mice and wild-type mice treated with the dual Pgp and BCRP inhibitor elacridar [405]. This suggests that dasatinib's brain penetration is limited by the activity of these two drug efflux pumps at the blood brain barrier. It is unclear whether eCF506 is also a Pgp substrate, as its higher brain:plasma ratio may have been achieved by saturation of the Pgp pumps due to its higher plasma concentration. Further studies are required to compare the brain exposure of eCF506 and dasatinib and to test whether eCF506 is a Pgp substrate, which is of importance for any potential use of eCF506 in CNS diseases. Nonetheless, the PK results obtained so far support eCF506's potential application in SFK-related diseases of the central nervous system and retina, such as type 4 medulloblastoma, Alzheimer's disease and diabetic retinopathy.

5.3.3. eCF506 and dasatinib have pro- and anti-tumour effects on MetBo2 cytokine secretion

An *in vitro* cytokine array showed that eCF506 and dasatinib have beneficial effects on the cytokine secretion profile of MetBo2 cells by triggering a strong upregulation of

IL-1 receptor antagonist (IL-1RA) and IGFBP5 secretion and a marked reduction of VEGF (see chapter 5.3.3).

IL-1RA is a natural antagonist of IL-1α and IL-1β signalling. Its recombinant form (anakinra) is used clinically to treat rheumatoid arthritis and has been investigated in several clinical trials of different cancers with some promising results [406]. IL-1β presence in the primary tumour was found to be a predictive biomarker for patients with stage II/III breast cancer that were at increased risk of disease recurrence and bone metastasis and it was found to drive breast cancer progression and bone metastasis in a mouse model [407,408]. Treatment of the mice with anakinra lead to a reduction in bone metastases by more than 50% as well as a reduction in subcutaneous tumour growth, with even higher efficacy when given preventatively [408]. This suggests that the increased secretion of IL-1RA in response to eCF506 and dasatinib treatment could at least in part be responsible for the strong anti-tumour effects seen in the MetBo2 bone metastasis and mammary fat pad studies.

Levels of secreted IGFBP-5 were also increased by both SRC inhibitors in MetBo2 cells. This factor has previously been associated with decreased cell migration of the MCF-7 cell line, tumour suppressor functions in human melanoma cells and inhibition of angiogenesis in an *ex vivo* assay [409–411]. Increased IGFBP5 secretion could therefore also contribute to eCF506 and dasatinib's anti-tumour effects.

Lastly, eCF506 potently inhibited the secretion of VEGF by MetBo2 cells *in vitro*, which is a key driver of angiogenesis in cancer (see chapter 1.2.3.4). VEGF can also prevent T-lymphocyte infiltration by inhibiting their ability to adhere to endothelial cells, a necessary step for extravasation and tumour infiltration [412]. SRC inhibition has previously been found to inhibit angiogenesis and this has been confirmed for eCF506 in *in vitro* and *ex vivo* models (see chapter 3.1.5). The finding that eCF506 and dasatinib can also reduce the secretion of pro-angiogenic VEGF by tumour cells could thus potentiate their anti-angiogenic properties in cancer and enable increased T-lymphocyte infiltration. High CD8+ T-cell infiltration was indeed observed in eCF506-treated MetBo2 mammary fat pad tumours in FVB mice and it is possible this could be related to eCF506's effects on MetBo2 cytokine signalling (see Figure 5.15); however, a better controlled study needs to confirm that this infiltration is indeed induced by eCF506 and not a time-dependent phenomenon associated with tumour progression.

Several other changes in cytokine secretion were observed in treated MetBo2 cells whose potential consequences are less clear or maybe counterproductive. The strong reduction of secreted CXCL2 in the cytokine array by over 75% by both eCF506 and dasatinib would likely have beneficial anti-cancer effects *in vivo*. Secretion of CXCL1/2 was found to increase metastatic potential and chemoresistance in breast cancer and an inhibitor of the primary CXCL1/2 receptor CXCR2 sensitised two metastatic mouse models to chemotherapy [413]. CXCL1/2 was also found to promote the expansion of myeloid-derived suppressor cells in tumours which hinder immunosurveillance [414]. However, CXCL1 secretion was upregulated 2- to 4-fold in response to treatment in the cytokine array, meaning it could compensate for at least some of the CXCL2 reduction, which makes the potential impact of changes in CXCL1/2 secretion less clear.

The moderate reduction of TNF-α secretion could either limit or promote tumour progression, as it was found to have context-dependent pro- and anti-tumour effects [415]. IL-6 secretion was decreased by low concentrations of both inhibitors but increased more than 12-fold by high doses of dasatinib; the roles of this cytokine in cancer are similarly complex, as IL-6 secreted by stromal cells or tumours promotes cell proliferation but also enables cytotoxic T-cell trafficking to the tumour [416]. The reduction of MMP-3 secretion with eCF506 likely reduces the malignancy of MetBo2 cells, as transgenic mice with activated MMP-3 develop invasive mammary tumours [417,418]. MMP-3 can also activate pro-MMP-9, which in turn increases tumour cell invasion and angiogenesis by releasing VEGF and promoting extracellular matrix degradation [419,420]. However, the increased secretion of osteopontin in response to eCF506 and dasatinib treatment (2- and 4-fold, respectively) is likely having counterproductive effects, as this chemokine-like factor is implicated in cell proliferation, metastasis, angiogenesis and drug resistance pathways with a special role in the bone microenvironment [421]. Moreover, CCL5 was increased by both compounds and has been linked to regulatory T-cell enrichment, which reduces anti-tumour immunity [422,423].

Overall, although the results from this study need to be taken with caution, the effects of eCF506 on IL-1RA and VEGF secretion could potentially contribute to its potent effects observed in the MetBo2 mouse models. Nevertheless, several cytokine changes in response to eCF506 or dasatinib treatment could indeed promote tumour growth and invasion. Future studies should investigate whether the same cytokine

patterns can be observed *in vivo*, in other cell lines and in other cancer models to conclude whether these are MetBo2-specific observations or general effects of SRC inhibitor treatment.

A recent study found that combining anti-IL-1β and anti-PD-1 antibodies in 4T1 mammary carcinoma in mice gave synergistic results by doubling CD8+ T-cell infiltration and almost completely abrogating tumour growth compared to monotherapy [424]. This provides an interesting rationale for testing the combination of eCF506 with PD-1 inhibitors in a MetBo2 mouse model, provided that the increased secretion of IL-1RA also occurs *in vivo*. Furthermore, inhibition of the SRC downstream target FAK is currently being tested in combination with anti-PD-1 and gemcitabine in a Phase 1/2 clinical trial of patients with advanced pancreatic cancer, based on synergistic results in mouse models [425,426]. Due to the close link between SRC and FAK activity, it is possible that eCF506 might produce a similar effect; however, unlike FAK, SFK inhibition might prevent T-cell activation due to the role of LCK in the TCR (discussed further in the following chapter), which would abolish the effect of PD-1 inhibition [104,427]. Comparing the effects of FAK and SRC inhibition in combination with anti-PD-1 in the pancreatic mouse model would be an interesting experiment to determine the impact of eCF506 on the anti-tumour immune response.

5.3.4. eCF506 is a potent inhibitor of tumour growth in some *in vivo* models

The efficacy of eCF506 *in vivo* has been assessed for the first time in different breast cancer models in mice with varying success; no potent anti-tumour activity was observed in a MDA-MB-231 xenograft model with either eCF506 or dasatinib (see chapter 5.2.1), while sustained tumour regression was seen with eCF506 in a bone metastasis and orthotopic murine breast cancer model (see chapter 5.2.2.3 and 5.2.2.4).

The results of the first *in vivo* study with eCF506 in an MDA-MB-231 xenograft were disappointing based on the high *in vitro* activity found in 2D culture. eCF506 had no impact on tumour growth whatsoever and dasatinib only inhibited it slightly toward the end of the study (see Figure 5.8). Since dasatinib has been studied extensively in MDA-MB-231 cells on its own or in combination with other anti-cancer agents, these

findings were surprising [172,308,428–430]. However, a search in the literature revealed only one published study in which dasatinib was tested in an *in vivo* model of this cell line, as the majority of papers only reports *in vitro* experiments [430]. In this study, 10 mg/kg dasatinib was given to nude mice every other day by oral gavage for a total of eight administrations, starting one week after inoculation with MDA-MB-231 cells (one million cells injected with Matrigel). Tumours were allowed to growth for four weeks after the end of treatment and significant differences in tumour size were first found 5 weeks after inoculation, with dasatinib reducing size by around 50% compared to control. While the study conducted in chapter 5.2.1 differs from the one done by Qian *et al.* in several ways (later treatment start, 2.5-fold higher dose, doubled dosing frequency, longer treatment period), stronger effects with dasatinib than those observed would still have been expected within the 25-day treatment period [430]. It is possible that the additional time prior to treatment start could have allowed tumours to be more established, compacted and treatment resistant due to either poor drug penetration and/or reduced dependency upon SRC for growth and survival in a complete 3D environment. This hypothesis is based on results from chapter 3.1.4, in which both eCF506 and dasatinib were much less potent against MDA-MB-231 spheroids than in 2D cell viability assays. Nonetheless, tumour sizes appeared to decrease after three weeks of treatment in the MDA-MB-231 mouse study (see Figure 5.8) and a longer observation period post-treatment as used by Qian *et al.* is needed to determine whether this trend is treatment-related, as some tumours in the control group also shrunk [430].

In contrast to the MDA-MB-231 xenograft, eCF506 caused tumour regression and even complete response in mouse studies with the bone-metastatic murine breast cancer cell line MetBo2. This cell line has been created and characterised by the group of Dr Bin-Zhi Qian and was found to be highly resistant to standard chemotherapy (*unpublished data*). Three *in vivo* experiments with MetBo2 have so far been completed: one in a bone metastasis model in immunocompetent mice and two in mammary fat pad primary tumours in immunocompetent and immunodeficient mice. eCF506 was able to reduce MetBo2 tumour size in nearly all mice (except for two in the bone metastasis model) and smaller size was maintained throughout the four weeks of initial treatment. Future studies with an open-ended initial treatment period are needed to determine whether eCF506 can control tumour size long-term.

While one mouse was cured in the mammary fat pad study, and two in the bone metastasis one maintained negligible BLI signal, the majority relapsed after treatment was stopped and exhibited re-growth of the original tumour (mammary fat pad experiment) or metastases in other sites of the body (bone metastasis experiment). Relapse can occur due to the survival of cancer stem cells and the results of an *in vitro* mammosphere assay suggest eCF506 can reduce stem cell activity but was unable to fully inhibit self-renewal at the concentration tested (chapter 5.2.2.1).
During the second round of treatment, all mice initially responded with a reduction in tumour size. However, in mammary fat pad tumours resistance emerged after around 10 days and tumours regrew at a similar rate to untreated controls in both mouse strains. Further investigation is currently under way using NanoString and Reverse Phase Protein Array methods to profile the pathways that are involved in this resistance mechanism. By mapping compensatory signalling pathways to drug target databases, the results could point toward rational drug combinations which increase the duration of response following eCF506 treatment.

A comparison of eCF506 in immunocompetent and immunocompromised mice showed similar efficacy in both models, which suggests that eCF506's anti-tumour activity is largely independent of the immune system. Therefore, the infiltration of CD8+ cells in eCF506-treated tumours of FVB mice does not appear to have contributed to tumour regression, as a similar reduction in size was found in CD1 nude mice, which lack a thymus and are thus unable to produce mature, differentiated T-cells [431]. CD8 is a marker for cytotoxic T lymphocytes which play important roles in immunosurveillance; their presence in the tumour microenvironment often correlates with better prognosis in breast and other cancers [432,433]. CD4+ and CD8+ T-cells are activated by binding of the T-cell receptor (TCR) to the antigen-presenting major histocompatibility complex (MHC) on antigen-presenting cells. This is the first in a multi-step process causing naïve CD8+ T-cells to become cytotoxic T-cells that can kill virus-infected or tumour cells by releasing cytotoxic granules or inducing apoptosis. One important protein downstream of the TCR is LCK kinase, a SRC kinase family member which is also potently inhibited by eCF506 and dasatinib (see chapter 1.2.3.6 and Table 3.4). Multiple studies have found that LCK inhibition by dasatinib inhibits TCR function and thus prevents CD8+ T-cell activation and effector functions *in vitro* and *in vivo* [434–438]. Increased cytotoxic T-cell mobilisation is observed in CML patients taking dasatinib and two *in vivo* studies found increased tumour

infiltration of CD8+ T-cells with dasatinib treatment, although one showed that these had a higher expression of PD-1, a marker of T-cell exhaustion [401,439,440]. It has recently been suggested to use dasatinib as a pharmacologic switch for chimeric antigen receptor T-cells (CAR-T) to temporarily reduce acute toxicity due to excessive activity [427]. Taken together, these findings suggest that eCF506 potentially induces T-cell infiltration into MetBo2 mammary fat pad tumours but simultaneously inhibits their activation and anti-tumour effects. This potential inactivation of the immunosurveillance could explain the similarity between the results seen in FVB and nude mice. Nevertheless, it is important to note that relapse in FVB mice after initial treatment only occurred after a lag phase of over one week, while the same tumours regrew immediately in CD1 nude mice. This does indicate that the presence of functional T lymphocytes might have some beneficial effect in this model during the initial treatment phase. Further studies are being considered to investigate the effect of eCF506 on T-cell infiltration and activation in this model and to compare it to dasatinib's effects *in vivo*.

Chapter 6. Final Discussion & Conclusion

The non-receptor tyrosine kinase SRC has repeatedly been associated with the progression of different cancers and the pathology of other diseases, such as Alzheimer's. Attempts to repurpose existing dual SRC/ABL inhibitors have so far been unsuccessful in gaining regulatory approval for their SRC inhibition alone. The recent discovery of the SRC/non-ABL inhibitor eCF506 offers the first opportunity to selectively inhibit SRC but not ABL kinase, which has the potential to improve upon the efficacy and safety profile of existing inhibitors. This thesis presents the continued preclinical investigation eCF506 in comparison to other SRC/ABL inhibitors in different models of cancer, which was carried out in collaboration with several partners from industry and academia.

The results of several *in vitro* experiments confirm that eCF506 is a potent inhibitor of SRC kinase activity with similar potency as the current best-in-class SRC/ABL inhibitor dasatinib. Both compounds were superior at inhibiting SRC signalling and 2D cell proliferation compared to the SRC/ABL inhibitors bosutinib and saracatinib. These results correlate directly with the relative potencies in cell-free kinase assays, where eCF506 and dasatinib showed the highest potency against SFKs. Kinome-wide profiling confirmed the overall selectivity of eCF506 for SFKs, with SRC identified as its main target and only one non-family member included in its top 10; dasatinib and bosutinib on the other hand exhibited relatively high promiscuity, as neither had SRC as one of their top 15 targets.

The attempts to confirm eCF506's selectivity over ABL in a cellular assay lead to the serendipitous discovery that eCF506 and dasatinib had opposite effects on the thermal stability of SRC kinase. Further investigation revealed that eCF506 has a distinct binding mode from dasatinib and bosutinib, as it stabilises SRC in its natural autoinhibited state, while the other two force it into an open conformation. As a result, dasatinib and bosutinib support the interaction between SRC and FAK, whereas eCF506 appears to prevent it. eCF506 can therefore inhibit both SRC's kinase and scaffolding activities. Saracatinib appears to bind SRC in a similar way as eCF506 based on its X-ray crystallography data, however its effects on the phosphorylation of SRC Y527 and FAK Y397 and the binding of SRC to FAK appear to be more similar to dasatinib and bosutinib. It is possible that the binding of saracatinib does not force SRC into a specific conformation, as eCF506 and dasatinib/bosutinib appear to do, and that the SRC-saracatinib complex can switch between open and closed conformations, with the latter potentially being favoured in crystallography.

While the differences in the SRC binding mode of eCF506 compared to the other inhibitors are interesting, it is not yet clear whether this has any wider implications on cellular signalling. Subcellular fractionations showed that dasatinib induces nuclear translocation of the SRC-FAK complex, however it is unclear whether this is due to the actions on SRC or overall increased cellular stress. Since both eCF506 and dasatinib gave very similar results when assessed by RPPA and in a cytokine secretion assay in different cell lines, it appears that the inhibition of SRC kinase activity may overshadow any scaffolding roles of the protein.

The last chapter of this thesis focuses on the assessment of eCF506 for its PK, toxicity and efficacy properties *in vivo*. The results of a first single dose toxicity study in rats revealed a high MTD (700 mg/kg); however, assessment of PK parameters in this species showed that eCF506 does not achieve the same high levels of exposure previously found in mice. The significantly better PK properties of dasatinib in rats are likely the reason it exhibits a much lower MTD than eCF506, which prevents a direct comparison of the toxicity of the two compounds in this species. It is possible that eCF506's main metabolite that was identified in a human hepatocyte stability assay retains potency; its activity and presence in rats need to be assessed, which will inform whether future PK studies should measure both compounds to accurately determine exposure. Nevertheless, additional PK experiments in mice confirmed eCF506's favourable properties in this species, as the compound was able to reach the brain and retina at relevant concentrations.

Efficacy studies with eCF506 in different *in vivo* models of breast cancer revealed cell line-specific differences, with no effect observed in a human xenograft model (MDA-MB-231), whereas tumours regressed and even disappeared in some cases in models of a murine bone metastatic breast cancer cell line (MetBo2). Interestingly, MetBo2 cells showed similar sensitivity to eCF506 as MDA-MB-231 cells in a 2D cell proliferation assay but much higher sensitivity in a 3D spheroid assay. This suggests that 3D assays might be the main predictor of *in vivo* response to eCF506, as the reduction in MetBo2 tumour size *in vivo* correlates with the reduction in spheroid size at low eCF506 concentrations *in vitro*. Nonetheless, a bigger comparative study is needed to confirm the predictive value of this 3D spheroid assay for eCF506's *in vivo* efficacy.

The potent *in vivo* effects of eCF506 led to the suggestion that the immune system may contribute to tumour clearance. However, a comparison of eCF506 in

immunocompetent and immunodeficient mice showed little differences, the most notable one being a longer delay until relapse in the immunocompetent mice. The infiltration of eCF506 treated tumours with CD8+ T-cells could be linked to treatment or be a time-dependent phenomenon and a properly controlled study is needed to distinguish between the two. However, the role of LCK in the activation of T-cells and the recent finding that dasatinib could be used as an on/off switch for CAR-T therapy suggests that SFK inhibition might indeed hinder tumour clearance by the immune system. Additional studies which assess both T-cell infiltration and activity can determine what impact, if any, eCF506 has on the immune system and might shed light on whether the delayed relapse in FVB mice is linked to the immune system.

Future studies

The preclinical investigation of eCF506 in cancer for this thesis explored its potency and selectivity *in vitro*, identified distinct molecular properties and provides a starting point for further *in vivo* experiments assessing efficacy, pharmacokinetics and side effects. Many follow-up and potential new experiments have been mentioned throughout the chapters, which would continue the characterisation of eCF506 as a novel selective SRC/non-ABL inhibitor. The challenge of future investigations will be to define a clear goal for the assessment of eCF506. While it would be interesting from a molecular perspective to follow up on the potential impact of the stable SRC-FAK interaction and nuclear translocation induced by dasatinib but not eCF506, the relevance of these observations for treatment outcomes is unclear. It is likely that the different selectivity profiles of SRC inhibitors lead to greater differences in cell signalling than differential conformations of kinase-inhibited SRC.

Greater focus should instead be placed on identifying relevant disease settings in which eCF506 shows efficacy and for which it could enter clinical development. The recent discovery that elevated SRC-ErbB4 signalling is the distinguishing feature of type 4 medulloblastoma provides a clear rationale to assess eCF506 in models of this disease. Notably, the kinome screen data shows that ErbB4 is also potently inhibited by eCF506 as well as dasatinib and bosutinib. Furthermore, the findings of this thesis warrant continued investigation into the potency of eCF506 in *ARID1A* mutant ovarian CCC, which should involve the testing of cell lines in a 3D spheroid assay prior to assessing sensitivity in *in vivo* models. Additional testing of primary patient-derived

CCC cells for sensitivity to eCF506 based on *ARID1A* status would be an important experiment in determining the clinical relevance of stratifying patients based on this marker. Lastly, an in-depth characterisation of the murine MetBo2 cell line could lead to potential new biomarkers for eCF506 sensitivity, which could then be screened for in human cancers.

In addition to the efficacy studies, further PK and toxicity studies with eCF506 are necessary to gain approval for clinical testing. The PK parameters need to be assessed in a second non-rodent species and the activity of its main metabolite needs to be tested. Prior screening of eCF506 stability in primary hepatocytes from different species might explain the different PK results seen in rats and mice and could help with the selection of a non-rodent species. The next steps for toxicity testing involve repeat-dose experiments and the confirmation of the safety of eCF506 in other species.

All of the PK, toxicology and *in vivo* efficacy experiments will require large quantities of pure eCF506, which exceeds the capacity of in-house synthesis. Therefore, the synthesis of a large batch of eCF506 has recently been outsourced with the support of the Institute of Genetics and Molecular Medicine. This will allow the continued preclinical development of eCF506 at the institute and in collaboration with partners in academia and industry.

Appendix

Appendix A.1. Dose-response curves of human breast and ovarian cancer (chapter 3.1.1.2) and chronic myeloid leukaemia (chapter 3.2.2) cell lines. 16 breast cancer, 13 ovarian cancer and 3 chronic myeloid leukaemia cell lines were treated with different SRC/ABL kinase inhibitors for 5 days. Effects on cell proliferation were measured using PrestoBlue™ reagent and curves were fitted using GraphPad Prism 7. Cell viability on the day of treatment was subtracted from final readings and results were normalised to DMSO treated control. All dose-response curves represent the average of three biological repeats with standard deviation.

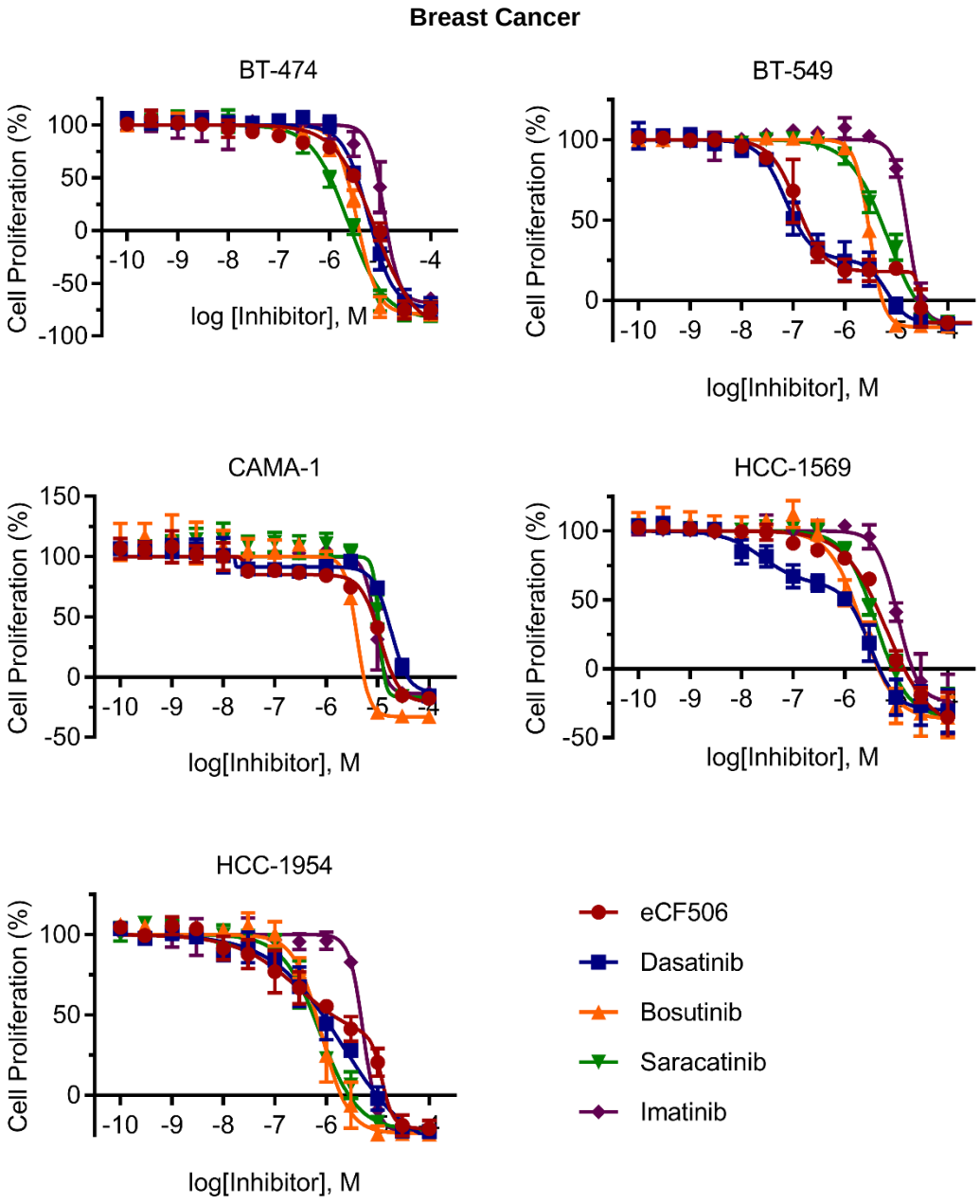

Figure continued on next page

Figure continued from previous page

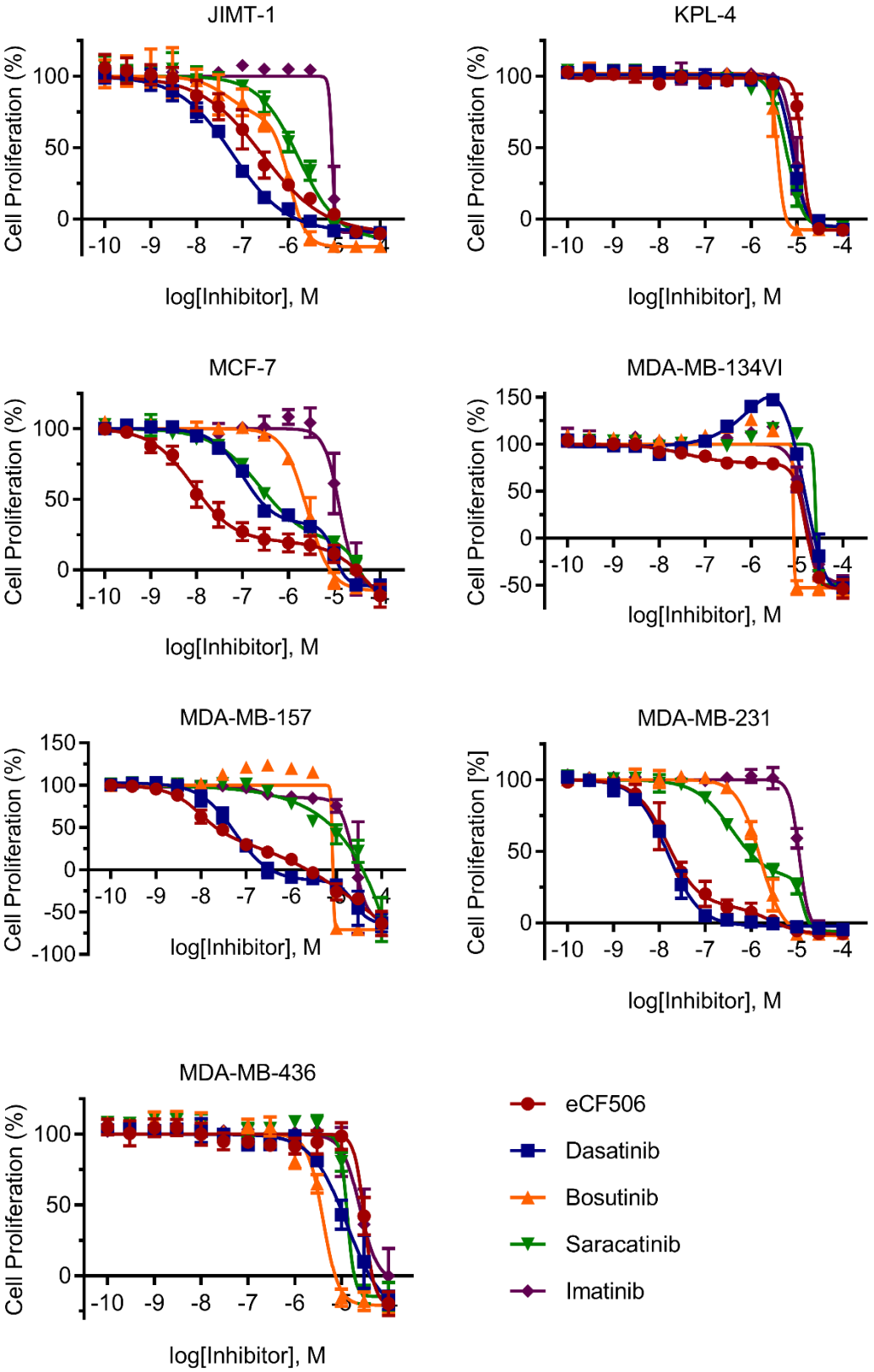

Figure continued on next page

Figure continued from previous page

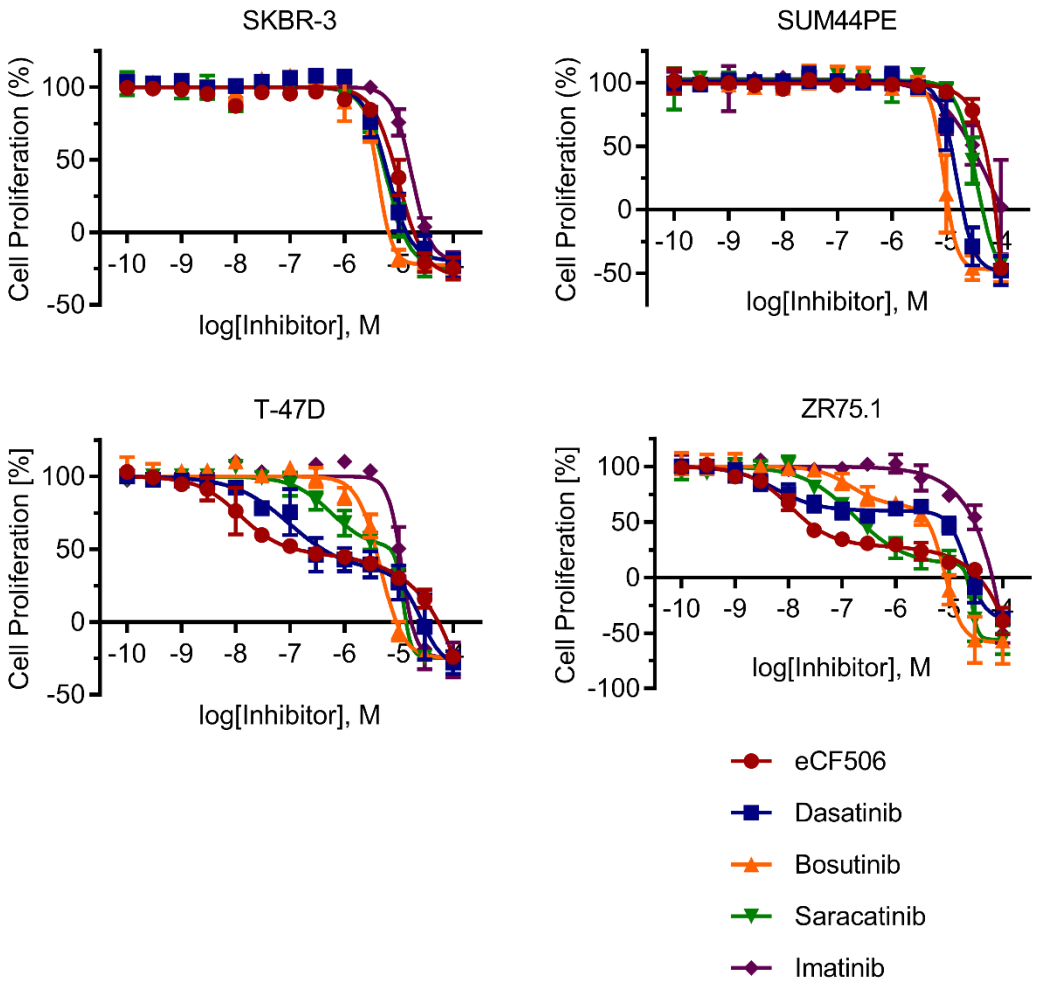

Ovarian Cancer

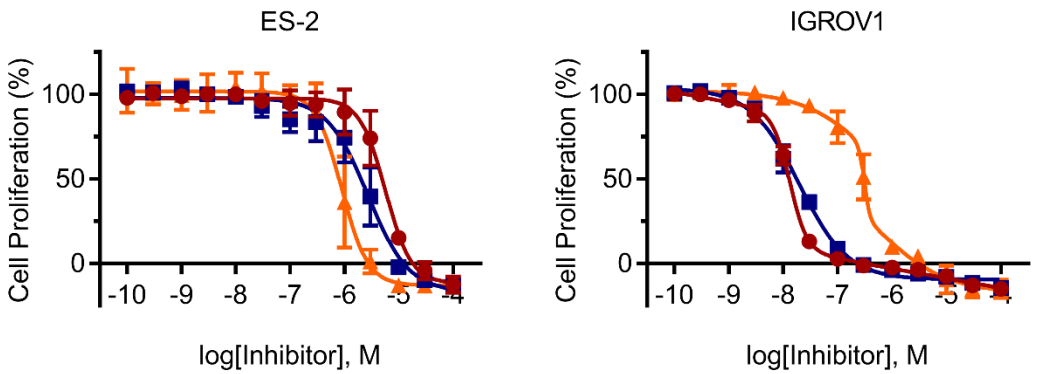

Figure continued on next page

Figure continued from previous page

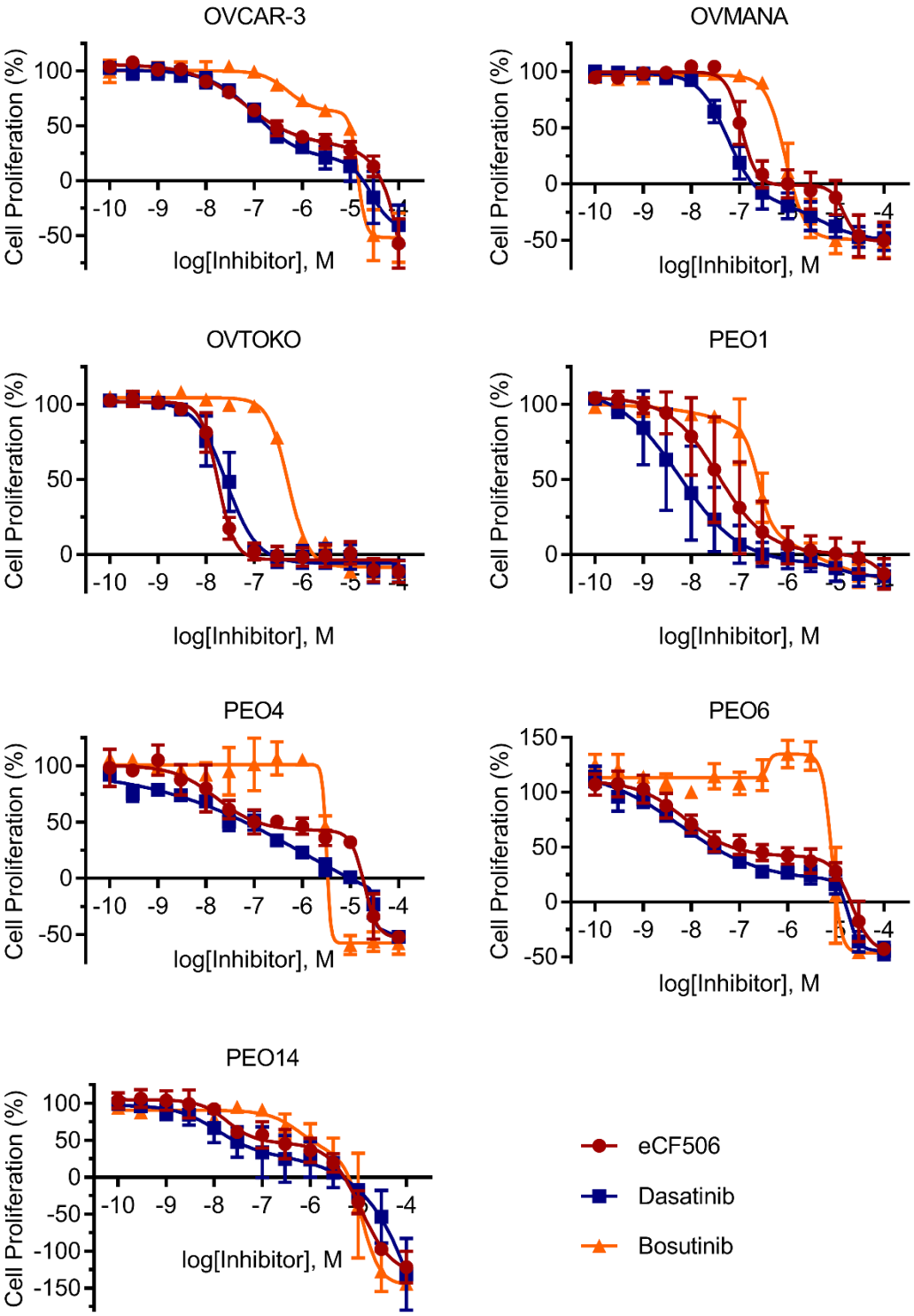

Figure continued on next page

Figure continued from previous page

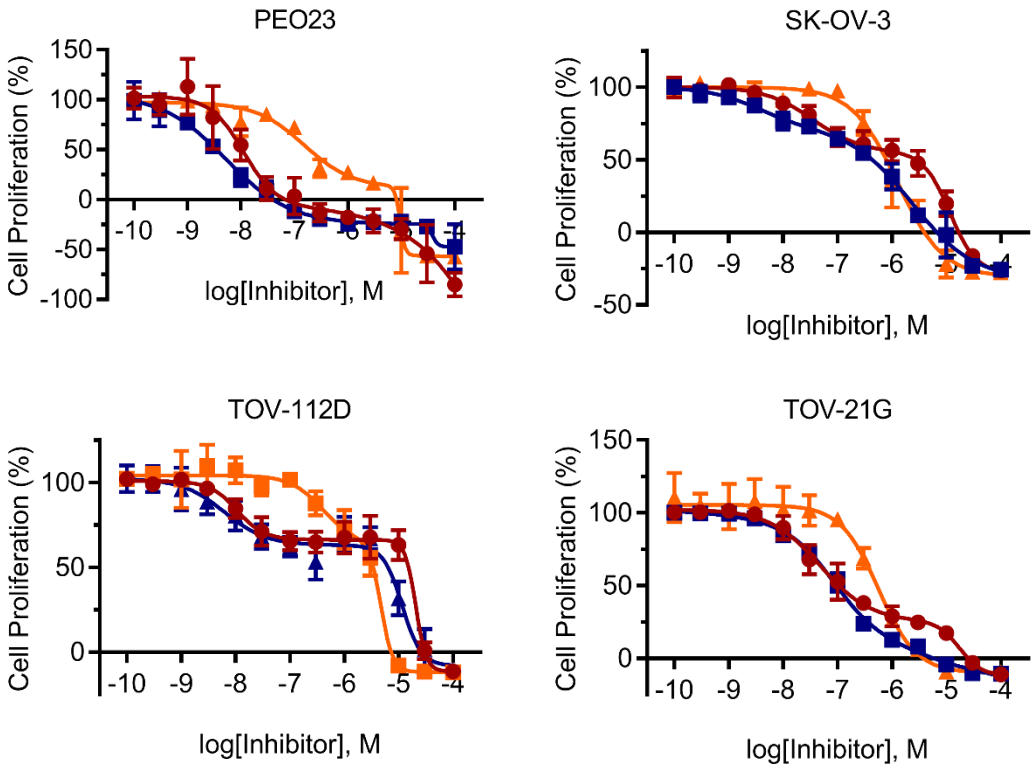

Chronic Myeloid Leukaemia

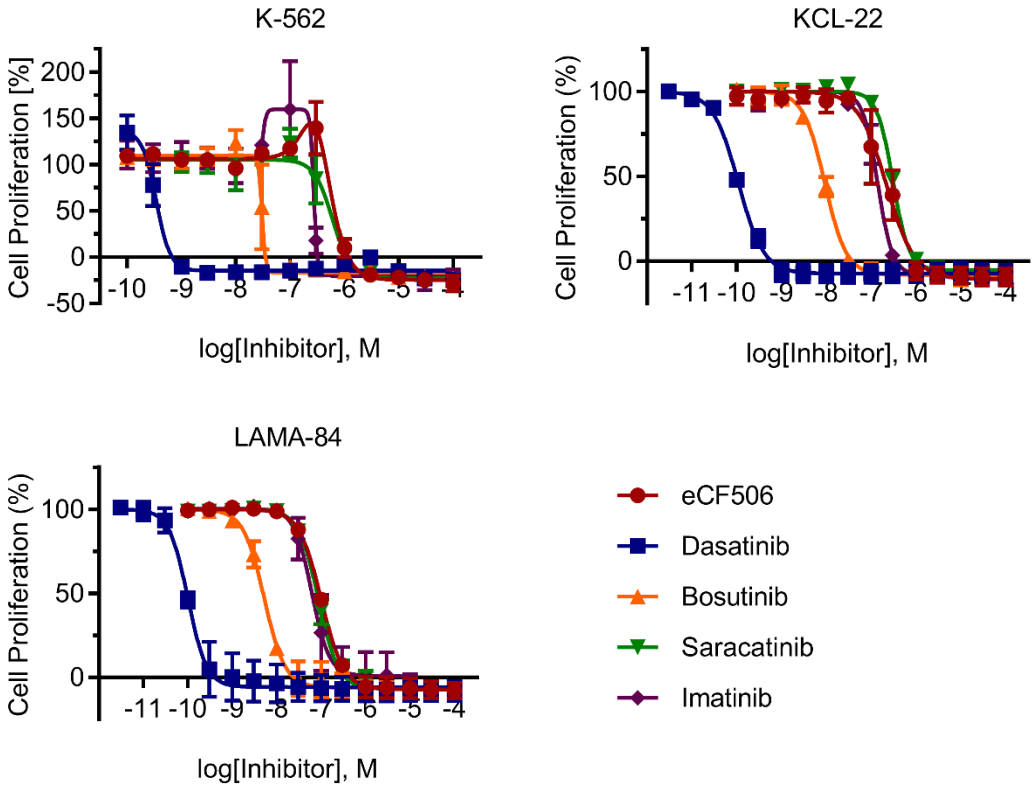

Appendix A.2. Dose-response curves of human oesophageal cancer high-throughput screen (chapter 3.1.1.3). Cells were treated for 48 hours prior to fixing, staining with DAPI and imaging. Number of cell nuclei is used as measure of cell survival and normalised to DMSO control. Graphs show average of three technical repeats with standard deviation.

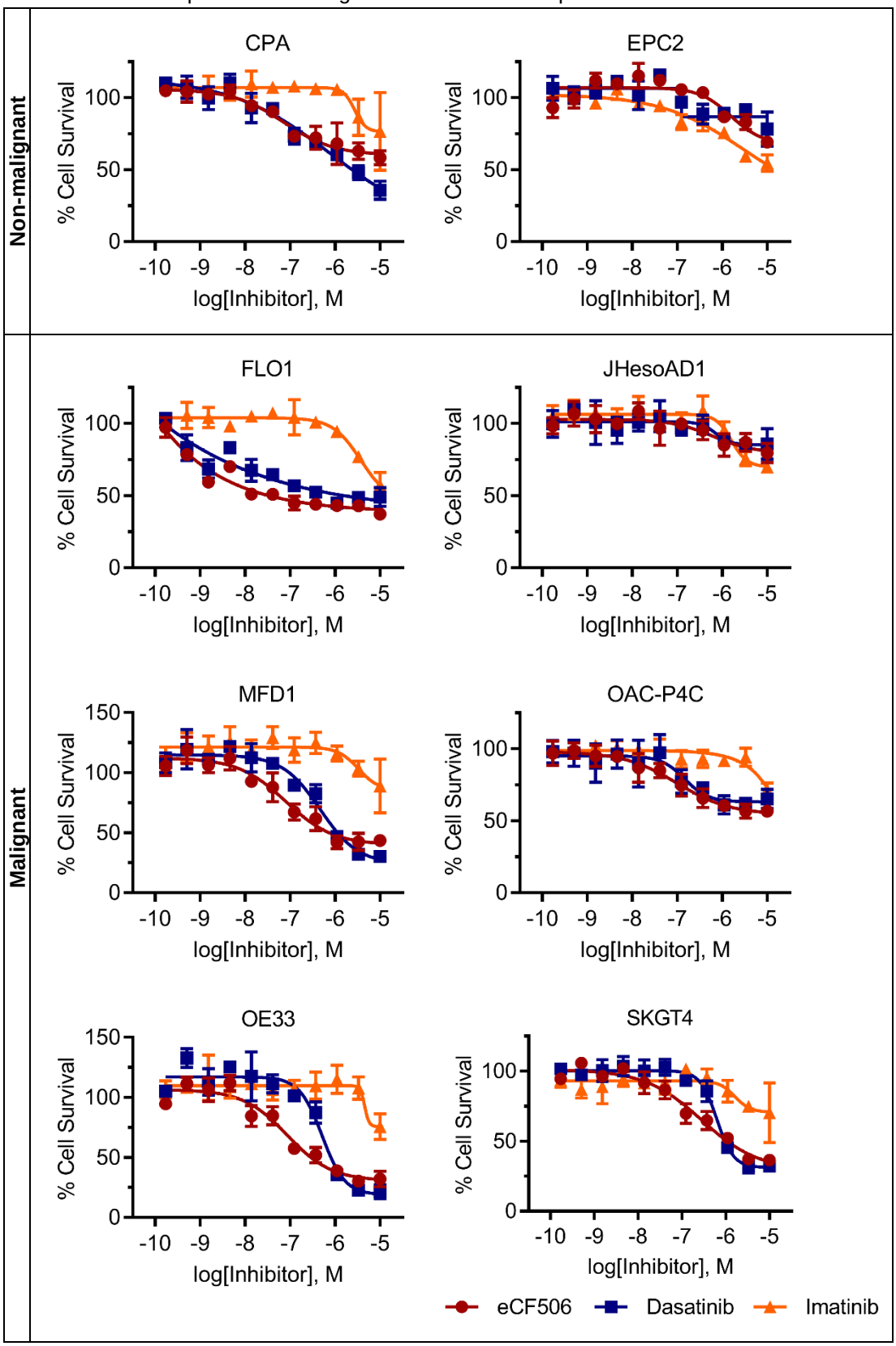

Appendix A.3. Full (phospho)-SRC and cell line sensitivity correlation analysis (chapter 3.1.3). (a) Phospho-SRC and total SRC levels were determined for all cell lines from Western blots and are plotted against eCF506 sensitivity from the 2D cell viability assays of chapter 3.1.1.2. Protein levels were determined from two biological replicates, normalised to MDA-MB-231 and are shown with standard error. Correlation analysis of combined breast and ovarian cancer cell line data was performed using GraphPad Prism 7.0. (b) Representative Western blots showing phospho-SRC and total SRC level of all cell lines. (c) GI_{25}, GI_{50}, GI_{75}, GI_{90} and TGI values of all cell lines for eCF506 treatment. Values (in µM) determined from three biological repeats and rounded to three significant figures.

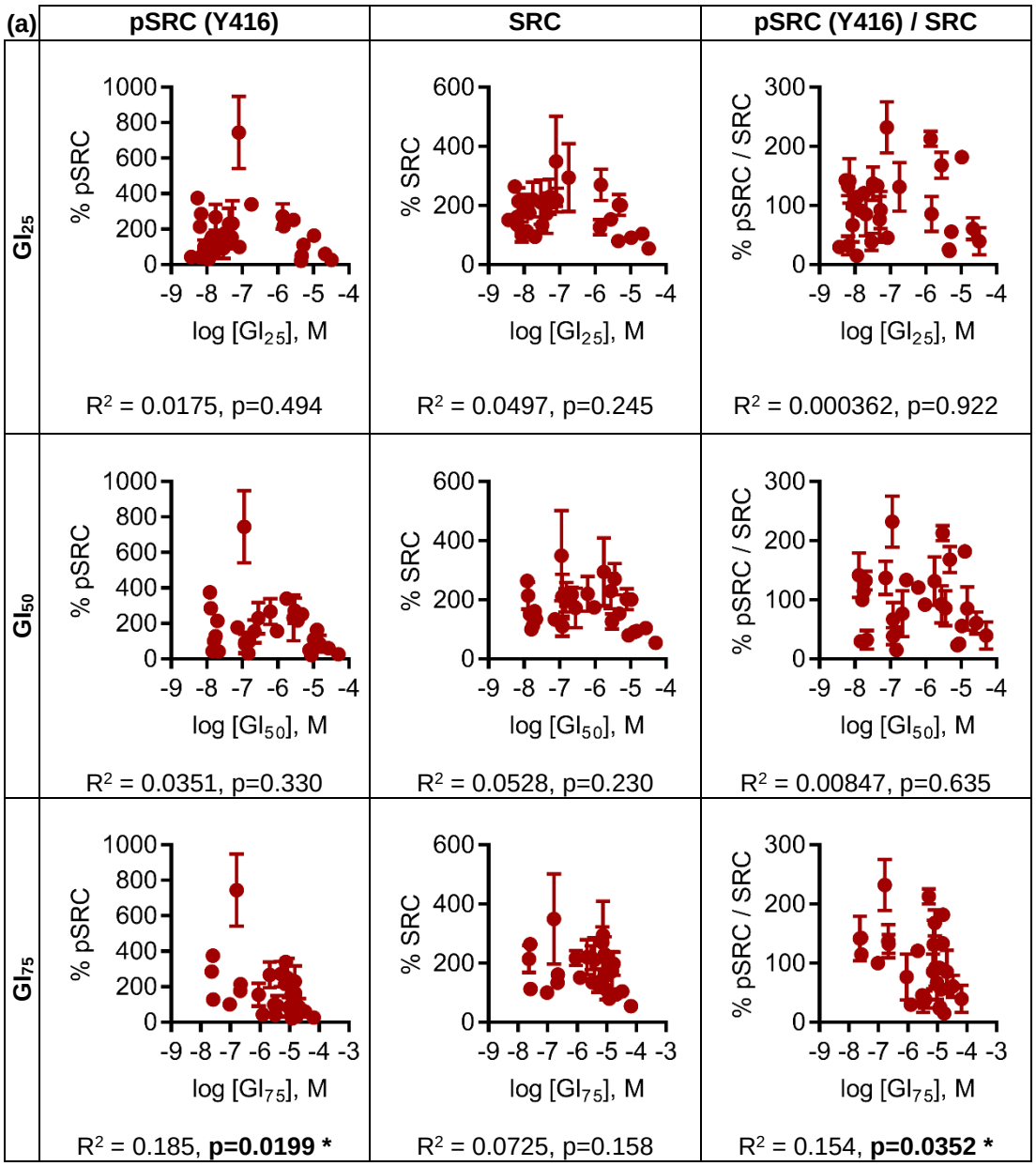

Figure continued on next page

Figure continued from previous page

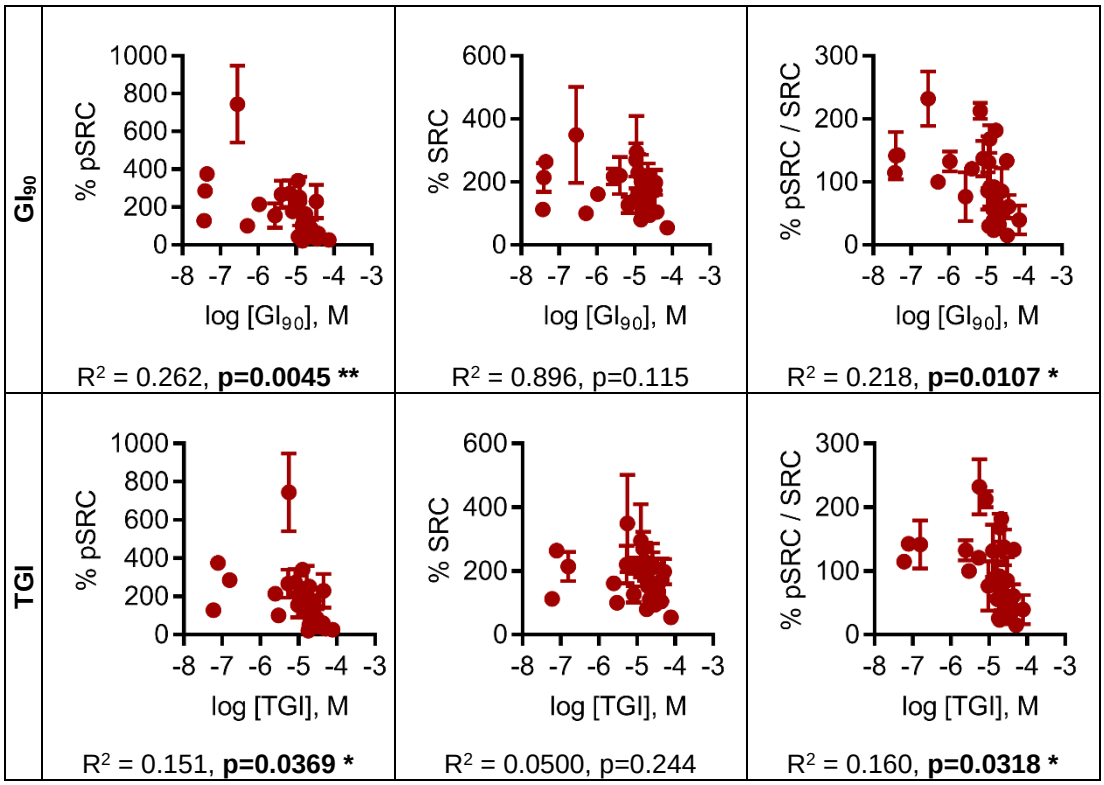

(b)

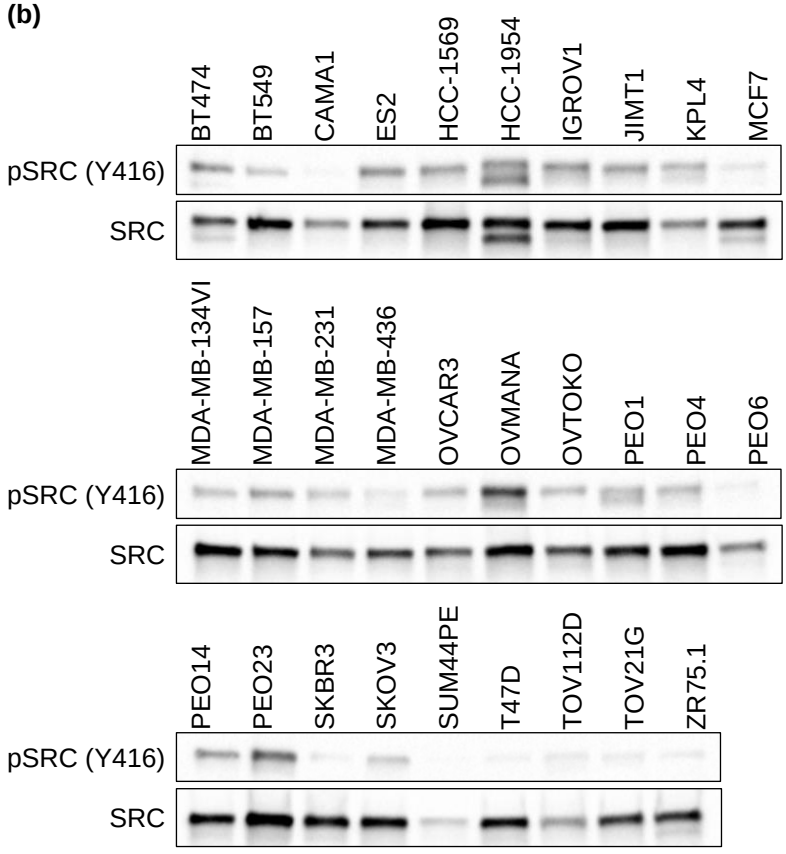

Figure continued on next page

Figure continued from previous page

(c)

	GI_{25}	GI_{50}	GI_{75}	GI_{90}	TGI
BT474	1.38	2.99	5.14	6.86	8.3
BT549	0.0832	0.155	3.05	22.3	25.9
CAMA	4.57	8.75	12.2	15.0	18.0
ES2	2.78	4.80	8.12	12.4	19.2
HCC1569	1.47	3.59	7.14	10.8	14.7
HCC1954	0.183	1.79	7.45	11.3	12.8
IGROV1	0.00693	0.0130	0.0234	0.0392	0.157
JIMT1	0.0505	0.222	0.895	2.76	9.65
KPL4	10.5	12.8	15.4	17.9	21.4
MCF7	0.00368	0.0147	1.24	11.5	30.3
MDAMB134VI	5.32	10.4	13.4	15.3	16.7
MDAMB157	0.00647	0.0200	0.221	1.07	2.47
MDAMB231	0.00868	0.0160	0.0944	0.518	3.04
MDAMB436	21.5	27.0	33.2	38.5	43.9
OVCAR3	0.0431	0.285	14.9	34.2	45.5
OVMANA	0.0798	0.113	0.163	0.285	5.58
OVTOKO	0.0121	0.0177	0.0260	0.0373	0.0596
PEO1	0.0323	0.0744	0.218	8.19	25.1
PEO14	0.0179	0.621	2.14	4.10	5.41
PEO23	0.00555	0.0123	0.0254	0.0444	0.0789
PEO4	0.0141	0.950	11.8	15.9	18.8
PEO6	0.00860	0.120	9.68	16.3	21.7
SKBR3	4.71	7.80	11.8	15.5	19.3
SKOV3	0.0528	2.80	8.48	12.6	16.6
SUM44PE	32.8	50.8	65.6	73.7	78.8
T47D	0.0114	0.149	16.8	36.1	52.0
TOV112D	0.0203	15.0	20.9	25.2	30.1
TOV21G	0.0293	0.120	3.83	15.3	25.1
ZR75.1	0.00639	0.0218	3.26	21.5	36.6

Appendix A.4. Spheroid assay results (chapter 3.1.4 and 5.2.2.1). Raw data of spheroid area as measured by Cell Profiler from collapsed images taken after 4 or 7 days of treatment with eCF506 or dasatinib. Table shows average of three biological repeats.

	MDA-MB-231		MCF-7		T-47D		MetBo2	
Concentration (μM)	Day 4	Day 7	Day 4	Day 7	Day 4	Day 7	Day 4	Day 7
eCF506								
10	38216	36324	56141	57265	61865	73619	34040	26519
3	38530	35314	67444	70501	64526	84845	29592	27657
1	42644	42910	72854	73878	66454	88379	24403	25008
0.3	39737	42111	70098	76403	65994	89789	19351	18341
0.1	39755	40914	66750	73332	68727	91654	18424	16401
0.03	41548	42668	65254	73612	63402	84107	14218	13603
0.01	39511	41447	74514	76715	69022	92256	14491	11197
0.003	38074	38211	73891	76611	66134	90607	21502	18413
DMSO	39720	42842	74817	83615	71154	95205	49517	75178
Dasatinib								
10	30430	28487	57105	58266	42746	51007	33299	25578
3	24704	20008	66688	67716	51444	63907	31760	28326
1	27796	22028	72916	74668	56913	70316	26679	26175
0.3	31382	24826	75611	74581	60071	77416	29562	26428
0.1	33050	27909	84410	88795	57838	76936	27783	24345
0.03	35465	33343	80475	81565	65359	86359	26335	23777
0.01	35530	34041	80625	76581	68253	90210	22655	20432
0.003	37840	38873	75142	80734	68172	91103	17549	13976
DMSO	39236	44026	80198	85207	68271	90819	56074	70146

Appendix A.5. Comparison of SRC activity between 2D and 3D cell models. Western blot comparison of phospho-SRC Y416 and total SRC amounts in MDA-MB-231 and MCF-7 cells grown on 6-well plates (2D) or as spheroids in non-adherent 96-well plates (3D) for a total of seven days. Data represents average of three biological replicates with standard deviation. Representative Western blots are shown. Statistical analysis was done using two-way ANOVA with Sidak correction for multiple comparison; $p>0.05$ ns, $p<0.05$ *, $p<0.001$ ***.

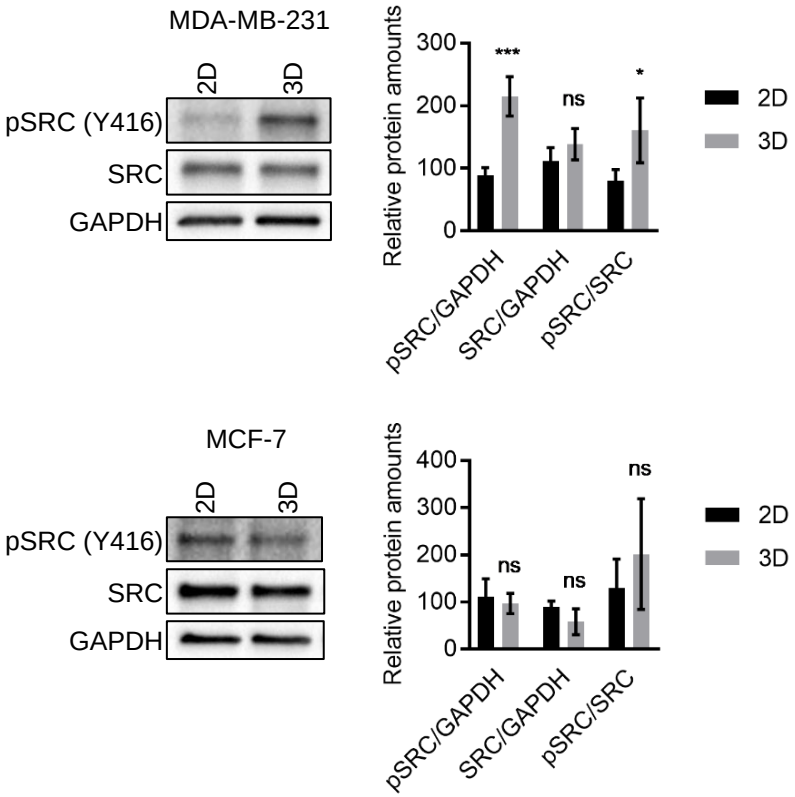

Appendix A.6. Full results of kinome screen of eCF506 (chapter 3.2.1.1). Table shows all 340 tested kinases in order of sensitivity to eCF506. % Activity shows the percentage of kinase activity left when treated with 1 µM eCF506 at 10 µM of ATP, relative to DMSO. Data represents average of two repeats.

Kinase	*% Activity*	*Kinase*	*% Activity*	*Kinase*	*% Activity*	*Kinase*	*% Activity*
SRC	0.1	MAP4K5	81.7	CK2a	92.8	PKG1a	96.6
BRK	0.2	RSK4	83.3	ROCK2	92.8	LRRK2	96.6
HCK	0.8	SGK3	83.4	CDK2/cyclin A1	92.9	CAMK1d	96.7
FGR	1.3	ZAK	83.4	DYRK3	93.0	PKCg	96.7
LYN	1.3	FGFR3	84.7	DAPK3	93.0	FLT3	96.8
LCK	1.4	ALK1	85.9	EPHB3	93.1	TAOK2	96.9
ARAF	1.7	EPHA1	86.7	NLK	93.1	ULK3	97.0
YES	1.8	MAP4K3	87.0	SRPK1	93.3	MAPKAPK2	97.0
LYN B	2.0	PAK3	87.3	CK1e	93.4	RSK2	97.1
FYN	2.3	MET	87.5	SIK2	93.6	CDK1/cyclin A	97.1
FRK	2.4	IKKa	87.6	VRK2	93.6	NEK9	97.1
BMX	2.8	MUSK	89.0	PRKG2	93.7	CDK3/cyclin E	97.2
BTK	3.8	LATS2	89.0	IKKe	93.8	TLK1	97.3
ERBB4	4.5	PKCb2	89.1	ULK1	93.9	MAP4K4	97.3
BLK	4.8	GSK3a	89.2	TESK1	94.3	MLK2	97.3
CSK	5.0	ERK7	89.4	DYRK1B	94.6	MST2	97.4
TXK	9.1	TYK2	89.6	GSK3b	94.6	p38-beta	97.4
RIPK3	12.1	BMPR2	89.6	MAPKAPK5	94.6	CAMK1a	97.4
RAF1	19.6	WNK3	90.3	PKG1b	94.6	JAK2	97.5
ABL2	28.7	CDK16/cyclin Y	90.4	FGFR4	94.9	PDPK1	97.5
LIMK2	30.0	PIM3	90.6	MSSK1	94.9	p38-alpha	97.5
MER	30.1	MAP4K2	90.6	TAOK1	95.0	NEK2	97.7
BRAF	34.5	CAMK1b	90.7	JNK3	95.1	MAPKAPK3	97.7
TEC	43.9	RON	90.9	ARK5	95.1	PKCd	97.8
SRMS	46.2	p38-gamma	90.9	HIPK2	95.2	MNK1	97.8
ACK1	54.3	CK1g2	90.9	HIPK3	95.2	MRCKa	97.9
ABL1	56.3	ACVR1B	90.9	CLK3	95.2	NEK3	98.0
AXL	64.1	RPS6KA5	91.1	CDK1/cyclin B	95.3	EPHA7	98.1
EPHB2	66.6	MEK1	91.1	PHKg2	95.3	TNIK	98.1
EPHB4	68.5	LCK2	91.2	DYRK1A	95.3	DYRK2	98.2
PAK2	71.2	CAMK2a	91.5	RPS6KB1	95.4	ALK3	98.2
RSK1	72.2	CAMK1g	91.5	MLK1	95.5	ITK	98.2
PKAcb	74.3	DMPK2	91.5	EPHA8	95.6	CK1g3	98.2
MAP3K8	74.6	IRAK1	91.8	CDK9/cyclin K	95.7	ERK5	98.4
Kit	75.1	EPHA5	92.0	STK16	95.7	PHKg1	98.5
NEK11	75.3	PKN1	92.1	PIM1	95.9	PKN3	98.5
RIPK2	76.8	CLK2	92.1	TRKB	95.9	RET	98.6
FGFR1	78.0	PKCtheta	92.1	STK33	96.2	PRKX	98.6
MEK2	78.8	IRAK4	92.4	WEE1	96.2	GRK7	98.6
DDR1	79.6	LTK	92.4	TAOK3	96.2	MARK4	98.6
LIMK1	79.8	MELK	92.5	BRSK2	96.4	MST4	98.7
MEKK3	80.2	CDK6/cyclin D3	92.6	PKCzeta	96.5	SIK1	98.9
NEK7	81.3	CAMK4	92.7	CDK4/cyclin D3	96.6	SGK1	98.9

Table continued on next page

Table continued from previous page

Kinase	*% Activity*	*Kinase*	*% Activity*	*Kinase*	*% Activity*	*Kinase*	*% Activity*
CHK2	98.9	INSRR	101.4	SIK3	104.0	MNK2	107.3
CDK5/p25	98.9	PIM2	101.4	GRK1	104.0	FER	107.5
TBK1	99.1	GRK5	101.5	TIE2	104.1	MAP3K12	108.2
AURKB	99.1	ROS1	101.5	AKT3	104.2	RPS6KB2	108.2
RPS6KA4	99.2	CDK2/cyclin E	101.6	TGFBR2	104.3	NEK5	108.5
WNK1	99.2	CK1d	101.6	SYK	104.3	PLK1	108.6
STK39	99.2	PAK6	101.7	JNK2	104.3	FES	108.6
PLK2	99.2	EPHA2	101.7	PDGFRb	104.3	PRKD1	108.7
CK1g1	99.2	PKCiota	101.8	VRK1	104.4	IKKb	109.1
MEKK2	99.3	PKAcg	101.8	LOK	104.5	GRK3	109.2
TRKC	99.3	AURKA	101.9	GRK2	104.5	CDK9/cyclin T1	109.2
GRK4	99.5	JAK1	101.9	TTBK1	104.5	ROCK1	109.7
DAPK2	99.5	CAMK2g	101.9	DAPK1	104.6	FGFR2	109.8
ERK2	99.5	CDK7/cyclin H	101.9	PKA	104.6	MLCK	109.8
MARK2	99.5	SLK	102.0	EPHA3	104.7	MST3	110.0
ASK1	99.6	CDK5/p35	102.0	MST1	105.0	RIPK5	110.0
CHK1	99.7	LATS1	102.1	HIPK4	105.0	TGFBR1	110.2
NEK6	99.7	TAK1	102.1	SNARK	105.0	TYRO3	110.5
MAP4K1	99.8	AURKC	102.2	PRKD3	105.0	PASK	110.6
PKCb1	99.8	CDK2/cyclin A	102.3	PLK3	105.1	PKN2	110.8
PKCepsilon	99.9	DDR2	102.4	CDK6/cyclin D1	105.2	JAK3	111.1
PKCa	99.9	GRK6	102.4	DMPK	105.2	CK1a1	111.4
SRPK2	100.0	ALK	102.5	MYO3b	105.2	IR	111.8
EPHA6	100.1	STK22D	102.5	ERK1	105.2	TSSK3	112.0
MEKK1	100.1	ZAP70	102.5	Haspin	105.3	YSK1	112.2
LKB1	100.1	CAMK2d	102.5	WNK2	105.4	PRKD2	113.0
STK38L	100.1	DCAMKL2	102.5	MYLK2	105.5	FAK	113.5
TRKA	100.1	TNK1	102.6	SGK2	105.6	BRSK1	114.7
CLK1	100.2	PKCeta	102.7	MRCKb	105.7	PDGFRa	115.1
MARK1	100.2	RSK3	102.8	ACVR1	105.7	EPHB1	115.5
MLK3	100.2	NEK4	102.8	NEK1	105.9	STK32C	116.0
HIPK1	100.3	DCAMKL1	102.8	TTBK2	106.0	CAMKK2	116.7
TLK2	100.4	OSR1	103.1	JNK1	106.0	PLK4	116.8
PYK2	100.5	SSTK	103.2	P38-delta	106.0	EGFR	117.3
PAK1	100.5	CSF1R	103.3	CDK1/cyclin E	106.1	STK32B	118.6
IGF1R	100.7	CAMK2b	103.5	AKT1	106.3	VEGFR2	119.5
CLK4	100.7	PAK5	103.5	FLT1	106.3	TSSK2	123.4
MEK3	100.8	STK17A	103.6	MAP2K6	106.3	ERBB2	126.3
MARK3	101.0	CAMKK1	103.6	EPHA4	106.5	FLT4	127.6
AKT2	101.0	CDK4/cyclin D1	103.7	CDC7/DBF4	106.9	MINK	128.9
MYLK3	101.1	ULK2	103.8	MAP2K4	107.0	STK38	175.7
DYRK4	101.3	PBK	103.9	PAK4	107.0	CK2a2	176.1

Appendix A.7. Dose-response curves of ABL1 modified MDA-MB-231 cells (chapter 3.2.2). MDA-MB-231 wild-type, MDA-MB-231 ABL1 knockout and MDA-MB-231 cells re-expressing ABL1 were treated with eCF506 or dasatinib for 5 days. Effects on cell proliferation were measured using PrestoBlue™ reagent and curves were fitted using GraphPad Prism 7. Cell viability on the day of treatment was subtracted from final readings and normalised to DMSO treated control. All dose-response curves represent the average of three biological repeats with standard deviation.

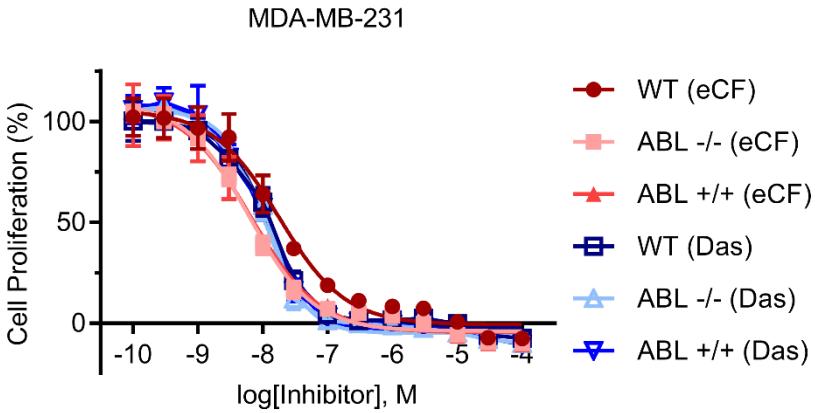

Appendix A.8. Western Blot analysis of pSRC (Y527) and pFAK (Y397) in MCF-7 cells (chapter 4.1.2.2 and 4.2.1). (a) Phospho-FAK (Y397) and Phospho-SRC (Y527) Western blot analysis after treatment of MCF-7 cells for 3 or 24 hours. Representative Western blot from three biological replicates. (b) Summary of phospho-SRC (Y527) and phospho-FAK (Y397) Western blots of MCF-7 cells showing average of three biological replicates with standard deviation. Band intensities were quantified using Bio-Rad ImageLab® software, adjusted for loading using GAPDH and normalised to DMSO. Concentrations given in µM.

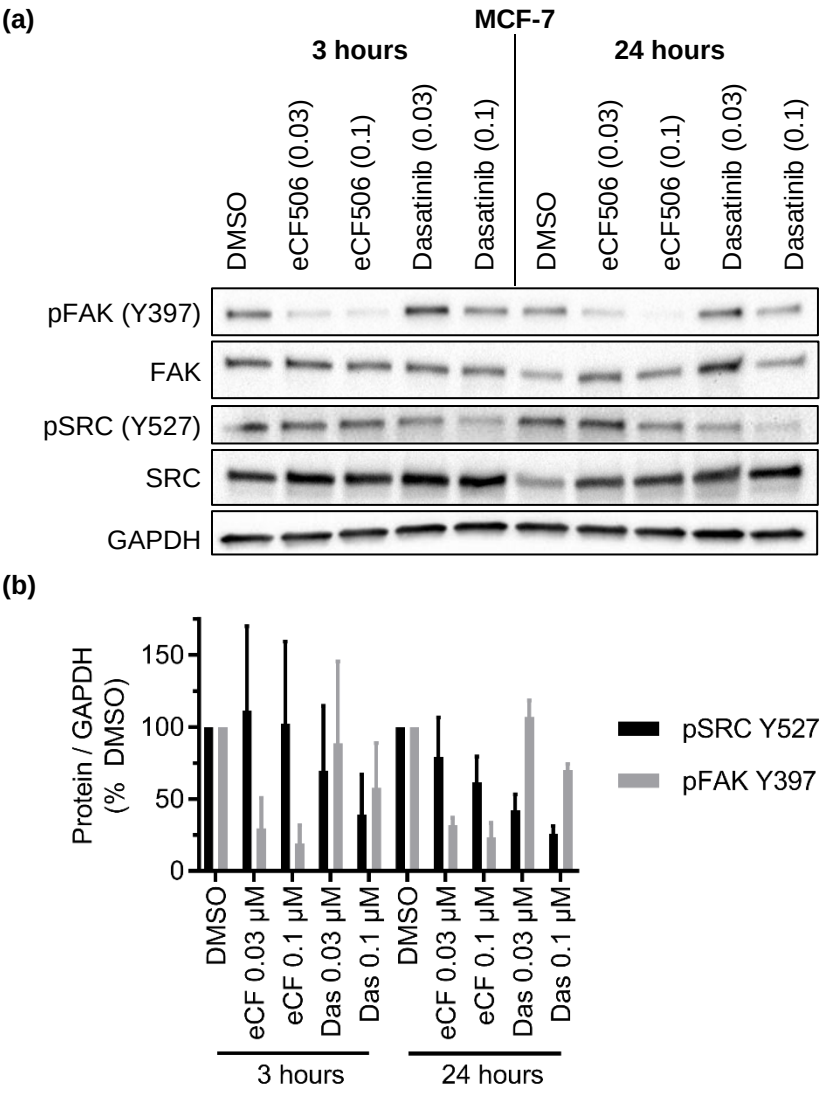

Appendix A.9. Western blot analysis of selected proteins assessed in the RPPA (chapter 4.2.1). MDA-MB-231 cells were treated with eCF506 or dasatinib for the time specified prior to lysis and analysis by Western blot. Images represent one biological replicate. Concentrations given in µM.

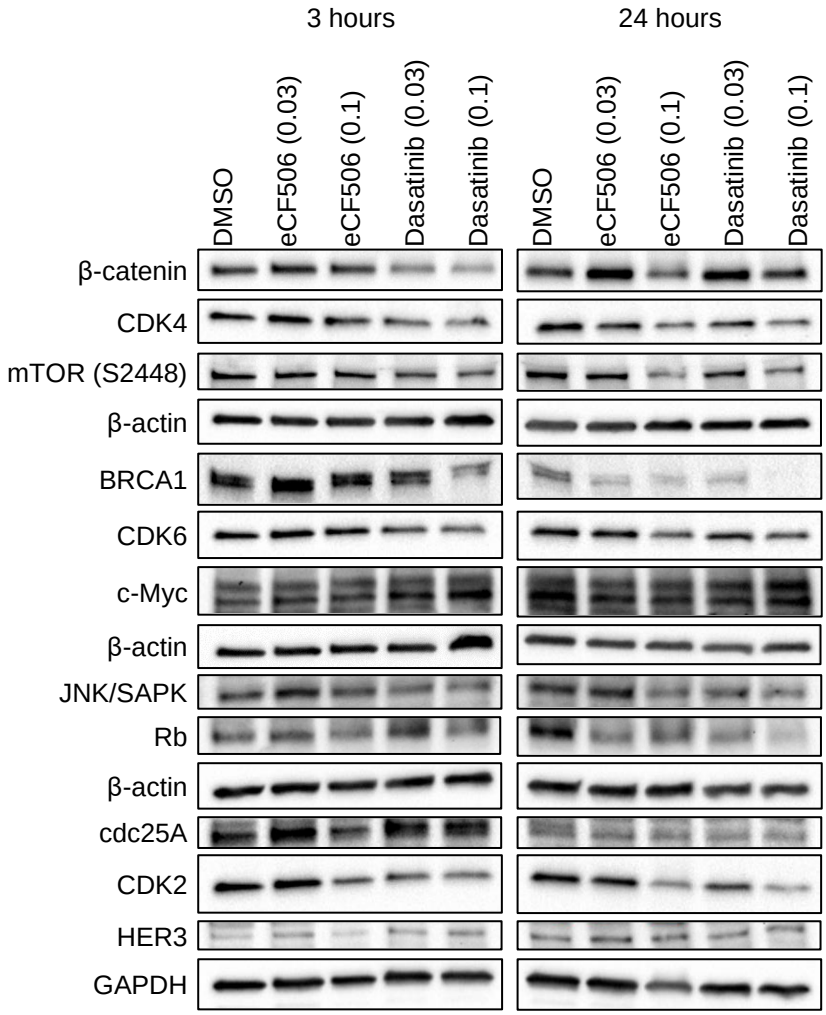

Appendix A.10. Exploratory co-immunoprecipitation of SRC, FAK, p85 PI3K, paxillin and ERα (chapter 4.2.2). (a) MDA-MB-231 or (b) MCF-7 cells were treated with eCF506 or dasatinib for 6 hours prior to cell lysis and co-immunoprecipitation using SRC (rabbit or mouse as specified) antibody overnight. Bound proteins were eluted and analysed using Western blot with total cell lysates as control. No SRC control in top right blot as strong background at similar molecular weight as SRC. Representative Western blots of one biological replicate. All concentrations given in µM.

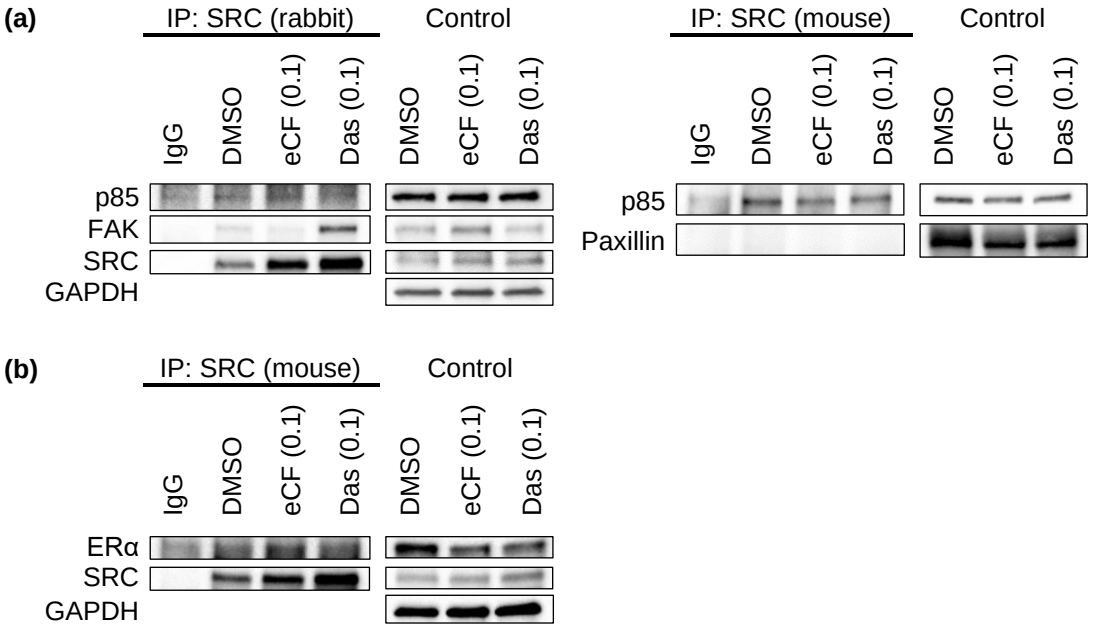

Appendix A.11. Subcellular fractionation of different cell lines (chapter 4.3.1 and 5.2.2.1). Subcellular fractionation of MetBo2, SCC, MCF-7, T-47D and ZR-75.1 cells treated with eCF506 or dasatinib (both 0.1 µM) for 6 hours prior to subcellular fractionation and analysis by Western blot. Representative Western blot of three (MetBo2, SCC, MCF-7) or one (T-47D, ZR75.1) biological repeats. (L.E.) = longer exposure. All concentrations given in µM.

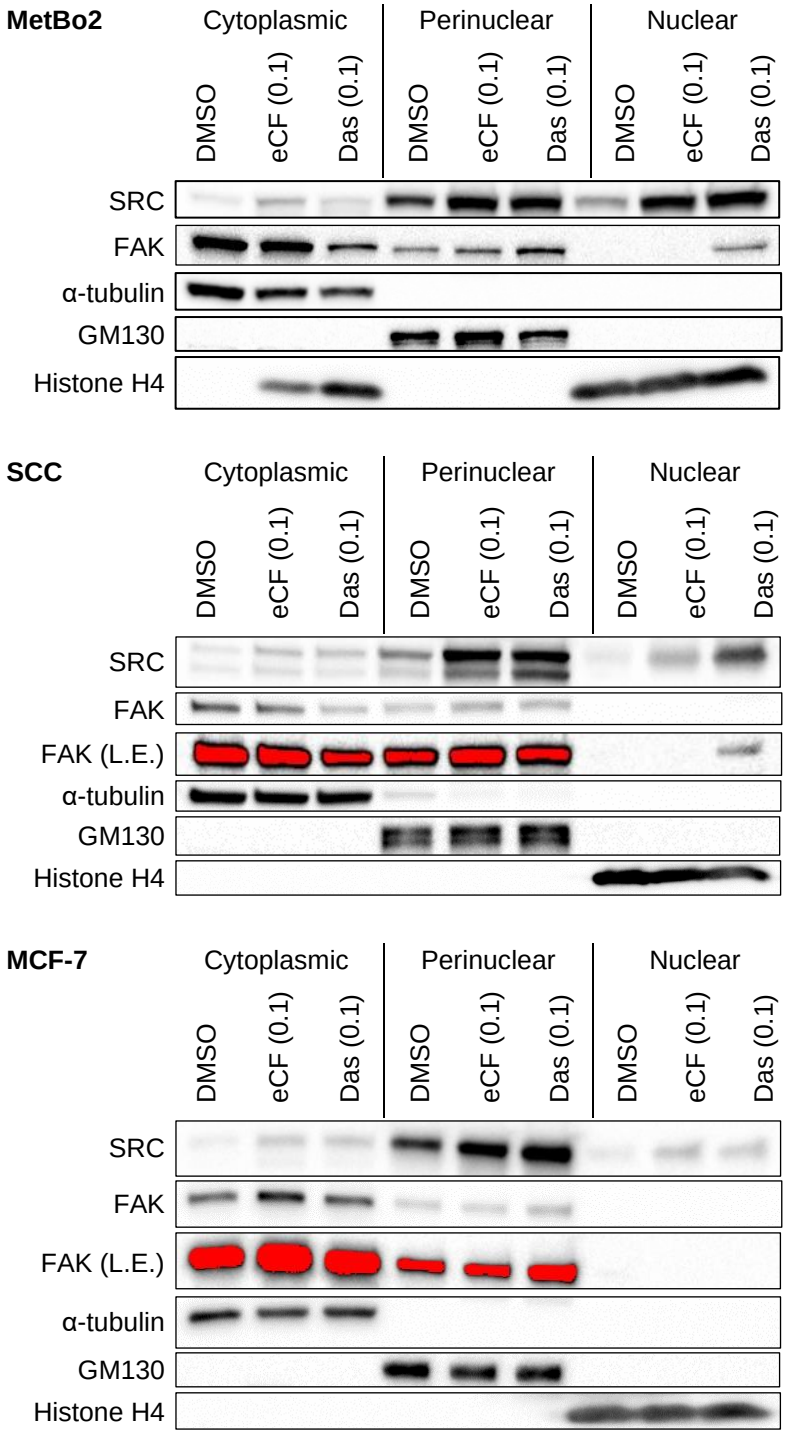

Figure continued on next page

Figure continued from previous page

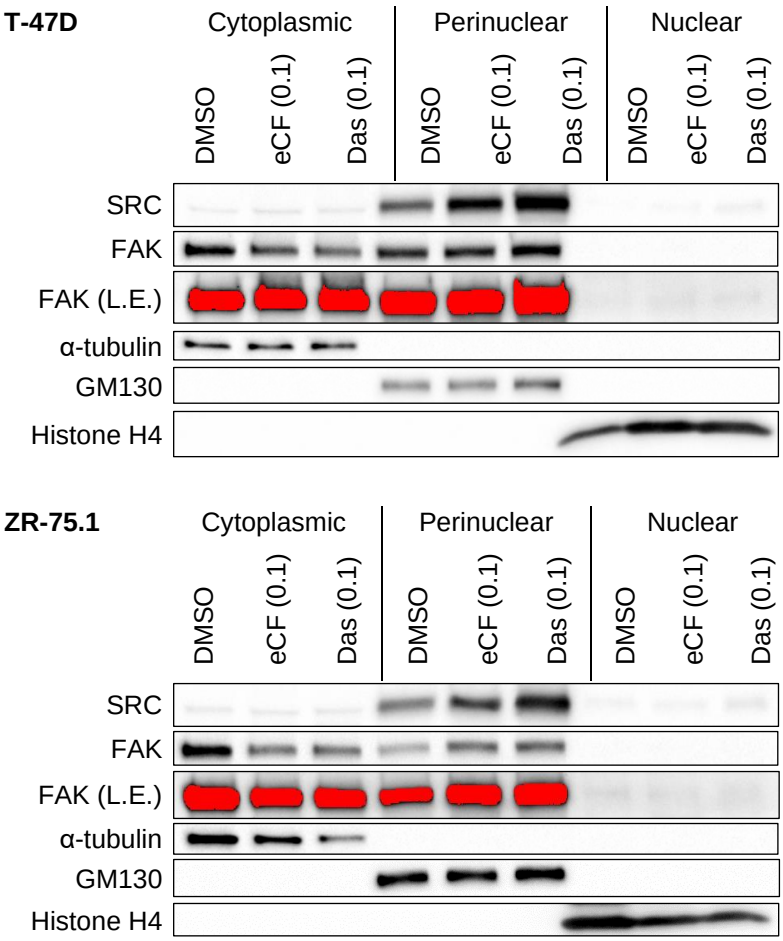

Appendix A.12. Dose-response curves of SCC cell lines treated with eCF506 or dasatinib (chapter 4.3.1). SCC, SCC FAK WT, SCC FAK -/- and SCC FAK NLS cells were treated with eCF506 or dasatinib for 5 days. Effects on cell proliferation were measured using PrestoBlue™ reagent and curves were fitted using GraphPad Prism 7. Cell viability on the day of treatment was subtracted from final readings and normalised to DMSO treated control. All dose-response curves represent the average of three biological repeats with standard deviation.

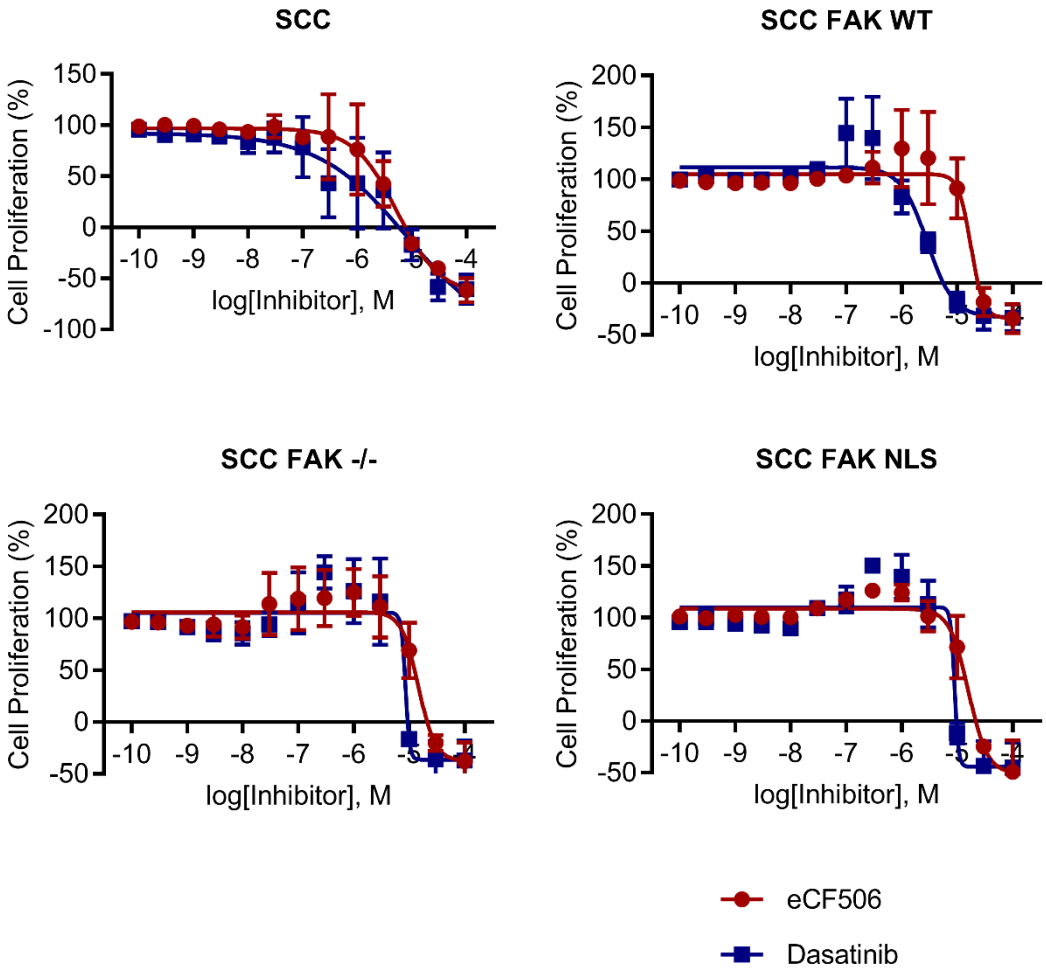

Appendix A.13. Pharmacokinetic data of eCF506 in Sprague-Dawley rats (chapter 5.1.2.1). Mean concentrations in ng/mL or µM from three animals per time point with standard deviation. BLQ = below limit of quantification (<10 ng/mL) in at least two of the three animals measured. Grey indicates no measurements taken at this time point.

	IV 1 mg/kg		**PO 10 mg/kg**		**PO 200 mg/kg**	
Time (h)	*ng/mL*	*µM*	*ng/mL*	*µM*	*ng/mL*	*µM*
0.03	172 (±27.3)	337 (±53.5)				
0.12	60.6 (±5.90)	119 (±11.6)				
0.25	30.9 (±5.61)	60.4 (±11.0)	BLQ		121 (±91.6)	0.237 (±0.179)
0.50	36.4 (±9.31)	71.3 (±18.2)	BLQ		82.7 (±71.6)	0.162 (±0.140)
0.75			BLQ		48.8 (±40.8)	0.0957 (±0.0799)
1.00	17.7 (±2.66)	34.6 (±5.21)	BLQ		54.4 (±31.0)	0.106 (±0.0608)
2.00	BLQ		11.3 (±1.23)	22.2 (±2.42)	270 (±150)	0.528 (±0.294)
4.00	BLQ		16.1 (±4.13)	31.6 (±8.09)	118 (±19.7)	0.231 (±0.0386)
6.00	BLQ		11.3 (±6.08)	22.1 (±11.9)	179 (±56.6)	0.351 (±0.111)
7.00	BLQ		9.38 (±3.81)	18.4 (±7.46)	160 (±65.3)	0.314 (±0.128)
24.00	BLQ		BLQ	BLQ	366 (±180)	0.717 (±0.352)

Appendix A.14. Detailed results of metabolite study (chapter 5.1.2.2). a) LC-MS chromatograms of the Q-Tof UPLC-MS/MS platform showing combined metabolite peaks after incubation of human hepatocytes with eCF506 for 0 minutes, 60 minutes or 120 minutes. (b) LC-MS chromatograms of the Q-Tof UPLC-MS/MS platform showing detailed metabolite peaks of m/z 527.3090 after incubation of human hepatocytes with eCF506 for 120 minutes.

(a) Combined metabolite peaks of samples incubated for 0, 60 or 120 minutes.

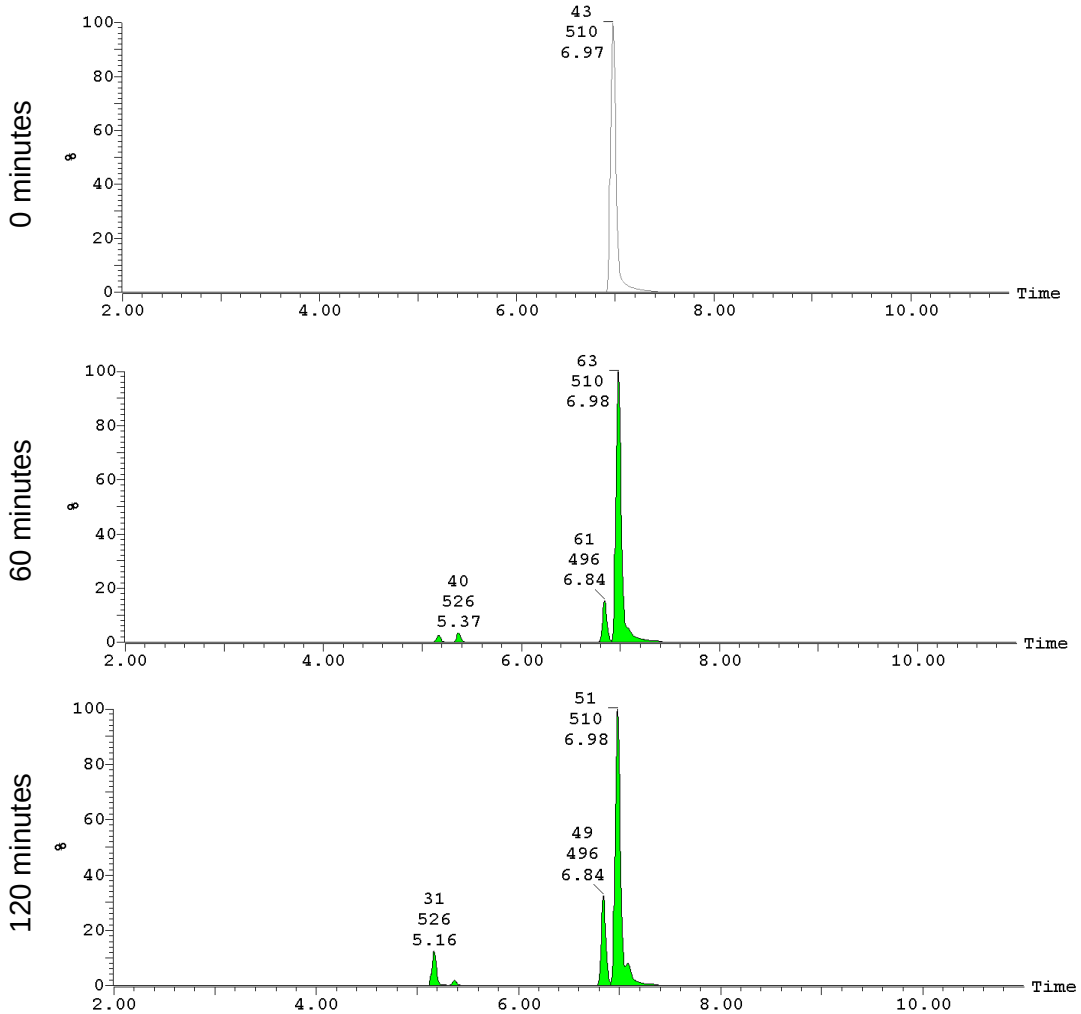

(b) eCF506 metabolites (m/z 527.3090) of sample incubated for 120 minutes.

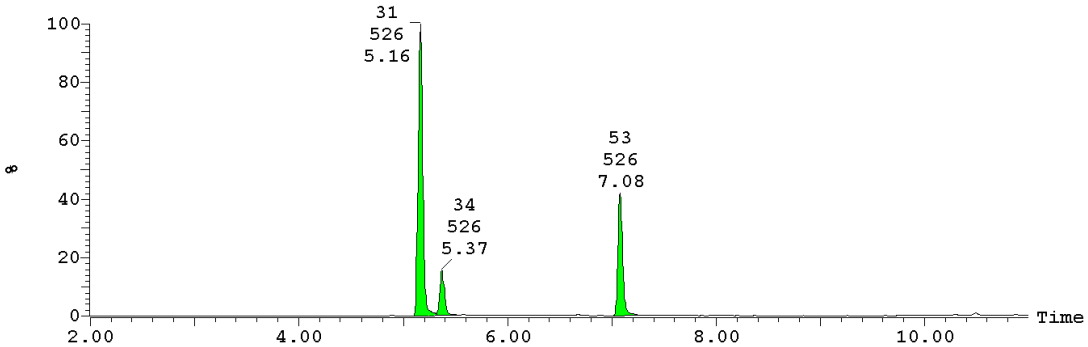

Appendix A.15. Dose-response curve of Met1 cells (chapter 5.2.2.1). Met1 cells were treated with five different SRC and/or ABL kinase inhibitors for 5 days. Effects on cell proliferation were measured using PrestoBlue™ reagent and curves were fitted using GraphPad Prism 7. Cell viability on the day of treatment was subtracted from final readings and normalised to DMSO treated control. All dose-response curves represent the average of three biological repeats with standard deviation.

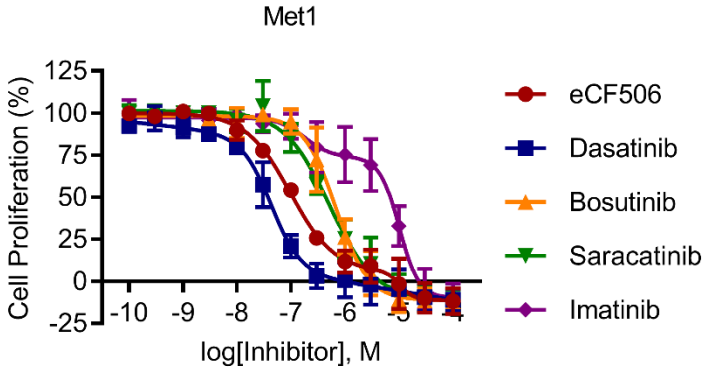

Appendix A.16. IHC of MetBo2 mammary fat pad tumours of FVB mice stained with Ki67 antibody (chapter 5.2.2.4). Immunohistochemical analysis of MetBo2 tumours in FVB mice stained with Ki67 antibody. Images show a necrotic core (white) and proliferative patches on the edge of the tumours (brown). Two representative images are shown per group. Scale bar shows 1 mm.

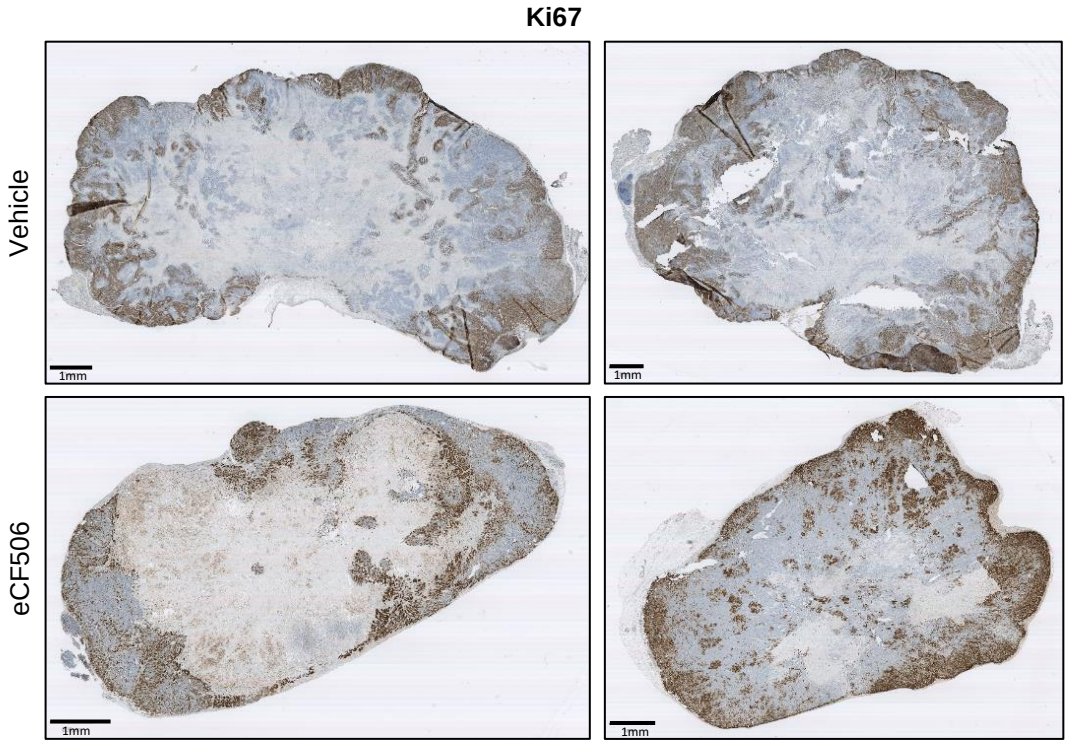

References

1. Fraser, C. *et al.* Rapid Discovery and Structure-Activity Relationships of Pyrazolopyrimidines That Potently Suppress Breast Cancer Cell Growth via SRC Kinase Inhibition with Exceptional Selectivity over ABL Kinase. *J. Med. Chem.* **59**, 4697–4710 (2016).
2. Bray, F. *et al.* Global cancer statistics 2018: GLOBOCAN estimates of incidence and mortality worldwide for 36 cancers in 185 countries. *CA. Cancer J. Clin.* **68**, 394–424 (2018).
3. Hanahan, D. & Weinberg, R. A. The Hallmarks of Cancer. *Cell* **100**, 57–70 (2000).
4. Hanahan, D. & Weinberg, R. A. Hallmarks of Cancer: The Next Generation. *Cell* **144**, 646–674 (2011).
5. GBD 2015 Risk Factors Collaborators. Global, regional, and national comparative risk assessment of 84 behavioural, environmental and occupational, and metabolic risks or clusters of risks for 195 countries and territories, 1990-2017: a systematic analysis. *Lancet (London, England)* **392**, 1923–1994 (2018).
6. Cao, Y., DePinho, R. A., Ernst, M. & Vousden, K. Cancer research: past, present and future. *Nat. Rev. Cancer* **11**, 749–754 (2011).
7. Friedman, A. A., Letai, A., Fisher, D. E. & Flaherty, K. T. Precision medicine for cancer with next-generation functional diagnostics. *Nat. Rev. Cancer* **15**, 747–756 (2015).
8. Bhullar, K. S. *et al.* Kinase-targeted cancer therapies: progress, challenges and future directions. *Mol. Cancer* **17**, 48 (2018).
9. Fabbro, D., Cowan-Jacob, S. W. & Moebitz, H. Ten things you should know about protein kinases: IUPHAR Review 14. *Br. J. Pharmacol.* **172**, 2675–700 (2015).
10. Du, Z. & Lovly, C. M. Mechanisms of receptor tyrosine kinase activation in cancer. *Mol. Cancer* **17**, 58 (2018).
11. Ong, F. S. *et al.* Personalized medicine and pharmacogenetic biomarkers: progress in molecular oncology testing. *Expert Rev. Mol. Diagn.* **12**, 593 (2012).
12. Klaeger, S. *et al.* The target landscape of clinical kinase drugs. *Science* **358**, eaan4368 (2017).
13. Martin, G. S. The hunting of the Src. *Nat. Rev. Mol. Cell Biol.* **2**, 467–475 (2001).
14. Martin, G. S. The road to Src. *Oncogene* **23**, 7910–7917 (2004).
15. Rous, P. A Sarcoma of the Fowl Transmissible by an Agent Separable from the Tumor Cells. *J. Exp. Med.* **13**, 397–411 (1911).
16. Rubin, H. Quantitative relations between causative virus and cell in the Rous No. 1 chicken sarcoma. *Virology* **1**, 445–473 (1955).
17. Svet-Moldavsky, G. J. Development of Multiple Cysts and of Hæmorrhagic Affections of Internal Organs in Albino Rats treated during the Embryonic or New-born Period with Rous Sarcoma Virus. *Nature* **180**, 1299–1300 (1957).
18. Zilber, L. A. & Kryukova, I. N. Haemorrhagic disease of rats due to the virus of chick sarcoma. *Acta Virol.* **1**, 156–160 (1957).
19. The Nobel Foundation. The Nobel Prize in Physiology or Medicine 1966. http://www.nobelprize.org/nobel_prizes/medicine/laureates/1966/ (1966).
20. Huebner, R. J. & Todaro, G. J. Oncogenes of RNA Tumor Viruses as Determinants of Cancer. *Proc. Natl. Acad. Sci.* **64**, 1087–1094 (1969).
21. Stehelin, D., Varmus, H. E., Bishop, J. M. & Vogt, P. K. DNA related to the transforming gene(s) of avian sarcoma viruses is present in normal avian DNA. *Nature* **260**, 170–173 (1976).
22. The Nobel Foundation. The Nobel Prize in Physiology or Medicine 1989. http://www.nobelprize.org/nobel_prizes/medicine/laureates/1989/ (1989).
23. Parker, R. C., Varmus, H. E. & Michael Bishop, J. Expression of v-src and chicken c-src in rat cells demonstrates qualitative differences between pp60v-src and pp60c-src. *Cell* **37**, 131–139 (1984).
24. Brugge, J. S. & Erikson, R. L. Identification of a transformation-specific antigen induced by an avian sarcoma virus. *Nature* **269**, 346–348 (1977).
25. Collett, M. S. & Erikson, R. L. Protein kinase activity associated with the avian

sarcoma virus src gene product. *Proc. Natl. Acad. Sci. U. S. A.* **75**, 2021–2024 (1978).
26. Levinson, A. D., Oppermann, H., Levintow, L., Varmus, H. E. & Bishop, J. M. Evidence that the transforming gene of avian sarcoma virus encodes a protein kinase associated with a phosphoprotein. *Cell* **15**, 561–572 (1978).
27. Hunter, T. & Sefton, B. M. Transforming gene product of Rous sarcoma virus phosphorylates tyrosine. *Proc. Natl. Acad. Sci.* **77**, 1311–1315 (1980).
28. Smart, J. E. *et al.* Characterization of sites for tyrosine phosphorylation in the transforming protein of Rous sarcoma virus (pp60v-src) and its normal cellular homologue (pp60c-src). *Proc. Natl. Acad. Sci.* **78**, 6013–6017 (1981).
29. Cooper, J. A., Gould, K. L., Cartwright, C. A. & Hunter, T. Tyr527 is phosphorylated in pp60c-src: implications for regulation. *Science* **231**, 1431–1434 (1986).
30. Courtneidge, S. A. Activation of the pp60c-src kinase by middle T antigen binding or by dephosphorylation. *EMBO J.* **4**, 1471–1477 (1985).
31. Roskoski Jr., R. Src protein-tyrosine kinase structure, mechanism, and small molecule inhibitors. *Pharmacol. Res.* **94**, 9–25 (2015).
32. Lowell, C. A. & Soriano, P. Knockouts of Src-family kinases: stiff bones, wimpy T cells, and bad memories. *Genes Dev.* **10**, 1845–57 (1996).
33. Boggon, T. J. & Eck, M. J. Structure and regulation of Src family kinases. *Oncogene* **23**, 7918–7927 (2004).
34. Frame, M. C. Src in cancer: deregulation and consequences for cell behaviour. *Biochim. Biophys. Acta - Rev. Cancer* **1602**, 114–130 (2002).
35. Irtegun, S., Wood, R. J., Ormsby, A. R., Mulhern, T. D. & Hatters, D. M. Tyrosine 416 Is Phosphorylated in the Closed, Repressed Conformation of c-Src. *PLoS One* **8**, e71035 (2013).
36. Parsons, S. J. & Parsons, J. T. Src family kinases, key regulators of signal transduction. *Oncogene* **23**, 7906–7909 (2004).
37. Yeatman, T. J. A renaissance for SRC. *Nat. Rev. Cancer* **4**, 470–480 (2004).
38. Lawson, C. *et al.* FAK promotes recruitment of talin to nascent adhesions to control cell motility. *J. Cell Biol.* **196**, 223–32 (2012).
39. Brunton, V. G., MacPherson, I. R. J. & Frame, M. C. Cell adhesion receptors, tyrosine kinases and actin modulators: a complex three-way circuitry. *Biochim. Biophys. Acta - Mol. Cell Res.* **1692**, 121–144 (2004).
40. Mitra, S. K. & Schlaepfer, D. D. Integrin-regulated FAK–Src signaling in normal and cancer cells. *Curr. Opin. Cell Biol.* **18**, 516–523 (2006).
41. Wozniak, M. A., Modzelewska, K., Kwong, L. & Keely, P. J. Focal adhesion regulation of cell behavior. *Biochim. Biophys. Acta - Mol. Cell Res.* **1692**, 103–119 (2004).
42. Huveneers, S. & Danen, E. H. J. Adhesion signaling - crosstalk between integrins, Src and Rho. *J. Cell Sci.* **122**, 1059–69 (2009).
43. Westhoff, M. A., Serrels, B., Fincham, V. J., Frame, M. C. & Carragher, N. O. SRC-mediated phosphorylation of focal adhesion kinase couples actin and adhesion dynamics to survival signaling. *Mol. Cell. Biol.* **24**, 8113–33 (2004).
44. Guarino, M. Src signaling in cancer invasion. *J. Cell. Physiol.* **223**, 14–26 (2009).
45. Frame, M. C. & Blobel, C. P. Newest findings on the oldest oncogene; how activated src does it. *J. Cell Sci.* **117**, 989–98 (2004).
46. Kowalczyk, A. P. & Nanes, B. A. Adherens junction turnover: regulating adhesion through cadherin endocytosis, degradation, and recycling. *Subcell. Biochem.* **60**, 197–222 (2012).
47. Avizienyte, E. *et al.* Src-induced de-regulation of E-cadherin in colon cancer cells requires integrin signalling. *Nat. Cell Biol.* **4**, 632–638 (2002).
48. McLachlan, R. W., Kraemer, A., Helwani, F. M., Kovacs, E. M. & Yap, A. S. E-Cadherin Adhesion Activates c-Src Signaling at Cell–Cell Contacts. *Mol. Biol. Cell* **18**, 3214–3223 (2007).
49. Lamouille, S., Xu, J. & Derynck, R. Molecular mechanisms of epithelial-mesenchymal transition. *Nat. Rev. Mol. Cell Biol.* **15**, 178–96 (2014).
50. Thiery, J. P. Epithelial–mesenchymal transitions in tumour progression. *Nat. Rev. Cancer* **2**, 442–454 (2002).
51. Patel, A., Sabbineni, H., Clarke, A. & Somanath, P. R. Novel roles of Src in cancer

cell epithelial-to-mesenchymal transition, vascular permeability, microinvasion and metastasis. *Life Sci.* **157**, 52–61 (2016).
52. Liu, X., Du, L. & Feng, R. c-Src regulates cell cycle proteins expression through protein kinase B/glycogen synthase kinase 3 beta and extracellular signal-regulated kinases 1/2 pathways in MCF-7 cells. *Acta Biochim. Biophys. Sin.* **45**, 586–592 (2013).
53. Bromann, P. A., Korkaya, H. & Courtneidge, S. A. The interplay between Src family kinases and receptor tyrosine kinases. *Oncogene* **23**, 7957–7968 (2004).
54. Zhang, S. & Yu, D. Targeting Src family kinases in anti-cancer therapies: turning promise into triumph. *Trends Pharmacol. Sci.* **33**, 122–8 (2012).
55. Lemmon, M. A. & Schlessinger, J. Cell signaling by receptor tyrosine kinases. *Cell* **141**, 1117–34 (2010).
56. Mayer, E. L. & Krop, I. E. Advances in Targeting Src in the Treatment of Breast Cancer and Other Solid Malignancies. *Clin. Cancer Res.* **16**, 3526–3532 (2010).
57. Yu, C. L. *et al.* Enhanced DNA-binding activity of a Stat3-related protein in cells transformed by the Src oncoprotein. *Science* **269**, 81–3 (1995).
58. Luttrell, D. K. & Luttrell, L. M. Not so strange bedfellows: G-protein-coupled receptors and Src family kinases. *Oncogene* **23**, 7969–7978 (2004).
59. McGarrigle, D. & Huang, X.-Y. GPCRs Signaling Directly Through Src-Family Kinases. *Sci. Signal.* **2007**, pe35 (2007).
60. Levin, E. R. & Hammes, S. R. Nuclear receptors outside the nucleus: extranuclear signalling by steroid receptors. *Nat. Rev. Mol. Cell Biol.* **17**, 783–797 (2016).
61. Shupnik, M. A. Crosstalk between steroid receptors and the c-Src-receptor tyrosine kinase pathways: implications for cell proliferation. *Oncogene* **23**, 7979–7989 (2004).
62. Weigel, N. L. & Moore, N. L. Steroid Receptor Phosphorylation: A Key Modulator of Multiple Receptor Functions. *Mol. Endocrinol.* **21**, 2311–2319 (2007).
63. Castoria, G. *et al.* Tyrosine phosphorylation of estradiol receptor by Src regulates its hormone-dependent nuclear export and cell cycle progression in breast cancer cells. *Oncogene* **31**, 4868–4877 (2012).
64. Chu, I. *et al.* Src promotes estrogen-dependent estrogen receptor alpha proteolysis in human breast cancer. *J. Clin. Invest.* **117**, 2205–15 (2007).
65. Kraus, S., Gioeli, D., Vomastek, T., Gordon, V. & Weber, M. J. Receptor for Activated C Kinase 1 (RACK1) and Src Regulate the Tyrosine Phosphorylation and Function of the Androgen Receptor. *Cancer Res.* **66**, 11047–11054 (2006).
66. Guo, Z. *et al.* Regulation of androgen receptor activity by tyrosine phosphorylation. *Cancer Cell* **10**, 309–319 (2006).
67. Asim, M., Siddiqui, I. A., Hafeez, B. B., Baniahmad, A. & Mukhtar, H. Src kinase potentiates androgen receptor transactivation function and invasion of androgen-independent prostate cancer C4-2 cells. *Oncogene* **27**, 3596–3604 (2008).
68. Razandi, M., Pedram, A., Park, S. T. & Levin, E. R. Proximal events in signaling by plasma membrane estrogen receptors. *J. Biol. Chem.* **278**, 2701–12 (2003).
69. Riley, D., Carragher, N. O., Frame, M. C. & Wyke, J. A. The mechanism of cell cycle regulation by v-Src. *Oncogene* **20**, 5941–5950 (2001).
70. Johnson, D., Frame, M. C. & Wyke, J. A. Expression of the v-Src oncoprotein in fibroblasts disrupts normal regulation of the CDK inhibitor p27 and inhibits quiescence. *Oncogene* **16**, 2017–2028 (1998).
71. Chu, I. *et al.* p27 Phosphorylation by Src Regulates Inhibition of Cyclin E-Cdk2. *Cell* **128**, 281–294 (2007).
72. Miyazaki, T., Neff, L., Tanaka, S., Horne, W. C. & Baron, R. Regulation of cytochrome c oxidase activity by c-Src in osteoclasts. *J. Cell Biol.* **160**, 709–18 (2003).
73. Feng, J. *et al.* Tyrosine phosphorylation by Src within the cavity of the adenine nucleotide translocase 1 regulates ADP/ATP exchange in mitochondria. *Am. J. Physiol. Physiol.* **298**, C740–C748 (2010).
74. Lluis, J. M., Buricchi, F., Chiarugi, P., Morales, A. & Fernandez-Checa, J. C. Dual Role of Mitochondrial Reactive Oxygen Species in Hypoxia Signaling: Activation of Nuclear Factor- B via c-SRC and Oxidant-Dependent Cell Death. *Cancer Res.* **67**, 7368–7377 (2007).

75. Jin, Y. *et al.* Src drives the Warburg effect and therapy resistance by inactivating pyruvate dehydrogenase through tyrosine-289 phosphorylation. *Oncotarget* **7**, 25113–24 (2016).
76. Zhang, J. *et al.* c-Src phosphorylation and activation of hexokinase promotes tumorigenesis and metastasis. *Nat. Commun.* **8**, 13732 (2017).
77. Smith, H. W. *et al.* An ErbB2/c-Src axis links bioenergetics with PRC2 translation to drive epigenetic reprogramming and mammary tumorigenesis. *Nat. Commun.* **10**, 2901 (2019).
78. Stetler-Stevenson, W. G. Matrix metalloproteinases in angiogenesis: a moving target for therapeutic intervention. *J. Clin. Invest.* **103**, 1237–41 (1999).
79. Niu, G. & Chen, X. Vascular endothelial growth factor as an anti-angiogenic target for cancer therapy. *Curr. Drug Targets* **11**, 1000–17 (2010).
80. National Cancer Institute. Angiogenesis Inhibitors. https://www.cancer.gov/about-cancer/treatment/types/immunotherapy/angiogenesis-inhibitors-fact-sheet (2018).
81. Eliceiri, B. P. *et al.* Selective requirement for Src kinases during VEGF-induced angiogenesis and vascular permeability. *Mol. Cell* **4**, 915–24 (1999).
82. Werdich, X. Q. & Penn, J. S. Src, Fyn and Yes play differential roles in VEGF-mediated endothelial cell events. *Angiogenesis* **8**, 315–326 (2006).
83. Kilarski, W. W., Jura, N. & Gerwins, P. Inactivation of Src family kinases inhibits angiogenesis in vivo: implications for a mechanism involving organization of the actin cytoskeleton. *Exp. Cell Res.* **291**, 70–82 (2003).
84. Niu, G. *et al.* Constitutive Stat3 activity up-regulates VEGF expression and tumor angiogenesis. *Oncogene* **21**, 2000–2008 (2002).
85. Pang, X. *et al.* Acetoxychavicol acetate suppresses angiogenesis-mediated human prostate tumor growth by targeting VEGF-mediated Src-FAK-Rho GTPase-signaling pathway. *Carcinogenesis* **32**, 904–912 (2011).
86. Cabrita, M. A. *et al.* Focal adhesion kinase inhibitors are potent anti-angiogenic agents. *Mol. Oncol.* **5**, 517–526 (2011).
87. Stone, R. L. *et al.* Focal adhesion kinase: an alternative focus for anti-angiogenesis therapy in ovarian cancer. *Cancer Biol. Ther.* **15**, 919–929 (2014).
88. Abu-Ghazaleh, R., Kabir, J., Jia, H., Lobo, M. & Zachary, I. Src mediates stimulation by vascular endothelial growth factor of the phosphorylation of focal adhesion kinase at tyrosine 861, and migration and anti-apoptosis in endothelial cells. *Biochem. J.* **360**, 255–264 (2001).
89. Boyce, B. F., Yoneda, T., Lowe, C., Soriano, P. & Mundy, G. R. Requirement of pp60c-src expression for osteoclasts to form ruffled borders and resorb bone in mice. *J. Clin. Invest.* **90**, 1622–1627 (1992).
90. Miyazaki, T., Tanaka, S., Sanjay, A. & Baron, R. The role of c-Src kinase in the regulation of osteoclast function. *Mod. Rheumatol.* **16**, 68–74 (2006).
91. Macedo, F. *et al.* Bone Metastases: An Overview. *Oncol. Rev.* **11**, 321 (2017).
92. Zhang, X. H. *et al.* Latent bone metastasis in breast cancer tied to Src-dependent survival signals. *Cancer Cell* **16**, 67–78 (2009).
93. Chiu, J.-H. *et al.* Role of estrogen receptors and Src signaling in mechanisms of bone metastasis by estrogen receptor positive breast cancers. *J. Transl. Med.* **15**, 97 (2017).
94. Myoui, A. *et al.* C-Src Tyrosine Kinase Activity Is Associated with Tumor Colonization in Bone and Lung in an Animal Model of Human Breast Cancer Metastasis. *Cancer Res.* **63**, 5028–5033 (2003).
95. Appel, C. K. *et al.* The Src family kinase inhibitor dasatinib delays pain-related behaviour and conserves bone in a rat model of cancer-induced bone pain. *Sci. Rep.* **7**, 4792 (2017).
96. De Felice, M., Lambert, D., Holen, I., Escott, K. J. & Andrew, D. Effects of Src-kinase inhibition in cancer-induced bone pain. *Mol. Pain* **12**, 1–14 (2016).
97. Saad, F. & Lipton, A. SRC kinase inhibition: Targeting bone metastases and tumor growth in prostate and breast cancer. *Cancer Treat. Rev.* **36**, 177–184 (2010).
98. Boyce, B. F. *et al.* Src Inhibitors in Metastatic Bone Disease. *Clin. Cancer Res.* **12**, 6291s-6295s (2006).
99. Davis, S. J. & van der Merwe, P. A. Lck and the nature of the T cell receptor trigger.

Trends Immunol. **32**, 1–5 (2011).
100. Lo, W.-L. *et al.* Lck promotes Zap70-dependent LAT phosphorylation by bridging Zap70 to LAT. *Nat. Immunol.* **19**, 733–741 (2018).
101. Zhang, W., Sloan-Lancaster, J., Kitchen, J., Trible, R. P. & Samelson, L. E. LAT: The ZAP-70 Tyrosine Kinase Substrate that Links T Cell Receptor to Cellular Activation. *Cell* **92**, 83–92 (1998).
102. Filipp, D. *et al.* Regulation of Fyn through translocation of activated Lck into lipid rafts. *J. Exp. Med.* **197**, 1221–7 (2003).
103. Palacios, E. H. & Weiss, A. Function of the Src-family kinases, Lck and Fyn, in T-cell development and activation. *Oncogene* **23**, 7990–8000 (2004).
104. Chapman, N. M., Connolly, S. F., Reinl, E. L. & Houtman, J. C. D. Focal adhesion kinase negatively regulates Lck function downstream of the T cell antigen receptor. *J. Immunol.* **191**, 6208–21 (2013).
105. Wiemer, A. J. *et al.* The focal adhesion kinase inhibitor PF-562,271 impairs primary CD4+ T cell activation. *Biochem. Pharmacol.* **86**, 770–781 (2013).
106. Gauld, S. B. & Cambier, J. C. Src-family kinases in B-cell development and signaling. *Oncogene* **23**, 8001–8006 (2004).
107. Chan, V. W. F., Meng, F., Soriano, P., DeFranco, A. L. & Lowell, C. A. Characterization of the B Lymphocyte Populations in Lyn-Deficient Mice and the Role of Lyn in Signal Initiation and Down-Regulation. *Immunity* **7**, 69–81 (1997).
108. Hibbs, M. L. *et al.* Sustained Activation of Lyn Tyrosine Kinase In Vivo Leads to Autoimmunity. *J. Exp. Med.* **196**, 1593–1604 (2002).
109. Xu, Y., Harder, K. W., Huntington, N. D., Hibbs, M. L. & Tarlinton, D. M. Lyn Tyrosine Kinase: Accentuating the Positive and the Negative. *Immunity* **22**, 9–18 (2005).
110. Abram, C. L. & Lowell, C. A. The diverse functions of Src family kinases in macrophages. *Frontiers in Bioscience* vol. 13 4426–4450 (2008).
111. Mócsai, A. *et al.* Integrin signaling in neutrophils and macrophages uses adaptors containing immunoreceptor tyrosine-based activation motifs. *Nat. Immunol.* **7**, 1326–1333 (2006).
112. Boulet, I. *et al.* Lipopolysaccharide- and interferon-gamma-induced expression of hck and lyn tyrosine kinases in murine bone marrow-derived macrophages. *Oncogene* **7**, 703–710 (1992).
113. Mitchell, J. *et al.* Src family kinase tyrosine phosphorylates Toll-like receptor 4 to dissociate MyD88 and Mal/Tirap, suppressing LPS-induced inflammatory responses. *Biochem. Pharmacol.* **147**, 119–127 (2018).
114. Ear, T., Tatsiy, O., Allard, F. L. & McDonald, P. P. Regulation of Discrete Functional Responses by Syk and Src Family Tyrosine Kinases in Human Neutrophils. *J. Immunol. Res.* **2017**, 4347121 (2017).
115. Kovács, M. *et al.* The Src family kinases Hck, Fgr, and Lyn are critical for the generation of the in vivo inflammatory environment without a direct role in leukocyte recruitment. *J. Exp. Med.* **211**, 1993–2011 (2014).
116. Gujar, R. *et al.* c-Src Suppresses Dendritic Cell Antitumor Activity via T Cell Ig and Mucin Protein-3 Receptor. *J. Immunol.* **197**, 1650–1662 (2016).
117. Maurya, N. *et al.* Immunoregulation of Dendritic Cells by the Receptor T cell Ig and Mucin Protein-3 via Bruton's Tyrosine Kinase and c-Src. *J. Immunol.* **193**, 3417–3425 (2014).
118. Kotenko, S. V & Pestka, S. Jak-Stat signal transduction pathway through the eyes of cytokine class II receptor complexes. *Oncogene* **19**, 2557–2565 (2000).
119. García-Martínez, J. M. *et al.* A non-catalytic function of the Src family tyrosine kinases controls prolactin-induced Jak2 signaling. *Cell. Signal.* **22**, 415–426 (2010).
120. Rowlinson, S. W. *et al.* An agonist-induced conformational change in the growth hormone receptor determines the choice of signalling pathway. *Nat. Cell Biol.* **10**, 740–747 (2008).
121. Liu, S. T., Pham, H., Pandol, S. J. & Ptasznik, A. Src as the link between inflammation and cancer. *Front. Physiol.* **4**, 416 (2013).
122. Silva, C. M. Role of STATs as downstream signal transducers in Src family kinase-mediated tumorigenesis. *Oncogene* **23**, 8017–8023 (2004).
123. Senis, Y. A., Mazharian, A. & Mori, J. Src family kinases: at the forefront of platelet

activation. *Blood* **124**, 2013–24 (2014).
124. Brave, M. *et al.* Sprycel for Chronic Myeloid Leukemia and Philadelphia Chromosome-Positive Acute Lymphoblastic Leukemia Resistant to or Intolerant of Imatinib Mesylate. *Clin. Cancer Res.* **14**, 352–359 (2008).
125. Chen, R., Wang, F., Zhang, X., Gao, C. & Chen, B. Severe thrombocytopenia after dasatinib treatment in a patient with Philadelphia chromosome-positive chronic myeloid leukemia. *Onco. Targets. Ther.* **8**, 955–7 (2015).
126. Mazharian, A., Ghevaert, C., Zhang, L., Massberg, S. & Watson, S. P. Dasatinib enhances megakaryocyte differentiation but inhibits platelet formation. *Blood* **117**, 5198–5206 (2011).
127. Kowata, S. *et al.* Dasatinib Induced Thrombocytopenia Might Be Due To The Inhibition Of Proplatelet Formation Of Megakaryocytes Via The Pathways Including Rho/Rock and Rac. *Blood* **122**, (2013).
128. Kalia, L. V, Gingrich, J. R. & Salter, M. W. Src in synaptic transmission and plasticity. *Oncogene* **23**, 8007–8016 (2004).
129. Salter, M. W. & Kalia, L. V. Src kinases: a hub for NMDA receptor regulation. *Nat. Rev. Neurosci.* **5**, 317–328 (2004).
130. Rauch, J., Volinsky, N., Romano, D. & Kolch, W. The secret life of kinases: functions beyond catalysis. *Cell Commun. Signal.* **9**, 23 (2011).
131. Schwartzberg, P. L. *et al.* Rescue of osteoclast function by transgenic expression of kinase-deficient Src in src-/- mutant mice. *Genes Dev.* **11**, 2835–44 (1997).
132. Kaplan, K. B., Swedlow, J. R., Morgan, D. O. & Varmus, H. E. c-Src enhances the spreading of src-/- fibroblasts on fibronectin by a kinase-independent mechanism. *Genes Dev.* **9**, 1505–1517 (1995).
133. Schlaepfer, D. D., Broome, M. A. & Hunter, T. Fibronectin-stimulated signaling from a focal adhesion kinase-c-Src complex: involvement of the Grb2, p130cas, and Nck adaptor proteins. *Mol. Cell. Biol.* **17**, 1702–13 (1997).
134. Palanisamy, A. P., Suryakumar, G., Panneerselvam, K., Willey, C. D. & Kuppuswamy, D. A Kinase-Independent Function of c-Src Mediates p130Cas Phosphorylation at the Serine-639 Site in Pressure Overloaded Myocardium. *J. Cell. Biochem.* **116**, 2793–2803 (2015).
135. Brunton, V. G. *et al.* Identification of Src-Specific Phosphorylation Site on Focal Adhesion Kinase: Dissection of the Role of Src SH2 and Catalytic Functions and Their Consequences for Tumor Cell Behavior. *Cancer Res.* **65**, (2005).
136. Cary, L. A., Klinghoffer, R. A., Sachsenmaier, C. & Cooper, J. A. SRC catalytic but not scaffolding function is needed for integrin-regulated tyrosine phosphorylation, cell migration, and cell spreading. *Mol. Cell. Biol.* **22**, 2427–40 (2002).
137. Katsuta, H., Tsuji, S., Niho, Y., Kurosaki, T. & Kitamura, D. Lyn-mediated down-regulation of B cell antigen receptor signaling: inhibition of protein kinase C activation by Lyn in a kinase-independent fashion. *J. Immunol.* **160**, 1547–51 (1998).
138. Xu, H. & Littman, D. R. A kinase-independent function of Lck in potentiating antigen-specific T cell activation. *Cell* **74**, 633–43 (1993).
139. Philipsen, L. *et al.* De novo phosphorylation and conformational opening of the tyrosine kinase Lck act in concert to initiate T cell receptor signaling. *Sci. Signal.* **10**, (2017).
140. Weis, S., Cui, J., Barnes, L. & Cheresh, D. Endothelial barrier disruption by VEGF-mediated Src activity potentiates tumor cell extravasation and metastasis. *J. Cell Biol.* **167**, 223–9 (2004).
141. Criscuoli, M. L., Nguyen, M. & Eliceiri, B. P. Tumor metastasis but not tumor growth is dependent on Src-mediated vascular permeability. *Blood* **105**, 1508–1514 (2005).
142. Sgroi, D. C. Breast Cancer Src Activity: Bad to the Bone. *Cancer Cell* **16**, 1–2 (2009).
143. Gupta, G. P. & Massagué, J. Cancer Metastasis: Building a Framework. *Cell* **127**, 679–695 (2006).
144. Jacobs, C. & Rübsamen, H. Expression of pp60c-src Protein Kinase in Adult and Fetal Human Tissue: High Activities in Some Sarcomas and Mammary Carcinomas. *Cancer Res.* **43**, 1696–1702 (1983).
145. Rosen, N. *et al.* Analysis of pp60c-src protein kinase activity in human tumor cell lines and tissues. *J. Biol. Chem.* **261**, 13754–13759 (1986).

146. Ottenhoff-Kalff, A. E. *et al.* Characterization of protein tyrosine kinases from human breast cancer: involvement of the c-src oncogene product. *Cancer Res.* **52**, 4773–4778 (1992).
147. Cartwright, C. A., Kamps, M. P., Meisler, A. I., Pipas, J. M. & Eckhart, W. pp60c-src activation in human colon carcinoma. *J. Clin. Invest.* **83**, 2025–2033 (1989).
148. Verbeek, B. *et al.* c-Src protein expression is increased in human breast cancer. An immunohistochemical and biochemical analysis. *J. Pathol.* **180**, 383–388 (1996).
149. Varkaris, A., Katsiampoura, A. D., Araujo, J. C., Gallick, G. E. & Corn, P. G. Src signaling pathways in prostate cancer. *Cancer Metastasis Rev.* **33**, 595–606 (2014).
150. Masaki, T. *et al.* pp60c-src activation in lung adenocarcinoma. *Eur. J. Cancer* **39**, 1447–1455 (2003).
151. Lutz, M. P. *et al.* Overexpression and Activation of the Tyrosine Kinase Src in Human Pancreatic Carcinoma. *Biochem. Biophys. Res. Commun.* **243**, 503–508 (1998).
152. van Oijen, M. G., Rijksen, G., ten Broek, F. W. & Slootweg, P. J. Overexpression of c-Src in areas of hyperproliferation in head and neck cancer, premalignant lesions and benign mucosal disorders. *J. Oral Pathol. Med.* **27**, 147–152 (1998).
153. Wiener, J. R. *et al.* Activated Src Protein Tyrosine Kinase Is Overexpressed in Late-Stage Human Ovarian Cancers. *Gynecol. Oncol.* **88**, 73–79 (2003).
154. Masaki, T. *et al.* pp60c-src Activation in hepatocellular carcinoma of humans and LEC rats. *Hepatology* **27**, 1257–1264 (1998).
155. Masaki, T. *et al.* Reduced C-terminal Src kinase (Csk) activities in hepatocellular carcinoma. *Hepatology* **29**, 379–384 (1999).
156. Tan, M. *et al.* ErbB2 promotes Src synthesis and stability: novel mechanisms of Src activation that confer breast cancer metastasis. *Cancer Res.* **65**, 1858–1867 (2005).
157. Talamonti, M. S., Roh, M. S., Curley, S. A. & Gallick, G. E. Increase in activity and level of pp60c-src in progressive stages of human colorectal cancer. *J. Clin. Invest.* **91**, 53–60 (1993).
158. Roseweir, A. K. *et al.* Nuclear expression of Lyn, a Src family kinase member, is associated with poor prognosis in renal cancer patients. *BMC Cancer* **16**, 229 (2016).
159. Wilson, G. R. *et al.* Activated c-SRC in ductal carcinoma in situ correlates with high tumour grade, high proliferation and HER2 positivity. *Br. J. Cancer* **95**, 1410–1414 (2006).
160. Allgayer, H. *et al.* Activation of Src kinase in primary colorectal carcinoma: an indicator of poor clinical prognosis. *Cancer* **94**, 344–351 (2002).
161. Elsberger, B. *et al.* Breast cancer patients' clinical outcome measures are associated with Src kinase family member expression. *Br. J. Cancer* **103**, 899–909 (2010).
162. Forget, A. *et al.* Aberrant ERBB4-SRC Signaling as a Hallmark of Group 4 Medulloblastoma Revealed by Integrative Phosphoproteomic Profiling. *Cancer Cell* **34**, 379-395.e7 (2018).
163. Benhar, M., Engelberg, D. & Levitzki, A. Cisplatin-induced activation of the EGF receptor. *Oncogene* **21**, 8723–8731 (2002).
164. Ischenko, I. *et al.* Inhibition of Src tyrosine kinase reverts chemoresistance toward 5-fluorouracil in human pancreatic carcinoma cells: an involvement of epidermal growth factor receptor signaling. *Oncogene* **27**, 7212–7222 (2008).
165. Peterson-Roth, E., Brdlik, C. M. & Glazer, P. M. Src-Induced Cisplatin Resistance Mediated by Cell-to-Cell Communication. *Cancer Res.* **69**, 3619–3624 (2009).
166. Hawthorne, V. S. *et al.* ErbB2-mediated Src and signal transducer and activator of transcription 3 activation leads to transcriptional up-regulation of p21Cip1 and chemoresistance in breast cancer cells. *Mol. Cancer Res.* **7**, 592–600 (2009).
167. George, J. A., Chen, T. & Taylor, C. C. Src Tyrosine Kinase and Multidrug Resistance Protein-1 Inhibitions Act Independently but Cooperatively to Restore Paclitaxel Sensitivity to Paclitaxel-Resistant Ovarian Cancer Cells. *Cancer Res.* **65**, (2005).
168. Duxbury, M. S., Ito, H., Zinner, M. J., Ashley, S. W. & Whang, E. E. siRNA directed against c-Src enhances pancreatic adenocarcinoma cell gemcitabine chemosensitivity. *J. Am. Coll. Surg.* **198**, 953–959 (2004).
169. Duxbury, M. S., Ito, H., Zinner, M. J., Ashley, S. W. & Whang, E. E. Inhibition of SRC tyrosine kinase impairs inherent and acquired gemcitabine resistance in human

pancreatic adenocarcinoma cells. *Clin. Cancer Res.* **10**, 2307–2318 (2004).
170. Buettner, R. *et al.* Activated STAT signaling in human tumors provides novel molecular targets for therapeutic intervention. *Clin. Cancer Res.* **8**, 945–954 (2002).
171. Tian, J. *et al.* Dasatinib sensitises triple negative breast cancer cells to chemotherapy by targeting breast cancer stem cells. *Br. J. Cancer* **119**, 1495–1507 (2018).
172. Pichot, C. S. *et al.* Dasatinib synergizes with doxorubicin to block growth, migration, and invasion of breast cancer cells. *Br. J. Cancer* **101**, 38–47 (2009).
173. Kopetz, S. *et al.* Synergistic Activity of the Src Family Kinase Inhibitor Dasatinib and Oxaliplatin in Colon Carcinoma Cells Is Mediated by Oxidative Stress. *Cancer Res.* **69**, 3842–3849 (2009).
174. Riggins, R. B. *et al.* Physical and Functional Interactions between Cas and c-Src Induce Tamoxifen Resistance of Breast Cancer Cells through Pathways Involving Epidermal Growth Factor Receptor and Signal Transducer and Activator of Transcription 5b. *Cancer Res.* **66**, 7007–7015 (2006).
175. Hiscox, S. *et al.* Dual targeting of Src and ER prevents acquired antihormone resistance in breast cancer cells. *Breast Cancer Res. Treat.* **115**, 57–67 (2009).
176. Tatarov, O. *et al.* Src Family Kinase Activity Is Up-Regulated in Hormone-Refractory Prostate Cancer. *Clin. Cancer Res.* **15**, 3540–3549 (2009).
177. Yang, C.-C. *et al.* Downregulation of c-SRC kinase CSK promotes castration resistant prostate cancer and pinpoints a novel disease subclass. *Oncotarget* **6**, 22060–22071 (2015).
178. Wheeler, D. L. *et al.* Epidermal growth factor receptor cooperates with Src family kinases in acquired resistance to cetuximab. *Cancer Biol. Ther.* **8**, 696–703 (2009).
179. Murakami, Y. *et al.* The activation of SRC family kinases and focal adhesion kinase with the loss of the amplified, mutated EGFR gene contributes to the resistance to afatinib, erlotinib and osimertinib in human lung cancer cells. *Oncotarget* **8**, 70736–70751 (2017).
180. Yoshida, R. *et al.* Activation of Src signaling mediates acquired resistance to ALK inhibition in lung cancer. *Int. J. Oncol.* **51**, 1533–1540 (2017).
181. Zhou, Q., Guo, X. & Choksi, R. Activation of Focal Adhesion Kinase and Src Mediates Acquired Sorafenib Resistance in A549 Human Lung Adenocarcinoma Xenografts. *J. Pharmacol. Exp. Ther.* **363**, 428–443 (2017).
182. Rexer, B. N. *et al.* Phosphoproteomic mass spectrometry profiling links Src family kinases to escape from HER2 tyrosine kinase inhibition. *Oncogene* **30**, 4163–4174 (2011).
183. Zhang, S. *et al.* Combating trastuzumab resistance by targeting SRC, a common node downstream of multiple resistance pathways. *Nat. Med.* **17**, 461–469 (2011).
184. Sato, H. *et al.* Src regulates insulin secretion and glucose metabolism by influencing subcellular localization of glucokinase in pancreatic β-cells. *J. Diabetes Investig.* **7**, 171–178 (2016).
185. Zhang, W. *et al.* Role of Src in Vascular Hyperpermeability Induced by Advanced Glycation End Products. *Sci. Rep.* **5**, 14090 (2015).
186. Kim, S. R. & Suh, W. Beneficial effects of the Src inhibitor, dasatinib, on breakdown of the blood-retinal barrier. *Arch. Pharm. Res.* **40**, 197–203 (2017).
187. Werdich, X. Q. & Penn, J. S. Src Family Kinases, New Therapeutic Targets for Intervention of VEGF–Mediated Retinopathy. *Invest. Ophthalmol. Vis. Sci.* **46**, 1426–1426 (2005).
188. Taniguchi, K. *et al.* Inhibition of Src kinase blocks high glucose-induced EGFR transactivation and collagen synthesis in mesangial cells and prevents diabetic nephropathy in mice. *Diabetes* **62**, 3874–86 (2013).
189. Wang, J. & Zhuang, S. Src family kinases in chronic kidney disease. *Am. J. Physiol. Physiol.* **313**, F721–F728 (2017).
190. Hu, M. *et al.* Therapeutic Targeting of Src Kinase in Myofibroblast Differentiation and Pulmonary Fibrosis. *J. Pharmacol. Exp. Ther.* **351**, 87–95 (2014).
191. AstraZeneca. US FDA grants saracatinib Orphan Drug Designation for idiopathic pulmonary fibrosis. https://www.astrazeneca.com/media-centre/press-releases/2019/us-fda-grants-saracatinib-orphan-drug-designation-for-idiopathic-pulmonary-fibrosis-18032019.html (2019).

192. Pham, H. *et al.* Essential Role of Lyn in Fibrosis. *Front. Physiol.* **7**, 387 (2016).
193. Li, Y., Xiong, L. & Gong, J. Lyn kinase enhanced hepatic fibrosis by modulating the activation of hepatic stellate cells. *Am. J. Transl. Res.* **9**, 2865–2877 (2017).
194. Mascarenhas, J. & Hoffman, R. Ruxolitinib: The First FDA Approved Therapy for the Treatment of Myelofibrosis. *Clin. Cancer Res.* **18**, 3008–3014 (2012).
195. Danysz, W. & Parsons, C. G. The NMDA receptor antagonist memantine as a symptomatological and neuroprotective treatment for Alzheimer's disease: preclinical evidence. *Int. J. Geriatr. Psychiatry* **18**, S23–S32 (2003).
196. Mota, S. I. *et al.* Impaired Src signaling and post-synaptic actin polymerization in Alzheimer's disease mice hippocampus — Linking NMDA receptors and the reelin pathway. *Exp. Neurol.* **261**, 698–709 (2014).
197. Liu, J., Chang, L., Song, Y., Li, H. & Wu, Y. The Role of NMDA Receptors in Alzheimer's Disease. *Front. Neurosci.* **13**, 43 (2019).
198. Ittner, L. M. *et al.* Dendritic Function of Tau Mediates Amyloid-β Toxicity in Alzheimer's Disease Mouse Models. *Cell* **142**, 387–397 (2010).
199. Um, J. W. *et al.* Alzheimer amyloid-β oligomer bound to postsynaptic prion protein activates Fyn to impair neurons. *Nat. Neurosci.* **15**, 1227–35 (2012).
200. Dhawan, G. & Combs, C. K. Inhibition of Src kinase activity attenuates amyloid associated microgliosis in a murine model of Alzheimer's disease. *J. Neuroinflammation* **9**, 563 (2012).
201. Mitrasinovic, O. M., Ryan, H., Poon, C. & Murphy, G. M. Src tyrosine kinase signaling regulates microglial protection of neurons from excitotoxicity. *Alzheimer's Dement.* **1**, S73–S74 (2005).
202. Kaufman, A. C. *et al.* Fyn inhibition rescues established memory and synapse loss in Alzheimer mice. *Ann. Neurol.* **77**, 953–71 (2015).
203. van Dyck, C. H. *et al.* Effect of AZD0530 on Cerebral Metabolic Decline in Alzheimer Disease. *JAMA Neurol.* **76**, 1219–1229 (2019).
204. Song, C., Zhang, Y., Parsons, C. G. & Liu, Y. F. Expression of polyglutamine-expanded huntingtin induces tyrosine phosphorylation of N-methyl-D-aspartate receptors. *J. Biol. Chem.* **278**, 33364–33369 (2003).
205. Salter, M. W. & Pitcher, G. M. Dysregulated Src upregulation of NMDA receptor activity: a common link in chronic pain and schizophrenia. *FEBS J.* **279**, 2–11 (2012).
206. Chu, J. J. H. & Yang, P. L. c-Src protein kinase inhibitors block assembly and maturation of dengue virus. *Proc. Natl. Acad. Sci. U. S. A.* **104**, 3520–3525 (2007).
207. de Wispelaere, M., LaCroix, A. J. & Yang, P. L. The small molecules AZD0530 and dasatinib inhibit dengue virus RNA replication via Fyn kinase. *J. Virol.* **87**, 7367–7381 (2013).
208. Liang, Y. & Roizman, B. State and role of SRC family kinases in replication of herpes simplex virus 1. *J. Virol.* **80**, 3349–3359 (2006).
209. Hirsch, A. J. *et al.* The Src Family Kinase c-Yes Is Required for Maturation of West Nile Virus Particles. *J. Virol.* **79**, 11943–11951 (2005).
210. Dupont, L. *et al.* Src family kinase activity drives cytomegalovirus reactivation by recruiting MOZ histone acetyltransferase activity to the viral promoter. *J. Biol. Chem.* **294**, 12901–12910 (2019).
211. Gilbert, C., Barat, C., Cantin, R. & Tremblay, M. J. Involvement of Src and Syk Tyrosine Kinases in HIV-1 Transfer from Dendritic Cells to CD4+ T Lymphocytes. *J. Immunol.* **178**, 2862–2871 (2007).
212. McCarthy, S. D. S., Sakac, D., Neschadim, A. & Branch, D. R. c-SRC protein tyrosine kinase regulates early HIV-1 infection post-entry. *AIDS* **30**, 849–858 (2016).
213. McCarthy, S. D. S., Jung, D., Sakac, D. & Branch, D. R. The c-Src and Pyk2 protein tyrosine kinases play protective roles in early HIV-1 infection of CD4+ T cell lines. *JAIDS J. Acquir. Immune Defic. Syndr.* **66**, 1 (2014).
214. Park, G. Bin *et al.* The Epstein-Barr Virus Causes Epithelial–Mesenchymal Transition in Human Corneal Epithelial Cells Via Syk/Src and Akt/Erk Signaling Pathways. *Investig. Opthalmology Vis. Sci.* **55**, 1770–1779 (2014).
215. Liu, S. *et al.* Lck/Hck/Fgr-Mediated Tyrosine Phosphorylation Negatively Regulates TBK1 to Restrain Innate Antiviral Responses. *Cell Host Microbe* **21**, 754-768.e5 (2017).

216. Brunton, V. G. & Frame, M. C. Src and focal adhesion kinase as therapeutic targets in cancer. *Curr. Opin. Pharmacol.* **8**, 427–432 (2008).
217. Puls, L. N., Eadens, M. & Messersmith, W. Current Status of Src Inhibitors in Solid Tumor Malignancies. *Oncologist* **16**, 566–578 (2011).
218. Lombardo, L. J. *et al.* Discovery of N -(2-Chloro-6-methyl- phenyl)-2-(6-(4-(2-hydroxyethyl)- piperazin-1-yl)-2-methylpyrimidin-4- ylamino)thiazole-5-carboxamide (BMS-354825), a Dual Src/Abl Kinase Inhibitor with Potent Antitumor Activity in Preclinical Assays. *J. Med. Chem.* **47**, 6658–6661 (2004).
219. Golas, J. M. *et al.* SKI-606, a 4-anilino-3-quinolinecarbonitrile dual inhibitor of Src and Abl kinases, is a potent antiproliferative agent against chronic myelogenous leukemia cells in culture and causes regression of K562 xenografts in nude mice. *Cancer Res.* **63**, 375–381 (2003).
220. Roskoski, R. Properties of FDA-approved small molecule protein kinase inhibitors. *Pharmacol. Res.* **144**, 19–50 (2019).
221. Anastassiadis, T., Deacon, S. W., Devarajan, K., Ma, H. & Peterson, J. R. Comprehensive assay of kinase catalytic activity reveals features of kinase inhibitor selectivity. *Nat. Biotechnol.* **29**, 1039–1045 (2011).
222. Lovera, S. *et al.* The Different Flexibility of c-Src and c-Abl Kinases Regulates the Accessibility of a Druggable Inactive Conformation. *J. Am. Chem. Soc.* **134**, 2496–2499 (2012).
223. Quintás-Cardama, A. *et al.* Preclinical characterization of the selective JAK1/2 inhibitor INCB018424: therapeutic implications for the treatment of myeloproliferative neoplasms. *Blood* **115**, 3109–17 (2010).
224. Green, T. P. *et al.* Preclinical anticancer activity of the potent, oral Src inhibitor AZD0530. *Mol. Oncol.* **3**, 248–261 (2009).
225. Duan, Y., Chen, L., Chen, Y. & Fan, X. c-Src binds to the cancer drug Ruxolitinib with an active conformation. *PLoS One* **9**, e106225 (2014).
226. O'Hare, T. *et al.* AP24534, a Pan-BCR-ABL Inhibitor for Chronic Myeloid Leukemia, Potently Inhibits the T315I Mutant and Overcomes Mutation-Based Resistance. *Cancer Cell* **16**, 401–412 (2009).
227. Roth, G. J. *et al.* Design, Synthesis, and Evaluation of Indolinones as Triple Angiokinase Inhibitors and the Discovery of a Highly Specific 6-Methoxycarbonyl-Substituted Indolinone (BIBF 1120). *J. Med. Chem.* **52**, 4466–4480 (2009).
228. Dalgarno, D. *et al.* Structural Basis of Src Tyrosine Kinase Inhibition with a New Class of Potent and Selective Trisubstituted Purine-based Compounds. *Chem. Biol. Drug Des.* **67**, 46–57 (2006).
229. Apsel, B. *et al.* Targeted polypharmacology: Discovery of dual inhibitors of tyrosine and phosphoinositide kinases. *Nat. Chem. Biol.* **4**, 691 (2008).
230. Gilani, R. A. *et al.* UM-164: A potent c-Src/p38 kinase inhibitor with in vivo activity against triple-negative breast cancer. *Clin. Cancer Res.* **22**, 5087–5096 (2016).
231. Kwarcinski, F. E. *et al.* Conformation-Selective Analogues of Dasatinib Reveal Insight into Kinase Inhibitor Binding and Selectivity. *ACS Chem. Biol.* **11**, 1296–1304 (2016).
232. King, E. R. & Wong, K.-K. Insulin-like Growth Factor: Current Concepts and New Developments in Cancer Therapy. *Recent Pat. Anticancer. Drug Discov.* **7**, 14 (2012).
233. Zhai, D., Deng, W., Huang, Z., Rogers, E. & Cui., J. J. Abstract 2132: The novel, rationally-designed, ALK/SRC inhibitor TPX-0005 overcomes multiple acquired resistance mechanisms to current ALK inhibitors. *Exp. Mol. Ther.* **76**, 2132 (2016).
234. Carna Biosciences Inc. Kinase Profiling Book. 5 https://www.carnabio.com/output/pdf/ProfilingProfilingBook_en.pdf (2019).
235. MW, M. *et al.* Novel 2-Aminopyrimidine Carbamates as Potent and Orally Active Inhibitors of Lck: Synthesis, SAR, and in Vivo Antiinflammatory Activity. *J. Med.* **49**, 4981–4991 (2006).
236. Bu, Y. *et al.* KXO1 (KX2-391), a Src-family kinase inhibitor targeting the peptide-binding domain, suppresses oncogenic proliferation in vitro and in vivo. *Exp. Mol. Ther.* **68**, 4983–4983 (2008).
237. Hanke, J. H. *et al.* Discovery of a novel, potent, and Src family-selective tyrosine kinase inhibitor. Study of Lck- and FynT-dependent T cell activation. *J. Biol. Chem.*

271, 695–701 (1996).
238. Girotti, M. R. *et al.* Paradox-breaking RAF inhibitors that also target SRC are effective in drug-resistant BRAF mutant melanoma. *Cancer Cell* **27**, 85–96 (2015).
239. Halaban, R. *et al.* A novel anti-melanoma SRC-family kinase inhibitor. *Oncotarget* **10**, 2237–2251 (2019).
240. Brandvold, R., Ste, M. E., Fox, C. C. & Soellner, M. B. Development of a Highly Selective c-Src Kinase Inhibitor. *ACS Chem. Biol.* **7**, 1393–1398 (2012).
241. Chan, W. W. *et al.* Conformational control inhibition of the BCR-ABL1 tyrosine kinase, including the gatekeeper T315I mutant, by the switch-control inhibitor DCC-2036. *Cancer Cell* **19**, 556–68 (2011).
242. Tian, G., Cory, M., Smith, A. A. & Knight, W. B. Structural Determinants for Potent, Selective Dual Site Inhibition of Human pp60 c-src by 4-Anilinoquinazolines. *Biochemistry* **40**, 7084–7091 (2001).
243. Arnold, L. D. *et al.* Pyrrolo[2,3-d]pyrimidines containing an extended 5-substituent as potent and selective inhibitors of lck I. *Bioorg. Med. Chem. Lett.* **10**, 2167–2170 (2000).
244. Blake, R. A. *et al.* SU6656, a Selective Src Family Kinase Inhibitor, Used To Probe Growth Factor Signaling. *Mol. Cell. Biol.* **20**, 9018–9027 (2000).
245. Kimura, S. *et al.* NS-187, a potent and selective dual Bcr-Abl/Lyn tyrosine kinase inhibitor, is a novel agent for imatinib-resistant leukemia. *Blood* **106**, 3948–3954 (2005).
246. U.S. National Institutes of Health. ClinicalTrials.gov. https://clinicaltrials.gov (2019).
247. Kennedy, L. C. & Gadi, V. Dasatinib in breast cancer: Src-ing for response in all the wrong kinases. *Ann. Transl. Med.* **6**, S60 (2018).
248. Finn, R. S. *et al.* Dasatinib as a single agent in triple-negative breast cancer: results of an open-label phase 2 study. *Clin. Cancer Res. An Off. J. Am. Assoc. Cancer Res.* **17**, 6905–6913 (2011).
249. Mayer, E. L. *et al.* A Phase 2 Trial of Dasatinib in Patients with Advanced HER2-Positive and/or Hormone Receptor-Positive Breast Cancer. *Clin. Cancer Res.* **17**, 6897–6904 (2011).
250. Llombart, A. *et al.* PD01-02: Randomized Phase II Study of Dasatinib vs Placebo in Addition to Exemestane in Advanced ER/PR-Positive Breast Cancer [BMS CA180-261 Study]. *Cancer Res.* **71**, PD01-02 (2011).
251. AACR. Split Verdict on Dasatinib-Letrozole for Metastatic Breast Cancer. *Cancer Discov.* **4**, 138–139 (2014).
252. Morris, P. G. *et al.* Phase II Study of Paclitaxel and Dasatinib in Metastatic Breast Cancer. *Clin. Breast Cancer* **18**, 387–394 (2018).
253. Sgroi, V. *et al.* Complete response in advanced breast cancer patient treated with a combination of capecitabine, oral vinorelbine and dasatinib. *Exp. Hematol. Oncol.* **7**, 2 (2018).
254. Moy, B. *et al.* Bosutinib in combination with the aromatase inhibitor exemestane: a phase II trial in postmenopausal women with previously treated locally advanced or metastatic hormone receptor-positive/HER2-negative breast cancer. *Oncologist* **19**, 346–347 (2014).
255. Moy, B. *et al.* Bosutinib in combination with the aromatase inhibitor letrozole: a phase II trial in postmenopausal women evaluating first-line endocrine therapy in locally advanced or metastatic hormone receptor-positive/HER2-negative breast cancer. *Oncologist* **19**, 348–349 (2014).
256. Araujo, J. C. *et al.* Docetaxel and dasatinib or placebo in men with metastatic castration-resistant prostate cancer (READY): a randomised, double-blind phase 3 trial. *Lancet Oncol.* **14**, 1307–1316 (2013).
257. McNeish, I. A. *et al.* A randomised, placebo-controlled trial of weekly paclitaxel and saracatinib (AZD0530) in platinum-resistant ovarian, fallopian tube or primary peritoneal cancer. *Ann. Oncol.* **25**, 1988–1995 (2014).
258. Pusztai, L. *et al.* Gene Signature–Guided Dasatinib Therapy in Metastatic Breast Cancer. *Clin. Cancer Res.* **20**, 5265–5271 (2014).
259. Herold, C. I. *et al.* Phase II Trial of Dasatinib in Patients with Metastatic Breast Cancer Using Real-Time Pharmacodynamic Tissue Biomarkers of Src Inhibition to

Escalate Dosing. *Clin. Cancer Res.* **17**, 6061–6070 (2011).
260. Schott, A. F. *et al.* Phase II studies of two different schedules of dasatinib in bone metastasis predominant metastatic breast cancer: SWOG S0622. *Breast Cancer Res. Treat.* **159**, 87–95 (2016).
261. Campone, M. *et al.* Phase II study of single-agent bosutinib, a Src/Abl tyrosine kinase inhibitor, in patients with locally advanced or metastatic breast cancer pretreated with chemotherapy. *Ann. Oncol.* **23**, 610–617 (2012).
262. Gucalp, A. *et al.* Phase II Trial of Saracatinib (AZD0530), an Oral SRC-inhibitor for the Treatment of Patients with Hormone Receptor-negative Metastatic Breast Cancer. *Clin. Breast Cancer* **11**, 306–311 (2011).
263. Wright, G. L. *et al.* PD01-01: Randomized Phase II Trial of Fulvestrant with or without Dasatinib in Postmenopausal Patients with Hormone Receptor-Positive Metastatic Breast Cancer Previously Treated with an Aromatase Inhibitor. *Cancer Res.* **71**, PD01-01 (2011).
264. Ocana Fernandez, A. *et al.* A phase II trial of dasatinib (D) in combination with trastuzumab (T) and paclitaxel (P) in the first line treatment of HER2 positive metastatic breast cancer (MBC) patients (pts): GEICAM/2010-04. *Ann. Oncol.* **28**, (2017).
265. Somlo, G. *et al.* Dasatinib plus capecitabine for advanced breast cancer: safety and efficacy in phase I study CA180004. *Clin. Cancer Res.* **19**, 1884–1893 (2013).
266. Fornier, M. N. *et al.* A phase I study of dasatinib and weekly paclitaxel for metastatic breast cancer. *Ann. Oncol.* **22**, 2575–2581 (2011).
267. Herbolsheimer, P. *et al.* Phase I trial of dasatinib and ixabepilone in patients with solid tumors. *Invest. New Drugs* **31**, 92–98 (2013).
268. Mitri, Z. *et al.* TBCRC-010: Phase I/II Study of Dasatinib in Combination with Zoledronic Acid for the Treatment of Breast Cancer Bone Metastasis. *Clin. Cancer Res.* **22**, 5706–5712 (2016).
269. Isakoff, S. J. *et al.* Bosutinib plus capecitabine for selected advanced solid tumours: results of a phase 1 dose-escalation study. *Br. J. Cancer* **111**, 2058–2066 (2014).
270. Tripathi, R., Liu, Z. & Plattner, R. Enabling Tumor Growth and Progression: Recent Progress in Unraveling the Functions of ABL Kinases in Solid Tumor Cells. *Curr. Pharmacol. Reports* **4**, 367–379 (2018).
271. Greuber, E. K., Smith-Pearson, P., Wang, J. & Pendergast, A. M. Role of ABL family kinases in cancer: from leukaemia to solid tumours. *Nat. Rev. Cancer* **13**, 559–571 (2013).
272. Srinivasan, D. & Plattner, R. Activation of Abl Tyrosine Kinases Promotes Invasion of Aggressive Breast Cancer Cells. *Cancer Res.* **66**, 5648–5655 (2006).
273. Srinivasan, D., Sims, J. T. & Plattner, R. Aggressive breast cancer cells are dependent on activated Abl kinases for proliferation, anchorage-independent growth and survival. *Oncogene* **27**, 1095–1105 (2007).
274. Lo, Y.-H., Ho, P.-C., Zhao, H. & Wang, S.-C. Inhibition of c-ABL sensitizes breast cancer cells to the dual ErbB receptor tyrosine kinase inhibitor lapatinib (GW572016). *Anticancer Res.* **31**, 789–795 (2011).
275. Weigel, M. T. *et al.* Enhanced expression of the PDGFR/Abl signaling pathway in aromatase inhibitor-resistant breast cancer. *Ann. Oncol.* **24**, 126–133 (2013).
276. Zhao, H. *et al.* Enhanced resistance to tamoxifen by the c-ABL proto-oncogene in breast cancer. *Neoplasia* **12**, 214–23 (2010).
277. Sirvent, A., Boureux, A., Simon, V., Leroy, C. & Roche, S. The tyrosine kinase Abl is required for Src-transforming activity in mouse fibroblasts and human breast cancer cells. *Oncogene* **26**, 7313–7323 (2007).
278. Gil-Henn, H. *et al.* Arg/Abl2 promotes invasion and attenuates proliferation of breast cancer in vivo. *Oncogene* **32**, 2622–2630 (2013).
279. Sawyers, C. L., McLaughlin, J., Goga, A., Havlik, M. & Witte, O. The nuclear tyrosine kinase c-abl negatively regulates cell growth. *Cell* **77**, 121–131 (1994).
280. Goga, A. *et al.* p53 dependent growth suppression by the c-Abl nuclear tyrosine kinase. *Oncogene* **11**, 791–799 (1995).
281. Morrison, C. D. *et al.* c-Abl inhibits breast cancer tumorigenesis through reactivation of p53-mediated p21 expression. *Oncotarget* **7**, 72777–72794 (2016).

282. Morrison, C. D., Chang, J. C., Keri, R. A. & Schiemann, W. P. Mutant p53 dictates the oncogenic activity of c-Abl in triple-negative breast cancers. *Cell Death Dis.* **8**, e2899–e2899 (2017).
283. Kain, K. H. & Klemke, R. L. Inhibition of Cell Migration by Abl Family Tyrosine Kinases through Uncoupling of Crk-CAS Complexes. *J. Biol. Chem.* **276**, 16185–16192 (2001).
284. Kain, K. H., Gooch, S. & Klemke, R. L. Cytoplasmic c-Abl provides a molecular 'Rheostat' controlling carcinoma cell survival and invasion. *Oncogene* **22**, 6071–6080 (2003).
285. Noren, N. K., Foos, G., Hauser, C. A. & Pasquale, E. B. The EphB4 receptor suppresses breast cancer cell tumorigenicity through an Abl–Crk pathway. *Nat. Cell Biol.* **8**, 815–825 (2006).
286. Varzavand, A. *et al.* a3b1 integrin suppresses prostate cancer metastasis via regulation of the Hippo pathway. *Cancer Res.* **76**, 6577–6587 (2016).
287. Qiu, Z., Cang, Y. & Goff, S. P. c-Abl tyrosine kinase regulates cardiac growth and development. *Proc. Natl. Acad. Sci.* **107**, 1136–114 (2010).
288. Kerkelä, R. *et al.* Cardiotoxicity of the cancer therapeutic agent imatinib mesylate. *Nat. Med.* **12**, 908–916 (2006).
289. Steegmann, J. L., Cervantes, F., le Coutre, P., Porkka, K. & Saglio, G. Off-target effects of BCR-ABL1 inhibitors and their potential long-term implications in patients with chronic myeloid leukemia. *Leuk. Lymphoma* **53**, 2351–2361 (2012).
290. Serrels, A. *et al.* Nuclear FAK Controls Chemokine Transcription, Tregs, and Evasion of Anti-tumor Immunity. *Cell* **163**, 160–173 (2015).
291. Li, B. *et al.* Epigenetic Regulation of CXCL12 Plays a Critical Role in Mediating Tumor Progression and the Immune Response In Osteosarcoma. *Cancer Res.* **78**, 3938–3953 (2018).
292. Dabovic, B. *et al.* Dual functions for LTBP in lung development: LTBP-4 independently modulates elastogenesis and TGF-β activity. *J. Cell. Physiol.* **219**, 14–22 (2009).
293. Canel, M. *et al.* Nuclear FAK and Runx1 Cooperate to Regulate IGFBP3, Cell-Cycle Progression, and Tumor Growth. *Cancer Res.* **77**, (2017).
294. Cho, S.-J., Park, M. H., Han, C., Yoon, K. & Koh, Y. H. VEGFR2 alteration in Alzheimer's disease. *Sci. Rep.* **7**, 17713 (2017).
295. Shaw, F. L. *et al.* A Detailed Mammosphere Assay Protocol for the Quantification of Breast Stem Cell Activity. *J. Mammary Gland Biol. Neoplasia* **17**, 111–117 (2012).
296. Jafari, R. *et al.* The cellular thermal shift assay for evaluating drug target interactions in cells. *Nat. Protoc.* **9**, 2100–22 (2014).
297. Macleod, K. G., Serrels, B. & Carragher, N. O. Reverse Phase Protein Arrays and Drug Discovery. *Methods Mol. Biol.* **1647**, 153–169 (2017).
298. Seeliger, M. A. *et al.* High yield bacterial expression of active c-Abl and c-Src tyrosine kinases. *Protein Sci.* **14**, 3135–3139 (2005).
299. Levinson, N. M. & Boxer, S. G. A conserved water-mediated hydrogen bond network defines bosutinib's kinase selectivity. *Nat. Chem. Biol.* **10**, 127–132 (2014).
300. Kabsch, W. XDS. *Acta Crystallogr. Sect. D Biol. Crystallogr.* **66**, 125–132 (2010).
301. Evans, P. R. & Murshudov, G. N. How good are my data and what is the resolution? *Acta Crystallogr. Sect. D Biol. Crystallogr.* **69**, 1204–1214 (2013).
302. McCoy, A. J. *et al. Phaser* crystallographic software. *J. Appl. Crystallogr.* **40**, 658–674 (2007).
303. Murshudov, G. N., Vagin, A. A. & Dodson, E. J. Refinement of Macromolecular Structures by the Maximum-Likelihood Method. *Acta Crystallogr. Sect. D Biol. Crystallogr.* **53**, 240–255 (1997).
304. Emsley, P. & Cowtan, K. *Coot* : model-building tools for molecular graphics. *Acta Crystallogr. Sect. D Biol. Crystallogr.* **60**, 2126–2132 (2004).
305. Shao, Z. *et al.* Choroid Sprouting Assay: An Ex Vivo Model of Microvascular Angiogenesis. *PLoS One* **8**, e69552 (2013).
306. Bankhead, P. *et al.* QuPath: Open source software for digital pathology image analysis. *Sci. Rep.* **7**, 16878 (2017).
307. Wellcome Trust Sanger Institute. Genomics of Drug Sensitivity in Cancer.

http://www.cancerrxgene.org/.
308. Park, B. J., Whichard, Z. L. & Corey, S. J. Dasatinib synergizes with both cytotoxic and signal transduction inhibitors in heterogeneous breast cancer cell lines--lessons for design of combination targeted therapy. *Cancer Lett.* **320**, 104–10 (2012).
309. Teoh, D. *et al.* Dasatinib (BMS-35482) interacts synergistically with docetaxel, gemcitabine, topotecan and doxorubicin in ovarian cancer cells with high SRC pathway activation and protein expression. *Int. J. Gynecol. Cancer* **24**, 218–225 (2014).
310. Konecny, G. E. *et al.* Activity of the multikinase inhibitor dasatinib against ovarian cancer cells. *Br. J. Cancer* **101**, 1699–708 (2009).
311. Simpkins, F. *et al.* Dual Src and MEK inhibition decreases ovarian cancer growth and targets tumor initiating stem-like cells. *Clin. Cancer Res.* **24**, 4874–4886 (2018).
312. Lieu, C. & Kopetz, S. The SRC family of protein tyrosine kinases: a new and promising target for colorectal cancer therapy. *Clin. Colorectal Cancer* **9**, 89–94 (2010).
313. Girotti, M. R. *et al.* Inhibiting EGF Receptor or SRC Family Kinase Signaling Overcomes BRAF Inhibitor Resistance in Melanoma. *Cancer Discov.* **3**, 158–167 (2013).
314. Spender, L. C. *et al.* Mutational activation of BRAF confers sensitivity to transforming growth factor beta inhibitors in human cancer cells. *Oncotarget* **7**, 81995–82012 (2016).
315. Kelber, J. A. *et al.* KRas Induces a Src/PEAK1/ErbB2 Kinase Amplification Loop That Drives Metastatic Growth and Therapy Resistance in Pancreatic Cancer. *Cancer Res.* **72**, 2554 (2012).
316. Fiorio Pla, A. *et al.* Differential sensitivity of prostate tumor derived endothelial cells to sorafenib and sunitinib. *BMC Cancer* **14**, 939 (2014).
317. Huang, D. *et al.* Sunitinib Acts Primarily on Tumor Endothelium rather than Tumor Cells to Inhibit the Growth of Renal Cell Carcinoma. *Cancer Res.* **70**, 1053–1062 (2010).
318. Ferreira, A. K. *et al.* Anti-Angiogenic and Anti-Metastatic Activity of Synthetic Phosphoethanolamine. *PLoS One* **8**, e57937 (2013).
319. Fraser, C. The Design and Development of Novel mTOR and SRC Family Kinase Inhibitors via a Phenotypic Drug Discovery Approach. (University of Edinburgh, 2015).
320. Brasher, B. B. & Van Etten, R. A. c-Abl has high intrinsic tyrosine kinase activity that is stimulated by mutation of the Src homology 3 domain and by autophosphorylation at two distinct regulatory tyrosines. *J. Biol. Chem.* **275**, 35631–7 (2000).
321. Meyn, M. A. *et al.* Src Family Kinases Phosphorylate the Bcr-Abl SH3-SH2 Region and Modulate Bcr-Abl Transforming Activity. *J. Biol. Chem.* **281**, 30907–30916 (2006).
322. de Jong, R., ten Hoeve, J., Heisterkamp, N. & Groffen, J. Tyrosine 207 in CRKL is the BCR/ABL phosphorylation site. *Oncogene* **14**, 507–513 (1997).
323. Mateus, A., Määttä, T. A. & Savitski, M. M. Thermal proteome profiling: unbiased assessment of protein state through heat-induced stability changes. *Proteome Sci.* **15**, 13 (2016).
324. Savitski, M. M. *et al.* Tracking cancer drugs in living cells by thermal profiling of the proteome. *Science* **346**, (2014).
325. Deininger, M., Buchdunger, E. & Druker, B. J. The development of imatinib as a therapeutic agent for chronic myeloid leukemia. *Blood* **105**, 2640–2653 (2005).
326. Quentmeier, H., Eberth, S., Romani, J., Zaborski, M. & Drexler, H. G. BCR-ABL1-independent PI3Kinase activation causing imatinib-resistance. *J. Hematol. Oncol.* **4**, 6 (2011).
327. Vultur, A. *et al.* SKI-606 (bosutinib), a novel Src kinase inhibitor, suppresses migration and invasion of human breast cancer cells. *Mol Cancer Ther* **7**, 1185–1194 (2008).
328. Chang, Y.-M. *et al.* Src family kinase oncogenic potential and pathways in prostate cancer as revealed by AZD0530. *Oncogene* **27**, 6365–6375 (2008).
329. Purnell, P. R. *et al.* The Src inhibitor AZD0530 blocks invasion and may act as a

radiosensitizer in lung cancer cells. *J. Thorac. Oncol.* **4**, 448–454 (2009).
330. Wu, Z.-H. *et al.* Src Inhibition Can Synergize with Gemcitabine and Reverse Resistance in Triple Negative Breast Cancer Cells via the AKT/c-Jun Pathway. *PLoS One* **11**, e0169230 (2016).
331. Nam, H.-J. *et al.* Antitumor Activity of Saracatinib (AZD0530), a c-Src/Abl Kinase Inhibitor, Alone or in Combination with Chemotherapeutic Agents in Gastric Cancer. *Mol. Cancer Ther.* **12**, 16–26 (2013).
332. Nam, A.-R. *et al.* Src as a Therapeutic Target in Biliary Tract Cancer. *Mol. Cancer Ther.* **15**, 1515–1524 (2016).
333. Lin, A. *et al.* Off-target toxicity is a common mechanism of action of cancer drugs undergoing clinical trials. *Sci. Transl. Med.* **11**, eaaw8412 (2019).
334. Li, L., Guris, D. L., Okura, M. & Imamoto, A. Translocation of CrkL to focal adhesions mediates integrin-induced migration downstream of Src family kinases. *Mol. Cell. Biol.* **23**, 2883–2892 (2003).
335. Plattner, R., Kadlec, L., DeMali, K. A., Kazlauskas, A. & Pendergast, A. M. c-Abl is activated by growth factors and Src family kinases and has a role in the cellular response to PDGF. *Genes Dev.* **13**, 2400–2411 (1999).
336. Tanis, K. Q., Veach, D., Duewel, H. S., Bornmann, W. G. & Koleske, A. J. Two distinct phosphorylation pathways have additive effects on Abl family kinase activation. *Mol. Cell. Biol.* **23**, 3884–3896 (2003).
337. Scott, A. J. *et al.* Evaluation of the efficacy of dasatinib, a Src/Abl inhibitor, in colorectal cancer cell lines and explant mouse model. *PLoS One* **12**, e0187173 (2017).
338. Langhans, S. A. Three-Dimensional in Vitro Cell Culture Models in Drug Discovery and Drug Repositioning. *Front. Pharmacol.* **9**, 6 (2018).
339. Arcaroli, J. J. *et al.* Gene array and fluorescence in situ hybridization biomarkers of activity of saracatinib (AZD0530), a Src inhibitor, in a preclinical model of colorectal cancer. *Clin. Cancer Res.* **16**, 4165–4177 (2010).
340. Mabuchi, S., Sugiyama, T. & Kimura, T. Clear cell carcinoma of the ovary: molecular insights and future therapeutic perspectives. *J. Gynecol. Oncol.* **27**, e31 (2016).
341. Manek, R. *et al.* Targeting Src in endometriosis-associated ovarian cancer. *Oncogenesis* **5**, e251 (2016).
342. Wiegand, K. C. *et al. ARID1A* Mutations in Endometriosis-Associated Ovarian Carcinomas. *N. Engl. J. Med.* **363**, 1532–1543 (2010).
343. Jones, S. *et al.* Frequent mutations of chromatin remodeling gene ARID1A in ovarian clear cell carcinoma. *Science* **330**, 228–231 (2010).
344. Miller, R. E. *et al.* Synthetic Lethal Targeting of *ARID1A* -Mutant Ovarian Clear Cell Tumors with Dasatinib. *Mol. Cancer Ther.* **15**, 1472–1484 (2016).
345. Caumanns, J. J., Wisman, G. B. A., Berns, K., van der Zee, A. G. J. & de Jong, S. ARID1A mutant ovarian clear cell carcinoma: A clear target for synthetic lethal strategies. *Biochim. Biophys. Acta - Rev. Cancer* **1870**, 176–184 (2018).
346. Berns, K. *et al.* ARID1A mutation sensitizes most ovarian clear cell carcinomas to BET inhibitors. *Oncogene* **37**, 4611–4625 (2018).
347. Wu, J. N. & Roberts, C. W. M. ARID1A Mutations in Cancer: Another Epigenetic Tumor Suppressor? *Cancer Discov.* **3**, 35–43 (2013).
348. Wellcome Sanger Institute. Cell Model Passports. https://cellmodelpassports.sanger.ac.uk.
349. Mariotti, V., McLeod, H. L. & Soliman, H. H. ARID1a as a marker of prognosis and increased sensitivity to CDK4/6, mTOR 1/2 and Src homology region 2 phosphatase (SHP 1/2) inhibitors in breast cancer (BC). *J. Clin. Oncol.* **37**, 1082–1082 (2019).
350. Samartzis, E. P. *et al.* Loss of ARID1A expression sensitizes cancer cells to PI3K- and AKT-inhibition. *Oncotarget* **5**, 5295–303 (2014).
351. Berns, K. *et al.* Loss of ARID1A Activates ANXA1, which Serves as a Predictive Biomarker for Trastuzumab Resistance. *Clin. Cancer Res.* **22**, 5238–5248 (2016).
352. Lin, Y.-F. *et al.* High-level expression of ARID1A predicts a favourable outcome in triple-negative breast cancer patients receiving paclitaxel-based chemotherapy. *J. Cell. Mol. Med.* **22**, 2458–2468 (2018).
353. Folkman, J. Angiogenesis in cancer, vascular, rheumatoid and other disease. *Nat.*

Med. **1**, 27–30 (1995).
354. Duh, E. J., Sun, J. K. & Stitt, A. W. Diabetic retinopathy: current understanding, mechanisms, and treatment strategies. *JCI insight* **2**, (2017).
355. NHS. Diabetic retinopathy. https://www.nhs.uk/conditions/diabetic-retinopathy (2018).
356. Tatton, L., Morley, G. M., Chopra, R. & Khwaja, A. The Src-selective Kinase Inhibitor PP1 Also Inhibits Kit and Bcr-Abl Tyrosine Kinases. *J. Biol. Chem.* **278**, 4847–4853 (2003).
357. von Raußendorf, F., de Ruiter, A. & Leonard, T. A. A switch in nucleotide affinity governs activation of the Src and Tec family kinases. *Sci. Rep.* **7**, 17405 (2017).
358. Rust, H. L., Moroco, J. A., Alvarado, J. J., Engen, J. J. & Smithgall, T. E. Abstract B190: Allosteric modulation of Src family kinases via SH3 domain displacement. *Mol. Cancer Ther.* **14**, B190 (2015).
359. Tokarski, J. S. *et al.* The Structure of Dasatinib (BMS-354825) Bound to Activated ABL Kinase Domain Elucidates Its Inhibitory Activity against Imatinib-Resistant ABL Mutants. *Cancer Res.* **66**, 5790–5797 (2006).
360. Roskoski, R. Classification of small molecule protein kinase inhibitors based upon the structures of their drug-enzyme complexes. *Pharmacol. Res.* **103**, 26–48 (2016).
361. Xu, W., Harrison, S. C. & Eck, M. J. Three-dimensional structure of the tyrosine kinase c-Src. *Nature* **385**, 595–602 (1997).
362. Xu, W., Doshi, A., Lei, M., Eck, M. J. & Harrison, S. C. Crystal Structures of c-Src Reveal Features of Its Autoinhibitory Mechanism. *Mol. Cell* **3**, 629–638 (1999).
363. Koudelková, L. *et al.* Novel FRET-Based Src Biosensor Reveals Mechanisms of Src Activation and Its Dynamics in Focal Adhesions. *Cell Chem. Biol.* **26**, 255-268.e4 (2019).
364. Ung, P. M.-U., Rahman, R. & Schlessinger, A. Redefining the Protein Kinase Conformational Space with Machine Learning. *Cell Chem. Biol.* **25**, 916-924.e2 (2018).
365. Elmore, S. Apoptosis: a review of programmed cell death. *Toxicol. Pathol.* **35**, 495–516 (2007).
366. Sun, H. *et al.* PTEN modulates cell cycle progression and cell survival by regulating phosphatidylinositol 3,4,5,-trisphosphate and Akt/protein kinase B signaling pathway. *Proc. Natl. Acad. Sci. U. S. A.* **96**, 6199–204 (1999).
367. Gheldof, A. & Berx, G. Cadherins and Epithelial-to-Mesenchymal Transition. *Prog. Mol. Biol. Transl. Sci.* **116**, 317–336 (2013).
368. Peng, S. *et al.* Dasatinib induces DNA damage and activates DNA repair pathways leading to senescence in non-small cell lung cancer cell lines with kinase-inactivating BRAF mutations. *Oncotarget* **7**, 565–79 (2016).
369. Lim, Y. *et al.* Focal adhesion kinase is negatively regulated by phosphorylation at tyrosine 407. *J. Biol. Chem.* **282**, 10398–404 (2007).
370. Calalb, M. B., Polte, T. R. & Hanks, S. K. Tyrosine phosphorylation of focal adhesion kinase at sites in the catalytic domain regulates kinase activity: a role for Src family kinases. *Mol. Cell. Biol.* **15**, 954–963 (1995).
371. Cabodi, S. *et al.* p130Cas interacts with estrogen receptor and modulates non-genomic estrogen signaling in breast cancer cells. *J. Cell Sci.* **117**, 1603–1611 (2004).
372. Castoria, G. *et al.* PI3-kinase in concert with Src promotes the S-phase entry of oestradiol-stimulated MCF-7 cells. *EMBO J.* **20**, 6050–6059 (2001).
373. Lim, S.-T. S. Nuclear FAK: a new mode of gene regulation from cellular adhesions. *Mol. Cells* **36**, 1–6 (2013).
374. Sun, S., Wu, H. J. & Guan, J. L. Nuclear FAK and its kinase activity regulate VEGFR2 transcription in angiogenesis of adult mice. *Sci. Rep.* **8**, 1–11 (2018).
375. Vijayan, R. S. K. *et al.* Conformational Analysis of the DFG-Out Kinase Motif and Biochemical Profiling of Structurally Validated Type II Inhibitors. *J. Med. Chem.* **58**, 466–479 (2015).
376. Davis, M. I. *et al.* Comprehensive analysis of kinase inhibitor selectivity. *Nat. Biotechnol.* **29**, 1046–1051 (2011).
377. Levinson, N. M. *et al.* A Src-Like Inactive Conformation in the Abl Tyrosine Kinase Domain. *PLoS Biol.* **4**, e144 (2006).

378. Caccia, D. *et al.* Dasatinib reduces FAK phosphorylation increasing the effects of RPI-1 inhibition in a RET/PTC1- expressing cell line. *Mol. Cancer* **9**, 278 (2010).
379. Liu, X. *et al.* Focal adhesion kinase activation limits efficacy of Dasatinib in c-Myc driven hepatocellular carcinoma. *Cancer Med.* **7**, 6170–6181 (2018).
380. Pleiman, C., Hertz, W. & Cambier, J. Activation of phosphatidylinositol-3' kinase by Src-family kinase SH3 binding to the p85 subunit. *Science* **263**, 1609–1612 (1994).
381. Frame, M. C., Patel, H., Serrels, B., Lietha, D. & Eck, M. J. The FERM domain: organizing the structure and function of FAK. *Nat. Rev. Mol. Cell Biol.* **11**, 802–814 (2010).
382. Lietha, D. *et al.* Structural Basis for the Autoinhibition of Focal Adhesion Kinase. *Cell* **129**, 1177–1187 (2007).
383. Kellett, M., Kessler, B., Mishall, K., Sharma, V. & Schweppe, R. SAT-574 Elucidating the Role of Nuclear Focal Adhesion Kinase (FAK) in Thyroid Cancer. *J. Endocr. Soc.* **3**, (2019).
384. International Council for Harmonisation of Technical Requirements for Registration of Pharmaceuticals for Human Use. ICH S9 Nonclinical Evalutation for Anticancer Pharmaceuticals. *ICH Harmonised Tripartite Guideline* https://www.ich.org/products/guidelines/safety/article/safety-guidelines.html (2009).
385. National Research Council (US) Committee on Chemical Environmental Mutagens. The Mutagenicity of Carcinogenic Compounds. in *Quantitative Relationship between Mutagenic and Carcinogenic Potencies: A Feasibility Study.* (National Academies Press (US), 1983).
386. European Medicines Agency. Sprycel: EPAR - Scientific Discussion. http://www.ema.europa.eu/docs/en_GB/document_library/EPAR_-_Scientific_Discussion/human/000709/WC500056995.pdf (2006).
387. Committee for Medicinal Products for Human Use (CHMP). Assessment Report: Bosulif. https://www.ema.europa.eu/en/documents/assessment-report/bosulif-epar-public-assessment-report_en.pdf (2013).
388. Bristol-Myers Squibb Pharmaceutical Research Institute. Investigator Brochure: Dasatinib BMS-354825. http://spirit-cml.org/isf/referencesafetyinformation/ (2007).
389. Chan, C. M. *et al.* Targeted inhibition of Src kinase with dasatinib blocks thyroid cancer growth and metastasis. *Clin. Cancer Res.* **18**, 3580–3591 (2012).
390. Golas, J. M. *et al.* SKI-606, a Src/Abl Inhibitor with *In vivo* Activity in Colon Tumor Xenograft Models. *Cancer Res.* **65**, 5358–5364 (2005).
391. Kamath, A. V *et al.* Preclinical pharmacokinetics and in vitro metabolism of dasatinib (BMS-354825): a potent oral multi-targeted kinase inhibitor against SRC and BCR-ABL. *Cancer Chemother Pharmacol* **61**, 365–376 (2008).
392. Luo, F. R. *et al.* Dasatinib (BMS-354825) Pharmacokinetics and Pharmacodynamic Biomarkers in Animal Models Predict Optimal Clinical Exposure. *Clin. Cancer Res.* **12**, 7180–7186 (2006).
393. Center for Drug Evalutation and Research. Bosutinib - Pharmacology Review(s). https://www.accessdata.fda.gov/drugsatfda_docs/nda/2012/203341Orig1s000PharmR.pdf (2012).
394. Hinson, J. A., Roberts, D. W. & James, L. P. Mechanisms of acetaminophen-induced liver necrosis. in *Handbook of Experimental Pharmacology* 369–405 (Springer, 2010). doi:10.1007/978-3-642-00663-0_12.
395. Christopher, L. J. *et al.* Biotransformation of [14C]dasatinib: In vitro studies in rat, monkey, and human and disposition after administration to rats and monkeys. *Drug Metab. Dispos.* **36**, 1341–1356 (2008).
396. Porkka, K. *et al.* Dasatinib crosses the blood-brain barrier and is an efficient therapy for central nervous system Philadelphia chromosome-positive leukemia. *Blood* **112**, 1005–12 (2008).
397. Batlle, E. & Clevers, H. Cancer stem cells revisited. *Nat. Med.* **23**, 1124–1134 (2017).
398. Thakur, R., Trivedi, R., Rastogi, N., Singh, M. & Mishra, D. P. Inhibition of STAT3, FAK and Src mediated signaling reduces cancer stem cell load, tumorigenic potential and metastasis in breast cancer. *Sci. Rep.* **5**, 10194 (2015).
399. Kolev, V. N. *et al.* Inhibition of FAK kinase activity preferentially targets cancer stem cells. *Oncotarget* **8**, 51733–51747 (2017).

400. Cariati, M. *et al.* Alpha-6 integrin is necessary for the tumourigenicity of a stem cell-like subpopulation within the MCF7 breast cancer cell line. *Int. J. Cancer* **122**, 298–304 (2008).
401. Song, N., Guo, H., Ren, J., Hao, S. & Wang, X. Synergistic anti-tumor effects of dasatinib and dendritic cell vaccine on metastatic breast cancer in a mouse model. *Oncol. Lett.* **15**, 6831–6838 (2018).
402. Jallal, H. *et al.* A Src/Abl kinase inhibitor, SKI-606, blocks breast cancer invasion, growth, and metastasis in vitro and in vivo. *Cancer Res.* **67**, 1580–1588 (2007).
403. Christopher, L. J. *et al.* Metabolism and Disposition of Dasatinib after Oral Administration to Humans. *Drug Metab. Dispos.* **36**, 1357–1364 (2008).
404. Agarwal, S. *et al.* Active Efflux of Dasatinib from the Brain Limits Efficacy against Murine Glioblastoma: Broad Implications for the Clinical Use of Molecularly Targeted Agents. *Mol. Cancer Ther.* **11**, 2183–2192 (2012).
405. Lagas, J. S. *et al.* Brain Accumulation of Dasatinib Is Restricted by P-Glycoprotein (ABCB1) and Breast Cancer Resistance Protein (ABCG2) and Can Be Enhanced by Elacridar Treatment. *Clin. Cancer Res.* **15**, 2344–2351 (2009).
406. Litmanovich, A., Khazim, K. & Cohen, I. The Role of Interleukin-1 in the Pathogenesis of Cancer and its Potential as a Therapeutic Target in Clinical Practice. *Oncol. Ther.* **6**, 109–127 (2018).
407. Nutter, F. *et al.* Different molecular profiles are associated with breast cancer cell homing compared with colonisation of bone: evidence using a novel bone-seeking cell line. *Endocr. Relat. Cancer* **21**, 327–341 (2014).
408. Holen, I. *et al.* IL-1 drives breast cancer growth and bone metastasis in vivo. *Oncotarget* **7**, 75571–75584 (2016).
409. Sureshbabu, A. *et al.* IGFBP5 induces cell adhesion, increases cell survival and inhibits cell migration in MCF-7 human breast cancer cells. *J. Cell Sci.* **125**, 1693–1705 (2012).
410. Wang, J. *et al.* Insulin-like growth factor binding protein 5 (IGFBP5) functions as a tumor suppressor in human melanoma cells. *Oncotarget* **6**, 20636–49 (2015).
411. Hwang, J. R. *et al.* The C-terminus of IGFBP-5 suppresses tumor growth by inhibiting angiogenesis. *Sci. Rep.* **6**, 39334 (2016).
412. Slaney, C. Y., Kershaw, M. H. & Darcy, P. K. Trafficking of T Cells into Tumors. *Cancer Res.* **74**, 7168–7174 (2014).
413. Acharyya, S. *et al.* A CXCL1 Paracrine Network Links Cancer Chemoresistance and Metastasis. *Cell* **150**, 165–178 (2012).
414. Shi, H. *et al.* Chemokine (C-X-C motif) ligand 1 and CXCL2 produced by tumor promote the generation of monocytic myeloid-derived suppressor cells. *Cancer Sci.* **109**, 3826–3839 (2018).
415. Wang, X. & Lin, Y. Tumor necrosis factor and cancer, buddies or foes? *Acta Pharmacol. Sin.* **29**, 1275–88 (2008).
416. Fisher, D. T., Appenheimer, M. M. & Evans, S. S. The two faces of IL-6 in the tumor microenvironment. *Semin. Immunol.* **26**, 38–47 (2014).
417. Sternlicht, M. D., Bissell, M. J. & Werb, Z. The matrix metalloproteinase stromelysin-1 acts as a natural mammary tumor promoter. *Oncogene* **19**, 1102–13 (2000).
418. Sternlicht, M. D. *et al.* The stromal proteinase MMP3/stromelysin-1 promotes mammary carcinogenesis. *Cell* **98**, 137–46 (1999).
419. Ramos-DeSimone, N. *et al.* Activation of matrix metalloproteinase-9 (MMP-9) via a converging plasmin/stromelysin-1 cascade enhances tumor cell invasion. *J. Biol. Chem.* **274**, 13066–76 (1999).
420. Bergers, G. *et al.* Matrix metalloproteinase-9 triggers the angiogenic switch during carcinogenesis. *Nat. Cell Biol.* **2**, 737–44 (2000).
421. Pang, X. *et al.* Osteopontin as a multifaceted driver of bone metastasis and drug resistance. *Pharmacol. Res.* **144**, 235–244 (2019).
422. Schlecker, E. *et al.* Tumor-infiltrating monocytic myeloid-derived suppressor cells mediate CCR5-dependent recruitment of regulatory T cells favoring tumor growth. *J. Immunol.* **189**, 5602–11 (2012).
423. Chang, L.-Y. *et al.* Tumor-Derived Chemokine CCL5 Enhances TGF- -Mediated Killing of CD8+ T Cells in Colon Cancer by T-Regulatory Cells. *Cancer Res.* **72**,

1092–1102 (2012).
424. Kaplanov, I. *et al.* Blocking IL-1β reverses the immunosuppression in mouse breast cancer and synergizes with anti-PD-1 for tumor abrogation. *Proc. Natl. Acad. Sci. U. S. A.* **116**, 1361–1369 (2019).
425. Jiang, H. *et al.* Targeting focal adhesion kinase renders pancreatic cancers responsive to checkpoint immunotherapy. *Nat. Med.* **22**, 851–60 (2016).
426. Symeonides, S. N., Anderton, S. M. & Serrels, A. FAK-inhibition opens the door to checkpoint immunotherapy in Pancreatic Cancer. *J. Immunother. Cancer* **5**, 17 (2017).
427. Mestermann, K. *et al.* The tyrosine kinase inhibitor dasatinib acts as a pharmacologic on/off switch for CAR T cells. *Sci. Transl. Med.* **11**, eaau5907 (2019).
428. Kurebayashi, J. *et al.* Preferential antitumor effect of the Src inhibitor dasatinib associated with a decreased proportion of aldehyde dehydrogenase 1-positive cells in breast cancer cells of the basal B subtype. *BMC Cancer* **10**, 568 (2010).
429. Tryfonopoulos, D. *et al.* Src: a potential target for the treatment of triple-negative breast cancer. *Ann. Oncol.* **22**, 2234–2240 (2011).
430. Qian, X.-L. *et al.* Dasatinib inhibits c-src phosphorylation and prevents the proliferation of Triple-Negative Breast Cancer (TNBC) cells which overexpress Syndecan-Binding Protein (SDCBP). *PLoS One* **12**, e0171169 (2017).
431. Kelland, L. R. “Of mice and men”: values and liabilities of the athymic nude mouse model in anticancer drug development. *Eur. J. Cancer* **40**, 827–836 (2004).
432. Chen, Z. *et al.* Intratumoral $CD8^+$ cytotoxic lymphocyte is a favorable prognostic marker in node-negative breast cancer. *PLoS One* **9**, e95475 (2014).
433. Gonzalez, H., Hagerling, C. & Werb, Z. Roles of the immune system in cancer: from tumor initiation to metastatic progression. *Genes Dev.* **32**, 1267–1284 (2018).
434. Schade, A. E. *et al.* Dasatinib, a small-molecule protein tyrosine kinase inhibitor, inhibits T-cell activation and proliferation. *Blood* **111**, 1366–77 (2008).
435. Weichsel, R. *et al.* Profound Inhibition of Antigen-Specific T-Cell Effector Functions by Dasatinib. *Clin. Cancer Res.* **14**, 2484–2491 (2008).
436. Blake, S., Hughes, T. P., Mayrhofer, G. & Lyons, A. B. The Src/ABL kinase inhibitor dasatinib (BMS-354825) inhibits function of normal human T-lymphocytes in vitro. *Clin. Immunol.* **127**, 330–339 (2008).
437. Fraser, C. K. *et al.* Dasatinib inhibits recombinant viral antigen-specific murine CD4+ and CD8+ T-cell responses and NK-cell cytolytic activity in vitro and in vivo. *Exp. Hematol.* **37**, 256–265 (2009).
438. Fei, F. *et al.* Dasatinib inhibits the proliferation and function of $CD4^+$ $CD25^+$ regulatory T cells. *Br. J. Haematol.* **144**, 195–205 (2009).
439. Hekim, C. *et al.* Dasatinib Changes Immune Cell Profiles Concomitant with Reduced Tumor Growth in Several Murine Solid Tumor Models. *Cancer Immunol. Res.* **5**, 157–169 (2017).
440. Iriyama, N., Hatta, Y. & Takei, M. Direct effect of dasatinib on signal transduction pathways associated with a rapid mobilization of cytotoxic lymphocytes. *Cancer Med.* **5**, 3223–3234 (2016).